Application of gold nanorods in cancer theranostics

Mohan Singh MRCS

The Hamlyn Centre for Robotic Surgery
Institute of Global Health Innovation
Department of Surgery and Cancer
Imperial College London
London, UK

2015

A thesis submitted for the degree of Doctor of Philosophy
to Imperial College London

Supervisors

Professor Daniel S Elson PhD
Hamlyn Centre for Robotic Surgery, Department of Surgery and Cancer
Imperial College London, South Kensington, London, UK

Professor George B Hanna PhD FRCS
Department of Surgery and Cancer, Imperial College London
St Mary's Hospital, London, UK

AUTHOR'S DECLARATION

I hereby declare that I am the sole author of this thesis and that all work within it is my own. Any individuals who carried out any collaborative work are duly credited.

Mohan Singh 25/12/2015

COPYRIGHT DECLARATION

The copyright of this thesis rests with the author and is made available under a Creative Commons Attribution Non-Commercial No Derivatives licence. Researchers are free to copy, distribute or transmit the thesis on the condition that they attribute it, that they do not use it for commercial purposes and that they do not alter, transform or build upon it. For any reuse or redistribution, researchers must make clear to others the licence terms of this work.

ABSTRACT

In the UK, oesophagogastric cancer is often diagnosed late resulting in only a third of patients being suitable for definitive treatment. The 5-year survival for oesophageal and gastric cancer is 12% and 17% respectively. Despite the need for early detection there remains an inherent risk of missing cancerous lesions during endoscopy.

In this research, the combined theranostic (therapy and diagnostic) potential of gold nanorods in gastrointestinal adenocarcinoma is scrutinised. The aims of this thesis were to assess the viability of applying photothermal therapy in human adenocarcinoma *ex vivo* tissues, determine their efficiency and safety within a rodent cancer model and to design a practical method for simultaneous imaging and therapy of cancer *in vivo*.

Studies were conducted to establish the optimal gold nanorod concentration and irradiation power required for inducing hyperthermic effects in human and porcine tissues and then evaluate the photothermal effects on *ex vivo* human oesophageal and gastric adenocarcinoma.

Multi-functionalised fluorescent gold nanorods were exposed to human adenocarcinoma cells to test *in vitro* targeting efficiency using immunohistochemistry and fluorescence microscopy.

A theranostic approach developed from *in vivo* studies is described and shown to be effective in identifying tumours and performing image-guided photothermal therapy. Key principles for successful photothermal therapy are outlined. The theranostic potential offered by functionalised gold nanorods have a place in early and late stage cancers, and can be a valuable adjunct in surgery and endoscopy.

Safety considerations of the application of gold nanorods and photothermal therapy are evaluated *in vivo*. Gold nanorods are appraised to be inherently safe while harbouring excellent translational potential as effective theranostic tools.

This work has shown that nanotechnology could now be considered for human gastrointestinal tumours. Providing an alternative means of treatment that is effective, cheap and rapid can incur significant improvements in patient prognosis, cancer treatment and quality of life.

PUBLICATIONS, PRESENTATIONS AND PRIZES

Publications

Application of gold nanoparticles for gastrointestinal cancer theranostics: A systematic review.
Singh, M., Harris-Birtill, D.C.C., Markar, S.R., Hanna, G.B., Elson, D.S.
Nanomedicine: Nanotechnology, Biology and Medicine Nov 2015, 11(8); 2083–2098.
doi: 10.1016/j.nano.2015.05.010.

Application of gold nanorods for photothermal therapy in *ex vivo* human oesophagogastric adenocarcinoma.
Singh, M. & Harris-Birtill, D.C.C., Zhou, Y., Gallina, M.E., Cass, A.E.G., Hanna, G.B., Elson, D.S.
Journal of Biomedical Nanotechnology 2016, 12(3), 481- 490. doi:10.1166/jbn.2016.2196.

Aptamer-conjugated, fluorescent gold nanorods as potential cancer theradiagnostic agents.
Gallina, M.E., Zhou, Y., Johnson, C.J., Harris-Birtill, D.C.C., Singh, M., Zhao, H., Ma, D., Cass, A.E.G., Elson, D.S.
Materials Science and Engineering: C, Feb 2016, 59; 324-332.
doi: 10.1016/j.msec.2015.09.101.

Gold nanorod reshaping *in vitro* and *in vivo* from a continuous wave laser.
Singh, M. & Harris-Birtill, D.C.C., Zhou, Y., Shah, A., Ruenraroengsak, P., Gallina, M.E., Hanna, G.B., Cass, A.E.G., Porter, A.E., Bamber, J., Elson, D.S.
Submitted.

Abstracts

Application of gold nanorods for *in vivo* theranostics of human oesophageal adenocarcinoma.
Singh, M., Nabavi, E., Zhou, Y., Zhao, H., Ma, D., Cass, A.E.G., Hanna, G.B., Elson, D.S.
Gut 2015;64:A471
doi:10.1136/gutjnl-2015-309861.1031

Application of gold nanorods for photothermal effect in upper gastrointestinal cancer tissue.
Singh, M., Harris-Birtill, D.C.C., Gallina, M.E., Hanna, G.B., Elson, D.S.
British J Surgery 2015; 102 (Suppl. 1): 72-73.

Application of gold nanorods for upper gastrointestinal cancer theranostics.
Singh, M., Nabavi, E., Zhou, Y., Zhao, H., Ma, D., Cass, A.E.G., Hanna, G.B., Elson, D.E.
British J Surgery April 2016; 103 (S3):46. doi: 10.1002/bjs.10158

Gold nanorod reshaping using a continuous wave laser.
Harris-Birtill, D.C.C. & Singh, M., Zhou, Y., Gallina, M.E., Cass, A.E.G., Elson, D.S.
Conference on Lasers and Electro-Optics (CLEO), San Jose, CA, June 2014. IEEE. Jan 2014.
Conference proceedings paper. doi: 10.1364/CLEO_AT.2014.JTh2A.95

Prizes

1. Best oral presentation award (MIA Prize) at the Royal Society of Medicine (RSM) Surgery Section and BASO-ACS Scientific Conference at the Royal Society of Medicine, Nov. 2015.
2. Best oral presentation award at the 9th London Surgical Symposium's plenary session, Imperial College London, September 2015.
3. ASiT-SARS Prize winner at the Association of Surgeons in Training (ASiT) Annual Surgical Conference, Liverpool, March 2016.
4. Best presentation award in the plenary session at The Society for Surgery of the Alimentary Tract (SSAT) Residents & Fellows Research Conference, San Diego, CA, May 2016.
5. Gerhard Buess Technology Award Session – Runner's up. 2nd of 7 best original presentations at the 24th International European Association of Endoscopic Surgery Congress in Amsterdam, The Netherlands, June 2016.

Oral Presentations

Application of gold nanoparticles for *in vivo* cancer theranostics
Singh, M., Nabavi, E., Zhou, Y., Zhao, H., Ma, D., Cass, A.E.G., Hanna, G.B., Elson, D.E.
- The Society for Surgery of the Alimentary Tract (SSAT) Residents & Fellows Research Conference, San Diego, CA, May 2016.
- Digestive Disease Week Plenary Session (Esophagus and Gastric), San Diego, CA, May 2016.
- Gerhard Buess Technology Award Session at the 24th International European Association of Endoscopic Surgery Congress in Amsterdam, The Netherlands, June 2016.

Gold nanoparticles for *in vivo* theranostics of human oesophageal adenocarcinoma.
Singh, M., Nabavi, E., Zhou, Y., Zhao, H., Ma, D., Cass, A.E.G., Hanna, G.B., Elson, D.E.
International Surgical Congress of the Association of Surgeons of Great Britain and Ireland, Belfast, May 2016.

Application of gold nanorods for oesophageal cancer theranostics.
Singh, M., Nabavi, E., Zhou, Y., Zhao, H., Ma, D., Cass, A.E.G., Hanna, G.B., Elson, D.E.
Association of Surgeons in Training Annual Surgical Conference, Liverpool, March 2016.

Fluorescence image-guided photothermal therapy of human oesophageal adenocarcinoma *in vivo* using multifunctional gold nanorods *in vivo*.
Nabavi, E., Singh, M., Zhou, Y., Gallina, M.E., Zhao, H., Ma, D., Cass, A.E.G., Hanna, G.B., Elson, D.E.
SPIE Photonics West BiOS, San Francisco, CA, USA, February 2016.

Application of gold nanorods for upper gastrointestinal cancer theranostics.
Singh, M., Nabavi, E., Zhou, Y., Zhao, H., Ma, D., Cass, A.E.G., Hanna, G.B., Elson, D.E.
Society of Academic and Research Surgery Annual Meeting, The Royal College of Surgeons of England, London, January 2016.

Application of gold nanorods for cancer theranostics.
Singh, M., Nabavi, E., Zhou, Y., Zhao, H., Ma, D., Cass, A.E.G., Hanna, G.B., Elson, D.E.
Royal Society of Medicine Surgery Section and BASO-ACS scientific conference at the Royal Society of Medicine, London, November 2015.

Application of gold nanorods for upper gastrointestinal cancer theranostics.
Singh, M., Nabavi, E., Zhou, Y., Zhao, H., Ma, D., Cass, A., Hanna, G.B., Elson, D.E.
9th London Surgical Symposium, Imperial College London, September 2015.

Targeted near-infrared photothermal therapy of human oesophageal adenocarcinoma in mice using multifunctional gold nanorods.
Nabavi, E., Singh, M., Zhou, Y., Gallina, M.E., Zhao, H., Ma, D., Cass, A.E.G., Hanna, G.B., Elson, D.E.
British Medical Laser Association Conference, Brighton, April 2015.

Application of gold nanorods for photothermal effect in upper gastrointestinal cancer tissue.
Singh, M., Harris-Birtill, D.C.C., Gallina, M.E., Zhou, Y., Cass, A.E.G., Hanna, G.B., Elson, D.S.
Association of Surgeons of Great Britain & Ireland International Surgical Congress, Harrogate, April 2014.

Application of gold nanorods for photothermal effect in human upper gastrointestinal cancer tissue.
Singh, M., Nabavi, E., Zhou, Y., Zhao, H., Ma, D., Cass, A., Hanna, G.B., Elson, D.E.
The Royal Society of Medicine Surgery Section Presidential Address, Royal Society of Medicine, London, October 2013.

Automatic image analysis of nanorods.
Harris-Birtill, D.C.C., Gallina, M.E., Zhou, Y., Lin, J., Singh, M., Elson, D.S.
Bio-Nano-Photonics Conference, Cardiff, September 2013.

Application of gold nanorods for photothermal effect in *ex vivo* upper gastrointestinal cancer tissue.
Singh, M., Harris-Birtill, D.C.C., Gallina, M.E., Zhou, Y., Cass, A.E.G., Hanna, G.B., Elson, D.S.
7th London Surgical Symposium, Imperial College London, September 2013.

Poster Presentations

Gold nanorod reshaping using a continuous wave laser.
Singh, M. & Harris-Birtill D.C.C., Zhou, Y., Shah, A., Gallina, M.E., Cass, A.E.G., Bamber, J., Hanna, G.B., Elson, D.S.
Bio-Nano-Photonics Symposium, Cardiff, Sept. 2015.

Application of gold nanorods for *in vivo* theranostics of human oesophageal adenocarcinoma.
Singh, M., Nabavi, E., Zhou, Y., Zhao, H., Ma, D., Cass, A.E., Hanna, G.B., Elson, D.S.
1. AUGIS Section of Digestive Disorders Federation, London ExCeL, June 2015.
2. Academic Trainees Annual Event, Imperial College London, May 2015.

Gold nanorod reshaping using continuous wave laser.
Harris-Birtill, D.C.C., Singh, M., Zhou, Y., Gallina, M.E., Cass, A.E.G., Elson, D.S.
CLEO (Conference on Lasers and Electro-Optics) in San Jose, CA, USA, June 2014.

Application of gold nanorods for photothermal effect in upper gastrointestinal cancer tissue.
Singh, M., Harris-Birtill, D.C.C., Gallina, M.E., Zhou, Y., Cass, A.E.G., Hanna, G.B., Elson, D.S.
1. Bio-Nano-Photonics Conference, Cardiff, Sept. 2013.
2. Medical Engineering Centres Annual Meeting and Bioengineering, Imperial College London, Sept. 2014. The UK's largest ever gathering of Biomedical Engineers, Bioengineers and Medical Engineers.

Mum

For your timeless encouragement and support

This work is as much yours as it is mine

ACKNOWLEDGEMENTS

This work is the culmination of the efforts of many people apart from myself. Pursuing a cancer research based project has been an attractive and thoroughly rewarding venture. I am very fortunate to complete the work whilst basking in the ambience of some incredibly bright, hardworking and cheerful people. I am cognisant that this work would neither have been possible nor worthwhile without their input and support. I look forward to many more years of continued friendship and collaboration.

Professor Daniel Elson, Supervisor. Thank you for taking me under your wing. I have benefited tremendously from your open-door policy, focused direction and innate ability to immediately solve any query I had. Your encyclopaedic knowledge, charisma and humility have made me realise that you a role model for academics everywhere and a world-class leader amongst them.

Professor George Hanna, Supervisor. Thank you for believing in me and providing gentle encouragement throughout the journey. Your extraordinary work ethic, guidance and humility are inspirational and have provided me ideals to strive for in my career.

Dr. Neil Clancy, co-worker. I have been lucky to catch a glimpse of how a young, enthusiastic, very bright yet grounded academic incessantly strives towards the pinnacle of academia. Thank you for answering my myriad of questions with your natural charm and the immense assistance you readily provided from the beginning.

Dr. Elham Nabavi, ever-present laboratory partner. Thank you for your hard work and dedication in making the hypothesis a reality. It has been a great pleasure conducting the *in vivo* experiments with you and witnessing the developments. I am delighted that you will be taking the work forward to the next stage.

Dr. David Harris-Birtill, co-worker. Thank you for your immense efforts in getting the project off the ground, your brilliant imaginative ideas, attention to detail, infectious positivity and devotion. You have been a formidable collaborator and it has been incredible to have had your unflinching support from the outset and throughout.

Drs. Yu Zhou & Maria Gallina, co-workers, Chemists par excellence. It has been staggering witnessing the diligence, evolution and eventual perfection of the chemistry involved in fabricating the ideal gold nanorods, the catalyst for the advancement of all the experiments within this thesis. Thank you for your perseverance and innovation.

Drs. Hailin Zhao and Daqing Ma, collaborators. Thank you for teaching me everything I needed to know about cell culture, immunohistochemistry, establishing tumour xenografts *in vivo*, and for your unswerving encouragement throughout.

Drs. Ji Qi, Jianyu Lin and Fernando Avila-Rencoret. Thank you for all your patience and immeasurable kindness in solving the multiple computing, formatting,

referencing and other issues I had, but also for helping me keep my balance with your delightful and cherished company over the years. I have learnt a great deal from you.

Miss Elena Schwan. Thank you for your skilful help with the figures, and your selflessness. They are indeed impressive. Without your experience, skills, imagination and Germanic perfectionism, they would appear mediocre, but you have evidently spruced them up to award-winning quality.

Professor Paul Sibbons and all the amazing staff at The Northwick Park Institute for Medical Research. Thank you for your enormous help with getting the *in vivo* studies underway and seeing me through it all. It has been an almighty effort and I am indebted to the entire department for the multi-source assistance received.

Dr. Pakatip Ruenraroengsak, co-worker. Thank you for your hard work in scrutinising and honing in on all those nanorods hiding within cells of tissues, and persevering to prove conclusively that they do in fact reshape with irradiation.

Mr. Stefan Antonowicz. Thank you for helping me getting started with the *in vitro* studies at Chelsea and the FLO-1 cells, which became the primary cell line used.

Mr. Sacheen Kumar, Mr. Nima Abbassi-Ghadi and Mr. Shobhit Arya. Thank you for all your help obtaining the numerous *ex vivo* samples and your valued support.

Professor Mark Rehkamper, Drs. Rebekah Moore and Adam Laycock. Thank you all for the great help in getting the many tissue samples processed with ICP-MS.

To my other friends and family. Thank you for your phenomenal understanding and encouragement over the period of research and write-up.

ABBREVIATIONS

ABC ATP-binding cassette
AOM Azoxymethane
AR Aspect ratio
Au Gold
[Au] Concentration of gold
BALB/c Bagg albino nude mice
BP Band-pass (filter)
C Celsius
CRC Colorectal cancer
CS-GNPs Chitosan-modified gold nanoparticles
CT Computed tomography
CTAB Cetyltrimethylammonium bromide
CW Continuous wave (laser)
DAPI 4', 6-diamidino-2-phenylindole
DLS Dynamic light scattering
DMEM Dulbecco's Modified Eagle's Medium
DNA Deoxyribonucleic acid
EDC N-(3-Dimethylaminopropyl)-N′-ethylcarbodiimide hydrochloride
EDTA Ethylenediaminetetraacetic acid
EDX Energy-dispersive X-ray spectroscopy
EGFR Epidermal growth factor receptor
EM Electron microscopy
EMA European Medicines Agency
EMCCD Electron multiplying charge coupled device
EMR Endoscopic mucosal resection
EPR Enhanced permeability and retention effect
ESD Endoscopic submucosal dissection
FA Folic acid receptors
FDA US Food and Drug Administration
FITC Annexin V-fluoroisothiocyanate
FLO-1 cells Distal oesophageal adenocarcinoma cell line
GA General anaesthesia
GES-1 Human gastric epithelium cells
GI Gastrointestinal
GNP Gold nanoparticle
GNR Gold nanorod
[GNR] Concentration of GNR
Gy Gray (Joule/kg)
H & E Haematoxylin & eosin (stain)
HeLa Human cervical cancer cells
HER-1 Human Epidermal Growth Factor Receptor 1
Het-1a Benign human squamous oesophageal epithelium cells
HNP Hybrid nanoparticles
HU Hounsfield Units
ICG Indocyanine green
ICP-MS Inductively coupled plasma mass spectrometry
IHC Immunohistochemistry
IPL Intense pulsed light
IRT Irinotecan
IT Intratumoural
IV Intravenous

K Kelvin
LP Long-pass (filter)
LSPR Longitudinal surface plasmon resonance
mag. magnification
MHRA Medicines and Healthcare products Regulatory Agency
MRI Magnetic resonance imaging
MTT 3-(4,5-dimethylthiazol-2-yl)-2,5-diphenyltetrazolium bromide assay
NHS N-Hydroxysuccinimide
NIR Near infra-red (laser/light)
nM nano Molar
nm nanometre
NPIMR The Northwick Park Institute for Medical Research
NPs Nanoparticles
OCT Optical coherence tomography
OD Optical density
OGJ Oesophagogastic junctional
OPO Optical parametric oscillator
PTT Photothermal therapy
PEG Polyethylene glycol
PAA Poly(acrylic) acid
PA (I) Photoacoustic (imaging)
PBS Phosphate buffered saline
PEL Establishment licence
PET Positron emission tomography
PFA Para-formaldehyde
PIL Procedural personal licence
$\mathbf{P_L}$ Laser power
PPL Project licence
PRISMA Preferred Reporting Items for Systematic Reviews and Meta-analysis
R1 resections microscopic evidence of tumour at resection margin
R2 (partial) resection macroscopic (gross) evidence of tumour at resection margin
RES Reticuloendothelial system/organs
RNA Ribonucleic acid
ROI Region of interest
RPMI Roswell Park Memorial Institute medium
s/c subcutaneous
SCID Severe combined immunodeficiency
se Standard error
SEM Scanning electron microscopy
SLN Sentinel lymph node
SPION Superparamagnetic iron oxide nanoparticles
SPR Surface plasmon resonance
STEM Scanning transmission electron microscope
T1 tumours tumours confined to the mucosal and submucosal layers
T2 tumours tumours growing into the muscularis propria layer
TEM Transmission electron microscopy
TNF Tumour necrosis factor
US Ultrasound
UV-Vis Ultraviolet–visible spectroscopy
VCAM-1 Vascular cell adhesion molecule-1
VEGF Vascular endothelial growth factor
W Watts

CONTENTS

ABSTRACT		iii
PUBLICATIONS, PRESENTATIONS AND PRIZES		iv
ACKNOWLEDGEMENTS		viii
ABBREVIATIONS		x
LIST OF FIGURES		xv
LIST OF TABLES		xix
CHAPTER 1 INTRODUCTION		1
1.1	THESIS MOTIVATION	4
1.1.1	EARLY DIAGNOSIS WITH OPTICAL IMAGING	4
1.1.2	PALLIATIVE PHOTOTHERMAL THERAPY	6
1.2	THESIS AIMS	7
1.3	OVERVIEW OF THE THESIS	8
CHAPTER 2 APPLICATION OF GOLD NANOPARTICLES FOR GASTROINTESTINAL CANCER THERANOSTICS: A SYSTEMATIC REVIEW		12
2.1	BACKGROUND	12
2.2	MATERIALS AND METHODS	19
2.3	RESULTS	20
2.4	SUMMARY OF EVIDENCE	30
2.5	DISCUSSION	35
2.6	CONCLUSIONS	37
METHODS AND MATERIALS		44
CTAB-GNR SYNTHESIS		44
MATERIALS		45
PREPARATION OF THE SEED SOLUTION		45
GROWTH OF GOLD NANORODS		45
PEGYLATION OF GNRs		46
FUNCTIONALISATION OF GNRs		46
CHARACTERISATION OF GNRs		47
OPTICAL DENSITY		47
TRANMISSION ELECTRON MICROSCOPY (TEM) AND EDX ANALYSIS		49
CHAPTER 3 GOLD NANOROD RESHAPING *IN VITRO* AND *IN VIVO* USING A CONTINUOUS WAVE LASER		51
3.1	INTRODUCTION	51
3.2	METHODS	52
3.2.1	SYNTHESIS	52
3.2.2	IRRADIATION AND MONITORING	52
3.2.3	CHEMICAL AND MICROSCOPIC ANALYSIS	54
3.2.4	THERMAL IMAGE ANALYSIS	54
3.2.5	PA DATA AND PULSED LASER ENERGY	55
3.2.6	*IN VIVO* ANALYSIS OF GNRS IN TUMOUR-BEARING AND TUMOUR-IRRADIATED MICE	56
3.2.7	TRANSMISSION ELECTRON MICROSCOPY (TEM)	56
3.3	RESULTS	57
3.4	DISCUSSION	64
3.5	CONCLUSION	69

CHAPTER 4 APPLICATION OF GOLD NANORODS FOR PHOTOTHERMAL THERAPY IN *EX VIVO* HUMAN OESOPHAGOGASTRIC ADENOCARCINOMA 72
4.1 INTRODUCTION 72
4.2 MATERIALS AND METHODS 73
4.2.1 GOLD NANOROD SYNTHESIS AND CHARACTERISATION 73
4.2.2 TEMPERATURE CHANGE WITH VARYING GOLD NANOROD CONCENTRATIONS 73
4.2.3 EFFECT OF GOLD NANOROD CONCENTRATION ON HEALTHY PORCINE OESOPHAGEAL TISSUES AND PHOTOTHERMAL RESPONSE 74
4.2.4 HUMAN OESOPHAGOGASTRIC TISSUE EXPERIMENTS 75
4.3 RESULTS 76
4.3.1 CHARACTERISATION OF GNRS 76
4.3.2 TEMPERATURE CHANGE WITH VARYING GNR CONCENTRATION 77
4.3.3 EFFECT OF GNR CONCENTRATION AND LASER FLUENCE ON HEALTHY PORCINE OESOPHAGEAL TISSUES AND PHOTOTHERMAL RESPONSE 78
4.3.4 PLASMONIC PHOTOTHERMAL THERAPY OF HUMAN OESOPHAGOGASTRIC TISSUES 80
4.4 DISCUSSION 81
4.5 CONCLUSIONS 85

CHAPTER 5 *IN VITRO* ASSESSMENTS OF FUNCTIONALISED GOLD NANORODS FOR IMAGING AND TARGETED THERAPY OF *IN VIVO* GASTROINTESTINAL CANCER 87
5.1 INTRODUCTION 87
5.2 SYNTHESIS OF GNRS AND FUNCTIONALISATION WITH FLUOROPHORE AND ANTI-EGFR ANTIBODY 88
5.3 HUMAN OESOPHAGEAL ADENOCARCINOMA (FLO-1) CELLS 88
5.4 TEM IMAGING OF FUNCTIONALISED GNRS 89
5.5 IMMUNOHISTOCHEMISTRY AND EPIDERMAL GROWTH FACTOR RECEPTOR (EGFR) ANTIGEN TARGETING 90
5.6 IMMUNOHISTOCHEMISTRY AND FLUORESCENCE MICROSCOPY OF FUNCTIONALISED GNRS IN CANCER CELLS 92
5.7 NIR LASER IRRADIATION OF OTHER CELLS INCUBATED WITH FUNCTIONALISED GNRS 93
5.8 ESTABLISHING HUMAN OESOPHAGEAL ADENOCARCINOMA TUMOUR XENOGRAFTS IN IMMUNODEFICIENT MICE 97
5.9 DISCUSSION 100

CHAPTER 6 APPLICATION OF FUNCTIONALISED GNRS FOR *IN VIVO* THERANOSTICS OF HUMAN OESOPHAGEAL ADENOCARCINOMA 103
6.1 INTRODUCTION 103
6.2 METHODS 104
6.2.1 ETHICS 105
6.2.2 STUDY DESIGN 105
6.2.3 EXPERIMENTAL PROCEDURES 106
6.2.4 EXPERIMENTAL ANIMALS 114
6.2.5 SAMPLE SIZE 115
6.2.6 EXPERIMENTAL OUTCOMES 115
6.2.7 CHARACTERISTICS OF THE FUNCTIONALISED GNRS USED IN *IN VIVO* STUDIES 116
6.3 RESULTS 116
6.3.1 FLUORESCENCE SPECTROSCOPY OF MICE INJECTED WITH FUNCTIONALISED GNRS 116

6.3.2 THE APPLICATION OF FUNCTIONALISED GNRS FOR FLUORESCENCE IMAGING OF TUMOURS 119
6.3.3 FLUORESCENCE IMAGING RESULTS FOR IV GNRS 120
6.3.4 FLUORESCENCE IMAGING RESULTS FOR IT GNRS 127
6.3.5 HEPATORENAL METABOLISM OF GNRS 129
6.4 THE APPLICATION OF FUNCTIONALISED GNRS FOR PTT 131
6.4.1 CONTROL MICE 131
6.4.2 RESULTS - INTRATUMOURAL (IT) GNRS AND NIR IRRADIATION 134
6.4.3 RESULTS - INTRAVENOUS (IV) GNRS AND NIR IRRADIATION 140
6.4.4 COMPARISON BETWEEN PHOTOTHERMAL TEMPERATURE RESPONSES WITH IV AND IT GNRS 144
6.5 THE THERANOSTIC APPLICATION OF GNRS *IN VIVO* 145
6.6 HISTOLOGICAL CONFIRMATION OF TUMOUR ABLATION 149
6.6.1 TEM – EVIDENCE OF INTRACELLULAR ENDOCYTOSIS OF GNRS IN TUMOUR CELLS 151
6.6.2 EVALUATION OF METASTASIS 153
6.7 THE 7 PRINCIPLES OF HIGHLY EFFECTIVE PHOTOABLATION 153
6.7.1 MULTIDIRECTIONAL INJECTION OF GNRS FOR IT ADMINISTRATION 154
6.7.2 ENSURING THE BEAM SIZE IS LARGER THAN THE LARGEST DIMENSION OF TUMOUR 156
6.7.3 SIZE CONSIDERATION OF LARGE TUMOURS 156
6.7.4 ADMINISTER A FRESH AND PURE SAMPLE OF FULLY FUNCTIONALIZED GNRS 160
6.7.5 ALLOW 24 HOURS AFTER IV ADMINISTRATION OF FUNCTIONALISED GNRS 160
6.7.6 DETERMINE THE APPROPRIATE OD (AND VOLUME) OF GNRS TO ADMINISTER 162
6.7.7 OBSERVE FOR 30 DAYS AND EVALUATE PATHOLOGY 163
6.8 SUMMARY OF FINDINGS 165
6.9 DISCUSSION – CLINICAL APPLICATIONS 167

CHAPTER 7 SAFETY CONSIDERATIONS IN THE APPLICATION OF FUNCTIONALISED GNRS FOR *IN VIVO* THERANOSTICS 171
7.1 INTRODUCTION 171
7.2 DETERMINATION OF THE MAXIMAL SAFE LASER FLUENCE 173
7.3 DETERMINATION OF THE MAXIMAL SAFE CONC. OF IT GNRS 174
7.4 DEPTH OF ENERGY TRANSFER 176
7.5 TOXICITY AND BIODISTRIBUTION OF GOLD 180
7.5.1 METHODS 180
7.5.2 ICP-MS RESULTS 181
7.5.3 DISCUSSION 183
7.6 HISTOLOGICAL EVALUATION OF RES ORGANS EXPOSED TO GNRS AND PTT 185
7.7 HAEMATOLOGICAL & BIOCHEMICAL ANALYSIS 186
7.8 PHYSICAL AND PSYCHOSOCIAL ATTRIBUTES OF TREATED ANIMALS 188
7.9 SUMMARY OF FINDINGS 189
7.10 DISCUSSION 190

CHAPTER 8 SUMMARY, FUTURE WORK AND CONCLUSION 193
8.1 CLINICAL APPLICATIONS 199
8.1.1 EARLY CANCERS 199
8.1.2 ADVANCED CANCERS 200
8.1.3 ADJUNCT TO SURGERY 200
8.2 KEY CHALLENGES REMAINING AND FUTURE WORK 200

LIST OF FIGURES

Fig. 1-1 Strategy for assessing the theranostic potential of GNRs in cancer. 7
Fig. M1 The (a) absorption and (b) fluorescence spectra with (c) ζ-potential values of multi-functionalised GNRs. Fluorescence emission of GNR-PEG-Anti-EGFR-Cy5.5 was done in a water solution after purification from any unreacted Cy5.5-Anti-EGFR antibody. 47
Fig. 3-1 The experimental set-up for monitoring GNR reshaping during CW laser application, using both PA and thermal imaging. Curved lines represent optical fibres and straight lines represent electronic connections. 54
Fig. 3-2 Example measured PA response (a), and after low pass filtering (b). Here the time periods corresponding to the background (magenta), the bottom of the sample (grey), and the top of the sample (black) are indicated between the vertical dashed lines. 55
Fig 3-3 Measured absorbance spectra of original GNRs (dotted lines), after PA pulsed laser only (dashed lines), and after 6 W/cm^2 CW laser light for 5 minutes (solid lines) across the three batches [red (sample $\boldsymbol{\alpha}$), blue (sample $\boldsymbol{\beta}$) and green (sample $\boldsymbol{\gamma}$)]. The magenta line refers to sample $\boldsymbol{\alpha}$ after 12 W/cm^2 laser light irradiation for 45 seconds. The black dashed line indicates the wavelength of the CW laser. 58
Fig. 3-4 The measured temperature profiles from each sample with (solid lines) and without (dotted lines) CW irradiation using the same line colours used in Fig. 3-3 to represent the different samples. GNR concentrations are labelled for each sample. 59
Fig. 3-5 Aggregation of GNRs can be observed in these TEM images (a) before CW laser irradiation and (b) after CW laser irradiation (60,000x magnification). The blue scale bars are 100 nm in length. 60
Fig. 3-6 Representative TEM images from sample $\boldsymbol{\alpha}$ showing GNRs (a) before laser irradiation, (b) after only PA pulsed laser light, (c) after 6 W/cm^2 CW irradiation, (d) after 12 W/cm^2 CW irradiation. The blue scale bars are 100 nm in length. 60
Fig. 3-7 (a) PA pulsed laser energy over time for each acquisition, illustrating the drift and pulse-to-pulse fluctuation in the laser energy, (b) the calculated PA signal mean of the three samples (thick line), with a standard error (shaded area) of the corrected signal, for CW laser on (black) and off (light blue). 61
Fig. 3-8 Thermal reaction, gradual healing and complete ablation of tumour xenograft seen *in vivo* in a mouse that received IT GNRs and CW NIR laser irradiation for three minutes. The numbering within pictures indicates the days post-irradiation while the first (un-numbered) image is the pre-irradiated tumour. The irradiated site was excised at day 30 and TEM analysis is shown in Figure 10 (d-h). 62
Fig. 3-9 Temperature rise seen *in vivo* after intratumoural (IT) GNRs administration and during CW laser irradiation for three minutes measured from the tumour site externally by the thermal imaging camera, after adjusting for background and baseline temperatures. 62
Fig. 3-10 TEM images of *in vivo* tumour sites following intratumoural (IT) administration of GNRs with pre- and post-irradiation with CW laser. TEM-EDX analysis also shown. 63
Fig. 4-1 (a) Tissue mounted onto a slide and laser diode catheter directed towards it (b) thermal imaging camera mounted above the tissue being irradiated by the laser. 75
Fig. 4-2 Example image captured by FLIR thermal imaging camera during tissue heating with a corresponding temperature response chart (y-axis), the blue box shows the selected background region of interest and the red box shows the selected tissue region of interest from which the mean temperature values are calculated. 76
Fig. 4-3 (a) Normalised optical density profile of GNRs with aspect ratio = 4, (b) TEM image of the GNPs produced. 77
Fig. 4-4 (a) Temperature increase over time with 3 ml of varying concentrations of GNRs in cuvettes, where the colour indicates the temperature rise in Celsius & (b) The temperature rise after 10 minutes of laser heating for 3 ml of various concentrations of GNRs with a line of best fit showing the linear relationship. The red circles show the mean values and the errors show the standard deviation of 3 repeats. 78

Fig. 4-5 Macroscopic appearances post laser irradiation of porcine oesophageal tissues incubated with a series of GNR solutions ranging from the most to least concentrated. 79
Fig. 4-6 Temperature rise with time for the tissue samples and conditions indicated. 79
Fig. 4-7 Temperature rise from porcine oesophageal tissues subjected to varying concentrations of laser power. The central marker is the mean value with the error bar showing the standard deviation of the three repeats. 80
Fig. 4-8 (a) Marked adherence of GNRs onto tissues that were incubated in a colloidal suspension of GNR which persisted despite thrice washing with PBS, in contrast to pale tissues incubated in RPMI (b). 80
Fig. 4-9 Temperature rises during irradiation with NIR laser in human *ex vivo* (a) oesophageal and (b) gastric tissues, incubated with either CTAB-GNRs or RPMI medium. 81
Fig. 5-1 Bright field (a) and dark field (b) STEM images of functionalised GNRs. 89
Fig. 5-2 Blue nuclear DAPI staining & anti-EGFR antibody fluorescent in green. The merged EGFR/DAPI image demonstrates binding of anti-EGFR antibody around the nuclei. 91
Fig. 5-3 The FLO-1 nuclei with DAPI & fluorescence from the Cy5.5-GNR-anti-EGFR-antibody in red. Merged Cy5.5-GNR-EGFR/DAPI fluorescence microscopy images demonstrating binding of FLO-1 cells to antibody- and fluorophore-conjugated GNRs. 92
Fig. 5-4 Laser set-up: The laser diode was directed on one particular well of the 48 well plate. Heating was recorded with a thermal imaging camera mounted above the well plate. 95
Fig. 5-5 Live/dead assay on HeLa cells with GNRs after (a) 5; (b) 10; and (c) 15 seconds of exposure to NIR laser. 96
Fig. 5-6 Creation of single tumour xenografts in SCID and BALB/c nude mice inoculated with subcutaneous injections of FLO-1 human oesophageal adenocarcinoma cells 98
Fig. 5-7 Histology (100x mag.) from the gastrointestinal tumours induced in mice with FLO-1 cells, indicating many ciliated columnar cells with some goblet cells present. There are also many crypts. 100
Fig. 6-1 Flow chart for the experimental group of the study. 106
Fig. 6-2 The experimental set-up for fluorescence imaging and photothermal therapy. 112
Fig. 6-3 The three fundamental experimental steps of the *in vivo* study. 113
Fig. 6-4 Fluorescence absorption and emission spectra from functionalised GNRs 117
Fig. 6-5 Use of a fluorescence spectrometer with a 690 nm long pass (LP) filter over the probe. The excitation light is emitted from a laparoscope mounted above. 117
Fig. 6-6 Fluorescence spectroscopy readings with both IV and IT GNRs, which were specifically enhanced over the area of tumour. Inset: Normalised UV-Vis spectroscopy of the GNR solution. 118
Fig. 6-7 (a) Schematic of fluorescence imaging set-up. Key LP = Long pass, BP = Band pass (b) Fluorescence imaging experimental actual set-up (with laser fibre optic in-situ). 120
Fig. 6-8 Live fluorescence image pre-IV injection with a constant area of fluorescence. 121
Fig. 6-9 (a) Constant fluorescence noted on left flank, (b) area demarcated under fluorescence image-guidance, (c) laparotomy to confirm bowel as the cause of the fluorescence. 121
Fig. 6-10 Images seen during live fluorescence imaging (needles in situ correspond to the external visible boundaries of tumour) in a mouse with tumour (b) and the absence of any fluorescence signal on the contralateral (tumour-free) flank (c) and the back (d). 122
Fig. 6-11 Live fluorescence signal (a) on the day of IV GNRs and (b) 24 hours post injection in the same mouse, (c) processed fluorescence image with background subtracted showing the fluorescence emission arising specifically from the tumour area. 122
Fig. 6-12 Line profiles of fluorescence emission signals over the tumour site correspond to peak fluorescence intensities in two different mice receiving IV GNRs. Graph also demonstrating the contrast in fluorescence intensity signals between pre- and 24 hours post-IV injection of GNRs (background subtracted). 124
Fig. 6-13 Live fluorescence imaging performed on a pilot mouse receiving only Cy5.5-anti-EGFR-antibody (without GNRs) demonstrating a gradual drop in fluorescence intensity over time. 125
Fig. 6-14 Degradation of fluorescence intensity over time in a pilot mouse receiving only Cy5.5-anti-EGFR-antibody, indicating a high initial signal intensity. 125

Fig. 6-15 Fluorescence imaging performed immediately before, after, and at 2 and 24 hours post injection. 126
Fig. 6-16 Decay of fluorescence imaging intensity signals from tumour sites at various time points after an IV injection of functionalised GNRs. 126
Fig. 6-17 Live fluorescence imaging of a mouse (a) pre- and (b) post- IT GNR injection. 127
Fig. 6-18 Live fluorescence imaging of another mouse (a) pre- and (b) post- IT GNR injection. 128
Fig. 6-19 (a) Fluorescence imaging illustrating the importance of photoquenching in highlighting GNR-deficient areas around the tumour pre-irradiation site with complete circumferential delivery of IT GNRs around the tumour site in (b) confirmed by fluorescence imaging after a 'top-up' GNR injection to the previously deficient region. 128
Fig. 6-20 Fluorescence images from the kidneys, spleen and liver (with picture of liver and gallbladder) of a mouse injected with IT GNRs. 129
Fig. 6-21 The lack of fluorescence in the faeces of control mice, and fluorescence from faeces after 1 and 2 days in mice that received IV GNRs. 130
Fig. 6-22 Temperature responses to laser irradiation of tumours without GNRs. 132
Fig. 6-23 Tumours of mice in the control group, showing images pre-intervention, then at stated days post-intervention, indicating continued tumour proliferation in control arms. 133
Fig. 6-24 Temperature charts recorded live during photothermal therapy from the thermal imaging camera, showing (a) the starting and (b) the final temperature rise after 3 minutes of NIR laser irradiation. The line across image (b) is a line profile across the measured region of the temperature change. 135
Fig. 6-25 The PTT responses in tumours of the 10 mice (initial tumours on the left column) which received IT GNRs, with their progression over days. 137
Fig. 6-26 Contrast seen from re-epithelialisation and regeneration of neo-collagen post PTT seen under polarised light microscopy. 138
Fig. 6-27 Intact collagen fibres in skin layers demonstrated following PTT. Shown under polarised light microscopy after staining with Picrosirius red with Miller's elastic stain. 138
Fig. 6-28 Representative temperature changes in a pilot mouse. Inset graph demonstrating the principle of Newtonian cooling behaviour observed after the laser was turned off, with a return to baseline after approximately 2 minutes. 140
Fig. 6-29 The PTT responses in tumours of the 10 mice (initial tumours on the left column) which received IV GNRs, with their progression over days. 142
Fig. 6-30 The mean and standard deviation of temperature rise in mice observed during PTT from all 10 mice in both IT and IV GNRs groups. 144
Fig. 6-31 The set-up for coupling fluorescence imaging with photothermal therapy. Fluorescence excitation light was delivered through the laparoscope and NIR light through the laser delivery fibre. 146
Fig. 6-32 The tumour xenograft (a) is initially identified and mapped [with needles, (b)] while under fluorescence guidance following an administration of IV GNRs. 146
Fig. 6-33 The fluorescent area was measured and marked (a), and without moving the markers, the laser aim-beam was brought into position (b). 148
Fig. 6-34 Temperature measurements obtained using the theranostic approach, at (a) 0 s and (b) 180 s, with a graphical representation of the measured temperature rise in (c). 148
Fig. 6-35 Representative histological appearances of three mice in the IT GNRs and PTT group showing fully regenerated epidermal & dermal layers with no evidence of tumour or proliferating cells. 149
Fig. 6-36 Representative histological appearances of three mice in the IV GNRs and PTT group showing fully regenerated epidermal & dermal layers with no evidence of tumour or proliferating cells. 149
Fig. 6-37 Histology from a study mouse showing potential aggregation of irradiated GNPs along a submuscularis fascial plane. 150
Fig. 6-38 (a) Perinuclear 'black dots' seen that may be GNPs under 800x & 1000x mag. in an area that received IT GNRs and PTT 30 days prior. (b) Large cells presumed to be macrophages phagocytosing GNPs. 151

Fig. 6-39 (a) TEM of a group of cells within the tumour tissue with an area of interest with gradual increase in magnifications in the ROI. Energy-dispersive X-ray spectroscopy graph showing the chemical analysis of the magnified ROI with the presence of gold indicated by peaks of 'Au' within the EDX. 152
Fig. 6-40 Pilot mouse that received a core delivery of GNRs into its tumour, with promising results and a clinical resolution of tumour by day 30. 155
Fig. 6-41 Hidden microscopic tumour within the muscularis layer despite a clinical (macroscopic) disappearance. 155
Fig. 6-42 Pilot mouse demonstrating a large tumour with a reasonable initial photothermal effect but developed a recurrence of tumour noticeable from day 21. 157
Fig. 6-43 Histology of the pilot mouse (on termination at day 30 post PTT). 157
Fig. 6-44 Within the central area of the tumour ablation site, there was some evidence of probable coalescing of GNPs. 158
Fig. 6-45 A sentinel lymph node seen adjacent to the tumour site with lymphatic tracts within the lymph node. 158
Fig. 6-46 GNPs seen inside lymphatic tracts of the lymph node as black dots. 159
Fig. 6-47 Pilot mouse received immediate PTT after IV administration of GNRs, showing a reasonable initial photothermal effect but a recurrence of tumour noticeable from day 8. 161
Fig. 6-48 Pilot mouse receiving half the normal OD/concentration of IV GNRs, with failure of tumour control. 162
Fig. 6-49 Temperature increases seen in the PTT of two mice receiving IV GNRs at different OD but the same irradiation parameters. 162
Fig. 6-50 Alarming temperature rise seen at the tumour site in a study mouse (Mouse 5) which received double (100 μl) the regular volume of IT GNRs at the same OD. The irradiation was ceased rapidly, and the mouse recovered satisfactorily. 163
Fig. 6-51 Pilot SCID mouse receiving IT GNRs and PTT with a good initial response, until a tumour was detected at the end of the study period. 164
Fig. 6-52 Histology from pilot SCID mouse: Regenerated epidermis and dermis with an underlying tumour present in the submuscularis plane. 164
Fig. 6-53 A cluster of GNPs seen within the tumour matrix of pilot mouse. 165
Fig. 7-1 Full thickness thermal burn in this pilot mouse with graph demonstrating the temperature rise during PTT. 173
Fig. 7-2 Thermal camera images showing the heating (immediately upon the commencement of irradiation) with corresponding temperature rise showing extension into the surrounding healthy tissues (at the concluding time point). 174
Fig. 7-3 Pilot mouse demonstrating thermal spot burn and its associated temperature rise (in red) compared to another mouse receiving half the OD and volume of GNRs. 175
Fig. 7-4 Typical clinical appearance of the early thermal reaction seen with PTT, with the corresponding temperature rise at the site of irradiation. 176
Fig. 7-5 Dissection of the irradiated site on day 2 post-PTT, exposing the underlying intercostals, left lung and left lobe of liver. 177
Fig. 7-6 Distance from surface of left lobe of liver affected by energy dissipation. 178
Fig. 7-7 Distance affected from the surface of the left lung by energy transmission. 178
Fig. 7-8 Depth of energy transfer from PTT and its histological extension from the epidermal layer to the underlying intercostal rib directly below the tumour. 179
Fig. 7-9 The average [Au] in tissues/blood at the end of study. 182
Fig. 7-10 Proportionate increase in [Au] seen in the RES organs of three mice receiving varying volumes of GNRs. 182
Fig. 7-11 Histology from the liver of at the end of 30 days post GNRs & PTT demonstrating no hepatocellular damage. 185
Fig. 7-12 Histology from the kidneys and spleen after of 30 days post GNRs & PTT showing no damage to renal cells, a morphologically active spleen but no splenocyte damage 185
Fig. 7-13 Box and whisker diagram of weight distribution of mice, demonstrating an increase in both groups with the medians, quartiles & minimum and maximum weight gains. 188

LIST OF TABLES

Table 2-1 The included studies, with the type of study, shape, size and concentration of GNPs used in the study. 21

Table 2-2 Types of *in vitro* and *in vivo* GI cancer models and methods of inducing cancer in rodents. 22

Table 2-3 Irradiation regimes used in each study model. 24

Table 3-1 The mean lengths, widths and aspect ratios of gold nanorods (GNRs) as measured manually from TEM images for two of the samples for each irradiation type. All errors show the standard deviation. 58

Table 3-2 Comparison of the energy and concentration of GNPs in other studies which have shown GNP reshaping with pulsed lasers in comparison to the fluences used in our *in vitro* and *in vivo* studies using CW laser. 65

Table 4-1 Concentration of the GNR solutions in which tissues were incubated, using an initial total volume of 2500 μL of concentrated GNR solution. 74

Table 4-2 Hydrodynamic diameter and ζ-potential values of GNRs measured by dynamic light scattering. 77

Table 6-1 The parameters of GNRs and laser used in the control groups, with the tumour sizes measured at the start and end dates of the control arm. 131

Table 6-2 The parameters of the 10 mice which received IT GNRs and PTT with NIR irradiation. 135

Table 6-3 The parameters of the 10 mice which received IV GNRs and PTT with NIR irradiation. 141

Table 6-4 Parameters used in Mouse 8 (IV GNRs and PTT group). 147

Table 6-5 The parameters for a pilot mouse in which the tumour regrew from the peripheries due to its large initial size. 157

Table 7-1 Parameters of pilot mouse which received IT GNRs and PTT at a high setting. 173

Table 7-2 Parameters of pilot mouse which received a high dose of IT GNRs before PTT. 174

Table 7-3 The average values of the concentration of Au ([Au]) found in tissues/blood at the end of study (given in μg of Au detected per gram of organ). 181

Table 7-4 The average blood results in the IV GNRs + PTT group (after 30 days). 187

Table 7-5 The average blood results in the IT GNRs + PTT group (after 30 days). 187

Table 7-6 The minimum, median, maximal and 1st and 3rd quartiles of weight gained by mice in each treatment arm of the study. 188

Chapter 1 Introduction

In 2010, an average of 430 people died from cancer daily in the United Kingdom, which equates to one person every four minutes. One in two people in the UK will develop cancer in their lifetime (1), while in the United States, one in three women and one in two men will develop cancer. In some nations, cancer will surpass heart disease as the commonest cause of mortality by 2020 (2). The incidence of gastrointestinal (GI) cancers is increasing since the mid-1970s in the UK, and primarily includes oesophageal, gastric and colorectal carcinomas, with a western preponderance towards adenocarcinomas. Colorectal and oesophageal cancers are now the 4th and 8th commonest cancers worldwide respectively (3). These cancers are often detected rather late in their course, as their detection relies heavily on symptomatic reporting and non-specific screening methods (4). Although oesophageal cancer is treatable, it is rarely curable. The 5-year survival rates of patients who are deemed suitable for definitive treatment range from 5-20% for oesophageal cancer, 10-15% for proximal gastric cancer and 6-75% for colorectal cancer (3, 5, 6)*.

The incidence of oesophageal adenocarcinoma has increased over three fold in the past three decades (7), rising from 3.8 to 23.3 cases per million. Oesophageal adenocarcinoma has overtaken oesophageal squamous cell carcinoma in the UK, USA and Western Europe, with most tumours found in the distal oesophagus. The cause for this alarming increase in adenocarcinomas and demographic shift is unknown. It is however known that most oesophageal adenocarcinomas arise from areas of columnar epithelium containing specialised intestinal metaplasia (8). A population-based, case-controlled study from Sweden found a strong causal link between symptomatic gastro-oesophageal reflux disease as a risk for developing oesophageal adenocarcinoma (9).

Generally the first-line treatment of solid and established gastrointestinal tumours in the UK is neoadjuvant chemo(radio)therapy, followed by surgical excision and then depending on the grade/stage of the tumour, adjuvant chemotherapy. Single modality treatment has been proven to be largely ineffective. Chemotherapy has a substantial failure and intolerance rate

---

*Some text within this chapter is adapted from the author's recently published paper in Nanomedicine: Nanotechnology, Biology, and Medicine. doi: 10.1016/j.nano.2015.05.010.

due to inadequate localisation of drugs to cancer-specific tissues and systemic side effects (10, 11). Radiation, on the other hand, is unable to eliminate all loco-regional recurrences and cure localised cancers due to the inherent resistance of some cancer cells towards ionising radiation (12). Neither radiotherapy nor chemotherapy has shown significant survival benefit (13), and the results from surgery as a sole entity without the summative and complementary effects from chemo-radiotherapy are meagre. The need for establishing personalised medicine as a means of providing tailor-made targeted delivery of therapy for specific cancers to individual patients seems increasingly essential.

The Nobel Prize winner Richard Feynman first proposed Nanotechnology in 1959 (14). "Nano" is Greek for "dwarf" and nanotechnology comprises particles that are of the order of 1 billionth of a meter (10^{-9} m). The National Nanotechnology Initiative (NNI) defines nanotechnology at dimensions of roughly 1 to 100 nanometres (nm) (15). By this definition, the largest nanoparticle (NP) is approximately six to eight hundred times smaller in linear size than the width of a strand of hair and approximately 100 – 10,000 times smaller than a human cell. The past 25 years has seen an intensified interest in nanotechnology, with the development of a multitude of differently shaped NPs for material science and nanomedicine. The commonest shapes include nanorods (16-18), nanospheres (19, 20) and nanoshells (21, 22), but the diversity also extends to nanocubes (23, 24), nanowires (25, 26), nanorockets (27) and nanostars (28, 29) to name a few. In general, NPs smaller than 100 nm have excellent tumour targeting ability (30), being small enough to permeate out from porous vascular endothelial fenestrations that surround a region of tumour.

Theranostics refers to agents that are simultaneously therapeutic and diagnostic. Theranostics using NPs implies a robust system which can diagnose, deliver targeted therapy and monitor response (31). When excited with laser energy of a wavelength that is tuned to the gold nanoparticle's specific surface plasmon resonance (SPR), valence electrons on the surface of gold nanoparticles (GNPs) exhibit very strong oscillatory energy, which induces high temperatures useful for eliciting localised tissue death. When these NPs are heated within cancer tissue, this is then termed photothermal therapy (PTT). The heating effect of illumination achieved by individual gold nanorods has been measured to be as high as 5897 K/W when irradiated with a 1064 nm continuous wave NIR laser, which coincided with the SPR of the nanorod (32). Studies have shown that GNPs have relatively negligible cytotoxicity for healthy cells, making them ideal for cancer-specific therapy.

This photothermal reaction can be applied to destroy cells within tumours, specifically in places that are difficult to reach surgically or require a palliative debulking procedure. GNPs have acted as agents for photothermal therapy on account of their enhanced absorption of

visible and NIR light, several orders of magnitude more intense than conventional laser phototherapy agents. Visible light is absorbed by naturally occurring chromophores, especially haemoglobin. However NIR light is only very weakly absorbed by water and chromophores, and this consequently allows for greater tissue penetration (33, 34) into living tissues than that afforded by visible light whilst exciting considerably less background fluorescence (35). Within the NIR spectrum (~650–900 nm), up to 10 cm depth of penetration through breast tissue was achieved even at low laser power (36-38). The first use of GNPs in photothermal ablation was described by Hirsch *et al*. in SKBr3 human breast epithelial carcinoma cells in 2003 (17). Currently, gold nanospheres (39, 40), gold nanorods (18, 41, 42) and gold nanoshells (43, 44) are the chief nanostructures that have been demonstrated in photothermal therapeutics. These structures are especially promising given their ease of preparation, capacity for multi-functionalisation and tunable optical properties.

NPs are also being used to deliver therapeutic chemicals directly to tumour sites, by extending their ability to also act as nano-carriers. Formulations of nanoparticles such as Doxil™, Abraxane™, Resovist® and Feridex® are already in clinical practice (45). Despite this progress, there remains considerable uncertainty and variation in methods and results from the application of GNPs in GI cancer that have been published. It is perhaps this existing variation and uncertainty that has forestalled the transition of GNPs in GI cancer theranostics from murine *in vivo* studies to human clinical trials. By applying GNPs that can target GI adenocarcinomas, the thermal effect that would result from irradiation by a light source could exert an ideal therapeutic effect on the cancer tissues.

Although there have been some human clinical trials and advances in the application of NPs in oral, breast, lung and prostate cancer therapy, their value in gastrointestinal (GI) cancer tissue remains contentious, with published studies being considerably disjointed in their focus, methods and materials, leading to a perplexing task of finding commonality and reproducibility. Although there have been some reported advances in *in vitro* and *in vivo* (rodent) studies, the lack of suitably comparable platforms obscures the evidence for the application of GNPs in GI cancer, resulting in concerns in translating nanotechnology to the clinical trials stage in GI oncology, despite progress in their application for other cancers.

1.1 Thesis Motivation

The systematic review described in Chapter 2 found a dearth of studies with effective and consistent theranostic results in GI cancer which also address the safety concerns that encompass the utilisation of photothermal therapy derived from gold nanoparticles. The emphasis in a majority of studies was usually either about optical imaging for cellular diagnosis or the thermal therapy of tumours, but rarely both. Although cytotoxicity from GNPs has been refuted by most *in vitro* studies, no firm conclusions can be drawn from objectively quantifiable parameters such as laser power, GNR concentration and volumes which could potentially be harmful *in vivo*. No study has shown the depth of penetration of the energy associated with GNP-induced thermal ablation *in vivo*. Consequently no study has ventured so far as to formulate and propose a simple, reliable and effective strategy for the combined theranostic approach for cancers, which, if established, would then make some headway in elevating this technology to a clinical trial. It is clear that *in vivo* studies have an advantage when attempting to address the challenges of providing consistency and reproducibility of results from both the imaging and therapeutic aspects of tumours, thus, this would form one of the primary focuses of this research.

Our biophotonics group has had some success in fabrication of GNPs and their application in the fluorescence detection and photothermal ablation of human cervical cancer cells (HeLa cells) (46) hence it provided an opportunity to experiment further on *ex vivo* human cancer tissues, and perform *in vivo* studies. Multifunctionalised GNRs were synthesised, to encourage the active pursuit of cancer cells which can then be identified via fluorescence imaging and thence upon irradiation with NIR laser, culminate in the photothermal destruction of cancerous cells.

It is envisioned that this technology could have an application in both early and late stages of cancer, and be an adjunct to surgery.

1.1.1 Early diagnosis with optical imaging

Mortality from cancer can be prevented with early disease detection. However early detection of upper GI cancer in the West remains disappointingly low. Late symptoms are often only detected when the tumour has penetrated the muscularis propria layer of the

oesophageal or gastric wall, with involvement of regional or remote lymph nodes or haematological spread to other organs. This results in only a third of cases of upper GI adenocarcinoma being suitable for surgical resection with curative intent (47). Western countries currently do not have any screening programs for upper GI malignancies, predominantly due to the significant costs associated with screening either with endoscopy or a contrast-enhanced swallow for diseases which have a relatively low incidence during routine endoscopy.

The occasional patient who presents with early (T1) disease has a much better chance of survival. However, some early cancers are missed despite patients undergoing endoscopy, the principle investigation for the diagnosis of gastro-oesophageal cancer. A single centre study (1075 patients) in the UK over 4.5 years demonstrated a 1.8% cancer miss rate attributed to clinical error, with a median diagnostic delay of 7.9 months (48). For those delayed more than six months, their chance of being offered curative surgery reduced from 24% to 6% (48). A Japanese study reported up to 85.2% of the missed upper GI cancers were at an early (T1) stage at diagnosis (49). However the Japanese are extraordinarily adept at picking up early cancers due to their much higher incidence of upper GI cancer (than the UK), a low threshold to investigate the upper GI tract and the presence of a national oesophago-gastric cancer screening program. Although cancer screening controversies have raged for a considerable time, Japan and South Korea are the only two countries which run a population-based screening program for gastric cancer (50, 51).

Although endoscopists maintain a high index of suspicion and are prepared to repeat an endoscopy early in the event of equivocal findings and persisting symptoms, there are undeniably subtle mucosal lesions, such as minor mucosal elevations or depressions (49, 52), that can be missed during endoscopy. Other potential sources of errors include a failure to recognise the significance of a lesion, deciding not to perform a biopsy or taking an insufficient number of biopsies (53, 54). A larger (2727 patients) retrospective study of medical records in England over one year demonstrated an 8.3% missed gastric cancer rates with patients having had an endoscopy within the preceding three years (55). The authors argue that given the slow growth of gastric cancers, it is likely that a lesion may possibly have been visible at a previous endoscopy if subjected to closer scrutiny in many patients. This study found that cancers which were subsequently detected at an early stage were more likely to have been missed in the past. Previous retrospective studies have reported the presence of abnormalities at endoscopy at the same site where cancer was diagnosed at subsequent endoscopy (49, 53). There is thus is a vital clinical need to develop better and innovative diagnostic techniques which will aid in the detection of early cancer.

This brings the need to clinically optimise cancer detection during endoscopy to the fore. Utilising novel and innovative optical imaging modalities such as those derived from the inherent optical contrast properties afforded by GNRs during minimally invasive procedures for upper GI malignancy will reduce the 100% reliance on the eyes and experience of the endoscopist (who could be a trainee) and improve detection rates of early and subtle lesions within the GI tract and the peritoneal cavity. Contrast enhancement from suspicious lesions highlighted by GNRs could enable image-guided 'optical biopsies', thereby enhancing the detection of early lesions by providing high amplitude contrast signals that will alert the endoscopist to the presence of an abnormality within that particular region, which may otherwise have received perfunctory attention. This area of illumination could then be a focal point to guide NIR light so as to avoid collateral damage and improve therapy. Thus the advantage of functionalised GNRs is not only can it support the clinical need for early cancer detection by fluorescence imaging, it can also be then used for tumour-targeted photothermal therapy should the lesion be a truly early one. Delivering effective laser therapy at relatively lower energies is thus capable of rendering the method truly theranostic and minimally invasive.

1.1.2 Palliative photothermal therapy

In 2012, 14.1 million new cases of cancer were diagnosed globally, and 32.6 million people were living with cancer (within 5 years of diagnosis) worldwide, with 57% (8 million) of new cancer cases, 5.3 million of the cancer deaths and 48% (15.6 million) of the 5 year prevalent cancer cases occurring in the less developed regions (Africa, Asia and Central and South America) (56). More than 80% of these new cases were found to be in an advanced stage of disease at the point of diagnosis (57). The heavy burden of the cost of cancer care affecting middle- and low-income countries makes it implausible to treat our way out of cancer, for it is apparent that even the highest-income countries struggle to grapple with the enormous bills arising from effective cancer treatment.

Increasing the surgical armamentarium in the face of such a large proportion of advanced cancers in an increasingly elderly population may provide an answer to reducing this rapidly expanding financial burden. Tumour photothermal therapy is a feasible potential application of GNRs as it might be able to provide symptomatic palliation in the face of inoperable malignant dysphagia from stenosing/occluding oesophageal tumours by tumour debulking, or be used in cases where residual disease (or margin involvement) is detected

microscopically after surgical resection. Thermal ablation such as that used for resectable colorectal liver metastases is seen as a viable alternative to surgery (hepatectomy) such that a new multicenter, open, pragmatic parallel randomised control trial will open in 2016 in the UK to compare disease free survival at 2 years from both treatment arms (58).

1.2 **Thesis aims**

Fluorescently labelled GNRs have the potential to provide optical contrast and heat under the appropriate excitation light, which would correspond to their fluorescence absorption and SPR peaks respectively. The aim of this research is to consolidate the knowledge from published studies, and then conduct studies to examine the effects and safety of the application of GNRs in the theranostics of upper gastrointestinal (GI) adenocarcinoma. The primary aims of this thesis are to:

1. Assess the viability of applying photothermal therapy in human (*ex vivo*) adenocarcinoma tissues
2. Determine its efficiency in rodent (*in vivo*) cancer models
3. Develop the application of fluorescence imaging for cancer detection *in vivo*.

The framework for the objectives of the thesis is illustrated in Fig. 1-1.

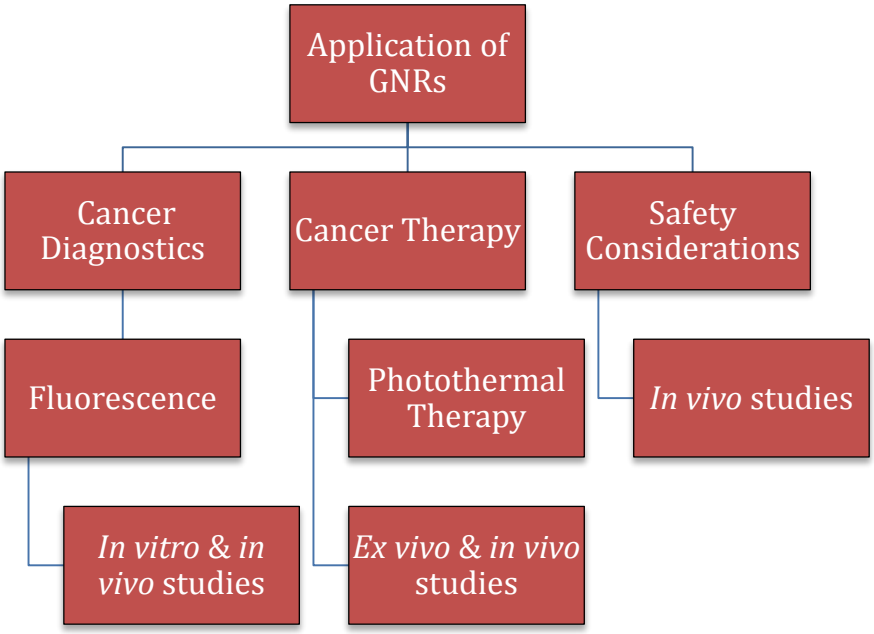


Fig. 1-1 Strategy for assessing the theranostic potential of GNRs in cancer.

1.3 Overview of the thesis

The work presented in this thesis is centred on the assessment of the viability, safety and efficiency of GNRs in the diagnosis and treatment of GI adenocarcinoma.

Chapter 2 serves as a main introduction to the principles underlying the mechanism of GNRs and to consolidate the progress from *in vitro* and *in vivo* applications of GNPs in GI cancer theranostics. It aims to highlight and provide objective evidence and insight into the current controversies that enshroud their application in the GI tract by discussing published findings relating to their size, shape, synthesis, surface charge, active and passive targeting efficiency, cellular uptake, biocompatibility, drug delivery and most crucially, their toxicity. The secondary aim is to formulate research that is then able to address the identified deficiencies.

Chapter 3 is focused on the whether sequential application of CW laser would be as photothermally effective as the initial laser application in the setting of irradiated GNRs within a tumour site. CW lasers are the most commonly used lasers for inducing PTT with GNRs in the context of tumour ablation. Reshaping or melting of GNRs after the initial laser application may render sequential irradiation ineffective due to an alteration in the optical absorption properties of irradiated GNRs. This is evaluated both *in vitro* and *in vivo*.

Chapter 4 aims to establish the optimal gold nanorod (GNR) concentration and laser power for inducing hyperthermic effects in tissues and to test this photothermal effect on porcine tissues and *ex vivo* human oesophagogastric adenocarcinoma tissues. The application of freshly dissected human adenocarcinoma tissue for PTT is in contrast with many studies that use animal tissues.

Chapter 5 involves optimising the surface properties of GNRs and experiments which test their suitability for specific cancer cell targeting. The properties of multifunctionalised GNRs are tested *in vitro* on human oesophageal adenocarcinoma cells. These cells are also used to establish tumour xenografts in mice.

Chapter 6 records the findings from detailed *in vivo* studies into the theranostic potential of functionalised GNRs, using oesophageal adenocarcinoma tumour as the tumour model.

Chapter 7 addresses the chief concern that still remains about the application of GNRs *in vivo* – safety. It evaluates the toxicity and biodistribution of circulating gold, while also estimating the depth of energy transfer from PTT.

Chapter 8 draws a conclusion from the studies above and formulates an outlook for the future application of this technology.

References

1. Ahmad AS, Ormiston-Smith N, Sasieni PD. Trends in the lifetime risk of developing cancer in Great Britain: comparison of risk for those born from 1930 to 1960. Br J Cancer. 2015;112(5):943-7.
2. Mukherjee S. The Emperor of all Maladies. A Biography of Cancer. Harper Collins Publisher. ISBN 978-0-00-725092-9. 2011.
3. UK Oesophageal Cancer Incidence Statistics, Cancer Research UK. http://www.cancerresearchuk.org/cancer-info/cancerstats/types/oesophagus/incidence/uk-oesophageal-cancer-incidence-statistics.
4. Mousa SA, Bharali DJ. Nanotechnology-based detection and targeted therapy in cancer: nano-bio paradigms and applications. Cancers. 2011;3(3):2888-903.
5. Bowel Cancer Statistics UK, Cancer Research UK http://www.cancerresearchuk.org/cancer-info/cancerstats/types/bowel/incidence/uk-bowel-cancer-incidence-statistics.
6. NCIN. Incidence of stomach cancer in England, 1998-2007. London: NCIN; 2010.
7. Pera M. Trends in incidence and prevalence of specialized intestinal metaplasia, Barrett's esophagus, and adenocarcinoma of the gastroesophageal junction. World J Surg. 2003;27(9):999-1008.
8. Haggitt RC, Tryzelaar J, Ellis FH, Colcher H. Adenocarcinoma Complicating Columnar Epithelium-Lined (Barrett) Esophagus. Am J Clin Pathol. 1978;70(1):1-5.
9. Lagergren J, Bergstrom R, Lindgren A, Nyren O. Symptomatic gastroesophageal reflux as a risk factor for esophageal adenocarcinoma. New Engl J Med. 1999;340(11):825-31.
10. Akhter S, Ahmad Z, Singh A, Ahmad I, Rahman M, Anwar M, Jain GK, Ahmad FJ, Khar RK. Cancer targeted metallic nanoparticle: targeting overview, recent advancement and toxicity concern. Curr Pharm Des. 2011;17(18):1834-50.
11. Feng S, Chien S. Chemotherapeutic engineering: Application and further development of chemical engineering priciples for chemotherapy of cancer and other diseases. Chem Eng Sci. 2003;58:4087-114.
12. Moeller B, Richardson R, Dewhirst M. Hypoxia and radiotherapy: opportunities for improved outcomes in cancer treatment. Cancer Metastasis Rev 2007;26(2):241-8.
13. Ku GY, Ilson DH. Role of neoadjuvant therapy for esophageal adenocarcinoma. Surg Oncol Clin N Am. 2009;18(3):533-46.
14. Feynman RP. There's plenty of room at the bottom. Presented at the Annual Meeting of the American Physical Society, December 29, 1959, California Institute of Technology, Pasadena, CA. http://www.zyvex.com/nanotech/feynman.html.
15. NNI. What is nanotechnology? http://www.nano.gov/nanotech-101/what/definition.
16. Black KCL, Yi J, Rivera JG, Zelasko-Leon DC, Messersmith PB. Polydopamine-enabled surface functionalization of gold nanorods for cancer cell-targeted imaging and photothermal therapy. Nanomedicine (Lond). 2013;8(1):17-28.
17. Huang X, El-Sayed IH, Qian W, El-Sayed MA. Cancer cell imaging and photothermal therapy in the near-infrared region by using gold nanorods. J Am Chem Soc. 2006;128(6):2115-20.
18. Huff TB, Tong L, Zhao Y, Hansen MN, Cheng J-X, Wei A. Hyperthermic effects of gold nanorods on tumor cells. Nanomedicine (Lond). 2007;2(1):125-32.
19. Gref R, Minamitake Y, Peracchia MT, Trubetskoy V, Torchilin V, Langer R. Biodegradable long-circulating polymeric nanospheres. Science. 1994;263(5153):1600-3.
20. Lu W, Melancon M, Xiong C, Huang Q, Elliott A, Song S, Zhang R, Flores Ln, Gelovani J, Wang L, Ku G, Stafford R, Li C. Effects of photoacoustic imaging and photothermal ablation therapy mediated by targeted hollow gold nanospheres in an orthotopic mouse xenograft model of glioma. Cancer Res. 2011;71(19):6116-21.
21. Gobin AM, Lee MH, Halas NJ, James WD, Drezek RA, West JL. Near-infrared resonant nanoshells for combined optical imaging and photothermal cancer therapy. Nano

letters. 2007;7(7):1929-34.
22. Loo C, Lin A, Hirsch L, Lee M-H, Barton J, Halas N, West J, Drezek R. Nanoshell-enabled photonics-based imaging and therapy of cancer. Technol Cancer Res Treat. 2004;3(1):33-40.
23. Ding H, Yang D, Zhao C, Song Z, Liu P, Wang Y, Chen Z, Shen J. Protein-gold hybrid nanocubes for cell imaging and drug delivery. ACS Appl Mater Interfaces. 2015;7(8):4713-9.
24. Wu X, Ming T, Wang X, Wang P, Wang J, Chen J. High-photoluminescence-yield gold nanocubes: for cell imaging and photothermal therapy. ACS Nano. 2010;4(1):113-20.
25. Su Y, Wei X, Peng F, Zhong Y, Lu Y, Su S, Xu T, Lee S-T, He Y. Gold nanoparticles-decorated silicon nanowires as highly efficient near-infrared hyperthermia agents for cancer cells destruction. Nano letters. 2012;12(4):1845-50.
26. Park G-S, Kwon H, Kwak DW, Park SY, Kim M, Lee J-H, Han H, Heo S, Li XS, Lee JH, Kim YH, Lee J-G, Yang W, Cho HY, Kim SK, Kim K. Full surface embedding of gold clusters on silicon nanowires for efficient capture and photothermal therapy of circulating tumor cells. Nano letters. 2012;12(3):1638-42.
27. Wu Z, Wu Y, He W, Lin X, Sun J, He Q. Self-propelled polymer-based multilayer nanorockets for transportation and drug release. Angew Chem Int Ed Engl. 2013;52(27):7000-3.
28. Chen H, Zhang X, Dai S, Ma Y, Cui S, Achilefu S, Gu Y. Multifunctional gold nanostar conjugates for tumor imaging and combined photothermal and chemo-therapy. Theranostics. 2013;3(9):633-49.
29. Dam DHM, Culver KSB, Sisco PN, Odom TW. Shining light on nuclear-targeted therapy using gold nanostar constructs. Ther Deliv. 2012;3(11):1263-7.
30. Wang A, Langer R, Farokhzad O. Nanoparticle Delivery of Cancer Drugs. Annual Reviews of Medicine 2012;63:185-98.
31. Rai P, Mallidi S, Zheng X, Rahmanzadeh R, Mir Y, Elrington S, Khurshid A, Hasan T. Development and applications of photo-triggered theranostic agents. Adv Drug Deliv Rev. 2010;62(11):1094-124.
32. Ma HY, Bendix PM, Oddershede LB. Large-Scale Orientation Dependent Heating from a Single Irradiated Gold Nanorod. Nano letters. 2012;12(8):3954-60.
33. Mahmood U, Weissleder R. Near-infrared optical imaging of proteases in cancer. Mol Cancer Ther. 2003;2(5):489-96.
34. Ntziachristos V, Bremer C, Weissleder R. Fluorescence imaging with near-infrared light: new technological advances that enable in vivo molecular imaging. European Radiology. 2003;13(1):195-208.
35. Boisselier E, Astruc D. Gold nanoparticles in nanomedicine: preparations, imaging, diagnostics, therapies and toxicity. Chemical Society Reviews. 2009;38(6):1759.
36. Dreaden EC, Mackey MA, Huang X, Kang B, El-Sayed MA. Beating cancer in multiple ways using nanogold. Chemical Society Reviews. 2011;40(7):3391.
37. Dreaden EC, Alkilany AM, Huang X, Murphy CJ, El-Sayed MA. The golden age: gold nanoparticles for biomedicine. Chem Soc Rev. 2012;41(7):2740-79.
38. Ntziachristos V, Yodh AG, Schnall M, Chance B. Concurrent MRI and diffuse optical tomography of breast after indocyanine green enhancement. Proc Natl Acad Sci U S A. 2000;97(6):2767-72.
39. Hainfeld JF, Slatkin DN, Smilowitz HM. The use of gold nanoparticles to enhance radiotherapy in mice. Phys Med Biol. 2004;49(18):N309-N15.
40. Huang XH, Jain PK, El-Sayed IH, El-Sayed MA. Determination of the minimum temperature required for selective photothermal destruction of cancer cells with the use of immunotargeted gold nanoparticles. Photochemistry and Photobiology. 2006;82(2):412-7.
41. Huang XH, El-Sayed IH, Qian W, El-Sayed MA. Cancer cell imaging and photothermal therapy in the near-infrared region by using gold nanorods. Journal of the American Chemical Society. 2006;128(6):2115-20.
42. Takahashi H, Niidome T, Nariai A, Niidome Y, Yamada S. Gold Nanorod-sensitized Cell Death: Microscopic Observation of Single Living Cells Irradiated by Pulsed Near-

infrared Laser Light in the Presence of Gold Nanorods. Chem Lett. 2006;35(5):500-1.
43. O'Neal DP, Hirsch LR, Halas NJ, Payne JD, West JL. Photo-thermal tumor ablation in mice using near infrared-absorbing nanoparticles. Cancer Letters. 2004;209(2):171-6.
44. Loo C, Lowery A, Halas N, West J, Drezek R. Immunotargeted Nanoshells for Integrated Cancer Imaging and Therapy. Nano letters. 2005;5(4):709-11.
45. Miele E, Spinelli G, Miele E, Tomao F, Tomao S. Albumin-bound formulation of paclitaxel (Abraxane ABI-007) in the treatment of breast cancer. Int J Nanomedicine. 2009;4:99-105.
46. Barriere C, Qi J, Allende PBG, Newton R, Elson DS. Multifunctional gold nanorods for image-guided surgery and photothermal therapy. Proc Spie. 2012;8234.
47. National Oesophago-gastric Cancer Audit 2010, taken from The NHS Information Centre. 2013.
48. Parsons S. Are we missing gastro-oesophageal cancer at endoscopy? Ann R Coll Surg Engl. 2010.
49. Hosokawa O, Tsuda S, Kidani E, Watanabe K, Tanigawa Y, Shirasaki S, Hayashi H, Hinoshita T. Diagnosis of gastric cancer up to three years after negative upper gastrointestinal endoscopy. Endoscopy. 1998;30(8):669-74.
50. Hamashima C, Ogoshi K, Okamoto M, Shabana M, Kishimoto T, Fukao A. A Community-Based, Case-Control Study Evaluating Mortality Reduction from Gastric Cancer by Endoscopic Screening in Japan. Plos One. 2013;8(11).
51. Kim BJ, Heo C, Kim BK, Kim JY, Kim JG. Effectiveness of gastric cancer screening programs in South Korea: organized vs opportunistic models. World J Gastroenterol. 2013;19(5):736-41.
52. Everett SM, Axon AT. Early gastric cancer in Europe. Gut. 1997;41(2):142-50.
53. Raftopoulos SC, Segarajasingam DS, Burke V, Ee HC, Yusoff IF. A Cohort Study of Missed and New Cancers After Esophagogastroduodenoscopy. Am J Gastroenterol. 2010;105(6):1292-7.
54. Yalamarthi S, Witherspoon P, McCole D, Auld CD. Missed diagnoses in patients with upper gastrointestinal cancers. Endoscopy. 2004;36(10):874-9.
55. Chadwick G, Groene O, Riley S, Hardwick R, Crosby T, Hoare J, Hanna GB, Greenaway K, Cromwell DA. Gastric Cancers Missed During Endoscopy in England. Clin Gastroenterol Hepatol. 2015;13(7):1264-70 e1.
56. GLOBOCAN. Estimated Cancer Incidence, Mortality and Prevalence Worldwide in 2012. http://globocan.iarc.fr/Pages/fact_sheets_cancer.aspx.
57. Stewart BW, Wild CP. World Cancer Report. 2014.
58. Thermal ablation versus surgery for patients with colorectal liver metastases. http://www.nets.nihr.ac.uk/projects/hta/1315304.

Chapter 2 Application of Gold Nanoparticles for Gastrointestinal Cancer Theranostics: A Systematic Review

*The aim of this systematic review is to compartmentalise and consolidate the progress of *in vitro* and *in vivo* applications of the most studied inorganic metallic NP – the GNP - in GI cancer. This highlights and provides objective evidence into some of the current controversies surrounding their application in the GI tract by discussing published variations with regards to their size, shape, synthesis, surface charge, active and passive targeting efficiency, cellular uptake, biocompatibility and drug delivery. GNPs have afforded new applications for a host of imaging platforms to enhance optical detection of these cancers and thus these are also reviewed. Where possible attempts are made to elucidate if there are any potential conclusions that can be drawn on their optimisation, efficacy and safety, and identify any potential issues that need addressing prior to elevating nanomedicine from the bench to bedside.

2.1 Background

Hyperthermia and Photothermal Therapy

Upon irradiation of GNPs with NIR light, surface electrons become excited and resonate vigorously. When these electrons return to the ground state, they emit energy in the form of heat and the surrounding temperature is raised (1). The temperature rise is primarily dependent upon the shape and concentration of the NPs, incubation time of GNP with tissues, laser fluence (power per unit area) and the laser exposure time (2, 3). The characteristic absorption spectrum of GNPs is dependant on the shape of the particles and is usually chosen to be within the NIR spectrum [between 650 and 900 nm for up to 10 cm depth of penetration (4-6)] where there is minimal background tissue absorption and high optical tissue penetration (7). In the case of gold nanorods (GNRs), altering and increasing their aspect ratio (length/width) during chemical synthesis shifts the absorptive peak of their longitudinal SPR band within the visible to the NIR (8-10). Gold nanospheres have rather limited spectral tunability due to their resonance peak at ~ 520 nm in the visible, which thus have a more limited clinical application in GI cancer due to the absorption and scattering of this light by tissue and endogenous chromophores.

---

* This chapter is adapted from the author's publication in Nanomedicine: Nanotechnology, Biology and Medicine, June 2015. doi: 10.1016/j.nano.2015.05.010

GNP heating can also release drugs directly into the site of particle accumulation by de-coupling heat-sensitive chemical bonds to the nanoparticles that act as cargo carriers or vectors. Furthermore, the photothermal effect may be channelled to rapidly transport drugs across membranes and damage DNA and proteins as well as generate oxygen free radicals (11, 12).

Within tissue, hyperthermia encourages a higher concentration of drugs to localise within a tumour by increasing regional blood flow. Hyperthermia also works at the cellular level by increasing cellular permeability and enables higher intracellular chemotherapy concentrations (11). Personalised medicine has given rise to 'activated therapy', namely enzyme-cleavable prodrugs (13, 14), which become active and release the parent drug after interacting with a specific biomarker inside the cell (15). Nanotechnology has allowed the progression of drug-delivery from bench to clinical application. For example, an albumin-bound 130 nm particle such as Paclitaxel (Abraxane®, Abraxis BioScience Inc.) has been approved by the US Food And Drug Administration (US FDA) for metastatic breast cancer (16). Another FDA-approved nanoparticle-based drug in use is doxorubicin (Doxil), which has been validated in a phase III multiple-myeloma trial and further indicated in metastatic ovarian cancer and AIDS-related Kaposi's sarcoma (17). Although there have been numerous drug delivery systems throughout the world, very few have made it through the rigours of the Medicines and Healthcare products Regulatory Agency (MHRA), the European Medicines Agency (EMA) or the US FDA, indicating a formidable "bottle neck" from translating bench to bed-side delivery (18, 19).

PTT using NIR light absorption to elicit thermal damage (7) is an established means of destroying cancer tissue, since tissues heated above a certain thermal threshold undergo various mechanisms of cellular damage (20, 21) such as protein structural changes or carbonisation of tissues. The term hyperthermia is used when an organ is heated to temperatures between 41 and 45°C. Hyperthermia can also enhance the efficacy of chemotherapy and radiation-induced tumour damage (22, 23), and there are also positive reports of an enhancement of the photodynamic (PDT) response (24) compared to PDT alone (25). Hyperthermia is an attractive therapy for it retains a lower side-effect profile than conventional cancer treatments, with the potential of repeated application without the concern of compounding the toxicity levels (26). One major challenge to local and regional PTT is the development of a homogeneous temperature distribution throughout the tissue (27), as the heating delivered from lasers generally follow a Gaussian profile. Temperature-dependent cell survival graphs have shown that each 1°C temperature rise above a 43°C threshold leads to doubling of cell death (12).

Techniques which employ temperatures above 45°C to produce irreversible cell damage are referred to as thermal ablation techniques (11), such as those used in radiofrequency or microwave ablation. This produces a specific area of cellular death bordered by regions experiencing less intense hyperthermia which are potentially viable. Cancer cells appear to be more sensitive to heat-induced damage than normal cells (28).

Rodent studies demonstrated that tissue depths of approximately 1 cm could be irradiated safely with NIR light using untargeted gold nanoshells with less than 10°C increases in normal tissues (29). These results concur with Shah *et al*. demonstrating that NIR light is able to penetrate to depths of more than 1 cm in tissues without visible damage (30). Depth of penetration and selectivity of PTT are some of the key challenges encountered in translating this technology to patients, where tumours may be extending 5–10 cm deep within parenchymal structures (31).

Enhanced Permeability and Retention Effect (EPR) and Tumour Targeting

First described by Maeda and Matsumura in 1986, the enhanced permeability and retention (EPR) effect provides an explanation for specific accumulation of GNPs at the tumour site (32, 33). They explained that NPs selectively accrue within solid tumour masses as a result of tumour physiology. Solid tumours contain leaky blood vessels with cell junction gaps ranging from 100 nm to 780 nm (34), compared with pore diameters of up to 20 nm in normal capillaries (35-37). Studies have repeatedly demonstrated that NPs with diameters up to 100 nm will pass through the reticuloendothelial system (RES) and into the circulation to extravasate and accumulate in the tumour region (35, 38-41). However, the sizes of these endothelial fenestrations are known to vary with tumour type and microenvironment (42). Once assembled inside the tumour interstitium, NPs are retained due to locally ineffective lymphatic drainage. This is a *passive* method of organising GNPs into cancerous regions, so that they are optimally positioned for PTT. For tumours less than 3 cm, local hyperthermia using targeting derived from passive GNP accumulation may be suitable (12, 43) but the biggest limitation is the considerable biological heterogeneity of tumours and hence the lack of bio-specificity. Tumours with poor vasculature, such as pancreatic or prostate cancer, may not amass GNPs via the EPR effect alone (28).

Active targeting has consequently been explored to enhance the GNP concentration within the tumour matrix by the attachment of a targeting moiety that is over-expressed by cancer cells. The GNP surface is chemically modified (functionalised) with an antibody or ligand

for receptor, antigen, carbohydrate or other type of targeting (41, 44). Antibodies that have been applied in targeting GI cancer include human epidermal growth factor receptor (EGFR) 1, vascular endothelial growth factor (VEGF), folic acid (FA) receptors and vascular cell adhesion molecule-1 (VCAM-1). Two distinct targeting mechanisms may be used to aid or enhance tumour targeting specificity.

Following conjugation to a specific receptor, GNPs internalise via the characteristic mechanism for that particular receptor; for example, GNPs targeting EGFR receptors become internalised within 15 minutes of receptor-ligand engagement (22) – see section below. The biggest limitation associated with active targeting is the fact that the GNPs are typically larger and experience difficulty in mass transport across bio-barriers, and also competitive uptake by non-target cell types or extracellularly (45). This may partly explain why the current GNPs in clinical use utilise passive targeting via the EPR effect rather than active biomolecular recognition, as well as the more complex clinical approval route for targeted agents (46).

Synthesis and Surface Coating of GNPs

In 1857 Michael Faraday pioneered the synthesis of colloidal gold; where he described a chemical synthesis of reducing gold chloride in a carbon disulfide solvent using phosphorous as a reducing agent (47). Today, there are three main methods to synthesize GNPs: physical, chemical and biological. The physical methods of synthesis comprise microwave irradiation (48), ultra-violet irradiation (49), laser ablation (50), sonochemical methods (51), thermolytic processes (52), photochemical and radical induced methods (53, 54). The biological method uses fungi or bacteria as nanofactories (55, 56).

In the synthesis of gold nanorods, which is the most widely used GNP in the PTT of GI cancer, the most commonly used method comprises a chemical seed-mediated approach whereby spherical ‘seed’ NPs (~4 nm) are added to a growth solution containing gold salt, silver nitrate, ascorbic acid and cetyltrimethylammonium bromide (CTAB) leading to the fabrication of GNPs with a rod-like morphology (i.e. GNRs) (57, 58). This was first described in the 1920s (59) and is a relatively simple and reproducible method of obtaining a high yield of GNRs with varying aspect ratios (60).

CTAB, a cationic surfactant coating, induces a positive charge to the surface of GNRs and in an aqueous medium, it prevents particle aggregation due to electrostatic repulsion (61). CTAB can be cytotoxic as it can cause biomembrane and peptide disintegration at micromolecular concentrations (62). Therefore, it is essential to replace or remove the CTAB

coating on GNRs in order to effectively apply GNRs in biomedical uses. While attempting to remove excess CTAB from newly synthesized GNRs with successive washings, centrifugation and removing the supernatant CTAB, CTAB-capped GNRs at a concentration of ~200 μg ml^{-1} still exhibited marked cytotoxicity (63). Thus, it is generally accepted that an outer protective coating on GNRs, such as PEGylation, silica or poly(acrylic) acid (PAA) is essential for most biological applications (61).

In order to exploit the EPR effect, hydrophobic GNPs must escape systemic recognition by the immune system. Cells of the RES, particularly macrophages, are scavengers that inhibit effective GNP treatment by phagocytosing or opsonising NPs and thus prohibit them from gaining access to tumour cells (64). Nevertheless, the surface of NPs is easy to modify; and by coating a hydrophilic 'stealth' conjugate such as polyethylene glycol (PEG) onto their surface, clearance by the RES organs such as the kidney, liver, spleen, and lymph nodes is decreased (22, 41, 44), while prolonging the circulatory half-life by 10 to 100 fold (34, 65). "PEGylation" of GNPs also provides an external shell for ligand conjugation and prevents particle aggregation. A disadvantage of PEGylation is that it can potentially shield the targeting agent, which reduces the likelihood of biorecognition (66).

Cellular Uptake of GNPs and Dependence on GNP Type and Shape

NPs traversing the GI tract bypass efflux by transmembrane ABC (ATP-binding cassette) transporters and subsequently enter cells via endocytosis (67). The process of GNR internalisation was studied by Chithrani *et al*. using transferrin-functionalised GNRs. The authors concluded that receptor-mediated endocytosis was the main mechanism behind internalisation based on a 70% decrease in cellular uptake at low temperatures (4°C), which is known to cease receptor-mediated endocytosis (68).

It is important to examine the distribution of GNPs in tumours at both tissue and cellular levels. As GNPs are electron-dense, transmission electron microscopy (TEM) or scanning electron microscopy (SEM) are both able to confirm internalisation of GNPs into GI cancer cells, observe aggregation as well as characterise the size and shape of the GNPs. EM can also display post-irradiation changes to intracellular architecture and organelles after NIR light absorption by intracellular GNPs. It can further be utilised to quantify non-selective uptake of GNPs by non-cancerous cells and the collateral spread of PTT-induced damage to adjacent healthy tissues. Inductively coupled plasma mass spectrometry can be used to give a precise quantification of the amount of administered gold which has been taken up by cells or tissues (62, 69).

There is some debate as to whether gold nanospheres, gold nanoshells or GNRs (the three most widely applied GNPs in the PTT of GI carcinoma) are preferable for biomedical targeting and delivery, as they all employ the same principle of SPR to release thermal energy to the surrounding tissues. Gold nanoshells (approximately 10–300 nm in diameter) comprise a dielectric core, usually silica, which is encompassed by a thin gold shell (29, 70). Huang *et al*. found that when targeted gold nanospheres and GNRs were compared with each other in terms of receptor binding to malignant oral epithelial cancer cells, many more GNRs appear to bind to malignant cells due to interactions between the surface of the rods and cell surface proteins (71). Huang also pointed out that on some occasions GNRs also accumulated in non-malignant cells due to non-specific interactions. von Maltzahn *et al*. further demonstrated that PEG-GNRs were superior to PEG-gold nanoshells in terms of intrinsic absorption and photothermal efficacy (GNRs generated more than 6 fold greater heat per gram of gold), as well as significantly longer circulation times *in vivo* (~17 hours for PEG-GNRs versus ~4 hours for PEG-gold nanospheres), which may be attributable to their polymer coating (72).

Chen *et al*. evaluated GNP size-associated toxicity over time. They found that GNPs ranging from 8 to 37 nm produced severe sickness in mice with side effects including fatigue, anorexia, fur colour changes and weight loss. The majority of mice injected with these sized GNPs died before the end of the fourth week (73). It is important to mention that the GNPs used were not PEGylated, rather somewhat unconventional surface modification peptides (pFMDV and pH5N1) were utilised. The authors also observed that very small GNPs (5 nm) or larger (50 -100 nm) were in fact non-toxic.

Desai *et al*. explored the relationship between GNP size and GI tract uptake and showed that GI cell endocytosis occurs more readily when NP sizes are below 130 nm (74). It is thus presumed that both active and passive targeting can be capitalised simultaneously to maximise the efficacy of GNP targeting, on the proviso that the combined particle-conjugate size remains approximately 130 nm or smaller to avoid uptake by the RES.

NPs have a large surface area to volume ratio which allows them to be held in suspension, incorporate targeting moieties, allow high pro-drug encapsulation and high loading capacity for imaging probes, but also permits extensive surface absorption (15, 75-77). It is known that most chemotherapy drugs distribute non-specifically within the body, which accounts for much of its toxicity and side effects. However GNPs loaded with cleavable pro-drugs are able to specifically internalise within cancer cells. This presents an elegant solution to the problem of non-specific biodistribution and poor bioavailability of conventional drugs.

Positively charged nanoparticles (from zeta potential measurements) were believed to be more likely to adhere to negatively charged cell membranes (78-80) by electrostatic interaction. However, doubt remains as to what extent the charge of GNPs influences the rate of cellular uptake (81). Arvizo *et al*. suggested that cell membrane potential significantly affects the uptake of GNP, and showed that cationic GNPs were much more efficient at depolarising the membrane and thus being taken up by both cancer and healthy cells, compared with anionic or neutral GNPs (82). Lund *et al*. were more sceptical of this theory and proposed that it is more likely that NPs either enter through pre-existing cell membrane pores or are capable of re-configuring the plasma membrane in order to create new pores (81). They used very small NPs (5 nm) and proposed passive internalisation by pathways which do not depend on energy, endocytosis or lipid-raft-mediated methods. Alkilany *et al*. studied the cellular uptake of differently charged GNRs, and found that particle surface charge bore no correlation to GNR uptake (62). Zahr *et al*. proposed that the higher the surface charge of a GNP, regardless of its polarity, the more likely it is to be phagocytosed by macrophages and removed from the circulation (83). In practice nanoparticle surface charge is often minimised by the incorporation of a neutral polymer such as PEG which limits electrostatic interactions with other components within the circulation.

Imaging Modalities and Diagnostics

Imaging the location of GNPs enables the potential diagnosis of cancer as NPs can be targeted to cancer using both the active and passive approaches discussed above. It is also important to image the location of NPs to understand their biodistribution and to target the laser to this precise location to gain a high level of specificity for directed therapy.

As gold nanoparticles are an excellent optical contrast agent (primarily through optical absorption of light attuned to their SPR wavelength band as well as their intrinsic luminescence under two-photon excitation) they may be imaged using imaging techniques which utilise this property, i.e. two-photon luminescence imaging (84-86), photoacoustic imaging (85, 87) narrow band imaging (88) and optical coherence tomography (OCT) (89, 90).

NIR fluorophores such as Cy5.5 may be conjugated to the surface of NPs for background-free diagnostic fluorescence imaging to clearly localise aggregates of GNPs within a tissue. Once fluorescence is identified within a cluster of nanoparticles, NIR laser illumination may then be directed to that location for PTT.

Non-optical methods have also been used with GNPs such as positron emission tomography (PET) and X-ray computed tomography (CT). They have been used with X-rays as gold has a higher atomic number and density compared to standard radiosensitive iodine-based reagents (91, 92). von Maltzahn *et al*. have shown preliminary evidence that GNRs appear to exhibit approximately two times more X-ray contrast than that of standard iodine per mole (72). Gold nanoshells (93, 94) and nanocages (95) have also been attached with the radionuclide ^{64}Cu to enable PET imaging of the NP location.

2.2 Materials and Methods

This systematic review was performed in accordance with guidelines from the Preferred Reporting Items for Systematic Reviews and Meta-analysis (PRISMA) (96).

Eligibility Criteria

Original peer-reviewed articles published in English on the application of GNPs in GI tract cancer (including oesophageal, gastric and colorectal carcinoma, but excluding oral, hepatic or pancreatic cancers) were considered. Studies using NPs without any gold element were excluded. Where multiple studies existed from the same institution, the most recent study was considered.

Information Sources and Search

A broad literature search was conducted in May 2013 using PubMed (1946 to date), Embase (1974 to date) and PsycINFO (1967 to date) databases. Additional searches using the Cochrane Library, Ovid SP and cross-referencing with Web of Science® were used to broaden the search. The MeSH search terms used were “gold nano*” and “*esophag*” or “gastr*” or “colo*” or “rectal” or “*intestinal” and “cancer”.

Study Selection and Data Collection Process

Two reviewers (M.S. and D.S.E.) independently reviewed all relevant articles from the literature search. The full text of each article was obtained and further screened for inclusion if it had relevance to application of GNPs in GI tract cancer. Studies were excluded if they were only conference abstracts without any extension to a full supporting paper due to the lack of data and methods, and studies were excluded if they only were on hepatic or pancreatic cancer. A high level of agreement existed between both reviewers, and minor

queries were discussed between the reviewers until a 100% concordance was achieved on the final studies included in this review.

Data Items

The following items were extracted from the studies: GNP type, shape, average size and concentration used, type of cancer cell lines or animal tumour model used (or both), charge of GNPs, employment of targeting agents, methods of confirming intracellular accumulation of GNPs, laser radiation type, fluence and regime, confirmation of PTT effects and temperature rises, confirmation of histological evidence of cellular destruction or cell viability studies (for cell studies), survival studies or follow up (for animal studies), imaging modalities used, and any evaluation of GNP toxicity.

2.3 Results

Initial searches using the MeSH terms above revealed 284 articles. There were nine conference abstracts (without accompanying full papers), which were excluded. A further 48 articles were identified through free text searches, the "related articles" feature and cross-referencing. Once duplicates were removed, finally 16 studies remained and were found to match the inclusion criteria, thus these are discussed in this systematic review.

GNP Type and Concentration

GNPs that were used in the theranostics of GI tract cancer involved a combination of GNPs conjugated with silica (97, 98), PEG (88, 99-101), chitosan (102, 103), iron core [with a gold shell (104)], pure shells (105), platinum-tethered (106), CTAB-coated GNR (107), gold-SPION hybrid NPs (108), PEG-conjugated hyaluronic acid NPs (109), PEG-Au-TNF (110) and poly(acrylic acid)-GNR (63). Although there are many shapes of NPs in existence, the three identifiable GNP shapes were rods, shells and spheres. The other identifiable characteristics of the studies are described in Table 2-1.

Study	Cells/Animals	Shape	Ave. Size (nm)	GNP Concentration
(97)	Cells + Mice	Rods	46 x 18	0.625 – 12.5 μM
(105)	Mice	Spheres	6-8	38.6 μg/ml
(102)	Cells + Rats	Particles	30-90	OD 1 (cells) or 3 x 10^{11} NP/ml OD 50 (animals)
(104)	Cells	Particles	10	10 μg/ml
(103)	Cells	Particles	15	20-100 μM, OD 0.6
(88)	Mice	Shells	135	2.66 x 10^{9} NP/ml, OD 1
(101)	Mice	Rods	45 x 14	4.5 ml/kg or OD 100 given IV to mice (2 x 10^{13} GNR/ml)
(106)	Cells	Particles	30-40	?
(107)	Cells	Rods	60 x 20	?
(108)	Mice	Hybrid Particles	6-18	PTT – 200 μL, 1 mg/ml MRI – 0.3 ml, 1 mg/ml
(100)	Mice	Shells	119	150 μL (1.5 x 10^{11}/ml)
(109)	Mice	Particles	238	?
(110)	Mice	Particles	33	5-24 μg
(99)	Mice	Shells	132-135	8 x 10^{8} /g body wt.
(63)	Cells	Rods	66 x 11	100 μg/ml
(98)	Mice	Shells	8-10	100 ml of 2.4 x 10^{11} NP/ml solution

Key: NP = Nanoparticle, OD = Optical Density, ? = Unknown/Unclear

Table 2-1 The included studies, with the type of study, shape, size and concentration of GNPs used in the study.

Charge of NPs

Zhang *et al*. measured 15 nm chitosan-coated GNPs using zeta potentials, and found they bore a charge of +30.0 ± 1.18 mV at a pH of 7.4 (103). They proposed that the positive charge promoted particle repulsion and prevented agglomeration, while enhancing endocytosis when interacting with negatively charged cell membranes. Huang *et al*. also measured the zeta potential of their synthesised GNPs, but it was unclear whether the authors considered this to have a bearing on GNP internalisation (97).

Passive or Active Targeting

Twelve (75 %) of the GI cancer studies did not involve functionalisation of GNPs with a targeting agent, relying instead solely on the EPR effect of passive accumulation of GNPs intracellularly and into the tumour tissue.

Folic acid was used as a targeting agent for MCG803 gastric cancer cells (97). Kirui *et al*. adopted immuno-targeting using humanised single-chain antibody conjugates (A33scFv) that target the A33 antigen expressed in 95% of primary and metastatic human colorectal cancer (CRC) cells, but is absent in most other normal tissues and tumour types (63, 108). Hyaluronic acid receptor (CD44) that is over-expressed in various cancer cells (109) has also been employed for targeting.

Cancer Models Used

The cancer models used were broadly categorised to either cellular studies (*in vitro*) and/or animal studies (*in vivo*) as shown in Table 2-2.

Study	Cells	Animals	Cell Line on Animals	Inoculation Method
(97)	MCG803 human gastric cancer	Nude mice	MCG803 gastric cancer	Flank s/c
(105)	No	BALB/c mice	CT26 colon carcinoma tumour	Flanks s/c
(102)	Het-1A, BAR-T and OE-19 human oesophageal lines	Sprague-Dawley rats		Esophago-duodenal anastomosis
(104)	Caco-2 and HT-29 human colon cancer cells	No		
(103)	Gastric Cancer MGC-803 and human gastric mucosa epithelial GES-1 cells	No		

(88)	No	Swiss nu/nu mice	HCT116, ATCC#CCL-247 Human colon cancer cells	Flank s/c
(101)	No	Balb/c mice	CT26.wt murine colon carcinoma (ATCC)	Flank s/c
(106)	HCT116, HCT15, HT29, RKO human colon cancer cells	No		
(107)	HCT-116 human colon cancer cells	No		
(108)	No	Balb/c nude mice	a) SW1222 cells (antigen-expressing human colorectal cancer cell line). b) Human colorectal cancer cell line (HT-29)	Left flank s/c Right flank s/c
(100)	No	BALB/c mice	CT-26, ATCC murine colon carcinoma cells	s/c
(109)	No		3 models:	
		BALB/c mice	HT29 human colon cancer cells	$1x10^7$ HT 29 cells in 100ml saline s/c into mice dorsa.
		BALB/c mice	Liver-implanted with CT26 colon cancer cells	Laparotomy & direct injection of $3x10^5$ CT26 cells into the left liver lobe.
		A/J Mice	Azoxymethane (AOM)-induced orthotopic colon cancer models.	Intraperitoneal injection
(110)	No	C57/BL6 mice	MC-38 colon carcinoma cells	s/c
(99)	No	Nude Swiss mice	HCT 116 human colorectal cancer cells	$\sim 2\times10^6$ cells s/c into right thigh.
(63)	SW 1222 (10^6 cells/ml) human colorectal cancer cells	No		
(98)	No	BALB/c AnNHsd Sprague–Dawley mice	CT26.WT murine colon carcinoma tumour cells (ATCC)	s/c into flank

Table 2-2 Types of *in vitro* and *in vivo* GI cancer models and methods of inducing cancer in rodents. Key: s/c = subcutaneous.

Irradiation Regimes

The irradiation regimes used with gold nanoparticles are shown in Table 2-3.

Study	Cells/Animals	Irradiation Used	Laser Power & Fluence	Duration of radiation
(97)	Cells + Mice	CW laser 808 nm	30 mW laser power 4 W/cm^2 laser fluence	3 mins
(105)	Mice	Intense Pulsed Light (IPL) (LumenisOne), a broadband (560-1200nm), pulsed, high energy light source + US	US: 2 W/cm^2, with frequency 1.1 MHz Light: 35 J/cm^2	US – 3 mins IPL – 9 pulses of 5 ms pulse duration
(102)	Cells + Mice	CW laser 818 nm – used both externally & via microendoscopy	3 W/cm^2	Cells & rats, 1 min at 3 W/ cm^2, or, 30 secs at 1 W/cm^2
(103)	Cells	X-rays	1 Gy/min	Cells exposed to 2, 6 & 10 Gy with corresponding irradiation times of 2, 6 & 10 min
(101)	Mice	CW laser 808 nm	3.5 W at 4.46 W/cm^2	180 seconds
(107)	Cells	Ti:Sapphire at 800 nm	1 mW (imaging), >10 mW for PTT with beam diam. approx. 20 µm	No time duration specified just states “4 passes"
(108)	Mice	CW laser 808 nm	5 W/cm^2, beam diam 6 mm	30 mins & 7 rounds therapy over 14 days
(100)	Mice	CW laser at 808 nm	4 W/cm^2, spot size 5 mm	3 mins
(99)	Mice	808 nm CW laser + a single 10 Gy dose of radiation therapy using 125 kV X-ray operated at 20 mA	0.6 W used, 75% duty cycle, average optical irradiance (350 mW/cm^2) Beam diam 10 mm	20 mins
(63)	Cells	CW laser 808 nm	5.1 W/cm^2, beam diam 4 mm	10 mins
(98)	Mice	CW laser 808 nm	4 W/cm^2, beam diam 5 mm	3 mins

Table 2-3 Irradiation regimes used in each study model.

Key: CW = Continuous Wave, US = Ultrasound, Gy = Gray (Joule/kg).

Proving Endocytosis of Gold Nanoparticles

A variety of different methods were used to identify the uptake of GNPs into cells and tissues. Almost all studies employed TEM imaging to visualise nanoparticles post synthesis, but three studies also used it to visualise NPs within cells (97, 103, 106) and one study used dark field microscopy (97). It was found that GNRs are virtually unchanged after internalisation and it is apparent that GNPs do not enter the nucleus, but agglomerate within intracellular vesicles (97, 103). The uptake and localisation of platinum-tethered NPs were also examined using inductively coupled plasma mass spectrometry, which confirmed the ability of GNPs to deliver platinum inside cells (106).

Fluorescent protein labelling of a colon cancer cell line was used by Black *et al*. (107) while Kirui *et al*. used NIR fluorescence imaging of localised intratumoural gold-SPION hybrid NPs (108). In a prior study, Kirui *et al*. (63) also showed that human CRC SW 1222 cells incubated with fluorescently-labelled A33scFv-GNRs had internalised into cells using fluorescent-based confocal microscopy analysis. Gobin *et al*. excised tumours and then cyrosectioned them with silver staining prior to microscopic analysis (100), confirming that nanoshells were present throughout the tumours. Li *et al*. similarly demonstrated GNP loading in cells via histology using silver staining (102).

A method used to identify iron-gold hybrid GNPs within cancerous tissues was using Perl's Prussian blue staining (108). Other excised tumour sections were lyophilised for gold content evaluation using neutron activation analysis (100), which was able to verify the presence of nanoshells within the tumour.

Photothermal Effect, Hyperthermia and Cancer Cell Destruction

Photothermal effects were evaluated in all studies that involved laser application. However, in one study suppression of cancer cell proliferation was noted without laser illumination, which was attributed to the GNP composition causing local cytotoxic effects. Wu *et al*. noted that iron clusters before oxidation in their iron core-gold shell nanoparticles specifically inhibited the growth of human CRC cells (CaCo-2 & HT-29), leaving healthy cells unaffected (104).

Ultrasound (US) irradiation alone showed an insignificant anti-tumour effect as shown by Sazgarnia *et al*. However, they showed that acoustic cavitation in the presence of GNP with intense pulsed light (IPL), a broadband (560-1200nm), pulsed, high energy light source,

could be used as a new method to improve therapeutic effects on tumours (105). The authors discovered that tumour inhibitory effect was significant when IPL and US and GNPs were used. They hypothesised that IPL irradiation on GNP enhances antitumour effects by establishing nucleation sites for acoustic cavitation.

Huang *et al*. noted that gastric cancer cells incubated with GNR-SiO_2-FA, destroyed cell spindle morphology, ruptured cell membranes and produced significant scarring after 3 minutes of NIR laser (4 W/cm^2) application (97). X-ray irradiation was also utilised on chitosan-modified GNPs (CS-GNPs), and the survival fractions of gastric cancer cells treated with CS-GNPs decreased when increasing the concentration of CS-GNPs and when compared to cells without CS-GNPs under the same X-ray radiation dose (103). Kirui *et al*. proved effective PTT of CRC cells that had been incubated with plasmon-resonant A33scFv-GNRs and treated with NIR laser (5.1 W/cm^2) for five minutes (63).

In measuring local tissue temperatures achieved from PTT, Goodrich *et al*. noted that in their mouse study, the average maximum temperature difference for GNR-infused and laser-treated animals was approximately 32.1 ± 9.0 °C (temperature rise) within tumour tissues as measured by a hypodermic needle thermocouple placed under the tumour and parallel to the laser fibre. With the laser-only control animals, the maximum temperatures rise within tissues was approximately 15.3 ± 2.8 °C. These temperature rises were noted over a 3-minute NIR laser (3 W) irradiation period (101). Kirui *et al*. noted a 30°C temperature rise for a concentration of 0.5 mg/ml hybrid NP using a regime of seven rounds of NIR CW irradiation (5 W/cm^2) over a fortnight (108). O'Neal *et al*. demonstrated after 30 seconds of NIR irradiation (4 W), the average temperature of laser-nanoshell treated colon cancer in mice was approximately 50°C and this was statistically significantly higher than the nanoshell-free (but NIR irradiated) controls. A complete tumour resorption was seen after 10 days of laser-nanoshell treatment (98).

Diagradjane *et al*. used H & E (haematoxylin & eosin) staining to demonstrate there were necrotic regions at a distance of ~1.4 mm from the tumour periphery in their thermoradiotherapy group, which showed a distortion of regional architecture characterised by patchy hypoxic regions in the tumour core with no identifiable regions of blood flow (99).

Histological Evidence of Destruction and Cell Viability Studies

The effects of PTT on cells using GNPs should be evaluated to ensure selective cellular destruction of cancer cells and the viability of healthy surrounding tissues post irradiation. Studies used a variety of methods in this endeavour to demonstrate cytotoxicity or apoptosis,

chiefly using trypan blue staining (97, 107), H & E staining and microscopy (99, 101, 102, 105), Annexin V-fluoroisothiocyanate (FITC) apoptosis detection kit I (104), ApopTag® apoptosis detection kit (102) and assays such as WST-1 (104), CCK-8 (97), MTT (102, 103, 106), TUNEL (102) and clonogenic cell survival assays (103). The clonogenic cell survival assay is an *in vitro* assay based on the ability of a single cell to reproduce to form a colony after ionising radiation, i.e. its survivability (103). The MTT assay is a quantitative colorimetric method to evaluate cytotoxicity while trypan blue is an *in vitro* cytotoxicity assay that measures cell membrane integrity.

Brown *et al*. evaluated the cytotoxicity of platinum-tethered GNPs (as a chemotherapy nanovector) against traditional PEGylated GNPs on human colon cancer cell lines using a tetrazolium dye-based microtitration assay (a MTT assay) and inductively coupled plasma-mass spectrometry. Tetrazolium salt assays measure mitochondrial activity. While the PEGylated NPs showed no cytotoxicity, the platinum-tethered gold nanoparticles in contrast were found to be 5.6-fold more cytotoxic than oxaliplatin (106). Another study also endeavoured to determine cellular viability using 0.5% trypan blue, a dye that does not penetrate the cytoplasm of viable cells, which was added prior to laser treatment of CTAB-coated GNR on a human colon cancer cell line, HCT-116 (107). After 10 minutes of illumination, it was noted that trypan blue had entered several cells within the laser region, and after 25 minutes, the entire irradiated region which had initially absorbed GNRs was stained with trypan blue, while other control regions remained unchanged. A subsequent wash of the stained cells on a slide led to the complete removal of thermally affected cells, suggesting major cellular damage.

PEG-conjugated hyaluronic acid nanoparticles (P-HA-NPs) that contained the anticancer drug Irinotecan (IRT) was studied on 3 BALB/c mice colon cancer xenografts. It was noted that IRT released gradually from NPs within 12 hours and then exerted a dose-dependent cytotoxicity on colon cancer cells (109). Kirui *et al*. conducted cell viability studies using a MTT assay of SW 1222 cells (an antigen-expressing human CRC cell line) after incubation with increasing concentrations of polyacrylic acid-GNRs against CTAB-GNRs. A dose-dependent toxicity was noted with a significantly higher cytotoxicity for cells which were incubated with CTAB-GNRs (63).

Survival Studies and Tumour Regression - *In vivo* animal studies

This review considered all longitudinal survival studies and tumour volume regression. Sazgarnia *et al*. (105) continued follow-up for 70 days after IPL+US+GNP treatment and

noted the survival fraction of these mice was the most significant compared with other control groups. In a different study involving mice inoculated with CT26 murine colon carcinoma, the mean survival time with various treatment modalities was established. For the "no treatment" group, mice lived for an average of 8 days, whilst mice in the “laser illumination only” group lingered for an average of 9.5 days, whilst the “NRs-only” group survived for 9.7 days. Most significantly, it was the photothermal ablation group of mice that survived the longest at 42.1 days (101). 44% of the GNR and laser-treated mice survived at day 60, together with evidence of complete tumour ablation. It was observed that the mean survival time of the photothermally-treated group was statistically higher than the control groups. O’Neal *et al*. observed colon tumour size and survival for 90 days following a single NIR irradiation treatment in mice receiving IV gold nanoshells. At 90 days post-treatment, 100% of the gold nanoshell irradiated mice remained healthy and free of tumours. However, tumours in both sham and control groups continued to develop rapidly (98).

In a study by Gobin *et al*., tumour size and animal survival was monitored seven weeks after NIR treatment in CRC induced in mice that were subjected to PEGylated gold nanoshells. All but two nanoshell-treated mice had complete tumour regression (100). A 14 day median survival was observed in the “saline + laser group”, and 10 days for the “no treatment” control group. After 21 days, the group with the most statistically significant survival was the “nanoshell + laser” group, which continued until the end points of the study. It was noted that the median survival time could not be calculated for this group, as the long-term survival was 83%. In a drug-delivery study, Choi *et al*. (109) used the anticancer drug Irinotecan (IRT) attached to PEG-hyaluronic acid nanoparticles (P-HA-NPs) on three mice bearing CRC xenografts. Tumour volume and survival rates were determined after IRT-P-HA-NPs were given intravenously every three days. The authors found that the “saline only” and “free IRT” groups experienced a rapid and significant increase in tumour size and growth. In contrast, significant tumour growth suppression was observed in the group treated with IRT-P-HA-NPs. 50% of mice treated with “free IRT” died after 15 days, and approximately 90% of mice in this group perished within 28 days, indicating IRT by itself results in severe systemic toxicity. Nonetheless the group treated with IRT-P-HA-NPs (using GNPs as a nanovector to deliver the drug into cells) exhibited a much higher survival rate than all control groups.

Imaging Modalities

Huang *et al*. evaluated the Hounsfield Units (HU) of GNR-SiO_2 by CT. Nude mice implanted with gastric cancer MGC803 cells were selected as the animal model and X-ray

imaging was used to monitor the targeting ability of GNR-SiO_2-FA into tissues (97). Puvanakrishnan *et al*. used NIR narrow band imaging in Swiss nu/nu mice inoculated subcutaneously with human CRC cells to image the accumulation of PEGylated gold nanoshells at the tumour site (88). NIR narrow band imaging was performed *ex vivo* on excised tumour tissue, and in four of five gold nanoshell-injected mice, the gold nanoshell regions were visible as dark areas (88). Kirui *et al*. implanted two colon cancer cell lines subcutaneously in murine models and injected intravenous targeted gold-SPION hybrid nanoparticles (HNPs)-A33scFv and then scanned the mice in a 7-T scanner. As a MRI agent, HNPs which had accumulated in subcutaneous CRC reduced the post-contrast T2 phase value by half (108). Gobin *et al*. used OCT imaging to evaluate PEGylated gold nanoshells in murine CRC. The results showed no enhancement in layers of normal tissue in mice treated with nanoshells, but there appeared to be significantly enhanced brightness in the region where nanoshells accumulated within a tumour, suggesting that gold nanoshells are able to provide substantial contrast in OCT imaging (100).

Toxicity of Gold Nanoparticles

Huang *et al*. showed using a CCK-8 assay that there was negligible cell death and physiological changes in MGC803 gastric cancer cells after exposure to GNR-SiO_2-FA. Even with the highest concentration of GNR-SiO2-FA, cell viability was greater than 90%, indicating that their GNPs were by themselves non-cytotoxic to MGC803 cancer cells within the concentration range studied (97). Similarly Zhang *et al*. evaluated the cytotoxicity of chitosan-modified GNPs (CS-GNPs) to MGC803 (gastric cancer) and GES-1 (human gastric epithelium) cells using the MTT assay. The cell viability of MGC-803 cells and GES-1 cells was more than 90% even when the concentration of CS-GNPs was increased to 100 μM, and no decline from this high survival rate was seen even after increasing the incubation time to 72 hours, implying very low levels of intrinsic cytotoxicity from CS-GNPs (103).

Li *et al*. showed that their chitosan GNP (CS-GGS) only heated and caused PTT in the presence of NIR irradiation when absorbed by cancerous oesophageal cell lines (OE-19). They induced orthotopic oesophageal cancer in rats by performing a surgical oesophagoduodenal anastomosis (102). The same GNP-laser combination did not have any effect on benign human squamous oesophageal epithelium cells (Het-1A) or Barrett's epithelium (BAR-T). However, the authors cautioned about selectivity of therapy, as they found some regions within oesophageal mucosa that included both cancerous and adjacent healthy tissues which were "burned" on exposure to NIR. They postulated that this could be due to infiltration of adjacent tissues by inflammatory cells such as phagocytes, and advised

that further evaluation of the specificity of GNP uptake in cancerous and benign tissues is required.

Goodrich *et al*. conducted biodistribution studies in twelve mice receiving infusions of high concentrations PEG-GNRs (optical density of 50 or 6.5 x 10^{12} GNR/ml, giving 6ml/kg body weight). At one, seven and 28 days post-infusion, some mice were sacrificed and blood and major organs (namely brain, heart, lungs, kidneys, liver, spleen and lymph nodes) were harvested for neutron activation analysis to determine gold content. They found concordance with other published results about the clearance and accumulation of GNPs by the organs of the reticuloendothelial system. The largest accumulation was found in the liver and spleen, where 75% of the total injected nanoparticles was noted 24 hours post injection, with negligible accumulation of gold in other organs. There was a gradual clearance of GNRs from the liver over the 28-day study. Reassuringly there were no signs of acute toxicity from GNRs even at 60 days (101).

Choi *et al*. used PEG-conjugated hyaluronic acid nanoparticles (P-HA-NPs) loaded with the anticancer drug Irinotecan (IRT) on three mice with colon cancer. Microscopic examination of major organs and tumours using H & E staining suggested that IRT-P-HA-NPs was effective at destroying tumour tissues, but only piecemeal necrosis was observed in the liver tissues (109).

Paciotti *et al*. (110) evaluated tumour volume regression resulting from various TNF treatments and treatment efficacy by varying the doses of TNF given either in its native form or colloidal-gold bound TNF (cAu-TNF) preparations. They noticed that at a dose of 24 μg of pure TNF per mouse, all the mice died, yet at the same dose of colloidal-gold-TNF preparation, not only was there a significant tumour volume reduction, none of the mice became sick or perished.

2.4 Summary of Evidence

Gold Nanoparticle type and Concentration

With the exception of one study that used GNPs of 238 nm (109), all the other studies used GNPs (of different shapes) below 135 nm in diameter/length. These sizes concur with other published studies looking at optimising the EPR effect, including Desai *et al*. who looked specifically at GI tract uptake (74). There have been a variety of differently shaped particles

being utilised in GI cancer targeting, including spheres, rods, shells and seven studies which only mention "nanoparticles", which is uncategorised as the final shape is not described.

It is difficult to categorise the concentrations of GNP solutions used, as most studies have not used a standardised system to report the concentrations used. There is a wide disparity in the Optical Densities (OD) of GNPs used in mice studies, some using concentrated solutions with an OD of 100 while another used an OD of 50 (102) or an OD of 1 (88). Two studies (98, 100) used virtually the same concentration of nanoshells in their mice studies, however they used vastly different volumes. They also had different sized nanoshells, which presents too many confounding factors to make the concentrations of various GNPs a comparable entity between studies. It therefore becomes impossible to elucidate an effective or optimal dose for cancer therapy, or to even establish a safe recommended dose. None of the studies ventured to quantify what dose may potentially be lethal or harmful *in vivo*.

Charge of Nanoparticles

There has really been only one proponent of maintaining a positive GNP charge (103), which, in itself suggests that charge is unlikely to be of any consequence. It appears that most GI cancer uptake studies rely primarily on the passive efflux from endothelial fenestrations via the EPR effect, and secondarily using biochemical targeting agents.

EPR Effect – Passive targeting

Most studies 12/16 (75%) did not involve GNP functionalisation with a targeting agent, solely utilising the EPR effect for tumour localisation. Goodrich *et al*. state that their previous experience using the concept of EPR for assessing the biodistribution of infused GNP to tumour found that less than 10% of the total injected dose actually reaches the tumour (101).

Biological Agents – Active targeting

Folic acid was used for targeting gastric cancer cells (97) while the A33 antigen (63, 108) and hyaluronic acid receptor (109) was used in targeting CRC. It remains to be proven if there is a definite combination of active and passive targeting that would provide ideal cancer targeting, but this would need to be balanced against the risks of provoking heat-induced bleeding or perforation if applied on more advanced (T3 or T4) cancers.

Cancer Models Used

There have been eleven *in vivo* rodent experiments, mostly with superficial tumours inoculated through subcutaneous injections of cancer cell lines in rodents (88, 97-102, 105, 108-110). Other ways of inducing cancer include intraperitoneal injection of Azoxymethane (AOM) in A/J mice. AOM treatment is used to induce colonic tumours as it mimics the adenoma-to-carcinoma sequence of CRCs in humans (109). Oesophageal cancer was induced orthotopically by mucosa-to-mucosa anastomosis between the lower oesophagus with the duodenum (102). In this study, GNPs were sprayed onto the surface of suspicious oesophageal mucosa via microendoscopy. The authors chose to do this as they cautioned that there is a real risk of GNPs becoming trapped in the interstitium of benign tissues with direct injection of GNPs.

The most common gastric cancer cell line used to induce cancer in murine models was MCG 803, while a variety of different cell lines were used to induce CRC, including (in order of popularity) CT26.wt (ATCC), HCT 116, HT-29, MC-38, SW1222 CRC cell lines. With regards to cancer cell studies, there is only one oesophageal study (102), one gastric cancer (103) and four colon cancer ones (63, 104, 106, 107). Overall, there has been a lack of published studies using the same cancer model, laser regime, fluorophore and GNPs (including similar concentrations) to make a valid and objective appraisal about the ideal protocol for a particular tumour type or the extent of its reproducibility. This is perhaps one key element that has hindered the progression of GNPs in clinical trials for GI cancer, whereas trials in other cancers have gone the distance. It highlights a need for more vigorous and streamlined reporting on key elements.

Irradiation Regimes

Vital pre-requisites for successful PTT include particle accumulation and appropriate laser dosimetry at an appropriate balance, for too high a laser exposure will entail excessive heating and collateral tissue damage, while too low a laser dose may result in incomplete ablation (101).

For cell studies, a mean laser fluence of 4.0 ± 1.1 W/cm^2 was used, while in rodents, a mean of 3.5 ± 1.7 W/cm^2 was applied for PTT. Most studies involving PTT used CW NIR laser, except one relying on acoustic cavitation induced by US (which also used intense pulsed light), two studies used X-rays and one a Ti:Sapphire laser. It is vital to accurately measure the thermal energy being delivered and the heating occurring, either with a thermal imaging

camera or a thermocouple. Equally crucial is the laser beam diameter and distance from the tip of the laser fibre to the tumour's surface for a real appreciation of the fluences required for the thermo-ablative responses seen.

Photothermal Effect, Hyperthermia and Cellular Destruction

While CW NIR lasers have been applied in eight studies for PTT and hyperthermia in GI cancer cells and tissues, only three have mentioned the temperature peaks achieved. One study used intense pulsed light in combination with US irradiation and GNP as a novel way to gain the desired therapeutic effect. X-ray irradiation was also used effectively in conjunction with CS-GNPs for thermal destruction of gastric cancer cells. The maximal temperatures obtained by irradiating *in vivo* GI cancer tissues in the presence of GNPs ranged from 50-62°C, but the three studies comprise different GNPs, concentrations and laser power. From these GNP studies, the mean laser fluence required to heat tissues to this temperature range was 4.5 W/cm^2.

It remains contentious whether there is a time-dependant peak of intracellular GNP concentration giving rise to an optimal therapeutic window for laser application. This issue should be addressed in future studies, and would involve imaging fluorophore-labelled GNPs at various time points.

Proving Endocytosis of Gold Nanoparticles

There is consensus that once internalised, GNPs do not enter the nucleus, but aggregate in vesicles within the cell. TEM is the most commonly used imaging modality employed to determine the size, shape and intracellular location of GNPs. Other techniques shown to be applicable for imaging, proving or quantifying GNPs within GI cells and tissues include dark field microscopy, inductively coupled plasma mass spectrometry, fluorescence protein labelling and imaging, fluorescent-based confocal microscopy, silver staining, Perl's Prussian blue staining (for iron-gold hybrid NPs) and neutron activation analysis.

Histological Evidence of Destruction and Cell Viability Studies

All studies used a variety of methods to assess cell viability after cell or tissue treatment with thermoradiation. The three most commonly used methods to demonstrate cytotoxicity or apoptosis were H & E staining and microscopy, followed by MTT assays and trypan blue staining.

Survival Studies / Follow-up - *In vivo* animal studies

Five studies presented longitudinal data from the application of GNPs and PTT. Two of these suggested that all murine models of CRC survived and nearly all had complete tumour regression after GNP and irradiation treatment (98, 100, 109). Where survival was studied, it is without doubt that the group of animals which received the combination of GNPs and laser lived the longest, and their survival was always statistically significant compared to other interventional arms or control groups (101, 105, 109). It is thus encouraging that when applied *in vivo* as a therapeutic modality for GI cancer, the GNP and NIR combination appears effective at regressing tumour and prolonging survival. This is the single most important therapeutic information that is consistently demonstrated in this review, and could potentially establish a firm foundation for clinical translation.

Imaging Modalities

GNPs have potential as X-ray and CT contrast agents due to their ability to induce strong X-ray attenuation (111) and are actively being investigated as a radiosensitiser. Within GI cancer, GNPs have been used as contrast agents in imaging modalities as diverse as MR, OCT, NIR Narrow Band Imaging and CT. The images obtained can also be used to monitor targeting and response to treatment. Kirui *et al*. synthesised iron-gold hybrid nanoparticles (HNP) and suggested that the iron oxide portion of the HNP served as the MR imaging agent, whilst the gold NP portion formed the hyperthermia agent (108).

Toxicity of Gold Nanoparticles

Data obtained from a host of methods including CCK-8, MTT assay, inductively coupled plasma mass spectrometry, neutron activation analysis and microscopy showed no apparent cytotoxicity from GNPs on cancer or healthy cells without the use of laser irradiation. This is important to know as there may be non-specific binding of GNPs to non-cancerous cells/tissues, and the route of administering GNPs into the systemic circulation avails itself to this probability. In an *in vivo* study comparing the different routes of administering GNPs and their corresponding toxicities, the authors noted that the oral and intraperitoneal routes demonstrated the highest toxicity levels, whilst the systemic route via the tail vein seemed to show the least toxicity (112).

The GNPs used in the studies have shown PEGylation is a reliable method of protecting cells from any potential cytotoxicity from CTAB. Goodrich *et al*. suggest that the largest

accumulation of GNPs *in vivo* was in the tumour followed by the liver and spleen, and the liver and spleen together accounted for approximately 75% of the injected GNPs on the first day (101), but this gradually cleared without any signs of acute toxicity throughout a 60 day period.

2.5 Discussion

The information presented here is encouraging in demonstrating that GNPs do have the potential to be excellent tumour targeting agents due to their ability to extravasate from leaky endothelial walls encompassing a GI tumour, and remain in-situ sufficiently long to absorb NIR light and generate heat that is then capable of destroying cancer cells. Active targeting to tumours can also be accomplished by conjugation with moieties that are over-expressed by cancer cells, namely antibodies, folic acid and peptides.

Further chemical refinement of NPs is being developed, such that the cytotoxicity of these particles is becoming much less pronounced. Despite the GI studies that have been conducted, we appear to be far away from conducting a clinical trial, unless there is a concerted effort to minimise variations in synthesised GNPs and the concentrations used in *in vivo* experiments. Thus further GI theranostics research needs to focus on the challenges remaining in representing nanotechnology as a viable and safe adjunct to surgery. This focus should not solely be on proving tumour regression, but also on examining acute and long term *in vivo* toxicity, with sufficiently powered studies which assess safe and optimal GNP doses and laser fluence.

This systematic review has identified a cohort of *in vivo* studies using GI cancer cells that have been implanted and grown subcutaneously in rodents, however there have only been two studies (102, 109) where the tumour has actually been established in an orthotopic (in-situ) model. Thermally ablating a superficial surface tumour with an external laser beam would present a lower risk profile than attempting the same endeavour intracorporeally with endoscopically-delivered NIR irradiation, where there would be additional factors and challenges to consider, but is vital to adequately assess and quantify that risk. In order to accomplish this, more orthotopic models of cancer should be studied with different modes of administering GNPs (intravenous, intratumoural or spraying) and laser treatment, in order to address the factors involved in bringing this technology to the forefront of clinical application. The depth of NIR penetration that can be efficaciously applied to a GI tumour region also needs to be quantified, so as to be certain about its applicability when given through the surface of the skin or organ. It is interesting in itself that none of the studies in

this review provided any information about the absorption or attenuation co-efficients of tissues with or without GNPs, but this is a factor that limits the depth of effective NIR delivery and thus heating.

It is without doubt that the NIR wavelength provides the optimal photo absorbance for clinical application, as it can be delivered deep into tissues by avoiding absorption or scattering by tissues and endogenous chromophores such as haemoglobin or bile. To take advantage of this clinically, it is imperative to be able to fibre-optically couple the delivery of NIR laser to pre-existing endoscopic and laparoscopic instruments, such that tumours that contain functionalised GNPs can be simultaneously identified and treated by NIR irradiation. Establishing this form of optical coupling and image-guided tumour therapy should be tested as a repeatable minimally-invasive procedure. Moving nanotechnology from the bench to the clinical arena will not only diminish the overall side-effects from non-specific systemic treatment (such as chemoradiation), it may also reduce collateral damage to healthy tissues.

Some of the impetus for improving the quality of *in vivo* GNP studies should be because it is anticipated that some cancers would be detected early through fluorescence imaging acquired during endoscopic procedures. Simultaneous PTT could then be performed at the same sitting while under sedation, arguably avoiding the need for general anaesthesia, while reducing personnel requirement, hastening post-procedural recovery and facilitating earlier discharge. It would also dramatically reduce surgical time, for example in early upper or lower GI cancers, performing endoscopic mucosal resection (EMR) or endoscopic submucosal dissection (ESD) would take the endoscopist a couple of hours, but the application of targeted laser via endoscopy would take a few seconds. This augurs well with today's enhanced recovery programmes, where there is a drive for more directed therapy, improved outcomes, reduction in soft tissue trauma, reduced complications/risks, reduced length of stay and cost-effectiveness. Nanotechnology also has the potential of being complementary to surgery, by being applicable post-operatively to tumour cavities and lymphatic tissues in order to reduce the risk of recurrence.

Equally important an issue for consideration in active targeting is tumour heterogeneity. Cancers are unique and vary from organ to organ, involving a mixture of malignant, non-malignant, stem and progenitor cells (113). It remains to be answered if it is possible to overcome this phenomenon by utilising the optical property of GNPs. It is envisaged that this could be performed by direct intratumoural injection of GNPs into the GI cancer, and then irradiating the site with NIR. This would have a particular palliative interest, primarily being useful in patients who are unfit for surgery or those who require tumour debulking for symptomatic relief, for instance from dysphagia due to tumour ingrowth from a stented

oesophageal carcinoma, vomiting and aspiration pneumonia from gastric outlet obstruction or subacute bowel obstruction from a difficult-to-stent and stenosing colorectal adenocarcinoma. Should there be sufficient grounds for a human clinical trial, it would be possible to extend this application to low volume metastatic lesions in the liver or peritoneum, whereby GNPs could be visually or ultrasonically injected intratumourally and NIR laser would be delivered through fibres during concurrent laparoscopy. The procedure is likely to need repeating, depending on the size and location of the lesion, but it should be relatively quick to do and uncomplicated, and could potentially significantly diminish the systemic inflammatory response syndrome and the surgical risks inherent from a hemi-hepatectomy. In addition to the benefits of utilising nanotechnology in late cancers, there remain unexplored yet intriguing avenues in the theranostics of early mucosal and submucosal tumours using a combination of optimal imaging techniques and targeted PTT, which are viable research platforms for the screening and early management of such lesions.

2.6 Conclusions

This systematic review has scrutinised the studies and collated results from the application of GNPs in the theranostics of upper and lower gastrointestinal cancer. The incorporation of a surface coating has certainly increased the biocompatibility and decreased the cytotoxicity of GNPs. Longitudinal survival studies of mice infused with varying volumes and OD of GNPs demonstrated much-needed objective confirmation that all the animals remained healthy during the study period, with evidence of prolonged survival in PTT studies. Although there appears to be an initial transient accumulation of gold chiefly in the liver and spleen after intravenous administration, this gradually dissipates sufficiently with no long-term sequelae or signs of toxicity in all *in vivo* studies.

The role of GNPs in providing diagnostic information is derived from the fact that GNPs are inherently dynamic optical contrast agents coupled with their ability to be further functionalised with NIR fluorophores which lends itself to being used in a variety of imaging techniques such as two-photon luminescence imaging, photoacoustic imaging, narrow band imaging and optical coherence tomography. This feature of optical absorption contrast and fluorescence to detect the location of GNPs within cancerous tissue would also guide the targeting of the NIR laser beam for therapy.

In terms of quantifying the efficacy of treatment on GI adenocarcinoma, all studies conducting photothermal therapy with gold nanoparticles showed cancer cell destruction and *in vivo* effects ranging from tumour volume regression to complete remission. The

hyperthermia induced by laser irradiation appeared to concentrate specifically on the tumour area, with sparing of surrounding healthy tissues, enabling this technology to ultimately be a useful adjunct to surgery and be delivered in a minimally invasive way. Before such an undertaking can be realised, concordance should be reached with regards to the type, size and concentration of GNPs, with the identification of a more robust, consistent and reproducible irradiation regime. Given the evidence of their safety and efficacy, achieving this congruity would provide the final necessary credentials to establish a much-needed clinical trial of gold nanoparticles in human GI cancer theranostics.

References

1. Akhter S, Ahmad M, Ahmad F, Storm G, Kok R. Gold nanoparticles in theranostic oncology: current state-of-the-art. Expert Opin Drug Deliv. 2012;9(10):1225-43.
2. Hutter E, Maysinger D. Gold nanoparticles and quantum dots for bioimaging. Microsc Res Tech. 2011;74(7):592-604.
3. Hutter E, Fendler JH. Exploitation of localized surface plasmon resonance. Adv Mater 2004;16(19):1685-706.
4. Dreaden EC, Alkilany AM, Huang X, Murphy CJ, El-Sayed MA. The golden age: gold nanoparticles for biomedicine. Chem Soc Rev. 2012;41(7):2740-79.
5. Dreaden EC, Mackey MA, Huang X, Kang B, El-Sayed MA. Beating cancer in multiple ways using nanogold. Chem Soc Rev. 2011;40(7):3391-404.
6. Ntziachristos V, Yodh AG, Schnall M, Chance B. Concurrent MRI and diffuse optical tomography of breast after indocyanine green enhancement. Proc Natl Acad Sci U S A. 2000;97(6):2767-72.
7. Rai P, Mallidi S, Zheng X, Rahmanzadeh R, Mir Y, Elrington S, Khurshid A, Hasan T. Development and applications of photo-triggered theranostic agents. Adv Drug Deliv Rev. 2010;62(11):1094-124.
8. Ahmad MZ, Akhter S, Rahman Z, Akhter S, Anwar M, Mallik N, Ahmad FJ. Nanometric gold in cancer nanotechnology: current status and future prospect. J Pharm Pharmacol. 2013;65(5):634-51.
9. Alkilany AM, Thompson LB, Boulos SP, Sisco PN, Murphy CJ. Gold nanorods: their potential for photothermal therapeutics and drug delivery, tempered by the complexity of their biological interactions. Adv Drug Deliv Rev. 2012;64(2):190-9.
10. Xu X, Cortie M. Shape change and color gamut in gold nanorods, dumbbells and dog-bones. Adv Funct Mater 2006;16:2170-6.
11. Hildebrandt B, Wust P, Ahlers O, Dieing A, Sreenivasa G, Kerner T, Felix R, Riess H. The cellular and molecular basis of hyperthermia. Crit Rev Oncol Hematol. 2002;43(1):33-56.
12. Oleson J, Samulski T, Leopold K, Clegg S, Dewhirst M, Dodge R, George S. Sensitivity of hyperthermia trial outcomes to temperature and time: implications for thermal goals of treatment. Int J Radiat Oncol Biol Phys 1993;25(2):289-97.
13. Huang X, Swierczewska M, Choi KY, Zhu L, Bhirde A, Park J, Kim K, Xie J, Niu G, Lee KC, Lee S, Chen X. Multiplex imaging of an intracellular proteolytic cascade by using a broad-spectrum nanoquencher. Angew Chem Int Ed Engl. 2012;51(7):1625-30.
14. Rautio J, Kumpulainen H, Heimbach T, Oliyai R, Oh D, Jarvinen T, Savolainen J. Prodrugs: design and clinical applications. Nat Rev Drug Discov. 2008;7(3):255-70.
15. Kim TH, Lee S, Chen X. Nanotheranostics for personalized medicine. Expert Rev Mol Diagn. 2013;13(3):257-69.

16. Retèl V, Hummel M, van Harten W. Review on early technology assessments of nanotechnologies in oncology. Molecular Oncology. 2009;3:394-401.
17. Hussein MA, Wood L, Hsi E, Srkalovic G, Karam M, Elson P, Bukowski RM. A Phase II trial of pegylated liposomal doxorubicin, vincristine, and reduced-dose dexamethasone combination therapy in newly diagnosed multiple myeloma patients. Cancer. 2002;95(10):2160-8.
18. Polanski M, Anderson NL. A list of candidate cancer biomarkers for targeted proteomics. Biomark Insights. 2007;1:1-48.
19. Anderson NL. The clinical plasma proteome: a survey of clinical asssays for proteins in plasma and serum. Clin Chem 2010;56:177-85.
20. Zhao Q, Wang L, Cheng R, Mao L, Arnold R, Howerth E, Chen Z, Platt S. Magnetic nanoparticle-based hyperthermia for head & neck cancer in mouse models. Theranostics. 2012;2:113-21.
21. Lim C, Shin J, Lee Y, Kim J, Oh K, Yuk S, Jeong S, Kwon I, S. K. Phthalocyanine-aggregated polymeric nanoparticles as tumor-homing near-infrared absorbers for photothermal therapy of cancer. Theranostics. 2012;2(9):871-9.
22. Milane L, Ganesh S, Shah S, Duan Z-F, Amiji M. Multi-modal strategies for overcoming tumor drug resistance: hypoxia, the Warburg effect, stem cells, and multifunctional nanotechnology. J Control Release. 2011;155(2):237-47.
23. Jordan A, Scholz R, Wust P, FaKhling H, Felix R. Magnetic fluid hyperthermia (MFH): Cancer treatment with AC magnetic field induced excitation of biocompatible superparamagnetic nanoparticles. Journal of Magnetism and Magnetic Materials. 1999;201(1-3):413-9.
24. Moore C, Pendse D, Emberton M. Photodynamic therapy for prostate cancer—a review of current status and future promise. Nat Clin Pract Urol. 2009;6:18-30.
25. Jang B, Park J, Tung C, Kim I, Choi Y. Gold nanorod-photosensitizer complex for near-infrared fluorescence imaging and photodynamic/photothermal therapy in vivo. ACS Nano. 2011;5(2):1086-94.
26. Allegra A, Penna G, Alonci A, Rizzo V, Russo S, Musolino C. Nanoparticles in oncology: the new theragnostic molecules. Anticancer Agents Med Chem. 2011;11(7):669-86.
27. Levi-Polyachenko NH, Stewart IV JH. Clinical Relevance of Nanoparticle Induced Hyperthermia for Drug Delivery and Treatment of Abdominal Cancers. The Open Nanomedicine Journal 2011;3:24-37.
28. Hu Z HF, Zhang Y, Chen C, Tu K, Jiang H, Wang L-Q. “Smart” Nanocarriers: A New Paradigm for Tumor Targeting Drug Delivery Systems. Drug Delivery Letters. 2011;1:67-84.
29. Hirsch LR, Stafford RJ, Bankson JA, Sershen SR, Rivera B, Price RE, Hazle JD, Halas NJ, West JL. Nanoshell-mediated near-infrared thermal therapy of tumors under magnetic resonance guidance. Proc Natl Acad Sci U S A. 2003;100(23):13549-54.
30. Shah N, Cerussi A, Eker C, Espinoza J, Butler J, Fishkin J, Hornung R, Tromberg B. Noninvasive functional optical spectroscopy of human breast tissue. Proc Natl Acad Sci U S A. 2001;98(8):4420-5.
31. Waldman SA, Fortina P, Surrey S, Hyslop T, Kricka LJ, Graves DJ. Opportunities for near-infrared thermal ablation of colorectal metastases by guanylyl cyclase C-targeted gold nanoshells. Future Oncol. 2006;2(6):705-16.
32. Maeda H. Tumor-selective delivery of macromolecular drugs via the EPR effect: background and future prospects. Bioconjug Chem. 2010;21(5):797-802.
33. Matsumura Y, Maeda H. A new concept for macromolecular therapeutics in cancer chemotherapy: mechanism of tumoritropic accumulation of proteins and the antitumor agent smancs. Cancer Res. 1986;46(12 Pt 1):6387-92.
34. Kommareddy S, Tiwari SB, Amiji MM. Long-circulating polymeric nanovectors for tumor-selective gene delivery. Technol Cancer Res Treat. 2005;4(6):615-25.
35. Sykes PD, Neoptolemos JP, Costello E, Halloran CM. Nanotechnology advances in upper gastrointestinal, liver and pancreatic cancer. Expert Rev Gastroenterol Hepatol.

2012;6(3):343-56.
36. Yuan F, Dellian M, Fukumura D, Leunig M, Berk D, Torchilin V, Jain R. Vascular permeability in a human tumor xenograft: molecular size dependence and cutoff size. Cancer Res 1995;55(17):3572-6.
37. Firth JA. Endothelial barriers: from hypothetical pores to membrane proteins. J Anat. 2002;200(6):541-8.
38. Perrault SD, Walkey C, Jennings T, Fischer HC, Chan WCW. Mediating tumor targeting efficiency of nanoparticles through design. Nano letters. 2009;9(5):1909-15.
39. Wisse E, Braet F, Luo D, De Zanger R, Jans D, Crabbé E, Vermoesen A. Structure and function of sinusoidal lining cells in the liver. Toxicol Pathol. 1996;24(1):100-11.
40. Carmeliet P, Jain RK. Angiogenesis in cancer and other diseases. Nature. 2000;407(6801):249-57.
41. Moghimi SM, Hunter AC, Murray JC. Long-circulating and target-specific nanoparticles: theory to practice. Pharmacol Rev 2001;53(2):283-318.
42. Hobbs SK, Monsky WL, Yuan F, Roberts WG, Griffith L, Torchilin VP, Jain RK. Regulation of transport pathways in tumor vessels: role of tumor type and microenvironment. Proc Natl Acad Sci U S A. 1998;95(8):4607-12.
43. Levine EA, Stewart JH, Russell GB, Geisinger KR, Loggie BL, Shen P. Cytoreductive surgery and intraperitoneal hyperthermic chemotherapy for peritoneal surface malignancy: experience with 501 procedures. J Am Coll Surg. 2007;204(5):943-53.
44. Sinha R, Kim GJ, Nie S, Shin DM. Nanotechnology in cancer therapeutics: bioconjugated nanoparticles for drug delivery. Mol Cancer Ther. 2006;5(8):1909-17.
45. Altintas I, Kok RJ, Schiffelers RM. Targeting epidermal growth factor receptor in tumors: from conventional monoclonal antibodies via heavy chain-only antibodies to nanobodies. Eur J Pharm Sci. 2012;45(4):399-407.
46. Ferrari M. Frontiers in cancer nanomedicine: directing mass transport through biological barriers. Trends Biotechnol. 2010;28(4):181-8.
47. Peter PE, John Meurig T. Gold in a metallic divided state—from Faraday to present-day nanoscience. Angew Chem Int Ed 2007;46:5480-6.
48. Tuval T, Gedanken A. A microwave-assisted polyol method for the deposition of silver nanoparticles on silica spheres. Nanotechnology. 2007;18:255601-8.
49. Abyaneh M, Paramanik D, Varma S, Gosavi S, Kulkarni S. Formation of gold nanoparticles in polymethylmethacrylate by UV irradiation. J Phys D Appl Phys 2007;40:3771-9.
50. Giorgetti E, Giusti A, Laza S, Marsili P, Giammanco F. Production of colloidal gold nanoparticles by picosecond laser ablation in liquids. Phys Status Solidi A 2007;204:1693-8.
51. Jin Y, Wang P, Yina D, Liu J, Qin L, Yu N, Xie G, Li B. Gold nanoparticles prepared by sonochemical method in thiol- functionalized ionic liquid. Colloid Surf A Physicochem Eng Aspects. 2007;302:366-70.
52. Nakamoto M, Yamamoto M, Fukusumi M. Thermolysis of gold(I) thiolate complexes producing novel gold nanoparticles passivated by alkyl groups. Chem Commun (Camb). 2002(15):1622-3.
53. Warren SC, Jackson AC, Cater-Cyker ZD, DiSalvo FJ, Wiesner U. Nanoparticle synthesis via the photochemical polythiol process. J Am Chem Soc. 2007;129(33):10072-3.
54. Mandal T, Fleming M, Walt D. Preparation of polymer coated gold nanoparticles by surface-confined living radical polymerization at ambient temperature. Nano Lett. 2002;2:3-7.
55. Alivisatos P. The use of nanocrystals in biological detection. Nat Biotechnol. 2004;22(1):47-52.
56. Katz E, Willner I. Integrated nanoparticle-biomolecule hybrid systems: synthesis, properties, and applications. Angew Chem Int Ed 2004;43:6042-108.
57. Murphy CJ, Sau TK, Gole AM, Orendorff CJ, Gao J, Gou L, Hunyadi SE, Li T. Anisotropic metal nanoparticles: Synthesis, assembly, and optical applications. J Phys Chem B. 2005;109(29):13857-70.
58. Stone J, Jackson S, Wright D. Biological applications of gold nanorods. Wiley

Interdiscip Rev Nanomed Nanobiotechnol. 2011;3(1):100-9.
59. Perez-Juste J, Pastoriza-Santos I, Liz-Marzan L, Mulvaney P. Gold nanorods: synthesis, characterization and applications. Coord Chem Rev 2005;249(1870-1901).
60. Yang D-P, Cui D-X. Advances and prospects of gold nanorods. Chem Asian J. 2008;3(12):2010-22.
61. Choi WI, Sahu A, Kim YH, Tae G. Photothermal cancer therapy and imaging based on gold nanorods. Ann Biomed Eng. 2012;40(2):534-46.
62. Alkilany AM, Nagaria PK, Hexel CR, Shaw TJ, Murphy CJ, Wyatt MD. Cellular uptake and cytotoxicity of gold nanorods: molecular origin of cytotoxicity and surface effects. Small. 2009;5(6):701-8.
63. Kirui DK, Krishnan S, Strickland AD, Batt CA. PAA-derived gold nanorods for cellular targeting and photothermal therapy. Macromol Biosci. 2011;11(6):779-88.
64. Ferrari M. Cancer nanotechnology: opportunities and challenges. Nat Rev Cancer 2005;5(3):161-71.
65. Ganta S, Devalapally H, Shahiwala A, Amiji M. A review of stimuli-responsive nanocarriers for drug and gene delivery. J Control Release. 2008;126(3):187-204.
66. Gabizon A, Martin F. Polyethylene glycol-coated (pegylated) liposomal doxorubicin. Rationale for use in solid tumours. Drugs. 1997;54 Suppl 4:15-21.
67. Davis ME, Chen ZG, Shin DM. Nanoparticle therapeutics: an emerging treatment modality for cancer. Nat Rev Drug Discov. 2008;7(9):771-82.
68. Chithrani B, Chan W. Elucidating the mechanism of cellular uptake and removal of protein-coated gold nanoparticles of different sizes and shapes. Nano letters. 2007;7(6):1542-50.
69. Takahashi H, Niidome T, Kawano T, Yamada S, Niidome Y. Surface modification of gold nanorods using layer-by-layer technique for cellular uptake. J Nanopart Res 2008;10:221-8.
70. Loo C, Lin A, Hirsch L, Lee M-H, Barton J, Halas N, West J, Drezek R. Nanoshell-enabled photonics-based imaging and therapy of cancer. Technol Cancer Res Treat. 2004;3(1):33-40.
71. Huang X, El-Sayed IH, Qian W, El-Sayed MA. Cancer cell imaging and photothermal therapy in the near-infrared region by using gold nanorods. J Am Chem Soc. 2006;128(6):2115-20.
72. von Maltzahn G, Park J-H, Agrawal A, Bandaru NK, Das SK, Sailor MJ, Bhatia SN. Computationally guided photothermal tumor therapy using long-circulating gold nanorod antennas. Cancer Res. 2009;69(9):3892-900.
73. Chen Y-S, Hung Y-C, Liau I, Huang GS. Assessment of the In Vivo Toxicity of Gold Nanoparticles. Nanoscale Res Lett. 2009;4(8):858-64.
74. Desai MP, Labhasetwar V, Amidon GL, Levy RJ. Gastrointestinal uptake of biodegradable microparticles: effect of particle size. Pharm Res. 1996;13(12):1838-45.
75. Hede S, Huilgol N. "Nano": the new nemesis of cancer. J Cancer Res Ther. 2006;2(4):186-95.
76. Moghimi S, Hunter A, Murray J. Nanomedicine: current status and future prospects. FASEB J 2005;19(3):311-30.
77. Thornton G. Materials science. Watching nanoparticles grow. Science. 2003;300(5624):1378-9.
78. Gratton SEA, Ropp PA, Pohlhaus PD, Luft JC, Madden VJ, Napier ME, DeSimone JM. The effect of particle design on cellular internalization pathways. Proc Natl Acad Sci U S A. 2008;105(33):11613-8.
79. Harush-Frenkel O, Rozentur E, Benita S, Altschuler Y. Surface charge of nanoparticles determines their endocytic and transcytotic pathway in polarized MDCK cells. Biomacromolecules. 2008;9(2):435-43.
80. Sahay G, Kim JO, Kabanov AV, Bronich TK. The exploitation of differential endocytic pathways in normal and tumor cells in the selective targeting of nanoparticulate chemotherapeutic agents. Biomaterials. 2010;31(5):923-33.
81. Lund T, Callaghan MF, Williams P, Turmaine M, Bachmann C, Rademacher T,

Roitt IM, Bayford R. The influence of ligand organization on the rate of uptake of gold nanoparticles by colorectal cancer cells. Biomaterials. 2011;32(36):9776-84.
82. Arvizo RR, Miranda OR, Thompson MA, Pabelick CM, Bhattacharya R, Robertson JD, Rotello VM, Prakash YS, Mukherjee P. Effect of nanoparticle surface charge at the plasma membrane and beyond. Nano letters. 2010;10(7):2543-8.
83. Zahr AS, Davis CA, Pishko MV. Macrophage uptake of core-shell nanoparticles surface modified with poly(ethylene glycol). Langmuir. 2006;22(19):8178-85.
84. Durr NJ, Larson T, Smith DK, Korgel BA, Sokolov K, Ben-Yakar A. Two-photon luminescence imaging of cancer cells using molecularly targeted gold nanorods. Nano letters. 2007;7(4):941-5.
85. Kim K, Huang S-W, Ashkenazi S, O'Donnell M, Agarwal A, Kotov N, Denny M, Kaplan M. Photoacoustic imaging of early inflammatory response using gold nanorods. Appl Phys Lett 2007;90:223901.
86. Park J, Estrada A, Schwartz JA, Diagaradjane P, Krishnan S, Dunn AK, Tunnell JW. Intra-organ Biodistribution of Gold Nanoparticles Using Intrinsic Two-photon Induced Photoluminescence. Lasers Surg Med. 2010;42(7):630-9.
87. Copland JA, Eghtedari M, Popov VL, Kotov N, Mamedova N, Motamedi M, Oraevsky AA. Bioconjugated gold nanoparticles as a molecular based contrast agent: implications for imaging of deep tumors using optoacoustic tomography. Mol Imaging Biol. 2004;6(5):341-9.
88. Puvanakrishnan P, Park J, Diagaradjane P, Schwartz JA, Coleman CL, Gill-Sharp KL, Sang KL, Payne JD, Krishnan S, Tunnell JW. Near-infrared narrow-band imaging of gold/silica nanoshells in tumors. J Biomed Opt. 2009;14(2):024044-.
89. Black KCL, Yi J, Rivera JG, Zelasko-Leon DC, Messersmith PB. Polydopamine-enabled surface functionalization of gold nanorods for cancer cell-targeted imaging and photothermal therapy. Nanomedicine (Lond). 2013;8(1):17-28.
90. Oldenburg AL, Hansen MN, Ralston TS, Wei A, Boppart SA. Imaging gold nanorods in excised human breast carcinoma by spectroscopic optical coherence tomography. J Mater Chem. 2009;19:6407-.
91. Cai Q-Y, Kim SH, Choi KS, Kim SY, Byun SJ, Kim KW, Park SH, Juhng SK, Yoon K-H. Colloidal gold nanoparticles as a blood-pool contrast agent for X-ray computed tomography in mice. Invest Radiol. 2007;42(12):797-806.
92. Kim D, Park S, Lee JH, Jeong YY, Jon S. Antibiofouling polymer-coated gold nanoparticles as a contrast agent for in vivo X-ray computed tomography imaging. J Am Chem Soc. 2007;129(24):7661-5.
93. Xie H, Goins B, Bao A, Wang ZJ, Phillips WT. Effect of intratumoral administration on biodistribution of 64Cu-labeled nanoshells. Int J Nanomedicine. 2012;7:2227-38.
94. Xie H, Wang ZJ, Bao A, Goins B, Phillips WT. In vivo PET imaging and biodistribution of radiolabeled gold nanoshells in rats with tumor xenografts. Int J Pharm. 2010;395(1-2):324-30.
95. Wang Y LY, Luehmann H, Xia X, Brown P, Jarreau C, Welch M, Xia Y. Evaluating the pharmacokinetics and in vivo cancer targeting capability of Au nanocages by positron emission tomography imaging. ACS Nano. 2012;6(7):5880-8.
96. Alessandro Liberati DGA, Jennifer Tetzlaff, Cynthia Mulrow, Peter C Gøtzsche, John P A Ioannidis, Mike Clarke, P J Devereaux, Jos Kleijnen, David Moher. The PRISMA statement for reporting systematic reviews and meta-analyses of studies that evaluate healthcare interventions: explanation and elaboration. British Medical Journal. 2009;339(b2535).
97. Huang P, Bao L, Zhang C, Lin J, Luo T, Yang D, He M, Li Z, Gao G, Gao B, Fu S, Cui D. Folic acid-conjugated silica-modified gold nanorods for X-ray/CT imaging-guided dual-mode radiation and photo-thermal therapy. Biomaterials. 2011;32(36):9796-809.
98. O'Neal DP, Hirsch LR, Halas NJ, Payne JD, West JL. Photo-thermal tumor ablation in mice using near infrared-absorbing nanoparticles. Cancer Lett. 2004;209(2):171-6.
99. Diagaradjane P, Shetty A, Wang JC, Elliott AM, Schwartz J, Shentu S, Park HC, Deorukhkar A, Stafford RJ, Cho SH, Tunnell JW, Hazle JD, Krishnan S. Modulation of in

vivo tumor radiation response via gold nanoshell-mediated vascular-focused hyperthermia: characterizing an integrated antihypoxic and localized vascular disrupting targeting strategy. Nano letters. 2008;8(5):1492-500.
100. Gobin AM, Lee MH, Halas NJ, James WD, Drezek RA, West JL. Near-infrared resonant nanoshells for combined optical imaging and photothermal cancer therapy. Nano letters. 2007;7(7):1929-34.
101. Goodrich GP, Bao L, Gill-Sharp K, Sang KL, Wang J, Payne JD. Photothermal therapy in a murine colon cancer model using near-infrared absorbing gold nanorods. J Biomed Opt. 2010;15(1):018001.
102. Li Y, Gobin AM, Dryden GW, Kang X, Xiao D, Li SP, Zhang G, Martin RCG. Infrared light-absorbing gold/gold sulfide nanoparticles induce cell death in esophageal adenocarcinoma. Int J Nanomedicine. 2013;8:2153-61.
103. Zhang C, Huang P, Bao L, He M, Luo T, Gao G, Cui D. Enhancement of gastric cell radiation sensitivity by chitosan-modified gold nanoparticles. J Nanosci Nanotechnol. 2011;11(11):9528-35.
104. Wu Y-N, Chen D-H, Shi X-Y, Lian C-C, Wang T-Y, Yeh C-S, Ratinac KR, Thordarson P, Braet F, Shieh D-B. Cancer-cell-specific cytotoxicity of non-oxidized iron elements in iron core-gold shell NPs. Nanomedicine. 2011;7(4):420-7.
105. Sazgarnia A, Shanei A, Taheri AR, Meibodi NT, Eshghi H, Attaran N, Shanei MM. Therapeutic effects of acoustic cavitation in the presence of gold nanoparticles on a colon tumor model. J Ultrasound Med. 2013;32(3):475-83.
106. Brown SD, Nativo P, Smith J-A, Stirling D, Edwards PR, Venugopal B, Flint DJ, Plumb JA, Graham D, Wheate NJ. Gold nanoparticles for the improved anticancer drug delivery of the active component of oxaliplatin. J Am Chem Soc. 2010;132(13):4678-84.
107. Black KC, Kirkpatrick ND, Troutman TS, Xu L, Vagner J, Gillies RJ, Barton JK, Utzinger U, Romanowski M. Gold nanorods targeted to delta opioid receptor: plasmon-resonant contrast and photothermal agents. Mol Imaging. 2008;7(1):50-7.
108. Kirui DK, Khalidov I, Wang Y, Batt CA. Targeted near-IR hybrid magnetic nanoparticles for in vivo cancer therapy and imaging. Nanomedicine. 2013;9(5):702-11.
109. Choi KY, Jeon EJ, Yoon HY, Lee BS, Na JH, Min KH, Kim SY, Myung S-J, Lee S, Chen X, Kwon IC, Choi K, Jeong SY, Kim K, Park JH. Theranostic nanoparticles based on PEGylated hyaluronic acid for the diagnosis, therapy and monitoring of colon cancer. Biomaterials. 2012;33(26):6186-93.
110. Paciotti GF, Myer L, Weinreich D, Goia D, Pavel N, McLaughlin RE, Tamarkin L. Colloidal gold: a novel nanoparticle vector for tumor directed drug delivery. Drug Deliv. 2004;11(3):169-83.
111. Popovtzer R, Agrawal A, Kotov NA, Popovtzer A, Balter J, Carey TE, Kopelman R. Targeted gold nanoparticles enable molecular CT imaging of cancer. Nano letters. 2008;8(12):4593-6.
112. Zhang X, Wu H, Di W, Wang Y, Chang J, Zhai Z, Meng A, Liu P, Zhang L, Fan F. Toxicologic effects of gold nanoparticles in vivo by different administration routes. Int J Nanomedicine 2010;5:771-81.
113. Bhattacharya S, Kudgus R, Bhattacharya R, Mukherjee P. Inorganic nanoparticles in cancer therapy. Pharm Res 2011;28(2):237-59.

Methods and Materials

CTAB-GNR synthesis

Mr. Yu Zhou MRes, a chemistry doctoral student at the Department of Chemistry, Imperial College London, fabricated the GNRs used for experiments using the seed-mediated approach described by Murphy *et al*. (1) and his own work. Cetyltrimethylammonium bromide (CTAB) was used as the surfactant (1) which forms a bilayer around the GNRs. Spherical 'seed' nanoparticles (~4 nm) are added to a growth solution containing gold sliver nitrate, salt, ascorbic acid and CTAB to produce GNRs with varying aspect ratios (AR) (2-4). Due to the variability in the absorption peak wavelength when creating GNRs using this method, many batches were made with different concentrations of silver nitrate until the absorption peak of the GNRs was at the appropriate wavelength of approximately 808 nm (measured with Perkin Elmer Lambda 25 UV/Vis Spectrophotometer, Waltham USA), which corresponds to the emission wavelength of our NIR laser diode. In Chapter 4 only CTAB-GNRs were used.

Chapters 3, 5, 6 and 7 used multifunctionalised GNRs. Multifunctionalised GNRs were fabricated when CTAB molecules on the surface of GNRs were replaced by carboxyl PEG. Subsequent EDC/NHS chemistry was used to functionalise GNRs with a fluorophore (Cy5.5) modified with an anti-EGFR antibody. Multifunctionalised GNRs were used in order to actively enhance tumour targeting efficiency rather than relying exclusively on the preferential passive accumulation of nanoparticles into tumours as a result of EPR. Although some authors have used purely PEGylated GNPs in tumour targeting, it is appreciated that the vast majority of these nanoparticles become absorbed by the reticuloendothelial system (RES) and < 10% of the injected GNPs actually reach the tumour site (5, 6). Functionalised GNRs are also more applicable for *in vivo* use, ensuring a higher intratumoural GNR accumulation, which then sets the stage for subsequent PTT.

We know from El-Sayed *et al*. (7) who have conjugated anti-EGFR-GNRs and then used them with irradiation on tumour cells, that by themselves anti-EGFR-GNRs do not exhibit cytotoxicity and yet selectively destroyed tumour cells without damaging healthy cells. It is known that many tumours over-express the EGFR antigen including those of the oesophagus, breast, colon, lung, ovary, head and neck, prostate and pancreas (8). The stepwise process of fabricating the multi-functionalised PEG-GNR-Cy5.5-anti-EGFR-antibody is described below.

Materials

CTAB was purchased from Calbiochem, while silver nitrate ($AgNO_3$), gold (III) chloride trihydrate ($HAuCl_4 \bullet 3H_2O$), sodium borohydride ($NaBH_4$), L-ascorbic acid (AA), N-(3-Dimethylaminopropyl)-N′-ethylcarbodiimide hydrochloride (EDC), N-Hydroxysuccinimide (NHS) and Potassium Carbonate (K_2CO_3) were all purchased from Sigma Aldrich. Heterobifunctional thiol carboxyl PEG [$HS\text{-}(O\text{-}CH_2\text{-}CH_2)_n\text{-}(CH_2)_2\text{-}COOH$], MW = 2 kDa was purchased from Nanocs, while DNAse/RNAse-free distilled water and phosphate buffered saline (PBS) solution were obtained from Life Technologies. Purified water (18.2 MΩ•cm) was produced by a Millipore water purification system. PerCP/Cy5.5 anti-human EGFR antibody was purchased from BioLegend® UK.

Preparation of the seed solution

9.75 ml of 0.1 M CTAB solution was added in a glass vial at 30°C under slow stirring. Meanwhile, 10 ml of 0.01 M $NaBH_4$ solution was prepared and inserted in ice for at least ten minutes. 0.25 ml of $HAuCl_4$ solution (0.01 M) was added into the CTAB solution followed by the addition of 0.6 ml of $NaBH_4$ solution under vigorous stirring. During this time, the colour of the solution should immediately change from bright yellow to brown. After five minutes, the solution was left undisturbed for one hour.

Growth of gold nanorods

The seed solution was then used to make GNRs. Different amounts of 0.01 M $AgNO_3$ (17 mg in 10 ml) in a water solution (130 µl $AgNO_3$ to achieve a GNR aspect ratio of 3.9, 0.01 M) were added to 9.5 ml of CTAB solution (0.1 M) under slow stirring at 30°C. Then 0.5 ml of $HAuCl_4$ solution (0.01 M), 55 µl of 0.1 M ascorbic acid (AA) solution and finally 12 µl of seed solution were also added to the mixture at 30°C. The colour of the solution changed from bright yellow to colourless after AA was added. The mixture was stirred for one minute and then left undisturbed in the dark for one hour. The colour change noted at approximately 15 minutes indicated the successful synthesis of GNRs.

After an hour, the solution was transferred into an eppendorf tube and centrifuged at 8500 rpm for 15 minutes at 30°C. Then the supernatant was decanted and the pellet was resuspended in 10 ml of PBS (pH=7.4). The GNR solution was stored at room temperature.

PEGylation of GNRs

Briefly, 10 ml of synthesised GNR solution was centrifuged twice at 8500 rpm for 15 minutes and then resuspended in 4 ml of water in order to reduce the CTAB concentration. Subsequently, 2 ml of K_2CO_3 buffer (2 mM) and 2 ml of HS-PEG-COOH solution (maintaining the stoichiometric ratio between GNRs and HS-PEG-COOH at 500,000:1) were added. The solution was sonicated for two hours to prevent aggregation and then left under continuous agitation overnight at room temperature in the dark. Next, the solution was centrifuged at 8500 rpm for 15 minutes at 30°C. The supernatant was decanted and the pellet precipitate was redispersed in 10 ml of PBS buffer (pH = 7.4) in an eppendorf tube covered with aluminum foil. Spectral and ζ-potential measurements were performed before and after ligand conjugation to confirm functionalisation of GNRs with thiol carboxyl PEG (COOH-PEG-GNRs).

Functionalisation of GNRs

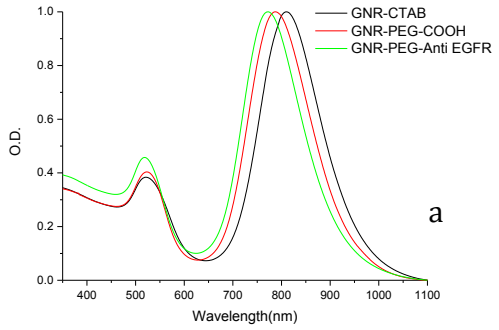
In a classical experiment, 4 ml of GNR-PEG-COOH solution was placed into a glass vial. Then 0.5 ml 0.4 M 1-Ethyl-3-[3-dimethylaminopropyl] carbodiimide hydrochloride (EDC) and 0.5 ml 0.1 M N-hydroxysulfosuccinimide (NHS) agents were added respectively. The mixture was put on a rotary shaker for 20 minutes and then centrifuged at 8500 rpm for fifteen minutes. The supernatant was decanted and distilled DNAse/RNAse-free water was added to the precipitate to make up to a total volume of 4 ml before adding modified Cy5.5 anti-human EGFR antibody (GNR:Anti-EGFR = 1:1000) (PerCP/Cy5.5 anti-human EGFR antibody, BioLegend®, London, UK). The solution was left on a rotary shaker for four hours and then centrifuged. The supernatant was decanted and the pellet was redispersed in 2 ml of distilled DNAse/RNAse-free water in an eppendorf tube covered with aluminium foil. Absorption spectra, ζ-potential measurements and fluorescence emission spectra were checked to verify GNR-PEG-Anti-EGFR-Cy5.5 conjugation (Fig. M1). The final solution was stored in the fridge at 4°C. The binding between GNR-PEG and Anti-EGFR-antibody-Cy5.5 is covalent. The size of the GNR is approximately 50 nm. PEG-Anti-EGFR which coats the GNRs is about 32 nm thick, and the Cy5.5 stands proud of this layer, making the Cy5.5 fluorophore approximately 32 nm away from the surface of the GNRs.

Characterisation of GNRs

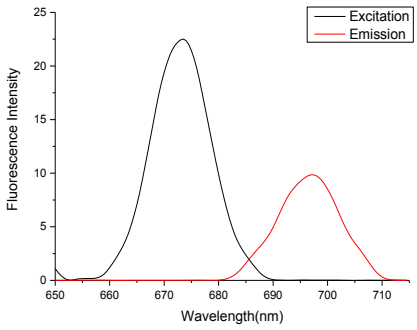
The optical density and light absorption profile of GNRs was measured using a UV-Vis spectrophotometer (Perkin Elmer, USA), while fluorescence spectra were measured using a Fluorolog-3 478 fluorometer (HORIBA, Jobin Yvon, USA). Pre- and post-functionalisation spectra were measured. ζ-potential was calculated using a Zetasizer Nano ZS90 dynamic light scattering (DLS) System (Malvern Instruments Ltd., Worcestershire, UK). Although an indirect means of characterising the surface of GNRs, its advantage lies in characterising the GNRs themselves and not any free molecules within the same solution. Fabricated GNRs were characterised further by transmission electron microscopy (TEM JEOL JEM-2000FX, Tokyo Japan). The stability of colloidal GNR suspension was carefully monitored over several weeks via UV-Vis spectrophotometry, DLS and ζ-potential measurements.

Optical density

Optical density is absorbance (A) that is normalised to the optical pass length (i.e. 'L' in Beer-Lambert law). OD = A/L. 'L' is the length of solution the light has to pass through (cm). In our experiments spectroscopic measurements were done in a cuvette of 1 cm. Therefore OD = A /1 or OD = A. The optical density is thus identical to the absorbance.



a



b

	Zeta Potential(mV)
GNR-CTAB	+ 62.8 ± 4
GNR-PEG-COOH	- 3 ± 1.5
GNR-PEG-Anti EGFR	- 11.6 ± 1.2

c

Fig. M1 The (a) absorption and (b) fluorescence spectra with (c) ζ-potential values of multi-functionalised GNRs. Fluorescence emission of GNR-PEG-Anti-EGFR-Cy5.5 was done in a water solution after purification from any unreacted Cy5.5-Anti-EGFR antibody.

The SPR of the GNRs was measured to be at 808 nm, which corresponded to an $OD_{\lambda = 808}$ of 26.4. Extinction spectra of PEGylated GNRs in normal saline suspensions did not show a peak shift, broadening or attenuation over a period of a month prior to injection. Although this OD is lower than those reported in some other *in vivo* studies, it was the highest concentration that was possible for us to synthesise, but was nevertheless fit for purpose in subsequent *in vivo* experiments. From the spectrophotometer results, we can see that the process of PEGylation, which is essential to mitigate the toxicity element for *in vivo* GNR application, neither mitigated the absorption co-efficient nor induced a wavelength shift, even after multi-functionalisation with fluorophore and anti-EGFR antibody. This strong stability was fundamental in ensuring that we would be optimising the SPR of the functionalised GNRs with our 808 nm NIR laser. This, together with the absence of plasmon coupling, further demonstrated that the particles remained well dispersed and did not aggregate during the functionalisation process, giving credence to the ability of PEG to effectively insulate GNPs from non-specific binding, remain stable and not aggregate, all of which are factors which will be particularly crucial *in vivo*.

The surface charge (zeta potential) of the GNRs after functionalisation was appropriately anionic. The change from a strongly positive to slightly negative charge meant there was good replacement of CTAB ligands on GNRs (9). Some studies suggest that cationic GNRs are more toxic when compared to neutral or anionic ones (10, 11). Murphy *et al*. (12, 13) argue that charge does not matter once GNRs are incubated in biological media, where strong interactions are established with proteins. These interactions would convert their ultimate charge to a negative one, whatever their initial charge may have been. Another study hypothesizes that intravenous administration of strongly negatively charged GNPs (-44 mV) leads to their rapid circulatory clearance and higher absorption by the reticuloendothelial system (RES) comprising chiefly of the liver/spleen (14). The relative inconsequence of the surface charge of GNRs has already been expounded in Chapter 2.

We observed good stability and dispersibility of the PEG-Cy5.5-anti-EGFR-antibody gold nanorods in both water and organic solutions, and, as with other studies, showed excellent biocompatibility *in vivo* through the process of PEGylation.

Transmission electron microscopy (TEM) of tissues and EDX analysis

Dr. Pakatip Ruenraroengsak PhD, a Research Associate, performed TEM analyses on tissues. Briefly, dissected tissue specimens were washed (x3) with 0.9% NaCl (saline) solution followed by another wash with sodium cacodylate buffer solution, at a pH of 7.4, before being fixed with 2.5% glutaraldehyde solution for two hours at 4°C. The tissue specimens were then washed three times with sodium cacodylate buffer solution, and stained with 1% osmium containing 2% potassium ferrocyanide for two hours, and washed with distilled deionised water (x3) and incubated overnight with 1% uranyl acetate in cacodylate buffer at 4°C before *en bloc* Walton's lead aspartate staining was performed. The samples were subsequently dehydrated with 25%, 50%, 70%, 90% and 100% anhydrous ethanol for 15 minutes (x3) each, before being placed in anhydrous ice-cold acetone and left at room temperature for 20 minutes (x3). Durcupan ACM is used as the resin. The samples are then placed into 25%, 50% and finally 75% Durcupan: acetone for two hours each. Tissues were placed in 100% Durcupan overnight, then into fresh 100% Durcupan for two hours. The resulting resin block was then sectioned with a diamond knife ultramicrotome. Each section was 50-70 nm thick, and placed on copper grids before viewing using TEM (TEM JEM 2100F, operated at 200 kV) and energy-dispersive X-ray spectroscopy (EDX/EDS) was used for further characterisation (X-Max 80 mm^2, Oxford Instruments, UK).

References

1. Yang JA, Lohse, S.E., Boulos, S.P., Murphy, C.J. The Early Life of Gold Nanorods: Temporal Separation of Anisotropic and Isotropic Growth Modes. J Clust Sci. 2012;23:799-809.
2. Stone J, Jackson S, Wright D. Biological applications of gold nanorods. Wires Nanomed Nanobi. 2011;3(1):100-9.
3. Murphy CJ, San TK, Gole AM, Orendorff CJ, Gao JX, Gou L, Hunyadi SE, Li T. Anisotropic metal nanoparticles: Synthesis, assembly, and optical applications. Journal of Physical Chemistry B. 2005;109(29):13857-70.
4. Yang DP, Cui DX. Advances and Prospects of Gold Nanorods. Chem-Asian J. 2008;3(12):2010-22.
5. Goodrich GP, Bao LL, Gill-Sharp K, Sang KL, Wang J, Payne JD. Photothermal therapy in a murine colon cancer model using near-infrared absorbing gold nanorods. Journal of Biomedical Optics. 2010;15(1).
6. Schwartz JA, Price RE, Gill-Sharp KL, Sang KL, Khorchani J, Goodwin BS, Payne JD. Selective Nanoparticle-Directed Ablation of the Canine Prostate. Laser Surg Med. 2011;43(3):213-20.
7. Huang XH, El-Sayed IH, Qian W, El-Sayed MA. Cancer cell imaging and photothermal therapy in the near-infrared region by using gold nanorods. Journal of the American Chemical Society. 2006;128(6):2115-20.

8. Yarden Y, Sliwkowski MX. Untangling the ErbB signalling network. Nat Rev Mol Cell Bio. 2001;2(2):127-37.
9. Liu XS, Huang N, Li H, Wang HB, Jin Q, Ji J. Multidentate Polyethylene Glycol Modified Gold Nanorods for in Vivo Near-Infrared Photothermal Cancer Therapy. Acs Appl Mater Inter. 2014;6(8):5657-68.
10. Loretz B, Bernkop-Schnurch A. In vitro cytotoxicity testing of non-thiolated and thiolated chitosan nanoparticles for oral gene delivery. Nanotoxicology. 2007;1(2):139-48.
11. Goodman CM, McCusker CD, Yilmaz T, Rotello VM. Toxicity of gold nanoparticles functionalized with cationic and anionic side chains. Bioconjugate Chem. 2004;15(4):897-900.
12. Alkilany AM, Murphy CJ. Toxicity and cellular uptake of gold nanoparticles: what we have learned so far? J Nanopart Res. 2010;12(7):2313-33.
13. Alkilany AM, Nagaria PK, Hexel CR, Shaw TJ, Murphy CJ, Wyatt MD. Cellular Uptake and Cytotoxicity of Gold Nanorods: Molecular Origin of Cytotoxicity and Surface Effects. Small. 2009;5(6):701-8.
14. Gormley AJ, Malugin A, Ray A, Robinson R, Ghandehari H. Biological evaluation of RGDfK-gold nanorod conjugates for prostate cancer treatment. J Drug Target. 2011;19(10):915-24.

Chapter 3 Gold nanorod reshaping *in vitro* and *in vivo* using a continuous wave laser

3.1 Introduction[1]

Continuous wave (CW) lasers with fluences of 2-10 W/cm^2 were used in several studies for testing photothermal therapy with GNRs (1-5). As CW lasers are generally less expensive, smaller and more portable than their pulsed counterparts, they are currently the more clinically compatible of the two types of photothermal therapy sources. It has also been shown by Kirui *et al*. (6) that there may be potential for fractionating the irradiation regime and delivering CW laser light over several rounds of therapy, using a laser fluence of 5 W/cm^2. Previous studies have shown that applying highly energetic pulsed nanosecond or femtosecond laser light pulses causes nanorods to deform or change shape via a melting process (7-15). This shape change causes the nanorod optical absorption peak to shift, and the optical absorption may decrease.

It has also been shown by Mohamed *et al.* (16) that heating with only a thermostatically controlled water bath can alter the GNR shape, decreasing their aspect ratio and SPR peak wavelength by increasing temperature. When tumours are large, photothermal therapy using GNRs may require repeated application. It has not been established whether re-application of CW laser to a previously irradiated site would be as photothermally effective as the initial laser application in the presence of pre-existing irradiated GNRs within the tumour site. This is because CW-induced GNR shape change from laser irradiation has not yet been investigated and is thus addressed by this study. This is a crucial factor since any reduction in absorption coefficient at the therapeutic laser wavelength due to GNR reshaping will reduce the heating effect and thus reduce the impact of the laser thermal therapy for subsequent irradiation at the same wavelength, making it significantly less effective.

Remote monitoring of the thermal heating of GNRs can be achieved, in solution and in tissue, using a thermal imaging camera. For instance Chou *et al.* (17) have shown a reduction in GNR sample heating after 5 and 60 seconds of 146 mW CW laser irradiation (785 nm), both when the sample was diluted and when the SPR peak was at a different wavelength. No analysis of the nanorods' shapes, or spectra, post CW laser irradiation was presented in this

[1] This chapter is adapted from a manuscript prepared for submission.

paper. Although GNR laser heating is dependent on the optical absorption, thermal imaging does not provide a direct measure of optical absorption; therefore it cannot measure GNR bleaching. The most common approach to measure changes in GNR optical properties is using optical spectroscopy. However, this is best done before and after the irradiation, as during irradiation the laser light may saturate the photodetector (normally a CCD or photodiode) in the spectral region of interest, and can therefore not be used to monitor the shape change dynamics during therapy.

Photoacoustics (PA) uses the optical absorption of pulsed laser light by materials to generate an acoustic wave that may be detected by an ultrasound transducer (18). GNRs have been shown to be a good PA contrast agent due to their strong optical absorption (18-24). Therefore PA should be able to monitor the destruction and reshaping of GNRs over time due to laser heating by a high power CW laser.

3.2 Methods

3.2.1 Synthesis

Three different batches of CTAB-GNRs (samples $\boldsymbol{\alpha, \beta}$ and $\boldsymbol{\gamma}$) were tested to check repeatability *in vitro*. For *in vivo* experiments, multifunctional GNRs (PEG-GNR-Cy5.5-Anti-EGFR-antibody) were used in rodents. Synthesis is described in Methods & Materials.

3.2.2 Irradiation and monitoring

These experiments were performed together with Dr. Davis Harris-Birtill PhD, a Research Associate. A preliminary validation experiment on a single concentrated GNR solution sample contained within an optically transparent cuvette (GNRs with an optical density of 0.75 at 808 nm, which corresponded to the emission peak of our CW laser) was tested with CW laser irradiation and the general effect on the GNRs post irradiation was visualised with a transmission electron microscope (TEM), (TEM JEOL JEM-2000FX, Tokyo Japan). Following this preliminary experiment, the actual study experiments comprised 3 ml aliquots of a newly prepared GNR solution (with varying optical densities) which were pipetted into an optically transparent membrane dish and irradiated for 5 minutes using a CW laser (DenLase-810/7, Beijing China) emitting at 808 nm with a power of 6 W and a beam area of 1 cm^2 at the sample surface. The solution was then removed and the dish was washed twice with water. One aliquot of GNRs was also used to evaluate the effect of increased CW laser

fluence. For this sample the beam area was reduced to 0.5 cm^2 while maintaining 6 W laser power, effectively increasing the fluence to 12 W/cm^2. For this case the irradiation time was reduced to 45 seconds, because the solution heated so rapidly that it started to boil.

To monitor the heating and GNR destruction, thermal imaging and photoacoustics were used; the experimental setup is shown in Fig. 3-1. To enable acoustic transmission from the sample to the ultrasound transducer, the base of the sample dish was in contact with the water bath below, and bubbles under the membrane were removed before starting. A very thin Mylar™ membrane was intentionally used (75 μm thick) to ensure minimal acoustic attenuation. For the PA light source a Nd:YAG pumped optical parametric oscillator (OPO) laser (Quantel Brilliant B with Rainbow OPO, Les Ulis France) was used which had a 7 ns laser pulse at 1 Hz repetition rate, a wavelength of 808 nm, a measured mean energy of 20.3 ± 1.5 mJ per pulse (where the error is the standard deviation measured over all 1800 pulses during the experiment), with a beam area at the sample surface of 200 mm^2. To check that the PA laser pulse did not cause GNR reshaping, a control was made for each sample with the CW laser switched off, and these samples were removed and analysed with spectroscopy and electron microscopy. The CW and PA lasers were both optimally attuned to the SPR wavelength of the GNRs. This enabled monitoring of any changes occurring to the GNRs arising from the CW laser using PA signal, as the GNRs would potentially be reshaped from the CW laser at that wavelength. This further enabled investigation into the reshaping effects arising from both lasers being delivered at the same wavelength.

For each laser pulse, a PC recorded the laser energy detected by the energy meter (Gentec-eo Solo2, Quebec Canada). An oscilloscope recorded the PA pulse detected by the ultrasound transducer[2] in response to the laser energy absorbed by the sample, using an electronic TTL (Transistor-Transistor Logic) pulse from the laser at the time of Q-switching as a trigger. The thermal imaging camera (FLIR Systems ThemaCAM S65, Wilsonville USA) was manually triggered at the beginning of the irradiation and set to acquire images at 1 Hz frame rate for the length of the irradiation. The thermal imaging camera has a field of view of 24° x 18°, with a thermal sensitivity of 0.08°C, a detector resolution of 320x240, a spectral range of 7.5 to 13 μm, and a reading accuracy of ± 2%. The CW laser was also manually triggered at the start of the PA and thermal imaging acquisitions.

[2] The ultrasound transducer has a measured 6.5 MHz centre frequency with a bandwidth of 4.5 MHz full width at half maximum (FWHM) amplitude, with a distance to focal maximum of 73.5 mm and FWHM pressure amplitude beam width of 17.5 mm axial by 1 mm radial measured using a beam profiling system (Precision Acoustics UMS).

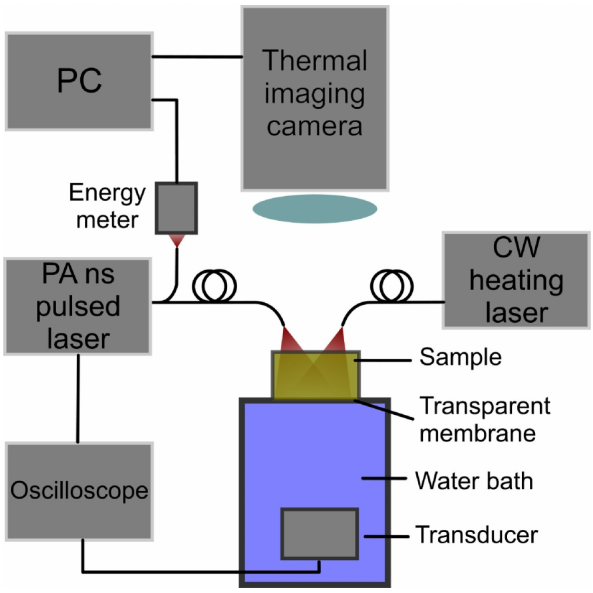


Fig. 3-1 The experimental set-up for monitoring GNR reshaping during CW laser application, using both PA and thermal imaging. Curved lines represent optical fibres and straight lines represent electronic connections.

3.2.3 Chemical and microscopic analysis

Samples from before and after irradiation were placed into cuvettes and the absorbance spectra were measured using the transmission spectrophotometer. A drop of each sample was then placed onto a carbon grid and air dried for imaging with TEM at 25,000x magnification. This allowed visualisation of the shape changes that occurred, and the length and width of each distinguishable GNR in all images acquired for all samples were measured. This involved manually locating the ends of each GNR in the images, and ignoring the spheres present, using ImageJ to measure the lengths, and then locating the centre to measure their widths. The aspect ratio of each GNR was calculated by dividing the length by the width, and the mean and standard deviation of the lengths, widths, and aspect ratios were then calculated.

3.2.4 Thermal image analysis

For each acquisition a region of interest (ROI) was selected for the sample and for a background region. The mean and standard deviation of the pixels within the ROI for each frame were then calculated. Any change in background temperature was subtracted from the

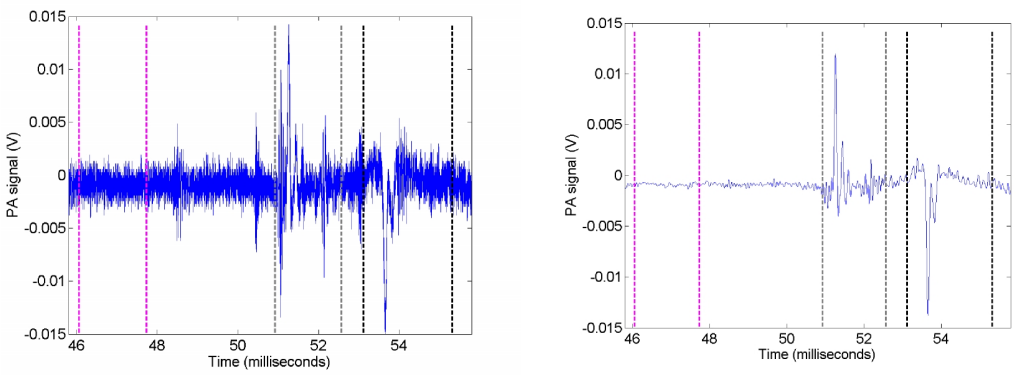
sample temperature to provide a background corrected temperature rise over time due to laser heating.

3.2.5 PA data and pulsed laser energy

A low pass filter (cut-off at 15 MHz) was applied in the frequency domain using Matlab to remove the PA high frequency noise, setting all frequency content above 15 MHz to zero, as illustrated in Fig. 3-2. Three intervals of the temporal PA response were extracted for analysis: one corresponding to the PA response from the top of the sample (V_{t}), one from the bottom of the sample (V_{b}), and one for the background (V_{b}), as illustrated by the dotted vertical lines in Fig. 3-2. The absolute value of the PA voltage response for each laser pulse was integrated over these intervals and divided by the interval time to obtain a measure of the sample PA strength (derived from V_{t} and V_{b}), and the background level (derived from V_{b}). The final PA signal was calculated by subtracting the background level from the sample PA strength and was normalised by the corresponding laser energy for each pulse ($F(t)$) using this equation:

$$V_{s}(t) = \frac{V_{t}(t) + V_{b}(t) - 2V_{bac}(t)}{F(t)} \quad [1]$$

This was repeated for each pulse in the sequence and for every sample.



(a) **(b)**

Fig. 3-2 Example measured PA response (a), and after low pass filtering (b). Here the time periods corresponding to the background (magenta), the bottom of the sample (grey), and the top of the sample (black) are indicated between the vertical dashed lines.

3.2.6 *In vivo* analysis of GNRs in tumour-bearing and tumour-irradiated mice

With ethics approval (UK Home Office project licence number PPL 70/7996), immunodeficient BALB/c nu/nu mice were inoculated subcutaneously with a human oesophageal adenocarcinoma cell line (FLO-1 cells) and developed solid tumours of at least 5 mm prior to any intervention. This generally matured within a fortnight following inoculation. Study mice were then injected intratumourally with 50 µl of aqueous GNR solution. These GNRs were PEGylated and functionalised with a fluorophore (Cy 5.5) modified with anti-EGFR antibody, and had an $OD_{\lambda\text{-}808nm}$ of 13.2. In one group of mice, tumour sites were biopsied for microscopic examination for the presence of intracellular GNRs. In another group of mice, tumours that received intratumoural (IT) injections of GNRs were then irradiated with the same CW NIR laser used in the previous *in vitro* study but now emitting at a power of 1.6 W with a beam diameter of 6 mm at the tumour surface for three minutes. NIR irradiation was performed under general anaesthesia (with an intraperitoneal injection of ketamine and xylazine) alongside post-procedural analgesia on the same day of administering GNRs. Temperature changes occurring within the irradiated tumour site was measured with the thermal imaging camera mounted above the mouse. Temperature rise analysis was performed in a manner akin to the *in vitro* study, with subtraction from background and baseline temperatures.

Tumours sites were examined on the day of GNR administration and daily until day 30 post-irradiation. One half of the tumour sample was processed for microscopic evaluation of tumour cells, while the other half of the sample was analysed using bright field transmission electron microscopy (TEM JEM 2100F) and energy-dispersive X-ray spectroscopy (EDX, X-Max 80 mm^2, Oxford Instruments, UK). The same examination was performed of irradiated tumour sites which were excised at day 30 post irradiation.

3.2.7 Transmission electron microscopy (TEM)

TEM analyses was performed on dissected tissue specimens which were fixed into a resin block which was then sectioned to 50-70 nm thick, and placed on copper grids before viewing using TEM (TEM JEM 2100F, operated at 200 kV) and EDX was used for further characterisation. At least 20 cells per ROI were observed from each tissue (n=2) with total view of 40 cells. The methods of tissue preparation have been mentioned in Methods and Materials.

3.3 **Results**

The absorbance of the samples showed consistent decreases in absorption of the SPRs at the laser wavelength (the second peak) after irradiation of all three samples, as shown in Fig. 3-3. With CW irradiation the spectral peak of GNRs shifted towards the blue, suggesting that the GNRs decreased in length (this is confirmed with their aspect ratio measurements in Table 3-1), while the absorption at wavelengths further from the laser was better preserved, suggesting the rods of the shape and size corresponding to high absorption at the laser wavelength were preferentially destroyed. There was a decrease in the GNR absorbance spectral peaks when irradiated with the PA pulsed laser, and yet the SPR peak wavelength did not change, therefore these GNRs are unlikely to have changed to shorter rods as this would lead to a SPR peak of shorter wavelength. This decrease in the longitudinal mode suggests a reduction in the number of GNRs, not a change in GNR length, as the spectral shape remains the same with PA pulsed wave laser irradiation. With CW laser the transverse mode peak (at around 530 nm) increased while their SPR peaks not only diminished but their wavelengths also decreased, suggesting some GNRs may be converted into spheres, as spheres contribute to this transverse mode peak and blue shift in SPR. The sample that received twice the CW laser fluence exhibited a further decrease in peak absorption and decrease in SPR wavelength.

Using the Beer-Lambert equation, the Absorption (A) = ε l c. As shown in Fig. 3-3, the peak absorption of sample α at 808 nm is 1.95. The optical path length l is 1 cm. The molar extinction coefficient ε was determined by plotting the absorption (same as the OD) of GNRs solution against concentration c. The gradient of this line of best-fit line equals the extinction coefficient of GNRs and was estimated to be $\varepsilon = 5.6 \pm 0.4 \times 10^{9}$ M^{-1} cm^{-1} at $SPR_{\lambda=808nm}$. Thus the concentration of GNRs at the $SPR_{\lambda=808nm}$ in sample α was calculated to be 3.5×10^{-8} M, sample β was 2.7×10^{-8} M and sample γ was 1.7×10^{-8} M.

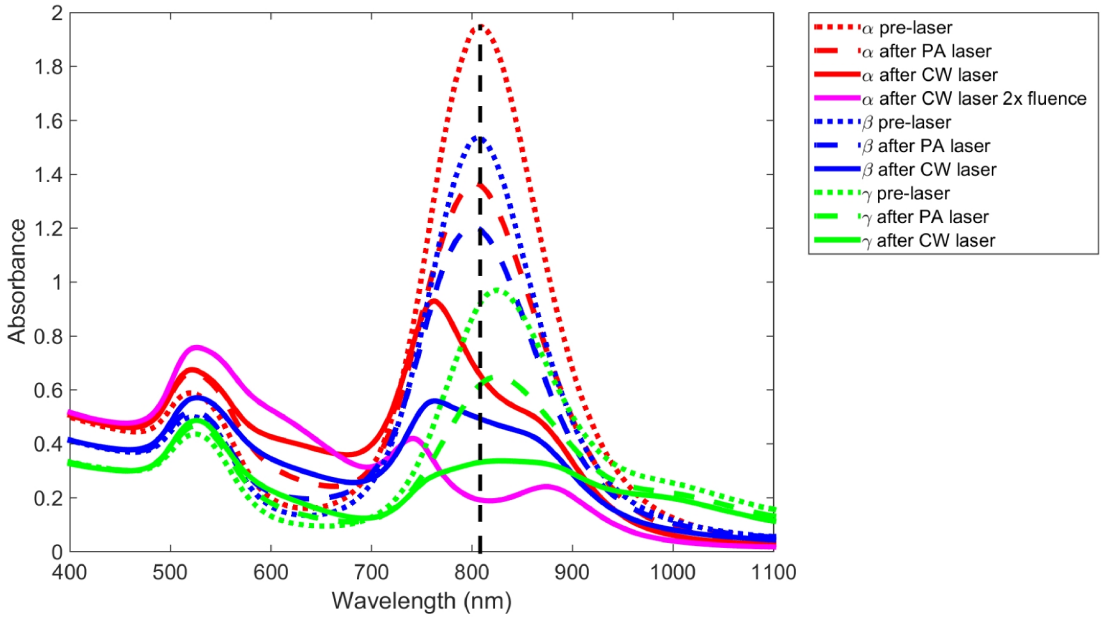


Fig. 3-3 Measured absorbance spectra of original GNRs (dotted lines), after PA pulsed laser only (dashed lines), and after 6 W/cm^2 CW laser light for 5 minutes (solid lines) across the three batches [red (sample α), blue (sample β) and green (sample γ)]. The magenta line refers to sample α after 12 W/cm^2 laser light irradiation for 45 seconds. The black dashed line indicates the wavelength of the CW laser.

Sample γ, with results represented with a green line in Fig. 3-3, had a slightly longer SPR peak than the laser wavelength. Therefore rods with an aspect ratio corresponding to the SPR peak were not heated optimally. Furthermore this sample was slightly less concentrated than the other samples, as shown by the original lower absorbance; both factors contributed to the lower temperature rise when compared with the other samples (as shown in Fig. 3-4).

	Sample α pre-laser	Sample α after pulsed laser	Sample α after CW laser	Sample α after 2x fluence CW laser	Sample β pre-laser	Sample β after CW laser
Number of GNPs measured	203	122	566	485	140	87
Length (nm)	43.1 ± 7.7	42.1 ± 6.8	39.5 ± 7.5	35.8 ± 6.6	44.3 ± 4.9	34.8 ± 8.2
Width (nm)	11.5 ± 2.3	13.3 ± 2.2	14.4 ± 2.5	16.2 ± 2.6	11.6 ± 1.2	13.4 ± 2.8
Aspect ratio	3.8 ± 0.5	3.3 ± 0.8	2.9 ± 0.9	2.3 ± 0.8	3.9 ± 0.6	2.8 ± 1.0

Table 3-1 The mean lengths, widths and aspect ratios of GNRs as measured manually from TEM images for two of the samples for each irradiation type. All errors show the standard deviation.

After measuring the lengths and widths, and subsequently calculating the aspect ratios of 1603 GNRs from TEM datasets, the mean dimensions were calculated for two of the three samples for all irradiation types, including before and after pulsed and CW laser irradiation, and these values are shown in Table 3-1. This consistently shows that the length of the rods is reduced while the width is increased leading to a decreased aspect ratio. These length and width measurements also illustrate that nanorods reshape to become more spherical, which in turn explains the increase in the 530 nm transverse plasmon resonance peak seen in the absorption spectra of the irradiated samples in Fig. 3-3. When twice the laser fluence was applied, a correspondingly larger effect was observed.

The temperature profile from each sample, with and without the 6 W/cm^2 CW irradiation is shown in Fig. 3-4. All three samples heated dramatically during irradiation with a rise between 10 and 25°C, with the majority of the heating occurring within the first 10 seconds.

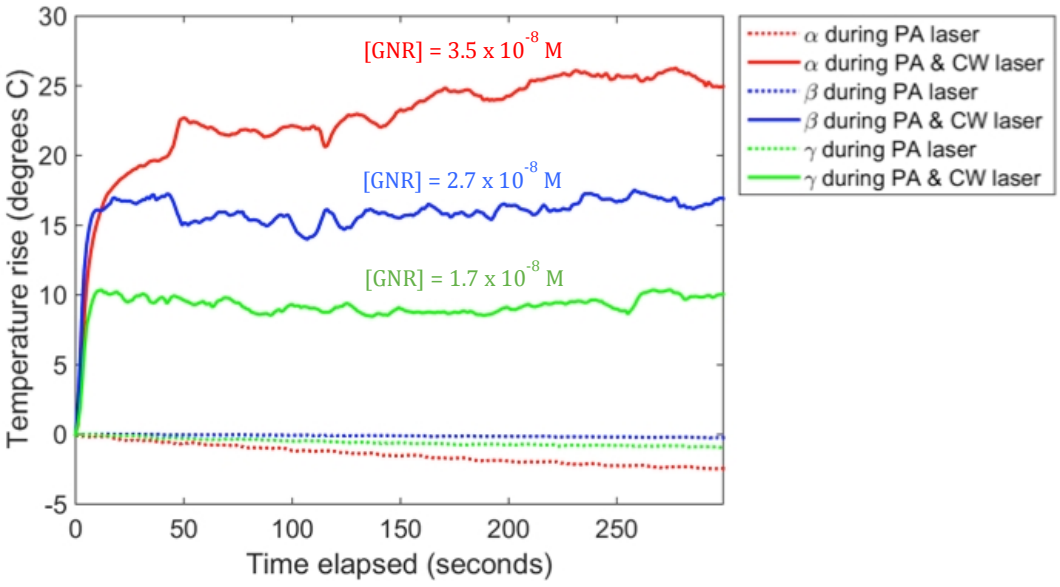


Fig. 3-4 The measured temperature profiles from each sample with (solid lines) and without (dotted lines) CW irradiation using the same line colours used in Fig. 3-3 to represent the different samples. GNR concentrations are labelled for each sample.

TEM images from the preliminary GNR sample with the higher GNR concentration that was irradiated is shown in Fig. 3-5 (a – pre-irradiation and b – post-irradiation) and this provided an early indication that reshaping and aggregation may be occurring to this irradiated sample. All subsequent study samples showed corresponding changes in nanorod shape after CW irradiation, confirming that the spectral changes seen were in fact due to shape changes; an example comparison is shown in Fig. 3-6. It appears that the nanorods become shorter

and wider, becoming more oval-shaped after laser heating, even tending towards spheres. As demonstrated in Fig. 3-6(d), the nanoparticles also exhibited aggregation post CW irradiation. When applying only the pulsed PA laser, the nanorods did not show a marked shape change as seen in Fig. 3-6(b). The gold nanoparticles in the TEM images appear aligned, possibly due to some surfactant remaining in the solution and the drying procedure for TEM preparation forming bubbles, pushing nanoparticles to the edges of the bubble.

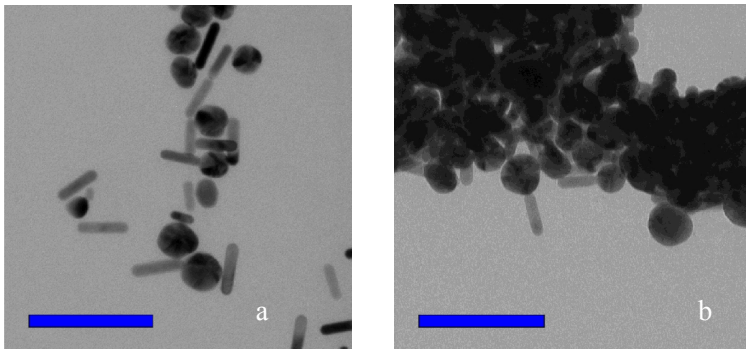


Fig. 3-5 Aggregation of GNRs can be observed in these TEM images (a) before CW laser irradiation and (b) after CW laser irradiation (60,000x magnification). The blue scale bars are 100 nm in length.

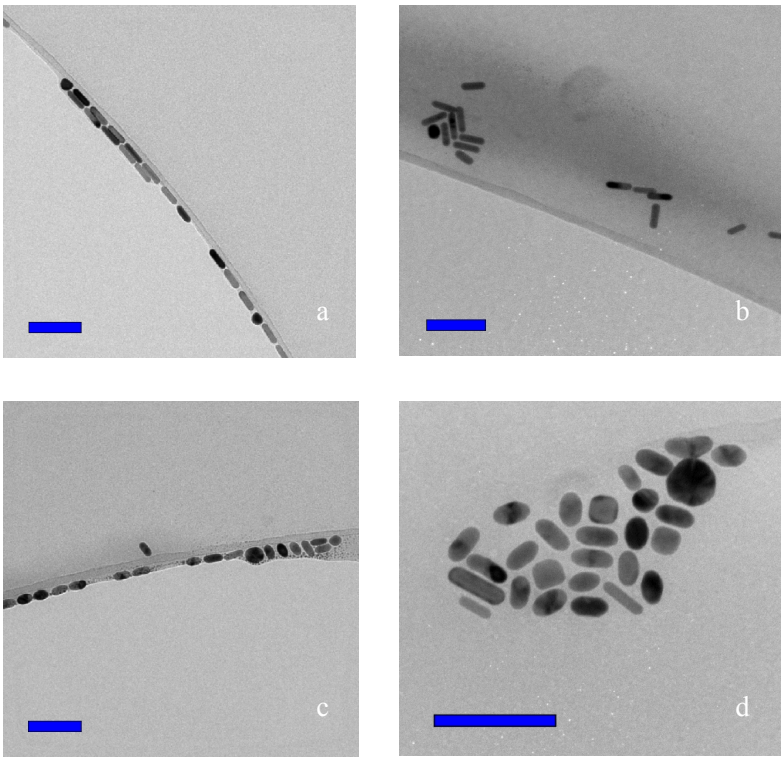
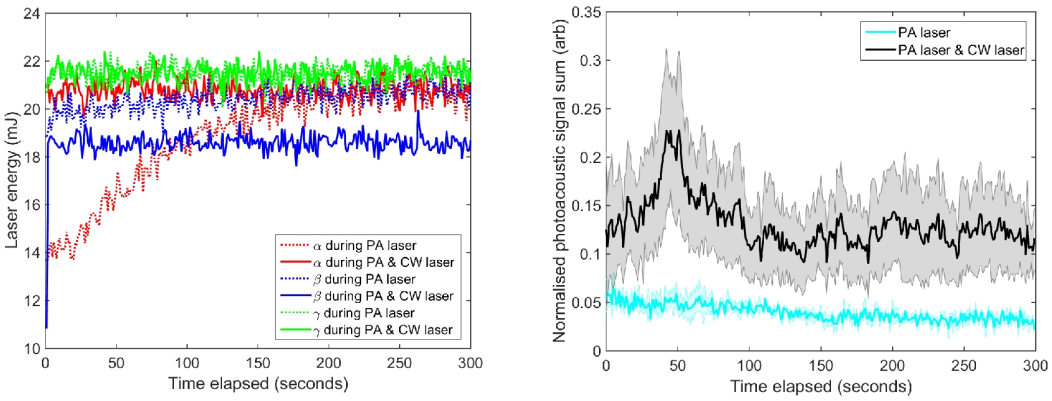


Fig. 3-6 Representative TEM images from sample α showing GNRs (a) before laser irradiation, (b) after only PA pulsed laser light, (c) after 6 W/cm^2 CW irradiation, (d) after 12 W/cm^2 CW irradiation. The blue scale bars are 100 nm in length.

The integrated PA signal (the sum of the absolute signal voltage over each interval) is from the 'top' and 'bottom' of the sample where the signal was low pass filtered using a 15 MHz cut-off and normalised to the laser energy. The means of the samples with and without the CW laser heating are shown in Fig. 3-7(b) with the standard error as the shaded regions and the thick lines as the means. For reference, the PA pulsed laser energy over time for each acquisition is shown in Fig. 3-7(a), illustrating a fluctuation in laser energy. These data were used to remove the laser energy pulse-to-pulse fluctuation from the PA signals by dividing the integrated signals by the energy for each pulse, according to equation [1].



(a) (b)

Fig. 3-7 (a) PA pulsed laser energy over time for each acquisition, illustrating the drift and pulse-to-pulse fluctuation in the laser energy, (b) the calculated PA signal mean of the three samples (thick line), with a standard error (shaded area) of the corrected signal, for CW laser on (black) and off (light blue).

Mice with tumours which received intratumoural (IT) administration of GNRs and irradiation with CW laser demonstrated a photothermal reaction within the subcutaneous tissues which was clearly observed during the first fortnight (as shown Fig. 3-8). This corresponded to a specific area of tumour necrosis occurring by virtue of the injected GNRs absorbing NIR light and thence eliciting a tumour photothermal response. Within the third week this organised into a scab which subsequently faded to reveal an underlying healed and tumour-free region by day 30 (Fig. 3-8). Microscopic examination of irradiated tumour sites displayed complete tumour ablation with the complete absence of any proliferating cancer cells. Neo-epithelialisation of epidermal and dermal skin layers was seen to occur through the process of neo-collagenesis and this was confirmed by polarised light microscopy (results shown in Fig. 6-27 and Fig. 6-28 in Section 6.4.2 in Chapter 6).



Fig. 3-8 Thermal reaction, gradual healing and complete ablation of tumour xenograft seen *in vivo* in a mouse that received IT GNRs and CW NIR laser irradiation for three minutes. The numbering within pictures indicates the days post-irradiation while the first (un-numbered) image is the pre-irradiated tumour. The irradiated site was excised at day 30 and TEM analysis is shown in Fig. 3-10(d-h).

During the three minute period of irradiation with NIR light, the temperature overlying the tumour sites was recorded externally by a thermal imaging camera, and the analysis of the temperature change from the baseline is shown in Fig. 3-9. A gradual rise in temperature was observed during irradiation with a final rise of 42°C.

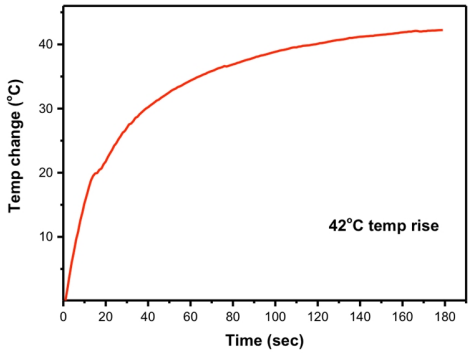


Fig. 3-9 Temperature rise seen *in vivo* after intratumoural (IT) GNRs administration and during CW irradiation for three minutes measured from the tumour site externally by the thermal imaging camera, after adjusting for background and baseline temperatures.

Tumour sites were examined with TEM following intratumoural (IT) administration of GNRs both pre- and post-irradiation with CW laser (Fig. 3-10). These sites were cross-examined with microscopic evaluation to confirm or refute the presence of tumour cells. It was observed that after intratumoural administration, GNRs became endocytosed and were contained within intracellular vesicles within tumour cells as shown in Fig. 3-10(a-c). These pre-irradiated GNRs retained their rod-like morphology and were confirmed to be GNRs by TEM-EDX analysis which corresponded to peaks of Au (gold) precisely at the location of the intracellular rods seen [Fig. 3-10(i)]. TEM images from post-irradiated tumour sites illustrated the biodistribution of GNRs within the cytoplasm of a single (damaged) cell as shown in Fig. 3-10(d). Both GNR aggregation and reshaping were seen within irradiated cells [Fig. 3-10(f & h)] and these morphed particles were proven to be irradiated GNRs by the presence of Au peaks from TEM-EDX analysis seen in Fig. 3-10(j & k).

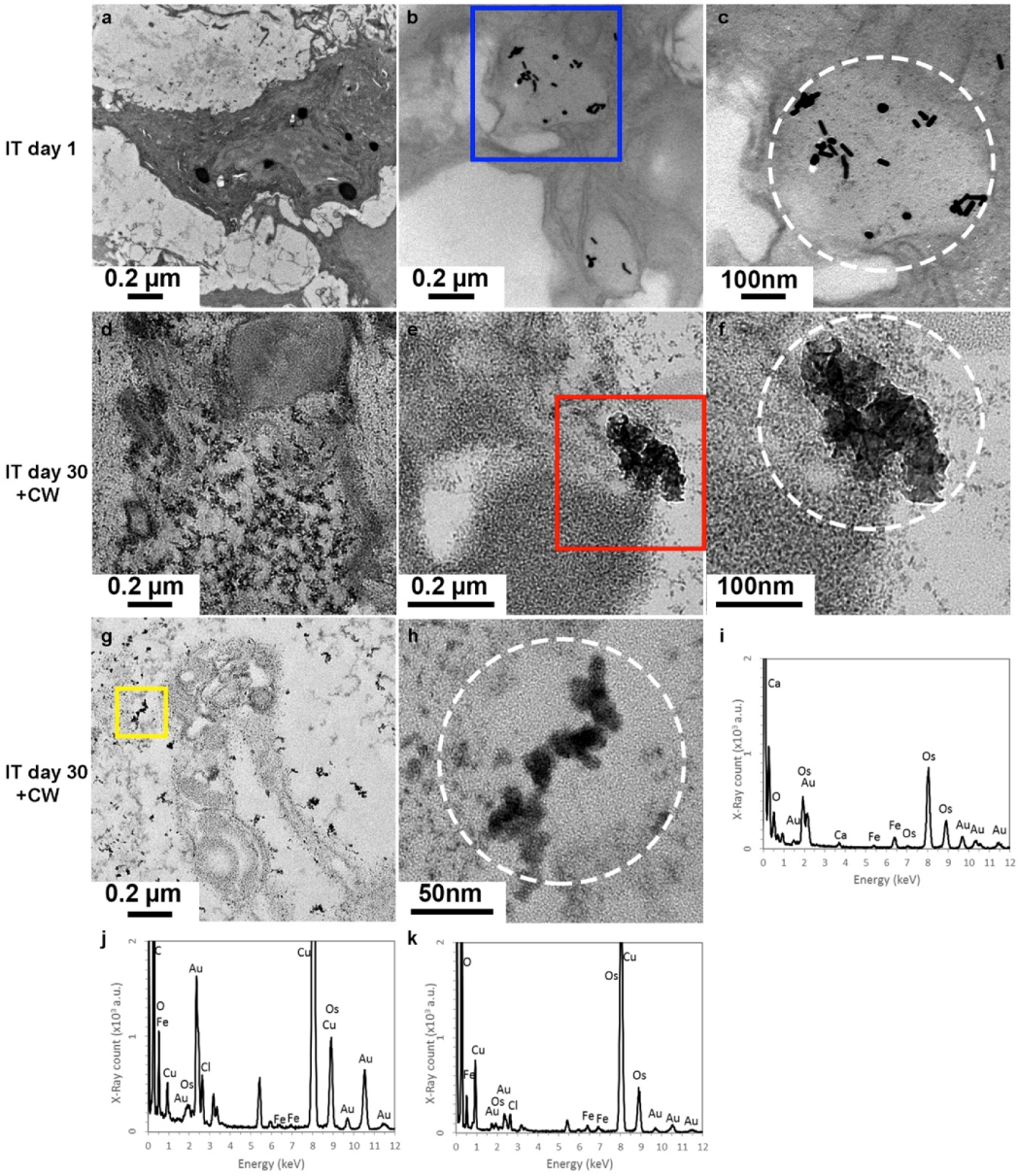


Fig. 3-10 TEM images of *in vivo* tumour sites following intratumoural (IT) administration of GNRs with pre- (a-c) and post-irradiation (d-h) with CW laser. (a) Low magnification image of day 1 pre-irradiated tumour tissue. (b) GNRs (black rod shaped) were contained in an intracellular (endolysosome) vesicle within a cancer cell. (c) High magnification image of the blue square in (b) showing the preservation of rod-like morphology of endocytosed GNRs pre-irradiation, which were confirmed by Au peaks from TEM-EDX analysis in (i). (d) Low magnification image of the post-irradiated site illustrating the distribution of irradiated particles within the cytoplasm of a single (radiation-damaged) cell. (e) GNR aggregation and reshaping seen within an irradiated cell following CW laser irradiation. (f) High magnification image of the red square in (e). Confirmation that this irregularly shaped structure was in fact morphed GNRs post-irradiation is shown by the presence of Au peaks seen from TEM-EDX analysis (in j). (g) Low magnification image of the post-irradiated site at day 30, illustrating a wide area of reshaped GNRs. (h) High magnification image of the yellow square in (g). The white circles in (c), (f) and (h) correspond to areas analysed and demonstrated as TEM-EDX spectrums in (i), (j) and (k) respectively.

3.4 **Discussion**

The difference in the temperature rise between the samples as seen in Fig. 3-4, can be explained by the difference in their optical absorption at the CW laser wavelength, a phenomenon which agrees with the findings of Chou *et al*. (17). This shows that reshaping can occur with a bulk temperature rise as low as 10-20°C. This however was a global temperature measurement and the local temperature of the centre of the heating laser spot would be much higher and the local temperature at the rod heating centre even higher. Due to convection currents, the GNRs will likely move in and out of the laser spot allowing the majority of the sample to be irradiated. The heat profiles also showed that there was no heating in the sample due to the PA pulsed laser although some exhibited a slight decrease in temperature. This small decrease is both due to cooling of the sample by the water bath giving an actual temperature decrease and the background ROI showing an apparent warming over time, due to temperature instability of the system, causing an apparent decrease in temperature rise after background subtraction.

Fluence (energy per unit area) was more commonly reported or calculable from a review of studies that have shown reshaping with pulsed lasers. It was not always possible to retrieve values for average power or intensity, due to missing laser specifications in some papers. Therefore a comparison of fluences was made between the values used in our *in vitro* and *in vivo* experiments for reshaping with CW excitation, and those reported by other authors who have demonstrated reshaping with pulsed lasers, and this is shown in Table 3-2.

A wide range of energies has been reported in the literature where nanoparticle reshaping has been demonstrated. Table 3-2 shows that the fluence values in our *in vivo* and *in vitro* experiments using CW laser are larger than those from pulsed lasers. The average concentration of GNRs is 2.90 x 10^{-10} M, which was only based on three papers which mentioned concentrations used, and this was higher than the GNR concentration in our *in vitro* and *in vivo* studies.

The irradiance (average power per unit area) used in our experiments was 6 W/cm^2 for *in vitro* and 5.66 W/cm^2 for *in vivo* experiments. Although it was not possible to determine the probability of reshaping from a single isolated GNR in our study as it was not directly measured, it can be extrapolated from a paper by Ma *et al.* (25) where reshaping was seen from a single nanorod with an irradiance of 1.8 x 10^6 W/cm^2 using a 1064 nm CW laser and optical trapping techniques. These results show, that it is possible to observe reshaping from a single nanorod using a CW laser *in vitro* even using irradiance values lower than those

described in our study as the heating is highly localised. We would expect to see reshaping as this is principally a laser irradiance-dependent effect since the temperature is always maximised locally at the absorption site. 'Melting' of individual GNRs could be observed in temperatures as low as ≈ 200°C, which is well below that of bulk gold.

Authors	Wavelength (nm)	Laser Type	Fluence (mJ/cm^2)	Concentration of GNPs (M)
Chang (13)	532 & 1064	Pulsed	6.74×10^{1}	Unknown
	532 & 1064	Pulsed	1.45×10^{1}	
	532 & 1064	Pulsed	1.45×10^{1}	
Gordel (11)	800	Pulsed	3.60	1.25×10^{-8}
	800	Pulsed	1.40	
Link (7)	800	Pulsed	1.02×10^{4}	5.70×10^{-10}
	800	Pulsed	5.60×10^{2}	
	800	Pulsed	2.00	
	800	Pulsed	1.00	
	800	Pulsed	2.00×10^{-1}	
	800	Pulsed	1.67×10^{4}	
	800	Pulsed	4.00×10^{3}	
	800	Pulsed	8.00×10^{2}	
	800	Pulsed	6.40×10^{2}	
Ungureanu (15)	810	Pulsed	4.30	3.00×10^{-10}
	810	Pulsed	2.10×10^{1}	
	810	Pulsed	6.20×10^{1}	
	532	Pulsed	1.10×10^{1}	
	532	Pulsed	6.10×10^{1}	
	700	Pulsed	2.00×10^{1}	
	700	Pulsed	1.00×10^{2}	
Zijlstra (12)	745	Pulsed	1.93	Unknown
	745	Pulsed	2.50	
AVERAGE		Pulsed	1.45×10^{3}	2.90×10^{-10}
Singh (*in vitro*)	808	CW	1.80×10^{6}	2.63×10^{-8}
Singh (*in vivo*)	808	CW	1.02×10^{6}	2.75×10^{-9}

Table 3-2 Comparison of the energy and concentration of GNPs in other studies which have shown GNP reshaping with pulsed lasers in comparison to the fluences used in our *in vitro* and *in vivo* studies using CW laser.

When the CW laser was applied to the sample, an increase in PA signal up to about 50 seconds was detected, as shown in Fig. 3-7(b). This is most probably due to the heating of the sample which is known to increase the Grueneisen coefficient and therefore increase the

effective PA signal, as shown by Shah et al. (26). The Grueneisen parameter (Γ) is defined as the factor which converts absorbed light energy into acoustic pressure:

$$p_0 = \mu_a F_0 \Gamma$$

where $\mu_a$is the optical absorption coefficient and F_0 and p_0 are the fluence and pressure at the sample (26). The temperature is the only factor which changes the Grueneisen parameter in this type of experiment as the Grueneisen parameter is also defined as $\Gamma = \frac{\beta c^2}{C_p}$, where *c* is the sound speed, β is the thermal expansion coefficient, and C_p is the specific heat capacity of the sample, of which *c* and β are temperature dependent (26).

After 50-60 seconds there was a gradual decrease in the PA signal, even though the temperature remained high. This suggests that the optical absorption coefficient of the sample was decreasing, since by this time point the Grueneisen coefficient should have stabilised, and this is confirmed by the absorbance spectra in Fig. 3-3 which clearly show a decrease. A correction factor could potentially be applied using knowledge of water and GNR Grueneisen temperature dependence, enabling probing of the actual change in absorption coefficient, although this could only be performed once the Grueneisen parameter of this type of solution as a function of temperature is known, also to make the results quantitative the system specific variables such as transducer sensitivity etc. would need to be factored in.

This study demonstrates for the first time that GNRs reshape both *in vitro* and *in vivo* after CW irradiation. Doubling the laser fluence (done here by reducing the laser beam diameter) led to a more dramatic change in morphology and absorption spectra. From the TEM images, it was shown that reshaping occurs in GNRs within five minutes of applying a CW laser *in vitro* and three minutes *in vivo*. This was demonstrated *in vivo* by applying NIR irradiation to the tumour at a fluence comparable to that used for PTT with CW lasers. Cancer cells showed that pre-irradiated functionalised GNRs delivered intratumourally were endocytosed, contained within endolysosomes of tumour cells and retained their original shape as demonstrated in Fig. 3-10(b-c). Proof that these were cancer cells was obtained by examining one half of the biopsied tumour tissue with haematoxylin and eosin staining under light microscopy which showed that the specimen comprised well-established adenocarcinoma from an alimentary tract origin. This endocytosis is likely to occur as a consequence of active antibody-antigen interaction resulting from an overexpression of

EGFR on the surface of cancer cells and the presence of anti-EGFR-antibodies on our functionalised GNRs.

Confirmation that these particles were in fact GNRs was obtained by EDX analysis [Fig. 3-10 (i-j)], which corresponded to peaks of Au and other organic compounds intrinsic to cells (C, O and Ca), those used as fixatives (Os and Fe) and the TEM grid (Cu). Post-irradiation aggregation and reshaping was observed at day 30 as spherical GNPs were found within the cytoplasm of membrane-damaged cells as shown in Fig. 3-10(d). Irradiation not only damaged tumour cell membranes but also resulted in the destruction of cellular organelles. It was further evident that these GNPs were found in the cytoplasm and did not become integral to the nucleus. The aggregation and reshaping seen *in vivo* [Fig. 3-10 (f, h)] was indeed comparable to *in vitro* results [Fig. 3-5(b) and Fig. 3-6(d)]. The temperature rise seen in the tumour three minutes after CW irradiation was shown in Fig. 3-9, and was greater than the temperature changes seen *in vitro*. More detailed scrutiny of the reshaped GNRs under high power magnification in Fig. 3-10(h) appears to illustrate a melting of nanorods. Histological assessment of the excised irradiated site demonstrated an absence of proliferating cancerous cells, with regeneration of new epithelium through the process of neo-collagenesis. Hence microscopic evaluation of irradiated sites was congruous with the clinical tumour regression seen macroscopically in Fig. 3-8.

The phenomenon of thermally-induced GNR reshaping occurred at relatively low bulk temperatures, well below the bulk melting point of gold as described by Taylor *et al.* (27). These changes were sustained throughout and beyond the period of irradiation, because a blue-shift and a considerable diminution in the absorption peak of GNRs had transpired, thus rendering any subsequent CW irradiation at the previous wavelength largely ineffective.

This result is important because CW lasers are more commonly used for photothermal therapy using gold nanoparticles, and it is noteworthy that any subsequent application of laser at the original wavelength may not produce cumulative or enhanced thermal effects due to the spectral shift and attenuation. As heat intensity increased, the blue-shift increased and the aspect ratio reduced. The GNRs also demonstrated a morphological change from rods to spherical-like particles, as shown in Table 3-1 and in TEM images. For example, sample α changes from an original aspect ratio of 3.8 to 2.9 after CW laser heating, decreasing further to 2.3 when the laser fluence is increased. This phenomenon was also described by Ng and Cheng (28) in subjecting GNRs to various annealing temperatures using water baths, they found that SPR bands decay exponentially with annealing time at all annealing temperatures.

When comparing the GNR absorbance spectra and temperature rise due to PA and CW lasers, it is apparent that the CW laser caused a much greater heating and spectral hole-burning than the PA laser, as demonstrated in Fig. 3-3 and Fig. 3-4. The average power using the PA laser over 1 second is 20.3 mW with a peak power of 2.9 MW, compared to the 6 W constant power of the CW laser. Therefore much more energy was deposited over the period of the illumination from the CW laser compared to the PA laser, leading to more GNR reshaping. It is clear that in comparing these two regimes, the determining factor in reshaping GNRs through laser irradiation is the average power from the laser rather than its peak power[3], although this may not be the case for different laser pulse properties. Heat diffusion will also affect heating, and consequently reshaping, as there would be less heat lost if same energy was applied over a shorter time period.

The results from the spectra shown in Fig. 3-3 and TEM analysis shown in Table 3-1 suggest that both the lengths of the GNRs and the number of GNRs are reduced after CW laser heating. The original lengths and aspect ratios of GNRs, which resulted in the absorption peak, have reduced, accompanied by a corresponding increase in their widths, as shown in Table 3-1, and the spectral blue shift after CW laser heating in Fig. 3-3. Furthermore the total number of GNRs may have reduced, as Fig. 3-3 shows the irradiated GNRs LSPR peak is not just blue shifted, the area under the LSPR peak is also reduced and has caused an increase in the TSPR peak at around 530nm, suggesting a conversion from rods to spheres. Prolonging the irradiation period may make all rods ultimately transform into spheres.

Although CTAB-GNRs were used in the *in vitro* studies, it has been previously shown that surface coating with PEG (thiol-terminated polyethylene glycol) also presented a similar attenuation in SPR absorption coefficients following irradiation with a nanosecond pulsed-laser, with the authors concluding that polymers such as PEG are not an effective heat barrier against the thermally-driven reshaping phenomenon (29). This concept was then proven with the reshaping of PEGylated GNRs seen in our *in vivo* study.

Significant aggregation was also seen as a separate entity alongside thermal reshaping post CW irradiation at fluences comparable to photothermal therapy, which would further affect the subsequent optical absorption capacity of GNRs [as seen *in vitro* in Fig. 3-5(b) and *in vivo* in Fig. 3-10(f)]. The TEM images of Fig. 3-5(b), Fig. 3-6(d) and Fig. 3-10(d-h) were all

[3] Using the equation Energy (J) = Power (W) x Time (secs), it is calculated that using the PA laser, with a mean pulse energy of 20.3 mJ with a repetition rate of 1 Hz and a 7 ns pulse length, the average power over 1 second is 20.3 mW and a peak power of 2.9 MW, compared to the 6 W continual power from the CW laser.

taken after the irradiated GNRs had cooled to room temperature, indicating an irreversible element to the aggregation. A hypothesis that may expound this is that the CTAB coating melted and dissociated from the surface of GNRs, eliminating the buffer interface and hence reducing the inter-particle distances. This has been studied in copolymer conjugation of gold nanoparticles via in situ small-angle X-ray scattering by Hamner and Maye (30). A further theory into the causation of this effect has been proposed by Heo *et al.* (31) where the authors suggest that at temperatures beyond 150°C achieved by annealing, aggregation occurs due to multiple hydrogen bonds being broken between random copolymer ligands of nanocomposites. Nam *et al.* (32) suggest that aggregates form rapidly *in vitro* due to electrostatic attractions between "smart" nanoparticles (pH-responsive and without any antibody conjugation), and a gradual accumulation occurs within cells as their exocytosis (clearance) from cells is blocked by the large size of the amorphous complexes. Aggregation was clinically demonstrated to be useful, selective and effective in cancer cells being irradiated with a 660 nm CW diode laser delivered at a relatively low fluence (32).

The spectral hole burning and shape change illustrated while using a CW laser with fluences comparable to those used in photothermal therapy are comparable to those demonstrated in the literature for pulsed laser irradiation. Therefore the effect of GNR reshaping during CW laser photothermal heating is a clearly observable occurrence, and should be taken into account when planning clinical therapy approaches using this method. Moreover photoacoustic measurements of GNR reshaping due to CW irradiation is demonstrated here, showing potential as a monitoring tool.

3.5 Conclusion

This is the first time reshaping has been shown using a CW laser both *in vitro* and in successful tumour ablations *in vivo*, which forms the most commonly applied method of laser irradiation on gold nanoparticles for photothermal therapy. The evolution of nanorod morphology should be evaluated or monitored during *in vivo* thermal therapy studies in conjunction with light fluence in order to better understand the implications on tissue heating, especially where sequential photothermal therapy is being considered for tumour regression. Reshaping of GNRs after the initial laser application will render subsequent irradiations largely ineffective and unlikely to provide any additional photothermal effect due to alterations in their optical absorption properties.

References

1. Huang XH, El-Sayed IH, Qian W, El-Sayed MA. Cancer cell imaging and photothermal therapy in the near-infrared region by using gold nanorods. Journal of the American Chemical Society. 2006;128(6):2115-20.
2. Kirui DK, Krishnan S, Strickland AD, Batt CA. PAA-derived gold nanorods for cellular targeting and photothermal therapy. Macromol Biosci. 2011;11(6):779-88.
3. von Maltzahn G, Park JH, Agrawal A, Bandaru NK, Das SK, Sailor MJ, Bhatia SN. Computationally Guided Photothermal Tumor Therapy Using Long-Circulating Gold Nanorod Antennas. Cancer Research. 2009;69(9):3892-900.
4. Choi WI, Kim JY, Kang C, Byeon CC, Kim YH, Tee G. Tumor Regression In Vivo by Photothermal Therapy Based on Gold-Nanorod-Loaded, Functional Nanocarriers. Acs Nano. 2011;5(3):1995-2003.
5. Goodrich GP, Bao LL, Gill-Sharp K, Sang KL, Wang J, Payne JD. Photothermal therapy in a murine colon cancer model using near-infrared absorbing gold nanorods. Journal of Biomedical Optics. 2010;15(1).
6. Kirui DK, Khalidov I, Wang Y, Batt CA. Targeted near-IR hybrid magnetic nanoparticles for in vivo cancer therapy and imaging. Nanomedicine. 2013;9(5):702-11.
7. Link S, Burda C, Nikoobakht B, El-Sayed MA. Laser-induced shape changes of colloidal gold nanorods using femtosecond and nanosecond laser pulses. Journal of Physical Chemistry B. 2000;104(26):6152-63.
8. Link S, El-Sayed MA. Spectroscopic determination of the melting energy of a gold nanorod. J Chem Phys. 2001;114(5):2362-8.
9. Link S, Burda C, Mohamed MB, Nikoobakht B, El-Sayed MA. Laser photothermal melting and fragmentation of gold nanorods: Energy and laser pulse-width dependence. J Phys Chem A. 1999;103(9):1165-70.
10. Link S, El-Sayed MA. Spectral properties and relaxation dynamics of surface plasmon electronic oscillations in gold and silver nanodots and nanorods. Journal of Physical Chemistry B. 1999;103(40):8410-26.
11. Gordel M, Olesiak-Banska J, Matczyszyn K, Nogues C, Buckle M, Samoc M. Post-synthesis reshaping of gold nanorods using a femtosecond laser. Phys Chem Chem Phys. 2014;16(1):71-8.
12. Zijlstra P, Chon JWM, Gu M. White light scattering spectroscopy and electron microscopy of laser induced melting in single gold nanorods. Phys Chem Chem Phys. 2009;11(28):5915-21.
13. Chang SS, Shih CW, Chen CD, Lai WC, Wang CRC. The shape transition of gold nanorods. Langmuir. 1999;15(3):701-9.
14. Link S, Burda C, Nikoobakht B, El-Sayed MA. How long does it take to melt a gold nanorod? A femtosecond pump-probe absorption spectroscopic study. Chem Phys Lett. 1999;315(1-2):12-8.
15. Ungureanu C, Kroes R, Petersen W, Groothuis TAM, Ungureanu F, Janssen H, van Leeuwen FWB, Kooyman RPH, Manohar S, van Leeuwen TG. Light Interactions with Gold Nanorods and Cells: Implications for Photothermal Nanotherapeutics. Nano letters. 2011;11(5):1887-94.
16. Mohamed MB, Ismail KZ, Link S, El-Sayed MA. Thermal reshaping of gold nanorods in micelles. Journal of Physical Chemistry B. 1998;102(47):9370-4.
17. Chou CH, Chen CD, Wang CRC. Highly efficient, wavelength-tunable, gold nanoparticle based optothermal nanoconvertors. Journal of Physical Chemistry B. 2005;109(22):11135-8.
18. Li CH, Wang LHV. Photoacoustic tomography and sensing in biomedicine. Phys Med Biol. 2009;54(19):R59-R97.
19. Taruttis A, Herzog E, Razansky D, Ntziachristos V. Real-time imaging of cardiovascular dynamics and circulating gold nanorods with multispectral optoacoustic

tomography. Opt Express. 2010;18(19):19592-602.
20. Agarwal A, Huang SW, O'Donnell M, Day KC, Day M, Kotov N, Ashkenazi S. Targeted gold nanorod contrast agent for prostate cancer detection by photoacoustic imaging. J Appl Phys. 2007;102(6).
21. Kim K, Huang SW, Ashkenazi S, O'Donnell M, Agarwal A, Kotov NA, Denny MF, Kaplan MJ. Photoacoustic imaging of early inflammatory response using gold nanorods. Appl Phys Lett. 2007;90(22).
22. Li PC, Wang CRC, Shieh DB, Wei CW, Liao CK, Poe C, Jhan S, Ding AA, Wu YN. In vivo Photoacoustic Molecular Imaging with Simultaneous Multiple Selective Targeting Using Antibody-Conjugated Gold Nanorods. Opt Express. 2008;16(23):18605-15.
23. Ha SH, Carson A, Agarwal A, Kotov NA, Kim K. Detection and monitoring of the multiple inflammatory responses by photoacoustic molecular imaging using selectively targeted gold nanorods. Biomedical Optics Express. 2011;2(3):645-57.
24. Shah AJ, Alles EJ, Box C, Eccles SA, Robinson SP, deSouza N, Bamber JC. Non-invasive molecular profiling of cancer using photoacoustic imaging of functionalized gold nanorods. Photons Plus Ultrasound: Imaging and Sensing 2014. 2014;8943.
25. Ma HY, Bendix PM, Oddershede LB. Large-Scale Orientation Dependent Heating from a Single Irradiated Gold Nanorod. Nano letters. 2012;12(8):3954-60.
26. Shah J, Park S, Aglyamov S, Larson T, Ma L, Sokolov K, Johnston K, Milner T, Emelianov SY. Photoacoustic imaging and temperature measurement for photothermal cancer therapy. J Biomed Opt. 2008;13(3):034024.
27. Taylor AB, Siddiquee AM, Chon JWM. Below Melting Point Photothermal Reshaping of Single Gold Nanorods Driven by Surface Diffusion. Acs Nano. 2014;8(12):12071-9.
28. Ng KC, Cheng WL. Fine-tuning longitudinal plasmon resonances of nanorods by thermal reshaping in aqueous media. Nanotechnology. 2012;23(10).
29. Horiguchi Y, Honda K, Kato Y, Nakashima N, Niidome Y. Photothermal Reshaping of Gold Nanorods Depends on the Passivating Layers of the Nanorod Surfaces. Langmuir. 2008;24(20):12026-31.
30. Hamner KL, Maye MM. Thermal Aggregation Properties of Nanoparticles Modified with Temperature Sensitive Copolymers. Langmuir. 2013;29(49):15217-23.
31. Heo K, Miesch C, Emrick T, Hayward RC. Thermally Reversible Aggregation of Gold Nanoparticles in Polymer Nanocomposites through Hydrogen Bonding. Nano letters. 2013;13(11):5297-302.
32. Nam J, Won N, Jin H, Chung H, Kim S. pH-Induced Aggregation of Gold Nanoparticles for Photothermal Cancer Therapy. Journal of the American Chemical Society. 2009;131(38):13639-45.

Chapter 4 Application of gold nanorods for photothermal therapy in *ex vivo* human oesophagogastric adenocarcinoma

4.1 Introduction[1]

As discussed in the previous chapter, gold nanoparticles are chemically fabricated and tuned to strongly absorb near infrared (NIR) light, enabling deep optical penetration and therapy within human tissues, where sufficient heating induces tumour necrosis. Although there have been initial human clinical trial advances in theranostic applications of nanoparticles in breast (1, 2), head and neck (3), lung (4) and prostate (5) cancers, their translational value in oesophagogastric cancer therapy remains unproven, with *in vitro* and rodent *in vivo* published studies varying considerably in their aims, methods and materials, leading to a perplexing task of finding commonality and reproducibility. There also remain unanswered questions about the acute and long-term toxicity from various *in vivo* animal studies (6, 7). Translation to clinical trials demands sufficiently powered and concurrent *in vitro* and *in vivo* studies which assess safe GNP concentrations, optimal laser fluence and efficacy.

In this chapter the aim was to establish the optimal gold nanorod (GNR) concentration and laser power for inducing hyperthermic effects in tissues and test this photothermal effect on *ex vivo* human oesophagogastric adenocarcinoma. Suitable GNR concentration and NIR laser power that could elicit sufficient hyperthermia for tumour necrosis was first determined using porcine oesophageal tissues. Human *ex vivo* oesophageal and gastric adenocarcinoma tissues were subsequently incubated with GNR solutions and a GNR-free control solution with corresponding healthy tissues for comparison, and then irradiated with NIR light for ten minutes. Corresponding temperature rises within these tissues were evaluated.

The photothermal therapy work presented herein evaluates the effect of GNRs on human oesophagogastric cancer and highlights areas requiring a unified focus in nanotechnology research involving GI cancer. The application of human tissue for PTT is in contrast with many studies that routinely use animal tissues. While data from *in vivo* studies in immunodeficient mice provides useful information, they are usually performed on

[1] This chapter is adapted from the author's publication in the Journal of Biomedical Nanotechnology, doi:10.1166/jbn.2016.2196.

synthetically induced subcutaneous tumour xenografts, it is vital to then be able to compare them to the results of these experiments performed in human cancer samples obtained from their naturally occurring sites within the upper gastrointestinal tract. To our knowledge this work is novel and relevant when considering the translational clinical potential of gold nanoparticles. Our group has already had success in the fabrication of multi-functionalised GNRs and their application in the fluorescent detection, targeting and photothermal ablation of human cervical cancer cells (HeLa cells) (8, 9). The work reported here is advancement in the application of PTT in human GI cancer tissue including imaging and thermal monitoring.

4.2 Materials and Methods

4.2.1 Gold nanorod synthesis and characterisation

Gold nanorods were fabricated with cetyltrimethylammonium bromide (CTAB) using the methods described in Methods and Materials, establishing CTAB-GNRs used in all the following experiments.

4.2.2 Temperature change with varying gold nanorod concentrations

In order to establish their heating profile, 3 ml of GNRs of varying concentrations were placed into a cuvette and subjected to irradiation with an 808 nm NIR laser (DenLase-810/7 CW laser, Beijing China) using 2 W of power for 10 minutes. Temperature was recorded using a thermal imaging camera (FLIR Systems ThermaCAM S65 Infrared Camera, Wilsonville USA), acquiring at 1 Hz. An initial 1000 μL sample of GNRs was used at its most concentrated, which had 12 x 10^9 GNPs per ml, and serial dilutions with water were made, maintaining a total volume of 1000 μL. This method could approximate the concentration of GNRs required to achieve hyperthermia levels (41-45°C) compatible with the photothermal destruction of tumour cells (10, 11).

4.2.3 Effects of gold nanorod concentration on healthy porcine oesophageal tissues and photothermal response

Healthy porcine oesophageal and gastric tissue was harvested from recently terminated animals less than 12 hours prior to experiments. Mucosa from the oesophagus was used to determine the photothermal effects observed by gradually decreasing the concentration of GNRs in which the tissues were incubated, then irradiating with NIR laser (2 W at 808 nm with a beam diameter of 12 mm) for 10 minutes. The incubation time was 45 minutes at room temperature.

The most concentrated GNR solution used for this experiment, based on absorption values obtained from UV-Vis spectrophotometry, was 12 x 10^9 GNRs per ml, and a series of concentrations was established using calculations based on the extinction coefficients of GNRs and by the addition of deionized water to make up the same final volume (Table 4-1).

Sample	No. of particles/ml (x10^9)
1	12
2	6
3	1.2
4	0.6
5	0.3
6	0.12
7	0.06
8	0.012

Table 4-1 Concentration of the GNR solutions in which tissues were incubated, using an initial total volume of 2500 μL of concentrated GNR solution.

A further study was conducted to determine the influence of altering the laser power on healthy tissue heating in the absence of GNRs, enabling a measure of what tissue damage may be done by the laser alone at varying powers. Healthy porcine oesophageal mucosal tissues were irradiated with varying laser powers for 10 minutes, commencing at 1 W and ending with 7 W, the maximum power of our DenLase-810 CW laser. Three repeats were analysed for each laser power.

4.2.4 **Human oesophagogastric tissue experiments**

Human oesophageal and gastric *ex vivo* tissues were obtained (with patient's consent and Regional Ethics Committee approval 04/Q0403/119) from oesophagectomy and gastrectomy cancer patients undergoing surgical resections. Both healthy and adenocarcinoma tissues were obtained from the same organs for comparative tests and each were incubated in a 2 ml solution of GNRs in a test tube under room temperature for 45 minutes. Healthy and cancerous tissues from the same organ were also incubated under room temperature in a test tube with 2 ml of RPMI, a culture medium widely used in cell culture. Tissue experiments were performed with CTAB-coated GNRs with the aim of testing the effect of photothermal therapy on tissues that had taken up GNRs.

After tissues had been incubated with either a GNR or RPMI solution for approximately 45 minutes, they were rinsed thrice with Dulbecco's Phosphate Buffered Saline (PBS). These tissues were then mounted onto a transparent microscope slide and a continuous wave NIR (808 nm) laser was directed toward the tissue (shown in Fig. 4-1).

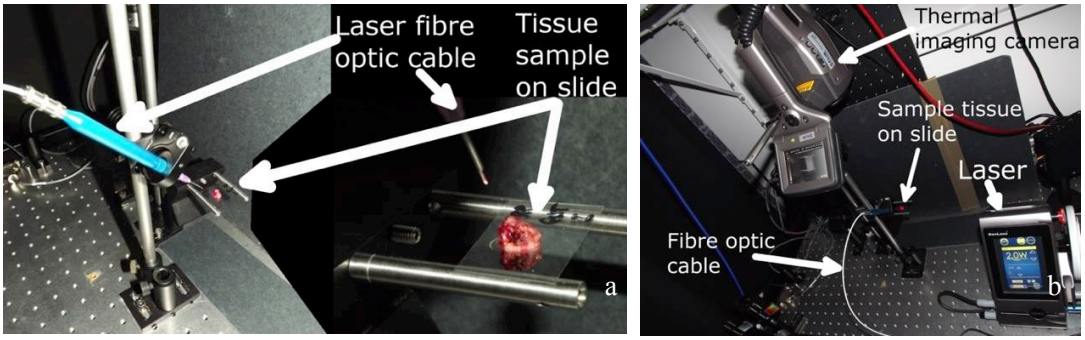


Fig. 4-1 (a) Tissue mounted onto a slide and laser diode catheter directed towards it (b) thermal imaging camera mounted above the tissue being irradiated by the laser.

The beam diameter was maintained at 12 ± 1 mm, and a power setting of 2 W was used. The laser fluence (power/unit area) used was kept constant throughout and was determined from results from experiments on *ex vivo* tissues presented in this chapter which eventually guided an avoidance in the use of fluences that would either char/carbonise tissues (excessively high) or cause a negligible effect (insufficiently low). This was learnt by scrutinising the effects on irradiating *ex vivo* tissues incubated at varying GNR concentrations whilst maintaining a particular laser fluence, or by varying the fluence while maintaining a constant GNR concentration. The NIR laser used emits at a wavelength of 808 nm with a maximal power of 7 W. The size of the specimen was kept relatively constant and similar to its

healthy counterpart i.e. approximately 1 cm^2 with a thickness of around 2 mm. The period of tissue irradiation was 10 minutes. Temperature monitoring during laser irradiation of the tissues was recorded by a thermal imaging camera, which was mounted directly above the specimen [Fig. 4-1 (b)]. 36 human oesophagogastric specimens were tested.

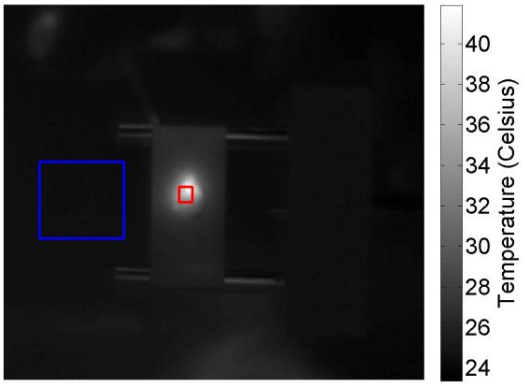


Fig. 4-2 Example image captured by FLIR thermal imaging camera during tissue heating with a corresponding temperature response chart (y-axis), the blue box shows the selected background region of interest and the red box shows the selected tissue region of interest from which the mean temperature values are calculated.

Regions of interest were selected to distinguish the temperature change occurring within the tissues or GNRs and the background temperature (Fig. 4-2). The mean and standard deviation of the pixels within the regions of interest was calculated. Then any background heating was subtracted from the heating occurring from within the specimen to give a measurement of the temperature rise within the tissues due to the laser. Plots of temperature rise over time were created using a Matlab program.

4.3 Results

4.3.1 Characterisation of GNRs

As alluded to in Methods and Materials, Fig. 4-3(a) shows that in the main, fabricated CTAB-GNRs had optical density peaks at 520 nm and 808 nm, corresponding to transverse and longitudinal SPRs of gold nanoparticles respectively. Nanospheres contribute only to the smaller transverse SPR peak, while GNRs contribute mainly to the longitudinal peak, which by design corresponds to the emission wavelength of the NIR laser (808 nm). The corresponding aspect ratio (AR = length/width) was found to be 4.0 (± standard error (se) of 0.08) by TEM measurements. The minimum number of GNRs analysed by TEM

measurement to determine the mean was 150. A representative TEM picture is shown in Fig. 4-3(b).

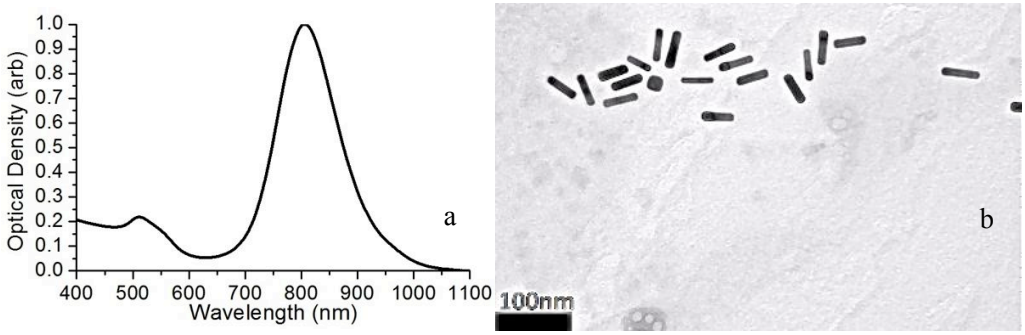


Fig. 4-3 (a) Normalised optical density profile of GNRs with aspect ratio = 4 (b) TEM image of the GNPs produced.

Stability studies were performed on the GNRs in their colloidal suspension, and Table 4-2 shows the zeta-potential and size measurement of CTAB-GNRs by DLS.

GNR functionalisation	Diameter [nm]	ζ-potential [mV]
CTAB-GNRs	44	+40

Table 4-2 Hydrodynamic diameter and ζ-potential values of GNRs measured by dynamic light scattering.

4.3.2 Temperature change with varying GNR concentration

The temperature increase during NIR laser irradiation for different GNR concentrations contained within cuvettes is illustrated in Fig. 4-4. The temperature profile over time for every concentration is shown in Fig. 4-4(a) and the measured temperature rise for the last time point after 10 minutes irradiation for each concentration is shown in Fig. 4-4(b).

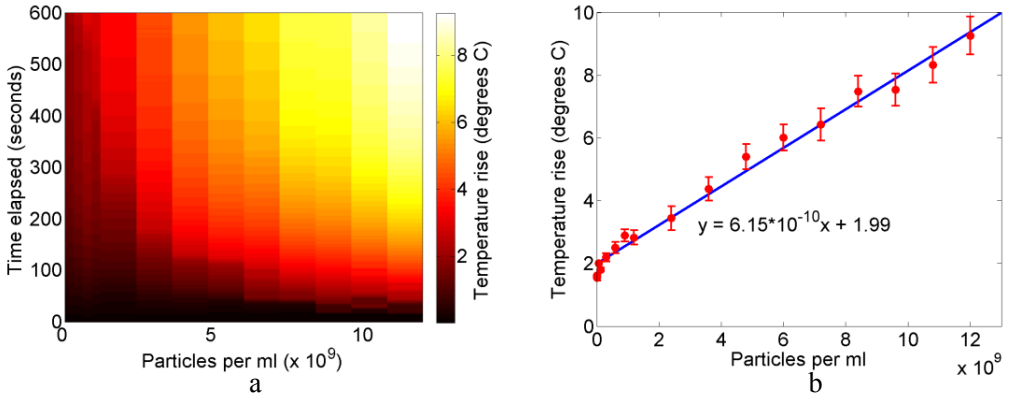


Fig. 4-4 (a) Temperature increase over time with 3 ml of varying concentrations of GNRs in cuvettes, where the colour indicates the temperature rise in Celsius. (b) The temperature rise after 10 minutes of laser heating for 3 ml of various concentrations of GNRs with a line of best fit showing the linear relationship. The red circles show the mean values and the errors show the standard deviation of 3 repeats.

4.3.3 Effects of GNR concentration and laser fluence on healthy porcine oesophageal tissues and photothermal response

The concentration of GNRs incubated with the tissue affects the temperature rise during NIR laser irradiation. The most concentrated solution had 12 x 10^9 GNRs per ml of solution with the least concentrated containing 1.2 x 10^7 GNRs per ml (as illustrated in Table 4-1). Macroscopic images of the tissue samples incubated with these varying GNR concentrations and then exposed to laser irradiation are illustrated in Fig. 4-5.

Tissues incubated in the first two (most concentrated) GNR solutions (12 x 10^9 GNRs and 6 x 10^9 GNRs per ml) underwent instantaneous charring/carbonisation under 2 W of NIR laser such that they crumpled and shrivelled. Consequently the thermal increments for these two samples were considerable (>60°C temperature rise). Hence a lower power laser setting (0.8 W) was selected for Sample 2 (half the original concentration), and the temperature profile is seen in Fig. 4-6 (red line), which demonstrated a 40°C temperature rise after ten minutes of NIR laser.

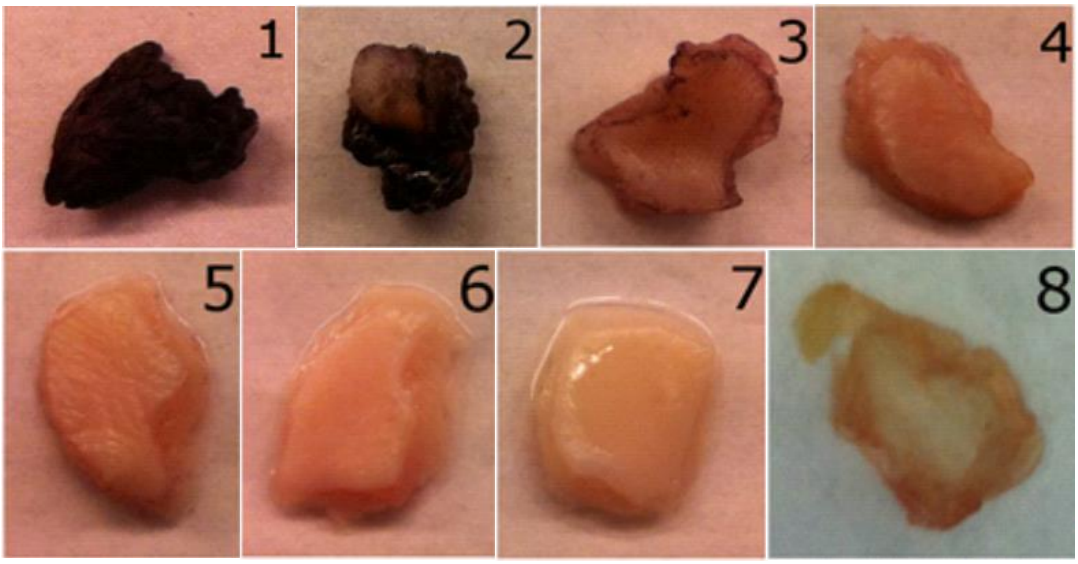


Fig. 4-5 Macroscopic appearances post laser irradiation of porcine oesophageal tissues incubated in a series of GNR solutions ranging from the most (1) to least concentrated (8).

Representative temperature profiles obtained from Samples 2, 4 and 8 are illustrated in Fig. 4-6. It is apparent that a gradual reduction in the concentration of GNRs incurs a lower thermal effect on tissues, such that at its most dilute concentration (Sample 8), only a 7°C temperature rise was recorded after 10 minutes' irradiation, which was identical to the temperature rise seen when the tissue was incubated with only water. More importantly there was a negligible thermal effect observed microscopically on the tissues incubated with an extremely low concentration of GNRs (i.e. Sample 8, with 1.2 x 10^7 GNRs/ml).

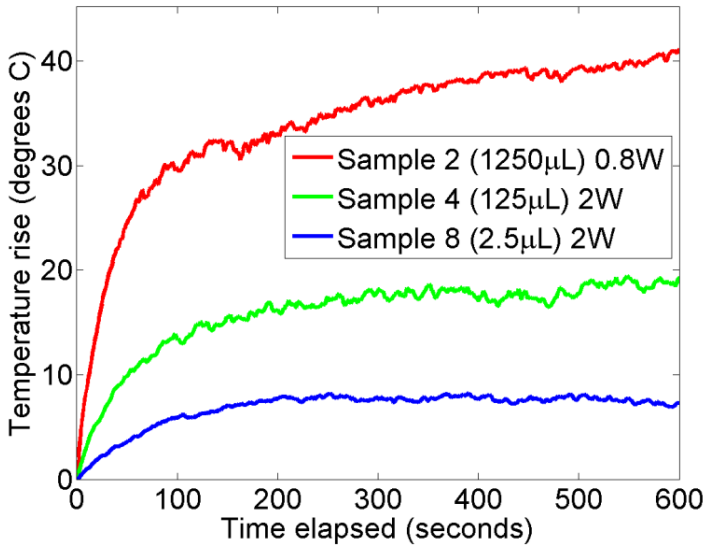


Fig. 4-6 Temperature rise with time for the tissue samples and conditions indicated.

A summary plot of the temperature rises obtained after ten minutes of heating tissues without GNRs with each laser power is illustrated, and it appears to also exhibit an approximately linear relationship (Fig. 4-7). These results henceforth guided the selection of the optimal GNR concentration and laser fluence in human *ex vivo* cancer experiments, as a therapeutic temperature rise is required from the nanorod treated tissue without causing damage to normal healthy tissue.

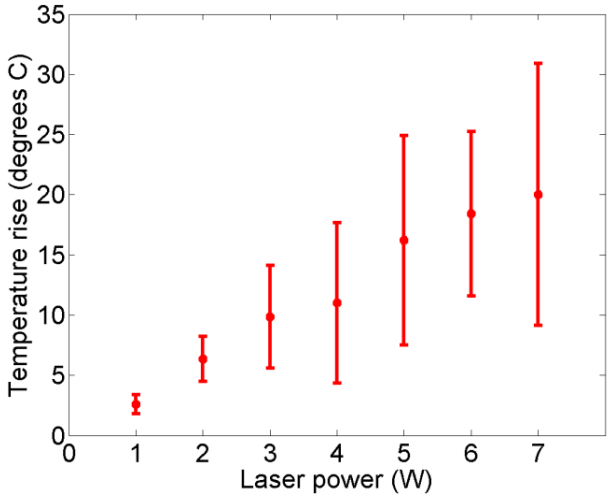


Fig. 4-7 Temperature rise from porcine oesophageal tissues subjected to varying concentrations of laser power. The central marker is the mean value with the error bar showing the standard deviation of the three repeats.

4.3.4 Plasmonic photothermal therapy of human oesophagogastric tissues

Staining of tissues was noted after rinsing tissues that had been incubated with GNRs, which persisted after thrice washing with PBS. Fig. 4-8 illustrates this marked contrast against the pale hue seen in tissues not exposed to GNRs. Oesophageal and gastric adenocarcinoma were obtained for experiments, and the temperature rises from the 2 W laser irradiation with corresponding healthy oesophageal and gastric tissues are shown in Fig. 4-9.

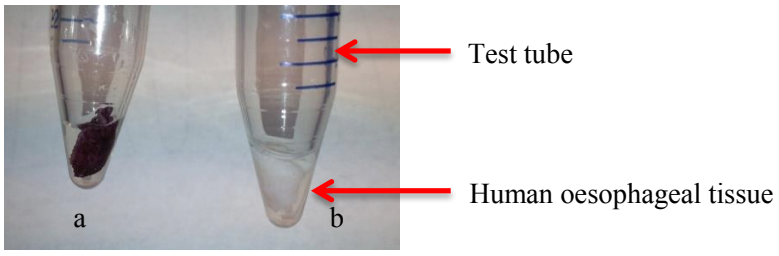


Fig. 4-8 (a) Marked adherence of GNRs onto tissues that were incubated in a colloidal suspension of GNR which persisted despite thrice washing with PBS, in contrast to pale tissues incubated in RPMI (b).

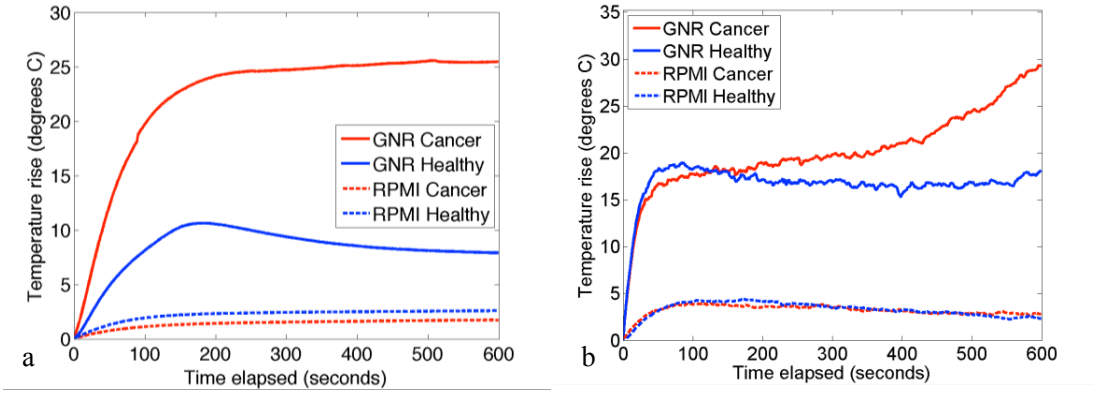


Fig. 4-9 Temperature rises during irradiation with NIR laser in human *ex vivo* (a) oesophageal and (b) gastric tissues, incubated with either CTAB-GNRs or RPMI medium.

4.4 Discussion

The ideal aspect ratio for the photothermal experiments conducted in *ex vivo* tissues was noted to be 4.0, as the longitudinal SPR peak of GNRs would then be located at 808 nm, which corresponds to the wavelength of the NIR laser and is a wavelength suitable for deep optical penetration into tissue. However, different aspect ratios could provide a similar photothermal effect as long as there is synchronicity between the absorption peak of GNRs and laser emission, although changes in optical penetration in tissue for a different laser wavelength would change the bulk heating dynamics. Stability studies demonstrated that apart from a slight shortening of GNR lengths observed only in solutions with a reduced amount of CTAB immediately after the first day post-synthesis (which was confirmed by TEM analysis), no changes were found in the particle size, zeta potential values and in the extinction profiles over a period of several months. The stability of the GNRs is also consistent with their ability to maintain a highly positive zeta-potential over time.

CTAB-coated GNRs were used for *ex vivo* experiments. It is known that CTAB exerts cytotoxic effects and should be avoided for *in vivo* studies (12-15). However it neither affects nor compromises the results of photothermal therapy of *ex vivo* tissues; instead it provides GNRs with an outer structure which mimics a phospholipid double layer, favouring cell membrane penetration and the incorporation of GNRs into tissue. Attempts of adopting polyethylene glycol (PEG) functionalised GNRs for our experiments were made, but, once tissues were rinsed with PBS, PEGylated GNRs did not adhere to tissues as effectively as

CTAB-coated GNRs and were washed away. CTAB and PEGylated GNRs are contrast agents which share identical absorption spectra, and it is their absorption spectrum that determines their heating properties. As human oesophagogastric tissues have similar optical properties, consequently the temperature rise seen with CTAB-GNRs would be the same as with PEG-GNRs.

Hyperthermia is the term applied when an organ or tissue is heated to temperatures between 41-45°C, which is capable of inducing cellular damage and necrosis (10, 11). By way of extrapolation from the linear concentration-temperature rise relationship in Fig. 4-4(b), the concentration required to obtain this level of hyperthermia can be deduced as approximately 3×10^{10} GNRs per ml. The most concentrated solution (12×10^{9} GNRs per ml) provided only a 9.2°C temperature rise after 10 minutes of irradiation. Although this rise may be sufficient for PTT *in vivo* where tissues have a higher core temperature (37°C) than cooler *ex vivo* tissues, it should be presumed that a large proportion of systemically delivered GNRs will not arrive specifically at the intended tumour site. Thus it is likely that future *in vivo* work would require the synthesis of higher concentrations of GNRs for adequate tumour-site accumulation. Water was used for comparison, which achieved a temperature rise of 1.6°C after 10 minutes.

A comparison of the illumination conditions and sample concentrations used in the previous chapter are considered. The illumination condition for Fig. 4-4 was that the laser fluence was 2 W/cm^2 for ten minutes and the fluence for Fig. 3-3 where reshaping was observed was 6 W/cm^2 over five minutes. At its maximal concentration, the temperature rise in Fig. 4-4 was approximately 9.5°C, while the temperature rise in Fig. 3-4 ranged from 10 to 25°C. The highest concentration of GNR samples shown in Fig. 4-4 was 6.6×10^{-12} M with an OD of 1 and the concentrations of GNRs in Fig. 3-4 ranged from 1.7 to 3.5×10^{-8} M with an OD of 2. Thus the samples used in the reshaping experiments were much more concentrated and the irradiation fluences higher but it is highly plausible that reshaping could occur with only a 10°C temperature rise in a given solution of GNRs as shown by sample γ in Fig. 3-4.

Testing this linear concentration-heating relationship on irradiated porcine oesophageal tissues showed consistency in the range of thermal effects achievable (Fig. 4-5). Tissues incubated in a very high concentration of GNRs experienced carbonisation upon irradiation with NIR, while very low GNR concentrations produced a negligible visible effect. The temperature increases recorded within tissues varied linearly with GNR concentration when exposed to NIR light (Fig. 4-6). In all samples the temperature rise shows a steep gradient in

the initial heating period until around 2 to 3 minutes, followed by a much shallower gradient. It is hypothesised that these temperature changes are due to the high optical absorption by the nanorods generating intense heating; the temperature gradient is then limited by a combination of 'melting' of the rods (as described in the previous chapter), the heat capacity of the tissue and the dissipation of heat into the surrounding environment. The temperature rise seen in Fig. 4-4 was for neat GNRs in a cuvette, while for Fig. 4-6 was for tissues incubated in GNRs and was appreciably much higher. This is likely to be because the GNRs are mainly on the surface of the tissue, and heating this thin layer generates more heat than the distributed heating throughout the depth and volume of GNRs in the cuvette. Laser power also affected tissue heating in a linear fashion independent of GNRs (Fig. 4-7). The variation in temperature rise for each power for the three repeats was large, and it is hypothesised that this is primarily due to variations between tissue samples such as blood spots. These optical absorption variations are at various spatial locations in the Gaussian profile of the laser beam thus causing inhomogeneous heating across each tissue sample. Due to the diverse range of thermal effects, it is vital to be comprehensive when pre-selecting the appropriate GNR aspect ratio, GNR concentration and laser fluence required in the PTT of adenocarcinomas, which in combination are factors not readily apparent from various published studies.

It was assumed that GNRs floating within a solution would diffuse into the incubated human oesophageal and gastric tissues and stick to them. The process of lavage/rinsing of all tissues thrice with PBS ensured that any GNRs that were merely floating on the surface of tissues were washed away leaving behind adherent molecules of GNRs that had either become endocytosed or integrated into the extracellular matrix of the tissues. The noticeable staining of tissues was observed after rinsing tissues that had been incubated with GNRs (Fig. 4-8) demonstrating substantial uptake or binding of GNRs. The amount and spatial distribution of GNR binding in tissues could be characterised in future studies using 3-D TEM image reconstruction of these tissues or by using inductively coupled plasma mass spectrometry. Conventional 2-D bright field imaging is unable to resolve whether GNRs directly translocate through the cellular membrane, or are essentially membrane-bound, or simply float on the surface of a TEM section (16). Laser heating experiments were conducted immediately after this incubation and rinsing period, minimizing, in as far as possible, the duration of tissue ischaemia.

We found that *ex vivo* human oesophagogastric tissues incubated in GNRs elicited the highest temperature rise of between 26-29°C after just 3.5 minutes of exposure to NIR light, which was sustained during irradiation. Only a modest 2°C temperature rise was seen in

tissues incubated in RPMI, even after 10 minutes of NIR irradiation (Fig. 4-9). Although these significant temperature rises were not consistently specific to adenocarcinoma tissues incubated in GNRs in all the 36 samples that were tested, the hyperthermia levels achieved were consistently much higher when compared to tissues that had only been incubated in RPMI. It is perceivable that lower temperature increments would still be effective if reproducible *in vivo*, due to higher core temperatures of *in vivo* tissues when compared to cooler *ex vivo* tissues. One postulation for the higher temperature increase seen in adenocarcinoma is that it possesses rougher and more irregular surfaces, within which more GNRs become entrapped, compared to the smooth compact uniformity of healthy tissues.

The lack of specificity in GNRs binding to cancerous tissue compared to healthy tissues is likely due to the properties inherent to *ex vivo* tissues themselves. Being *ex vivo*, the EPR mechanism of GNRs extravasating from vascular endothelial fenestrations and then accumulating around a tumour site is not possible due to the absence of a blood supply. Furthermore there is a degree of undetermined ischaemic insult that commences the moment tissues are excised from the body, which may preclude cell-GNR interaction. The GNR themselves were not functionalised with cancer-specific targeting agents. Thus both active and passive targeting methods of GNR localisation to tumour were not fully utilised, relying then on passive diffusion or a hypothetical osmosis of GNRs through cell membranes or pores emerging within devascularised tissue matrix. Specific GNR-cancer targeting modes would need to be exploited within the systemic circulation to take advantage of passive diffusion (EPR effect) and active targeting (receptor-antibody complex) of multi-functionalised GNRs in tumour theranostics.

Another feature is the tissue-GNR incubation period of 45 minutes. Most published *in vivo* experiments in rodents have generally allowed a 24 hour period after injecting GNRs prior to commencing laser irradiation, which permits time for GNRs to immerse into the tumour's matrix or become endocytosed. A shorter incubation period could confront the additional issue of being subjected to the various phases of the cell cycle, whereby cells that are synchronisingly dividing or in the quiescent phase of the cell cycle (S, G0 or G1 phase) may not instantaneously take up GNRs (17). This is particularly true in some cancer cells such as HeLa (human cervical cancer) cells, where the total cell cycle lasts 20-24 hours long. To account for this phenomenon, a longer incubation period would be needed for adequate GNR uptake, but this would adversely impact on the quality of tissues that have been devoid of oxygen during this time (despite being exposed to salient nutrients from the culture medium).

With regard to heating tissues, the general temperature rise for tissues incubated in GNRs was noted to be at least 20°C, which was consistent and hence would be sufficient, if reproducible *in vivo*, to incur irreversible cellular, protein and DNA damage to the area targeted for photothermal ablation. Other factors to consider would be the location, depth of invasion and surface area (or width) of the tumour. Multiple consecutive treatments could be required to obtain satisfactory thermal ablation in large tumours; much like fractionated radiotherapy regimes. However unlike radiotherapy, the concept of hyperthermia favours repeated applications while negating issues surrounding radiosensitivity.

4.5 Conclusions

We have demonstrated successful fabrication of GNRs with aspect ratios designed for photothermal effect as a first stage towards application for *in vivo* theranostics of oesophagogastric malignancy. Although CTAB-GNRs were used in these *ex vivo* experiments, PEGylated GNRs could be more suitable for *in vivo* applications due to their enhanced biocompatibility, which is not a concern *ex vivo*, and an identical photothermal effect would be seen due to their identical absorption spectra.

Experiments on gold nanorod solutions and in tissues showed that within the range of parameters explored, GNR concentration causes the temperature to rise in a linear manner during laser irradiation. It is deduced that a high concentration of GNR solution will be required for *in vivo* studies to obtain a sufficiently hyperthermic response suitable for the photothermal destruction of oesophagogastric adenocarcinoma. We have shown that the temperature rise is proportional to laser power and there may be some influence on heating due to variations in normal tissue chromophores.

To our knowledge this is the first time that the plasmonic photothermal effect from GNRs has been evaluated on human *ex vivo* oesophagogastric tissues. We note a substantial but indiscriminate heating of tissues incubated in GNRs then irradiated with NIR light. This temperature rise, if reproducible *in vivo*, would be effective for therapy of cancerous lesions as clinical application is possible with endoscopic coupling of laser fibres. The strong absorption of light by GNRs at relatively low laser energies renders the therapy method minimally invasive with minimal collateral damage expected in healthy tissues free from GNRs.

References

1. Miele E, Spinelli GP, Miele E, Tomao F, Tomao S. Albumin-bound formulation of paclitaxel (Abraxane (R) ABI-007) in the treatment of breast cancer. Int J Nanomed. 2009;4(1):99-105.
2. Capecitabine and Paclitaxel (Albumin-Stabilized Nanoparticle Formulation) in Treating Women Undergoing Surgery for Stage II or Stage III Breast Cancer. http://www.cancer.gov/clinicaltrials/search/view?cdrid=513169&version=HealthProfessional&protocolsearchid=12643264.
3. Staves B. Pilot study of Aurolase™ therapy in refractory and/or recurrent tumors of the head and neck. National Institutes of Health.
4. Efficacy Study of AuroLase Therapy in Subjects With Primary and/or Metastatic Lung Tumors. http://www.cancer.gov/clinicaltrials/search/view?cdrid=739962&version=HealthProfessional&protocolsearchid=12643286.
5. Magnetic Nanoparticle Thermoablation-Retention and Maintenance in the Prostate: A Phase 0 Study in Men. http://www.cancer.gov/clinicaltrials/search/view?cdrid=756661&version=HealthProfessional&protocolsearchid=12643296.
6. Rai P, Mallidi S, Zheng X, Rahmanzadeh R, Mir Y, Elrington S, Khurshid A, Hasan T. Development and applications of photo-triggered theranostic agents. Adv Drug Deliver Rev. 2010;62(11):1094-124.
7. Akhter S, Ahmad MZ, Singh A, Ahmad I, Rahman M, Anwar M, Jain GK, Ahmad FJ, Khar RK. Cancer Targeted Metallic Nanoparticle: Targeting Overview, Recent Advancement and Toxicity Concern. Curr Pharm Design. 2011;17(18):1834-50.
8. Barriere C, Qi J, Allende PBG, Newton R, Elson DS. Multifunctional gold nanorods for image-guided surgery and photothermal therapy. Proc Spie. 2012;8234.
9. Garcia-Allende PB, Barriere C, Sauvage VS, Qi J, Elson DS. Method to determine optimal illumination wavelengths for gold nanoparticle detection in tissue using reflectance spectroscopy. Clinical and Biomedical Spectroscopy and Imaging Ii. 2011;8087.
10. Zhao Q, Wang LN, Cheng R, Mao LD, Arnold RD, Howerth EW, Chen ZG, Platt S. Magnetic Nanoparticle-Based Hyperthermia for Head & Neck Cancer in Mouse Models. Theranostics. 2012;2(1):113-21.
11. Lim CK, Shin J, Lee YD, Kim J, Oh KS, Yuk SH, Jeong SY, Kwon IC, Kim S. Phthalocyanine-Aggregated Polymeric Nanoparticles as Tumor-Homing Near-Infrared Absorbers for Photothermal Therapy of Cancer. Theranostics. 2012;2(9):871-9.
12. Alkilany AM, Nagaria PK, Hexel CR, Shaw TJ, Murphy CJ, Wyatt MD. Cellular uptake and cytotoxicity of gold nanorods: molecular origin of cytotoxicity and surface effects. Small. 2009;5(6):701-8.
13. Huang P, Bao L, Zhang C, Lin J, Luo T, Yang D, He M, Li Z, Gao G, Gao B, Fu S, Cui D. Folic acid-conjugated silica-modified gold nanorods for X-ray/CT imaging-guided dual-mode radiation and photo-thermal therapy. Biomaterials. 2011;32(36):9796-809.
14. Kirui DK, Krishnan S, Strickland AD, Batt CA. PAA-derived gold nanorods for cellular targeting and photothermal therapy. Macromol Biosci. 2011;11(6):779-88.
15. O'Neal DP, Hirsch LR, Halas NJ, Payne JD, West JL. Photo-thermal tumor ablation in mice using near infrared-absorbing nanoparticles. Cancer Lett. 2004;209(2):171-6.
16. Al-Jamal KT, Nerl H, Muller KH, Ali-Boucetta H, Li SP, Haynes PD, Jinschek JR, Prato M, Bianco A, Kostarelos K, Porter AE. Cellular uptake mechanisms of functionalised multi-walled carbon nanotubes by 3D electron tomography imaging. Nanoscale. 2011;3(6):2627-35.
17. Kim JA, Aberg C, Salvati A, Dawson KA. Role of cell cycle on the cellular uptake and dilution of nanoparticles in a cell population. Nature Nanotechnology. 2012;7(1).

Chapter 5 *In vitro* assessments of functionalised gold nanorods for imaging and targeted therapy of *in vivo* gastrointestinal cancer

5.1 Introduction

While the plasmon photothermal effect has been shown to potentially be an effective method of clinically inducing irreversible tumour photodestruction in human *ex vivo* oesophageal and gastric adenocarcinoma, it is prudent to investigate this further in an *in vitro* setting. This required the fabrication of coated GNRs which can be taken up by live cancer cells. In order for this to be a viable process for both *in vitro* and *in vivo* application including imaging, the surface of GNRs required a stealth coating such as PEG and multi-functionalisation with a fluorescent dye and a targeting ligand. Cumulatively this would enable appropriately functionalised GNRs to be biocompatible, optically detectable and cancer specific. This feature of multi-functionality further required GNRs to possess an aspect ratio and SPR absorption peak that was optimally tuned to the NIR.

In this chapter the fabrication of these target-specific fluorescent GNR constructs is described. Exposing these nano-constructs to a combination of human adenocarcinoma and healthy cells tested their efficiency at tumour targeting. FLO-1 cells are human oesophageal adenocarcinoma cells which were chosen as a robust and verified cell line suitable for representing GI adenocarcinoma cells in general, within the context of PTT.

Epidermal growth factor receptor (EGFR), found on the surface of cells, is commonly upregulated in a variety of epithelial malignancies, including oesophageal, gastric and colon adenocarcinomas. EGFR inhibitors such as Cetuximab are indicated in the treatment of metastatic colorectal cancer, metastatic non-small cell lung cancer and head and neck cancer. They have been explored in patients with upper GI cancers, and it is apparent that distal oesophageal and oesophagogastic junctional (OGJ) tumours may be more sensitive to EGFR blockade than distal gastric adenocarcinomas (1). In oesophageal cancer, immunohistochemistry (IHC) proven EGFR overexpression is very common, occurring in approximately 80% of patients with adenocarcinoma and squamous cell carcinoma (2). In the work described in this chapter, the expression of epidermal growth factor receptors (EGFR) on FLO-1 cells was thus tested with IHC. In addition to this, *in vitro* IHC and

fluorescence microscopy was performed to evaluate the FLO-1 cellular uptake of anti-EGFR-antibody modified GNRs. The concept of *in vitro* photothermal therapy of cancer cells with GNRs is also reported and discussed. This chapter concludes by expounding on the application of FLO-1 cells in an *in vivo* model for establishing human oesophageal adenocarcinoma tumour xenografts. Hence the concept and potential for multi-functionalised GNRs in providing tumour theranostics is explored *in vitro* as a precursor to *in vivo* work.

5.2 Synthesis of GNRs and functionalisation with fluorophore and anti-EGFR antibody

GNRs were fabricated using the seed-mediated method described by Murphy *et al*. (3) and work done by Mr. Yu Zhou, as described in Methods and Materials. CTAB molecules on the surface of GNRs were replaced by carboxyl PEG. Subsequent EDC/NHS chemistry was used to functionalise GNRs with a fluorophore (Cy5.5) modified with an anti-EGFR antibody.

5.3 Human oesophageal adenocarcinoma (FLO-1) cells

FLO-1 cells have been verified as a true human oesophageal adenocarcinoma cell line and are recommended for research on oesophageal adenocarcinoma (4). These cells were obtained from Mr. Stefan Antonowicz MB ChB, MSc, MRCS a Clinical Research Fellow at the Department of Surgery and Cancer, Imperial College London. FLO-1 cells were established from a primary distal oesophageal adenocarcinoma in a 68-year-old Caucasian male in 1991. They are of epithelial origin and have an adherent growth mode (5). The subculture routine involves splitting sub-confluent cultures (70-80%) into 1:4 to 1:8, i.e. seeding at 1-3 x 10,000 cells/cm^2 using trypsin/EDTA; 5% CO_2; 37°C. The saturation density is approximately 10^5 cells/cm^2.

Cells were thus passaged routinely and incubated at 37°C in humidified air with 5% CO_2 and maintained in a state of logarithmic growth. They were cultured in T175 flasks (Flask EZ Nunclon 175 cm^2 Angled Neck Filter Sterile, VWR International Ltd., Lutterworth, UK). Cell culture work was performed at Chelsea and Westminster Hospital, London. The culture medium for FLO-1 cells is Dulbecco's Modified Eagle's Medium (DMEM) – 4500 mg

glucose/ml (Sigma-Aldrich Company Ltd. Dorset, UK) and the following was added to a standard 500 ml container of DMEM:

- 10% Foetal Bovine Serum (Sigma-Aldrich).
- 2 nM L-Glutamine Solution Bioxtra 200 mm (Sigma-Aldrich).
- 100 U/ml Penicillin + 100 mg/ml Streptomycin solutions (Sigma-Aldrich).

5.4 TEM imaging of functionalised GNRs

The aspect ratios (AR) of GNRs were determined using TEM (JEOL 2100 FEG-TEM). A small drop of ~8 μL of diluted aqueous GNR solution was pipetted onto a holey carbon film on 300 mesh copper grids (Agar Scientific, UK) and subsequently allowed to dry at room temperature. TEM images were routinely acquired using a JEOL 2010 high resolution TEM at an acceleration voltage of 200 kV. The image shown in Fig. 5-1, using bright field and dark field contrast, demonstrate an average GNR length of 70 nm, with an AR of 4. These images of our functionalised GNRs (courtesy of Experimental Techniques Centre, Brunel University London, using a Scanning Transmission Electron Microscope, STEM, taken at 80 kV), also showed that there were some nanospheres within the solution, produced as by-products, which correspond to the smaller spectral peak at 520 nm.

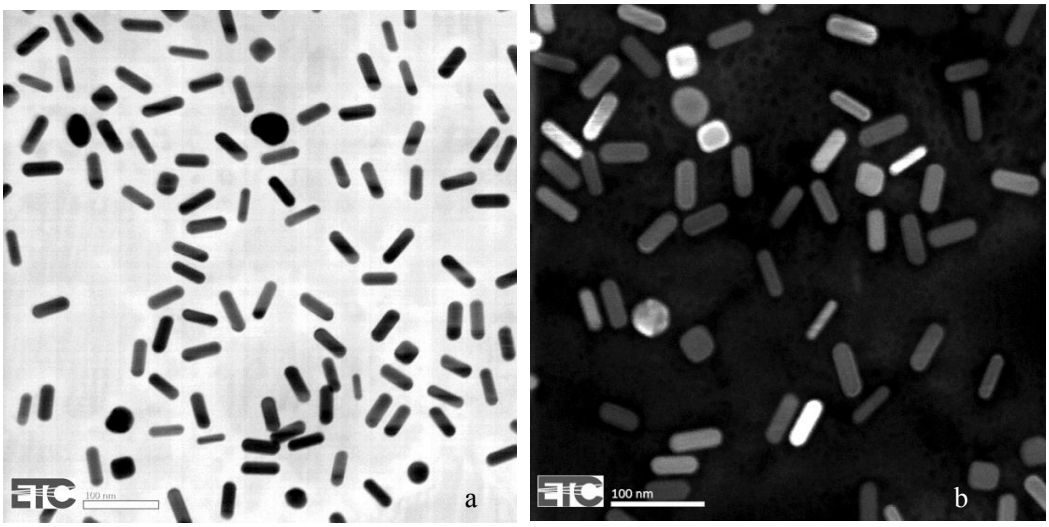


Fig. 5-1 Bright field (a) and dark field (b) STEM images of functionalised GNRs (courtesy of ETC, Brunel University London). Scale bars = 100 nm.

Scanning electron microscopy (SEM) was attempted to delineate the presence of GNRs within FLO-1 cells. However we were unable to clearly identify the presence of GNRs using

this method. It was thus decided that the best way to identify their intratumoural presence was to use TEM, which is more commonly used in nanoparticle characterisation and localisation. We subsequently performed and demonstrated this more definitely *in vivo* (refer to Section 6.6.1 in Chapter 6).

5.5 Immunohistochemistry and Epidermal Growth Factor Receptor (EGFR) Antigen Targeting

"*Immunohistochemistry is used to detect the presence or location of antigens (e.g. proteins) in cells of a tissue section by application of the principle that antibodies bind specifically to antigens in biological tissues. It is used particularly to diagnose cancerous cells, and the distribution/localisation of biomarkers and differently expressed proteins in different parts of a biological tissue*" (6).

EGFR is a family of transmembrane proteins with an extracellular receptor domain regulating an intracellular tyrosine kinase (7). EGFR (HER-1) is commonly over-expressed by many cancers including breast, GI and head and neck adenocarcinomas. It is important in signalling pathways, regulation of angiogenesis, cell proliferation and tumour metastases (8, 9).

Surface modification by attachment of an anti-EGFR antibody could increase the yield of GNRs within cancerous cells that overexpresses the EGF receptor. Kao *et al*. conjugated GNPs with cetuximab, an antibody-targeting EGFR, and further labelled the GNPs with In-111, which created EGFR-targeted AuNPs. Their results suggest that anti-EGFR-antibody-conjugated GNPs are a useful anti-tumour tool for the treatment of EGFR-overexpressed cancers (10). This overexpression of the EGF receptor on the surface of cancer cells, combined with the specificity of antibody binding, has been found to require only half the laser energy to destroy normal cells when both cell types were incubated in the same concentration of nanorod bioconjugates, which is a feature of selective PTT (11). Kwon *et al*. demonstrated that their intravenously delivered EGFR-NPs had a higher affinity for human breast tumours in mice at all time points in comparison to antibody-free NPs, from which it was concluded that the EGFR-specific-antibody-NP is more effective for cancer targeting *in vivo* (12). These tumours responded well to photothermal therapy with NIR laser irradiation.

The antibody attached to our GNR was an anti-EGFR antibody which was also conjugated to a fluorophore (Cy5.5), acquired from a commercial source, which was aimed at aiding detection via immunofluorescence. 4', 6-diamidino-2-phenylindole (DAPI) was used as a counterstain to highlight the location of cell nuclei.

For *in vitro* fluorescence microscopy, we stained our FLO-1 cell nuclei with DAPI and purchased fluorescent anti-EGFR antibody which was added to the cells in culture medium. These immunohistochemistry experiments were performed with Dr. Hailin Zhao PhD, a Research Associate at Chelsea and Westminster Hospital. The method is described below:

FLO-1 cells were fixed in paraformaldehyde in 0.1 mol/l PBS solution. Cells were then incubated in 10% normal donkey serum in 0.1 mol/l PBS-Tween 20 and then incubated overnight with rabbit anti-EGFR (1:200, Abcam) followed by incubation with donkey anti-rabbit secondary antibody for 1 hour. The slides were counterstained with nuclear dye DAPI and mounted with VECTASHIELD Mounting Medium (Vector Laboratories, Burlingame, CA). Cells were examined using an Olympus (Watford, UK) BX4 microscope using 20x objective.

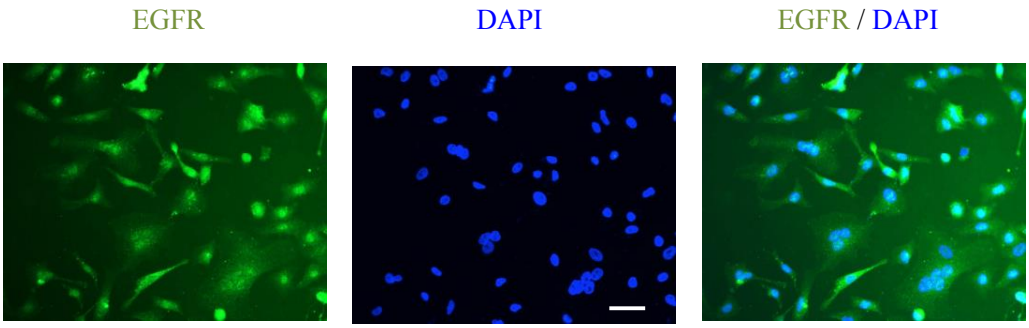


Fig. 5-2 Blue nuclear DAPI staining and anti-EGFR antibody fluorescent in green. The merged EGFR/DAPI image demonstrates binding of anti-EGFR antibody around the nuclei. Scale bar = 50 μm.

Results from immunohistochemistry experiments as shown in Fig. 5-2 demonstrated that our chosen cancer cells express the EGFR receptor as they take up free anti-EGFR antibody and we should therefore similarly target these cancer cells for *in vivo* experiments by conjugating GNRs with anti-EGFR-antibody.

5.6 Immunohistochemistry and fluorescence microscopy of functionalised GNRs and cancer cells

FLO-1 cells were fixed on two coverslips. 2 ml of cells with their medium was pipetted onto four coverslips and incubated overnight at 37°C. The next day, the medium was removed and 1 ml of 4% para-formaldehyde (PFA) added. After 15 minutes, PFA was removed and replaced by PBS such that the cells in the dish were adequately bathed.

Cy5.5-PEG-anti-EGFR-antibody functionalised GNRs were then added in a ratio of 1:200 dilution (diluted with PBS). Thus for two coverslips, 1.5 µL GNR solution is added to 298.5 µL PBS making a total of 300 µL of PBS-GNR inside a test tube. This was mixed for a few seconds with a vortex stirrer. 150 µL of this PBS-GNR mixture was added onto one coverslip, and another 150 µL onto a second coverslip (total volume used was thus 300 µL). This was then left overnight to incubate with the functionalised GNRs in the dark to allow ≥16 hours for the optimal expression of an antigen. The next day, all GNRs were removed and all coverslips washed thrice with PBS. DAPI drops were pipetted onto a slide to stain the cell nucleus. The coverslips with cells were turned over to face the DAPI. After 24 hours or more of DAPI staining, fluorescence microscopy was performed.

For *in vitro* fluorescence staining, cells were fixed in paraformaldehyde in 0.1 mol/l PBS solution. Cells were then incubated in 10% normal donkey serum in 0.1 mol/l PBS-Tween 20 before being incubated overnight with the functionalised GNR. The slides were counterstained with nuclear dye DAPI and mounted with VECTASHIELD Mounting Medium (Vector Laboratories, Burlingame, CA). Sections were examined using an Olympus (Watford, UK) BX4 microscope using 20x magnification.

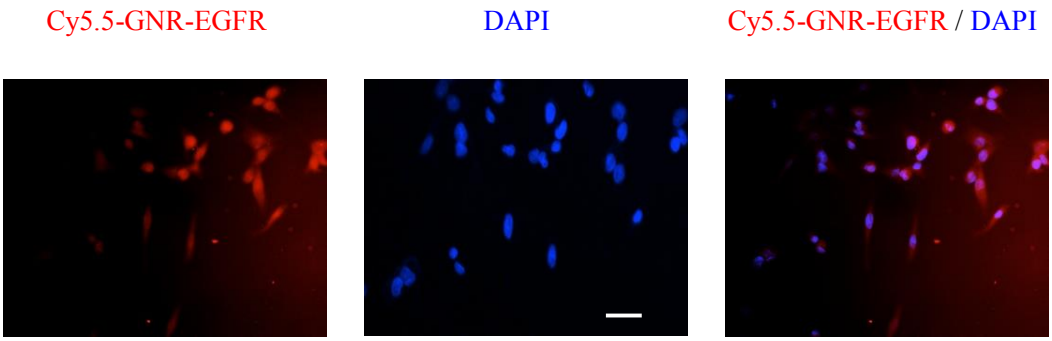


Fig. 5-3 The FLO-1 nuclei with DAPI and fluorescence from the Cy5.5-GNR-anti-EGFR-antibody in red. Merged Cy5.5-GNR-EGFR/DAPI fluorescence microscopy images demonstrating the binding of FLO-1 cells to antibody- and fluorophore-conjugated GNRs. Scale bar = 50 µm.

The results of immunohistochemistry and microscopy represented in Fig. 5-3 demonstrate that FLO-1 nuclei fluoresces blue under DAPI staining. The fluorophore Cy5.5 attached to a pure sample of anti-EGFR-antibody-functionalised GNRs shows that they too were fluorescent. The superimposed images of both Cy5.5-GNR-EGFR/DAPI showed that the GNRs were perinuclear and intracellular and there were no fluorescent signals coming from isolated, untargeted or free-floating fluorophores. The binding was efficient and suitable for PTT. This experiment was repeated thrice, showing good degree of binding on all occasions. We did not however observe this binding with Het-1A cells (a healthy squamous oesophageal cell line). In a separate experiment, the fluorescence properties of the functionalised GNRs were measured with a plate reader. The fluorescence of functionalised GNRs was well above the corresponding supernatant of the centrifuge solution, meaning that the fluorescence seen (in red) in Fig. 5-3 was unlikely to be from free fluorophores present in solution, but from functionalised GNRs.

We also used a different human oesophageal adenocarcinoma cell line (OE-33) for immunohistochemistry and for *in vivo* application. Despite showing encouraging fluorescence microscopy results of uptake of functionalised GNRs, OE-33 cells proved to be challenging to culture in two different cell culture laboratories, and as such, FLO-1 cells which were noted to be more robust and reliable, and also had a good rate of GNR uptake, were preferentially chosen for both *in vitro* and *in vivo* studies.

5.7 NIR laser irradiation of other cells incubated with functionalised GNRs

Dr. Clément Barrière PhD, a previous Research Associate in our group performed this *in vitro* experiment. It is included here to demonstrate that our group had previously tested the concept of *in vitro* photothermal therapy which has also been demonstrated by various other groups. We had no intention of reproducing the experiment *in vitro* with our FLO-1 cells as it would not add value to the information already gained from *ex vivo* tissue and already known from literature, where cellular and tissue destruction was possible with a combination of GNRs and laser irradiation. However the results adequately illustrate the effect of PTT on cells using a classic live/dead assay, thus it is mentioned here for completeness. The following is adapted from a paper drafted for publication but not yet submitted.

HeLa (human cervical cancer) or OSEC2 (normal ovarian epithelial) cells were grown in a 48 well plate. The GNRs used were functionalised with either an aptamer (AS1411) or folic acid. AS1411 is an oligonucleotide which can be specifically endocytosed by cancer cells, its uptake being nucleolin-driven, where nucleolin is the receptor which is overexpressed on the membrane and in the cytoplasm of tumour cells (13). The viability and the proliferation of cells in the presence of functionalised GNRs were assessed. Viability tests were made on HeLa cells, in 48 well plates. 20,000 cells per well were plated. Experiments were repeated on three different wells, to reduce any random errors. The solutions were cultured for one day in the corresponding complete media, either complete DMEM (for HeLa cells) or complete RPMI (for OSEC2 cells). This was followed by 24-72 hours of incubation with a solution of GNRs dissolved in biological media (0.5 ml with 10^{11} GNRs per well). Live/dead assays (Calcein/Ethidium homodimer) were purchased from Invitrogen and the standard procedure was followed to assess the permeability of the nucleus membrane of the cells. Briefly, the GNRs solution was carefully removed, and each well was rinsed with 0.5 ml PBS. A solution of 23 mM of ethidium homodimer (dead) and 1 mM of calcein AM (live) was prepared in PBS. Each well was then incubated with 0.5 ml of this solution for 20 minutes.

Toxicity and cellular damage experiments were designed to assess the potential toxicity of the combination of GNRs with laser irradiation on HeLa cells (cell death was assessed with a classic live/dead assay). Cells were plated (10,000 HeLa cells per well) in a 48 well plate two days before the experiment in their corresponding media. This method was used to insure complete coverage of each well. For each sample of multi-functionalised GNRs, three wells were filled. Two of those were exposed to the laser while the last one was used as a control. After two days of incubation, the media was removed and replaced by multi-functionalised GNRs solutions dissolved in complete DMEM (for HeLa cells) and the well plate was incubated for four hours. The solution for the live/dead assay was prepared just before the laser experiment and left in the dark. All the wells were emptied of their respective solution and rinsed once with PBS. The control well was used to assess whether the cells were still alive after this treatment. The live/dead assay was performed as soon as possible after the PTT experiment. Should the cells be alive, they would show up as green, and if dead, they should declare themselves as red.

A thermal camera (FLIR S65 Thermal Imaging camera – 320×240 pixel LWIR detector – 80 mK) was used which could indicate the emissivity over a large area and record temperature variation efficiently. A NIR laser diode (ThorLabs, L808P1WJ, 808 nm, 0.3 nm bandwidth, maximum power: 1 W) was used to heat the GNRs-cells.

The well plate was placed in front of the laser as per the set-up illustrated in Fig. 5-4. A standard experiment used 0.78 W of laser power. Images were recorded for 20 seconds to assess the background noise and temperature properties. Subsequently the shutter blocking the laser beam was removed for one minute. This procedure was repeated for all the wells except for controls. The live/dead assay was performed immediately after this experiment. An inverted microscope (Olympus IX51) was used to detect cell fluorescence with a 100 W mercury lamp and an Olympus DP70 colour camera while the Olympus software (DP controller and manager V3.1.1) was used to visualise the images.

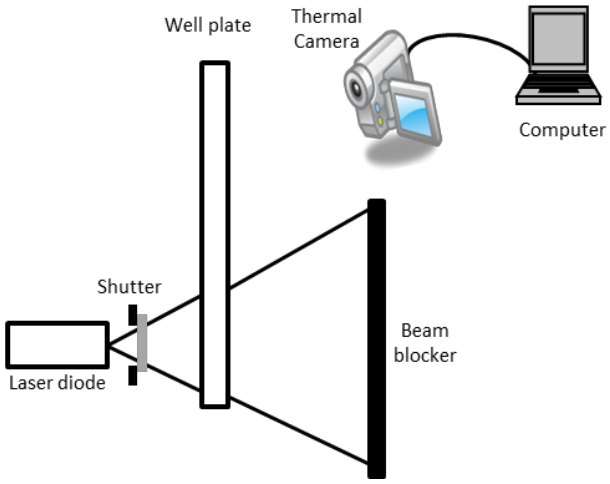


Fig. 5-4 Laser set-up: The laser diode was directed on one particular well of the 48 well plate. Heating was recorded with a thermal imaging camera mounted above the well plate.

Results

No temperature increase was detected in cells which were not incubated with or exposed to GNRs. The influence of the laser on cells incubated with GNRs was studied using a live/dead assay. Fig. 5-5(b) shows that after just 10 seconds, some cells have already been photothermally destroyed (red staining). The area destroyed after 15 seconds in Fig. 5-5(c) was already slightly larger than the spot size of the laser, showing that the heat quickly dissipated to the periphery, where red and dead cells are stained. The central area of irradiation is totally devoid of any staining, as completely obliterated cells are not able to pick up the stain.

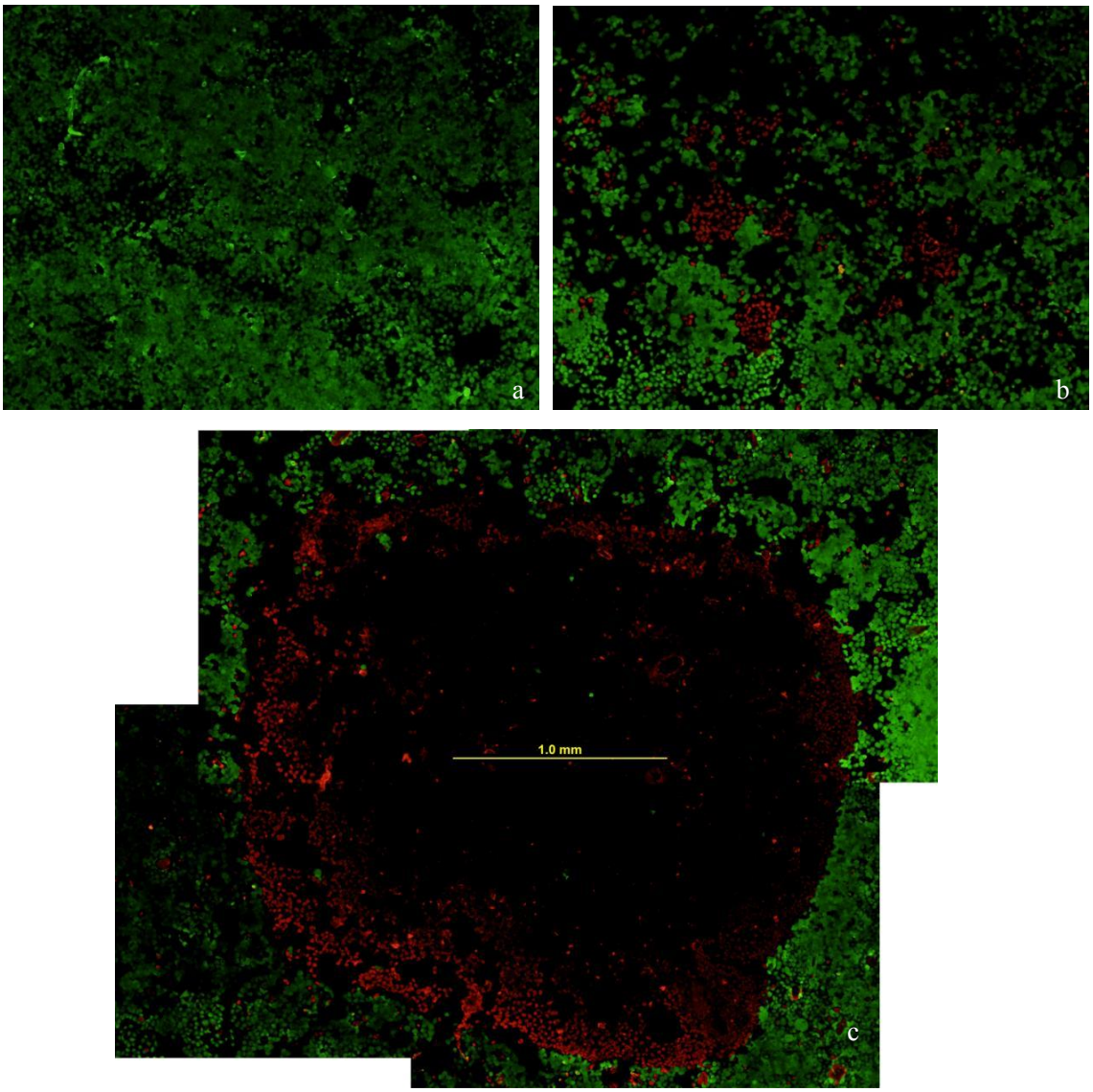


Fig. 5-5 Live/dead assay on HeLa cells with GNRs after (a) 5; (b) 10; and (c) 15 seconds of exposure to NIR laser (Scale bar = 1 mm).

Temperature profile data showed that all negative control cells (with/without application of laser light or with/without non-targeted GNRs) demonstrated good viability after the experiment. The results with neutral PEG (SH-PEG-CH_3) showed no toxicity with the live/dead assay and were comparable to the negative control. It is important to note that when left for only four hours (the time required to perform the subsequent laser experiment), no toxicity was observed.

Only active targeting with folic acid or the aptamer AS1411 led to cell death. As observed by the thermal imaging camera, the area of dead cells increased proportionately with the final temperature reached. This study demonstrated the effectiveness and selectivity of photothermal destruction of cells incubated with appropriately functionalised GNRs which were then irradiated. To target cells, it was possible to functionalise GNRs with either folic acid or the aptamer AS1411. Both compounds are biocompatible, but it was noted that using an aptamer provided greater heat intensity and better specificity to tumour cells. While this photothermal effect is confirmed *in vitro*, it was thus necessary to study this phenomenon *in vivo*.

5.8 Establishing human oesophageal adenocarcinoma tumour xenografts in immunodeficient mice

Although we have been successful in the application of imaging and photothermal therapy for tumour localisation in cells and *ex vivo* tissues, this has been thus far limited by the lack of a circulatory system, which is the route by which GNRs get to the site of the tumour *in vivo*. The previous work was essential in laying the foundations for successful GNR synthesis and functionalisation with fluorophores and antibodies/aptamers, and to estimate the concentrations of GNRs and laser fluence required to produce adequate hyperthermia.

In an *in vivo* study, GNRs would target cancer cells by exploiting tumour physiology (EPR effect) and also by utilising the active antibody-antigen principles of selective targeting. There are semi-permeable vessels surrounding a tumour, where GNPs, due to their size, can diffuse through once delivered into the systemic circulation. Towards this a full physiological system is required including blood flow, lymph activity and, for the photothermal effect and subsequent healing, the full complement of the coagulation cascade.

Ethical approval was sought under the Animals (Scientific Procedures) Act 1986 and was granted by the Secretary of State for a small animal project licence (PPL number 70/7996) on the 14th of August 2014. The author was the project licence holder and had a personal licence to carry out regulated procedures on living animals (PIL number 70/25542). Rodent work was conducted at The Northwick Park Institute for Medical Research (NPIMR).

FLO-1 cells were grown and incubated in T175 flasks at the cell culture laboratory at the Department of Anaesthetics, Chelsea and Westminster Hospital, London. When cells were approximately 95% confluent, the culture medium was aspirated and replenished with fresh

medium to remove dead and detached cells. Subsequently, the entire medium was removed and cells washed with 20 ml of PBS. Approximately 5-6 ml of 0.05% trypsin-EDTA was added (Trypsin 0.05% EDTA, Life Technologies Limited, Paisley, UK) to disperse cells. The trypsinised cells were re-incubated at 37°C for 10 minutes prior to being transferred into a 50 ml sterile test tube, which was then centrifuged immediately at or below 1500 rpm for 5 minutes. Viable cells could be counted using a hemocytometer. The supernatant was decanted and the cell pellet was suspended in medium such that there was approximately 100 µl medium added per flask of confluent cells. As a rough guide, one confluent T 175 cm^2 flask of approximately 15-20 x 10^6 cells was needed to grow a tumour in one mouse. Ultimately a 100 µl suspension of both cells and medium was injected subcutaneously into each mouse. Cells were transported in a sterile test tube to NPIMR where immunodeficient mice were housed in an aseptic environment and handled with aseptic technique.

8-9 weeks old male immunodeficient BALB/c nu/nu (comprising 92% of the total number used) and CB-17 SCID (severe combined immunodeficiency) mice (8%) were obtained from Charles River UK Ltd. (Kent, England). They underwent an acclimatisation period after arrival. The inoculation area was shaved (if necessary), then cleaned and sterilised with ethanol and/or iodine solutions. A 30-gauge needle was used to mix the cells with their medium and a 0.5 ml insulin syringe was used to draw the cells into the syringe. Under manual restraint, 15-20 x 10^6 cells were injected subcutaneously (s/c) at one site, usually into either flanks (or the back) of the mice. NIR therapy could then be started after approximately a fortnight when the tumours reached a minimum of 5 mm in any one dimension, measured regularly with digital callipers (Electronic Vernier Calliper, Sealey Group, Bury St. Edmunds, Suffolk, UK) as shown in Fig. 5-6.

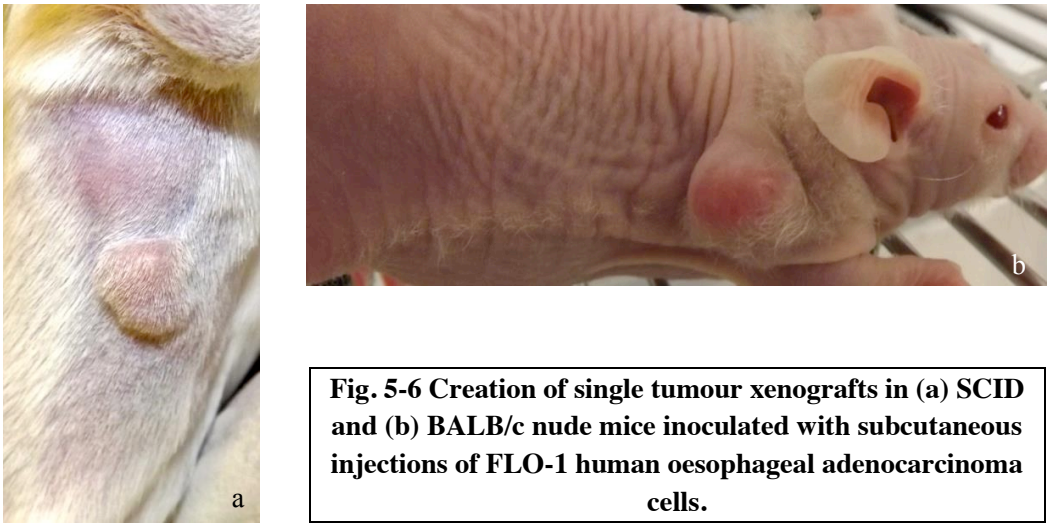


Fig. 5-6 Creation of single tumour xenografts in (a) SCID and (b) BALB/c nude mice inoculated with subcutaneous injections of FLO-1 human oesophageal adenocarcinoma cells.

When proportionally compared to the height of a nude mouse (typically 6.5 cm), these 5-6 mm tumours would, in a typically built adult human male (175 cm), conform to a tumour that is roughly the size of a hand (14 cm), with the depth of a fist (5 cm). They were noted to grow aggressively, reaching appropriate size for experimentation within approximately 10-14 days. In our small animal project licence it was decreed that in the case of a single tumour attaining a mean diameter exceeding 1.2 cm, the animal would be humanely killed (abiding by the National Cancer Research Institute guidelines). The high growth rate of these tumours meant that they would often grow to their maximal dimension within 17 days after becoming suitable for intervention.

It is expected that for a tumour to become clinically evident, a threshold of sufficiently actively replicating cancer cells has to be overcome before uncontrolled division and oncogenic propagation can lead to tumour formation. Pilot tumour growth studies using 2 -3 mice were performed to determine which patterns of local growth were reproducible. This also showed any potential adverse effects associated with tumour progression and enabled humane endpoints to be identified (14). An insufficient number of cancerous cells will suppress the induction of tumour through the immune system, even in immune-compromised mice. The criteria for success in the process of subcutaneous cancer cell implantation was to have at least 80% of animals producing tumours of 5 mm minimum in two axes measured (measured using callipers in three directions; maximum length, width and depth) within eight weeks as published by E. Oikonomou *et al*. (15). We expected that the success rate of tumour induction would be in excess of 80% as the previous work quoted above suggests that 100% is achievable. At the end of this experiment the first go/no-go decision was made - if no tumours, insufficient numbers of tumours (less than 80%) or no adequately sized tumours are produced, the project could not progress further and further *in vitro* optimisation work would become necessary. When appropriate tumours were induced, some of the animals became the control arm of all ensuing experiments to ensure that the induced tumours were not self-limiting, that GNRs by themselves would not elicit tumour regression or that laser alone would not induce a thermal therapy of tumours. Tumours were also biopsied with core (punch) biopsy where histological confirmation of adenocarcinoma was evaluated.

Confirmation that the tumours which developed from subcutaneous injections of FLO-1 cells was obtained through punch biopsies and histological evaluation. This was consistent with active and well-established adenocarcinoma of an alimentary tract origin (shown in Fig. 5-6).

Throughout the period of the animal study there was no morbidity or mortality suffered by the animals from any adverse reactions from either the inoculation procedure or tumour growth.

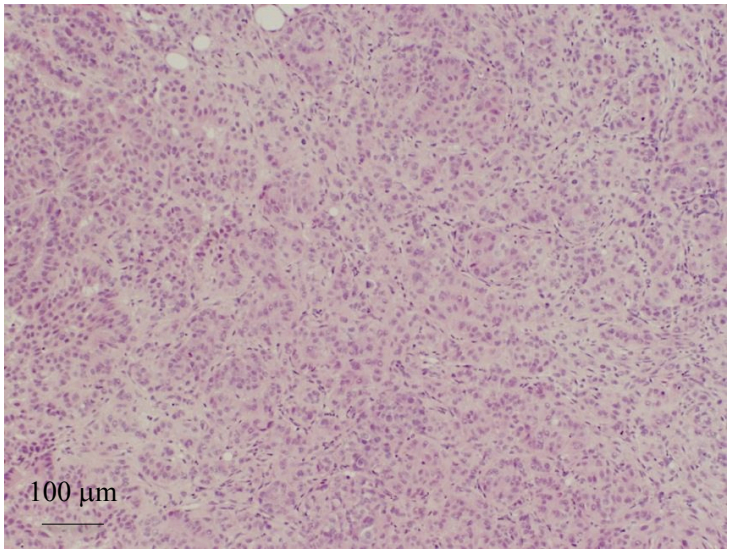


Fig. 5-6 Histology (100x mag.) from the gastrointestinal tumours induced in mice with FLO-1 cells, indicating many ciliated columnar cells with some goblet cells present. There are also many crypts.

5.9 Discussion

The main purpose of this work was the fabrication of suitably functionalised GNRs which would then be able to target tumours *in vivo* for the purpose of imaging (diagnosis) and tumour ablation (therapy). Consequently these GNRs had to fulfil numerous criteria – they had to be coated with PEG to improve biocompatibility and reduce aggregation; they had to possess a SPR which was attuned to strongly absorb light at approximately 808 nm (which would correspond both to the therapeutic optical window of tissues being in the NIR, as well as match the emission of our CW diode laser); they had to be suitably concentrated (with a high optical density) for *in vivo* application and be functionalised with a fluorophore (Cy5.5) as well as a targeting ligand. Anti-EGFR antibody was the ligand of choice as EGFR is not only overexpressed in oesophageal cancers, but numerous other cancers and hence our results could potentially be transferable to a broader application. Validation, stability and characteristics of these functionalised particles were demonstrated via UV-Vis spectroscopy, zeta potential measurements and TEM. A mean GNR length of 70 nm and an aspect ratio of four was identified with TEM.

FLO-1 cells were chosen as a verified representative for GI tract adenocarcinoma. These cells were shown by immunohistochemistry techniques and fluorescence microscopy to express an abundance of EGFR on their cell surface, which should in theory bind to the ligand attachment on the surface of our functionalised GNRs. This specific antibody-antigen mechanism of binding was subsequently confirmed *in vitro* by fluorescence microscopy on FLO-1 cells which were incubated with fluorophore- and antibody-functionalised GNRs. The photothermal destruction of cancer cells was illustrated by the previous work done by our group using live/dead assay on cancer cells incubated with functionalised GNRs and then irradiated for a very short duration with NIR laser. As it was crucial to then test this effect *in vivo* by establishing a live tumour model, FLO-1 tumour xenografts were established in immunodeficient mice in order to scrutinise the intricate interplay between physiology and tumour pathology in response to GNRs and photothermal therapy.

References

1. Dragovich T, Campen C. Anti-EGFR-Targeted Therapy for Esophageal and Gastric Cancers: An Evolving Concept. J Oncol. 2009;2009:804108.
2. Takaoka M, Harada H, Andl CD, Oyama K, Naomoto Y, Dempsey KL, Klein-Szanto AJ, El-Deiry WS, Grimberg A, Nakagawa H. Epidermal growth factor receptor regulates aberrant expression of insulin-like growth factor-binding protein 3. Cancer Research. 2004;64(21):7711-23.
3. Yang JA, Lohse, S.E., Boulos, S.P., Murphy, C.J. The Early Life of Gold Nanorods: Temporal Separation of Anisotropic and Isotropic Growth Modes. J Clust Sci. 2012;23:799-809.
4. Boonstra JJ, van Marion R, Beer DG, Lin L, Chaves P, Ribeiro C, Pereira AD, Roque L, Darnton SJ, Altorki NK, Schrump DS, Klimstra DS, Tang LH, Eshleman JR, Alvarez H, Shimada Y, van Dekken H, Tilanus HW, Dinjens WNM. Verification and Unmasking of Widely Used Human Esophageal Adenocarcinoma Cell Lines. J Natl Cancer I. 2010;102(4):271-4.
5. Public Health England. General Cell Collection: FLO-1.
6. Ramos-Vara JA, Miller MA. When Tissue Antigens and Antibodies Get Along: Revisiting the Technical Aspects of Immunohistochemistry-The Red, Brown, and Blue Technique. Vet Pathol. 2014;51(1):42-87.
7. Harari PM. Epidermal growth factor receptor inhibition strategies in oncology. Endocrine-Related Cancer (England: Society for Endocrinology) 2004;11(4):689–708.
8. Waksal HW. Role of an anti-epidermal growth factor receptor in treating cancer. Cancer Metast Rev. 1999;18(4):427-36.
9. Citri A, Yarden Y. EGF-ERBB signalling: towards the systems level. Nat Rev Mol Cell Bio. 2006;7(7):505-16.
10. Kao HW, Lin YY, Chen CC, Chi KH, Tien DC, Hsia CC, Lin WJ, Chen FD, Lin MH, Wang HE. Biological characterization of cetuximab-conjugated gold nanoparticles in a tumor animal model. Nanotechnology. 2014;25(29).
11. Dickerson EB, Dreaden EC, Huang XH, El-Sayed IH, Chu HH, Pushpanketh S, McDonald JF, El-Sayed MA. Gold nanorod assisted near-infrared plasmonic photothermal therapy (PPTT) of squamous cell carcinoma in mice. Cancer Letters. 2008;269(1):57-66.

12. Kwon KC, Ryu JH, Lee JH, Lee EJ, Kwon IC, Kim K, Lee J. Proteinticle/Gold Core/Shell Nanoparticles for Targeted Cancer Therapy without Nanotoxicity. Advanced Materials. 2014;26(37):6436-41.
13. Soundararajan S, Wang L, Sridharan V, Chen WW, Courtenay-Luck N, Jones D, Spicer EK, Fernandes DJ. Plasma Membrane Nucleolin Is a Receptor for the Anticancer Aptamer AS1411 in MV4-11 Leukemia Cells. Mol Pharmacol. 2009;76(5):984-91.
14. Workman P, Aboagye EO, Balkwill F, Balmain A, Bruder G, Chaplin DJ, Double JA, Everitt J, Farningham DAH, Glennie MJ, Kelland LR, Robinson V, Stratford IJ, Tozer GM, Watson S, Wedge SR, Eccles SA, Navaratnam V, Ryder S, Inst NCR. Guidelines for the welfare and use of animals in cancer research. Brit J Cancer. 2010;102(11):1555-77.
15. Oikonomou E, Kothonidis K, Zografos G, Nasioulas G, Andera L, Pintzas A. Newly established tumourigenic primary human colon cancer cell lines are sensitive to TRAIL-induced apoptosis in vitro and in vivo. Brit J Cancer. 2007;97(1):73-84.

Chapter 6 Application of functionalised GNRs for *in vivo* theranostics of human oesophageal adenocarcinoma

6.1 Introduction

In previous studies we have noted a substantial but indiscriminate heating of human *ex vivo* tissues incubated in GNRs then irradiated with NIR light. We hypothesised that this temperature rise, if reproducible *in vivo*, would be effective therapy for tumour ablation. The strong absorption of GNRs at relatively low laser energies renders the therapy method minimally invasive with minimal collateral damage expected in (healthy) tissues free from GNRs. Our encouraging *in vitro* and *ex vivo* results requires further investigation using a model with a circulatory and physiological system akin to humans. The *in vivo* work presented in this chapter thus incorporates applying the knowledge and lessons learnt from the preceding *ex vivo* and *in vitro* experiments.

We propose, by direct application of a fibre optic catheter, to deliver NIR laser light to nude mice inoculated with a subcutaneous tumour xenograft derived from implantation of a human oesophageal adenocarcinoma cell line after systemically or locally administering functionalised GNRs. These GNRs would be coated with polyethylene glycol (PEG), and functionalised with a fluorophore (Cy5.5) and a targeting agent (anti-EGFR antibody). The fluorophore dye will aid visualisation of the tumour and provide a region of interest with which to direct the NIR laser beam for subsequent photothermal therapy (PTT).

Developing this application for PTT and an endoscopic fluorescent cancer detection system would address a clinical need for improved cancer theranostics. The anticipation is that some form of tumour regression and shrinkage will be evident due to the hyperthermia caused from the absorption and conversion of NIR light into thermal energy.

The rationale behind utilising an oesophageal cancer model is that oesophageal cancer rates have risen by 65% in men and 14% in women since the mid-1970s, and it tends to be a largely indolent but aggressive tumour with the propensity for presenting at advanced stages. There is also a miss rate associated with early oesophago-gastric lesions on endoscopy which could be overcome by image-guided ‘optical biopsies’ as alluded to in Chapter 1. The incidence rate in the UK is second highest in Europe for males and the highest for females

(1). In the national oesophago-gastric (O-G) cancer audit conducted from April 2011-March 2012, the estimated number of patients diagnosed in England with O-G cancer was 13,003 (2). Out of these 2,253 received surgery, 5,155 received primary chemo/radiotherapy and 1,557 received an endo-palliative procedure. The median length of stay for oesophagectomy was 13 days and 11 days for a gastrectomy. For colorectal cancer, 29,445 patients underwent surgery in England and Wales (April 2011-March 2012), with a median length of stay of 7 days. In GI cancers, neoadjuvant chemo(radio)therapy has become increasingly more successful at downstaging both early and moderate disease to either complete pathological response or microscopic residual tumours. Although this can present with a resect-or-not-resect conundrum to the surgeon, we anticipate that a proportion of early or microscopic residual (T1 N0) and late (palliative) adenocarcinomas (T4) could benefit from PTT in either providing cure (early) or reducing tumour volume (late). As these cases could be performed endoscopically as day cases, it will also save on in-patient admission. There would also be a reduction in the reliance on radical or bypass surgery, as this method if successfully delivered endoscopically as intended, would be minimally invasive.

In this chapter the main aims of the *in vivo* study are to:

1. Reproduce an appropriate mouse subcutaneous tumour model using GI adenocarcinoma cells
2. Evaluate non-invasive fluorescence imaging to correctly and specifically identify tumour tissue using functionalised GNRs as the contrast agent
3. Confirm the ability of GNR-induced photothermal therapy to reduce or destroy cancer tumours
4. Demonstrate an integrated theranostic application of GNRs feasible for clinical translation (for *in situ* diagnosis and concurrent therapeutic application)
5. Discuss the application of this nanotechnology in clinical practice.

6.2 Methods

The structure of reporting the *in vivo* methodology and results here is in line with the ARRIVE (Animal Research: Reporting of *In Vivo* Experiments) guidelines which are currently endorsed by scientific journals, major funding bodies and learned societies (3).

6.2.1 Ethics

Ethical approval was sought under the Animals (Scientific Procedures) Act 1986 and was granted by the Secretary of State under the following licences:

- A small animal project licence (PPL number 70/7996) granted on the 14th of August 2014 (the initial submission of this application to the Home Office was on the 19th of December 2013)
- A personal licence to carry out regulated procedures on living animals (PIL number 70/25542) obtained on the 22nd of August 2013
- The establishment licence at the Northwick Park Institute for Medical Research, Harrow, Middlesex (PEL number 70/4714).

6.2.2 Study Design

The design incorporated the use of two main experimental groups and three control groups. A pilot study was conducted to determine the propensity for tumour growth, the optimal GNR dose, laser fluence and duration of irradiation. The experimental groups were randomised to receive either intravenous (IV) or intratumoural (IT) GNRs. At a specific time point for each group, fluorescence imaging was performed, followed by NIR laser irradiation of the tumour site for PTT. The control groups were allocated into mice with tumours which received either IV or IT GNRs without laser, or laser alone. After completing a pilot study with 15 mice, a further 30 mice were used in the experimental and control arm. The animals were suitable for either treatment or control once their tumours reached a minimum size of 5 mm in any axis. Allocation of mice to either the experimental or control arm was performed randomly to minimise bias. The result from each animal was assessed separately as a single entity. The end of study in the experimental arm was 28-30 days after the commencement of laser irradiation with an excision biopsy of the irradiated tumour site and a thorough post mortem examination of other organs. For those with persisting tumour growth, especially in the control groups, a single tumour attaining a mean diameter exceeding 1.2 cm in any two axes prompted humane termination under National Cancer Research Institute guidelines.

A flow diagram for the experimental group is illustrated in Fig. 6-1.

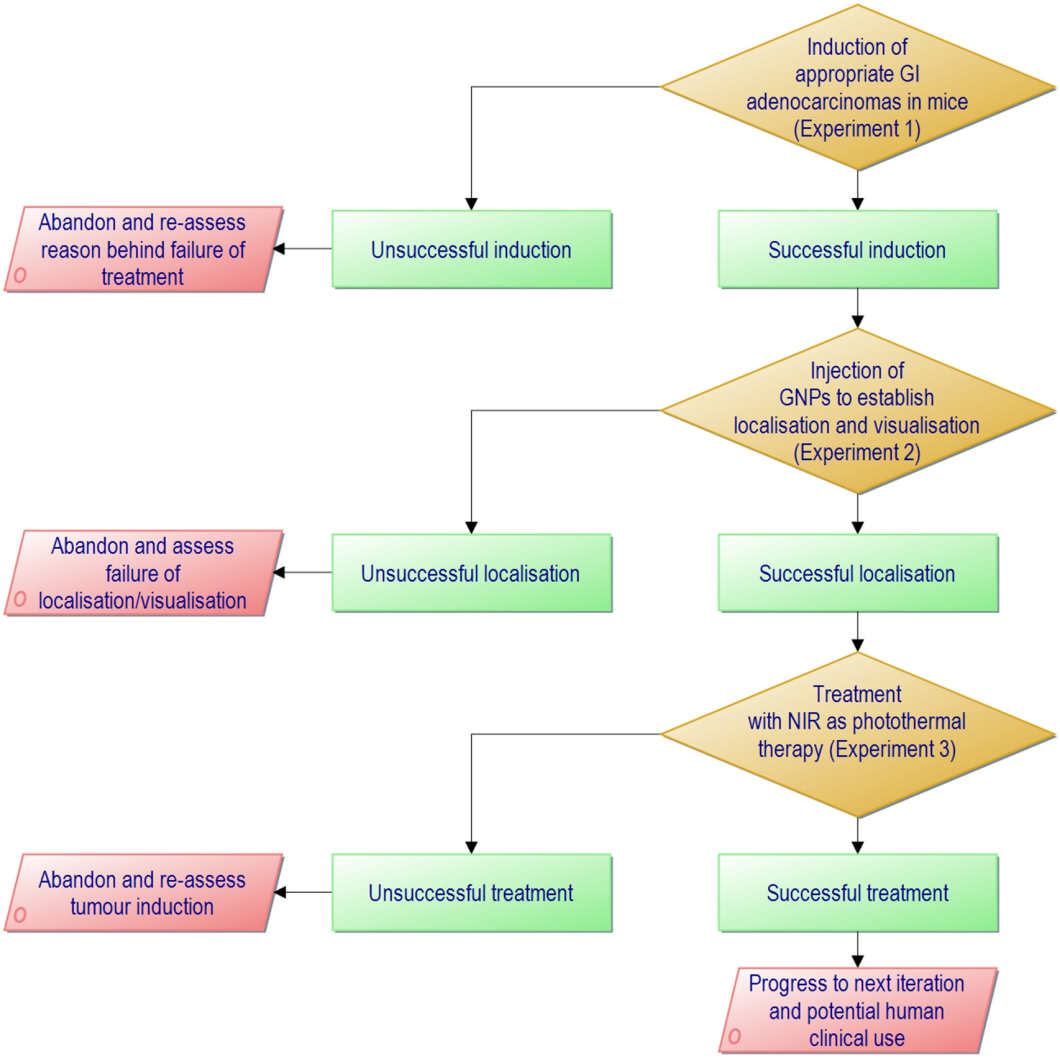


Fig. 6-1 Flow chart for the experimental group of the study.

6.2.3 Experimental Procedures

This project can be logically separated into three sequentially dependent experiments with two go/no-go decision points for progression.

Experiment 1 – Induction of a tumour xenograft

FLO-1 human oesophageal adenocarcinoma cells were cultured and used as the cell line inoculated for tumour growth in immunocompromised SCID or BALB/c nude mice. A single bolus of up to 10^6 - 10^7 FLO-1 cells in 100 µL culture medium was implanted, using manual restraint, subcutaneously at a single site in 45 mice. Hair removal was performed in

SCID mice to expose the areas of tumour. Tumours were allowed to grow to 5 mm prior to commencement of study (usually 10-14 days). At the end of this experiment the first go/no-go decision was made - if no tumours, insufficient numbers of tumours (less than 80%) or no adequately sized tumours were produced, the project did not progress to Experiment 2. In this case all animals would be terminated at this point and different cells would be assessed as to their tumour induction potential *in vitro*. Some of the animals were used as the control arm of the ensuing experiments to ensure that the induced tumours were not self-limiting. All animals were culled if and when the tumours exceeded 1.2 cm in diameter in two axes.

Experiment 2 – Administration of functionalised GNRs and non-invasive imaging

Provided Experiment 1 was successful, animals with tumours of at least 5 mm diameter in any two axes measured would, under general anaesthesia, have a single bolus of GNRs injected either directly into the tumour (intratumoural, IT) or systemically (intravenous, IV). GNRs were coated with PEG and functionalised with Cy5.5 fluorophore which was modified with anti-EGFR-antibody. Tumour size was measured in two dimensions with electronic callipers (Electronic Vernier Calliper, Sealey Group, Bury St. Edmunds, Suffolk, UK). The anaesthetic administered was 30 µl or 0.03 ml of a combination of Ketamine (100 mg/ml):Xylazine (23.32 mg/ml) given at a 2:1 ratio intraperitoneally, which generally provided about one hour of general anaesthesia (GA). For IT injections, 50-75 µl of functionalised GNRs with an $OD_{\lambda = 808}$ = 13.2 was administered and for IV injections, 100 µl of GNRs with an $OD_{\lambda = 808}$ = 26.4 was administered. All IV injections were performed via the tail vein. Tumour uptake of intravenously delivered GNRs was perceived to be dependant on the extent of tumour angiogenesis (EPR theory) and limited by the rate of uptake by the RES, thus functionalised GNRs were utilised to increase the probability of tumour targeting. After a pilot study was completed, 20 mice were randomised such that half the experimental animals would receive IT GNRs while the other half would be injected with IV GNRs. The control arm of this experiment with mice which received only GNRs (or NIR light alone) should show that the induced tumours and their malignant propagation were neither responsive to the administration of local or systemic GNRs, nor from the application of laser.

Assessment of GNR localisation within the tumour via fluorescence spectroscopy or fluorescence imaging took place at several time points during a 0-24 hour period post GNR injection. This was performed to establish the efficacy of this type of diagnostic modality in the identification of cancerous versus normal tissue. The criterion for success in this experiment is the visualisation of fluorescence emission from tumour sites using non-

invasive imaging. Dr. Elham Nabavi PhD, a Research Associate, performed these fluorescence studies together with the author.

Experiment 3 - Photothermal therapy and evaluation of treatment

Dr. Elham Nabavi PhD, together with the author, performed the following studies. Mice with appropriate tumours received GNRs, then received, under general anaesthetic, non-invasive near infrared (NIR) light between 1.0 – 2.6 W for up to three minutes. The selection of laser power was dependant on the size of the tumour. For mice receiving IT GNRs, PTT was done within 30 minutes of delivery, while the ones receiving IV GNRs underwent PTT after 24 hours of delivery. This was to ensure there was adequate time for systemically delivered functionalised GNRs to circulate to the targeted site and achieve maximal intratumoural accumulation. Previous studies have shown that GNP accumulation was noted in tumours after 24 hours of circulation, and as such this was used as a reference time point for our IV GNR PTT experiments (4). NIR-induced PTT was performed extracorporeally using an inexpensive, small and portable CW diode NIR 808 nm laser (DenLase-810/7 laser). The laser was calibrated and its power checked with a power meter prior to every application. The maximal laser fluence (or power density, P_D) was 5 W/cm^2, which was ascertained from the literature review as being the optimal laser fluence used in successful and published *in vivo* PTT experiments using gold nanoparticles. The laser power used in each of our experiments was thus variable and tailored according to the single largest axial diameter of the tumour measured on the day of irradiation. The following formula was used in calculating the laser power (P_L) that would be chosen for a particular tumour.

$$\text{Laser Fluence, } P_D = P_L / \pi r^2 \quad [P_D \text{ Max} = 5 \text{ W/cm}^2]$$

$$\text{Thus } P_L = 5\pi r^2 \text{ (radius, r = ½ Maximal tumour diameter, in cm)}$$

The laser beam diameter (determined using the aim beam function of the laser) initially only covered the tumour size (exactly) during pilot studies, but a refinement was subsequently made during the experimental stages to cover at least the diameter of the tumour plus an additional 1-2 mm area circumferentially. The laser was centred at the core of the tumour and the path of the beam was ensured to be as perpendicular to the tumour as possible, and the distances from the tip of the laser fibre optic to the surface of the tumour were recorded. This distance was generally noted to be between 15-20 mm, depending on the beam diameter required. It was important to ensure that the tumour was directly below the tip of the laser,

and the laser spot was checked at different positions to ensure complete coverage of the tumour. Once the appropriate beam diameter was determined, P_L was calculated using the formula. Laser exposure time was three minutes. This time period was an extrapolation from our *ex vivo* tissue data as well as analysis from published *in vivo* studies (4) which demonstrate that > 90% of the heating actually occurs within the first three minutes. Full laser safety precautions were adhered to and the eyes of the mice were covered and protected during fluorescence and irradiation, and the experiments were conducted in the daytime in a laser-safe room in NPIMR. The control arm of this experiment received NIR irradiation appropriate for their tumour size (without GNRs) and should demonstrate that the induced tumours and their growth were not responsive to this energy alone.

Heat profile assessment

Background and baseline body temperatures were pre-determined prior to laser application using a thermal imaging camera (FLIR Systems ThemaCAM S65 Infrared Camera – 76,000 pixel display, Wilsonville USA). This was manually triggered at the beginning of the irradiation and set to acquire images at 1 Hz frame rate for the length of the irradiation. The CW laser was also manually triggered at the start of the thermal image acquisitions. The heating effect on both healthy and tumour tissues were observed. Temperature rises were calculated and plotted by measuring the heating occurring in a manually selected ROI within the irradiated tumour site and subsequently subtracting from the background temperature which was defined as an area remote to the mouse. The general temperature rise for *ex vivo* tissues incubated with GNPs was noted to be approximately 20°C, which would be sufficient, if reproducible *in vivo*, to incur irreversible cellular, protein and DNA damage to the area targeted for photothermal ablation.

Psychosocial, weight and tumour site assessments

Animals were observed for four weeks during which serial photographs of progress were taken. The animals were weighed once weekly while tumour and/or irradiation sites and psychosocial behaviour was reviewed daily. Monitoring was by at least thrice weekly clinical examinations and physical measurements of tumour size if there was still a tumour present post irradiation. Criteria for success in this experiment was arbitrarily set to be a reduction in size of the tumours by at least 50% within four weeks with histologically proven destruction of tumour cells identified from tumours sites excised at termination. The end point of the study was four weeks after the application of NIR light or when tumours exceeded 12 mm in any two axes.

Histological assessment

Samples of tissue from tumour sites were taken for microscopic assessment in all experimental mice and from selected pilot mice. In selected cases histological examination was conducted on major organs. Histology was performed on day 30 post irradiation (the end period of study) on excision biopsies of the tumour sites which incorporated a margin of healthy surrounding tissue. The specimen was fixed in 10% neutral buffered formal saline and embedded in paraffin prior to performing 5 μm sections which were then stained with haematoxylin & eosin (H & E) and 0.1% Picrosirius red with Miller's elastic stain to demonstrate collagen. Picrosirius red stain is widely used in the histological visualisation of collagen I and III fibers and muscle in tissue sections. This stain was viewed using polarised light microscopy resulting in birefringence of the collagen fibers to distinguish between type I and type III (5, 6). Histological slides were imaged with an Olympus BX 40 light microscope and with polarised light.

Transmission electron microscopy (TEM) and EDX analysis

Tissue from tumour sites was harvested during terminations in mice that received either IV or IT GNRs (without laser) and also from tumour sites that underwent PTT. This was to visualise the position of GNRs within the tumour tissue from both routes of GNR administration, both before and after irradiation. This was visualised with TEM (TEM JEOL JEM-2100FX, Tokyo, Japan) and energy-dispersive X-ray spectroscopy (EDX/EDS) was used for further characterisation. The preparation of tissues has been described in Methods and Materials.

Clinical examination

All mice in the treatment arm of the study underwent a thorough post-mortem clinical examination of tumour sites, the peritoneum, liver, spleen, omentum and lungs at termination for an assessment of metastasis.

Blood profile assessment

Under terminal general anaesthesia blood was drawn by intracardiac venesection for clinical pathology screen. Blood was examined for biochemical parameters which included urea, creatinine, liver function and a full blood count. This was assessed on mice which received

both IV and IT GNRs and PTT at the end of 30 days. These blood values were compared to published normal data for the type of mice and used to identify any systemic toxicity, haematological or biochemical abnormalities from either GNRs or PTT.

Inductively coupled plasma mass spectrometry (ICP-MS)

The concentration of gold ([Au]) within organs was determined at the end of the study using ICP-MS. This was performed on blood using intracardiac venesection during terminal anaesthesia, and harvesting organs such as liver, spleen, kidneys, lungs, heart, brain and tumour sites. Each sample was dry weighed prior to freezing for subsequent ICP-MS analysis. The [Au] at 30 days (or end of study) was also contrasted with [Au] at the tumour sites and in vital organs on Day 0 (defined as the day after IV injections of GNR or the day of IT injections) to see the initial [Au] concentration values at the time when PTT would be instituted and to observe its variation at the end of 30 days.

The aims of the experiments are outlined below and the set up and design of the study are illustrated in Fig. 6-2 and Fig. 6-3:

Experiment 1: prove the efficacy of the chosen GI adenocarcinoma cell line and supply tumour-bearing animals for Experiments 2 and 3.

Experiment 2: determine which of, or whether, both routes of administering GNRs can result in localisation of the GNPs within the tumour. Clinically, it was hoped that both routes will be appropriate as direct intratumoural injection, where possible, may be a route of choice in some human subjects. Additionally, this experiment should establish the ability of non-invasive optical imaging in identifying and contrasting tumour tissue from that of normal tissue.

Experiment 3: show whether NIR light can excite GNRs to produce local energy sufficient to kill tumour cells. Additionally, samples taken at the termination of this experiment will be used to establish the presence and effect of GNRs both at the site of PTT and remote from this site. This should supply data concerning the biodistribution of GNRs and any histo-morphological changes associated with their presence.

The protocol of the study is summarised as follows:

1. Subcutaneous injection of human oesophageal adenocarcinoma cells, one site per animal.
2. Monitor tumour sizes using callipers.
3. Application of non-invasive fluorescence imaging (background).
4. Intravenous or intratumoural injection of GNRs.
5. Application of non-invasive fluorescence imaging (post intervention).
6. Application of non-invasive NIR light.
7. Monitor tumour sites.
8. Observation for up to 4 weeks.
9. Under terminal general anaesthesia, removal of blood by intracardiac venesection.
10. Termination by a Schedule 1 method followed by tissue retrieval.

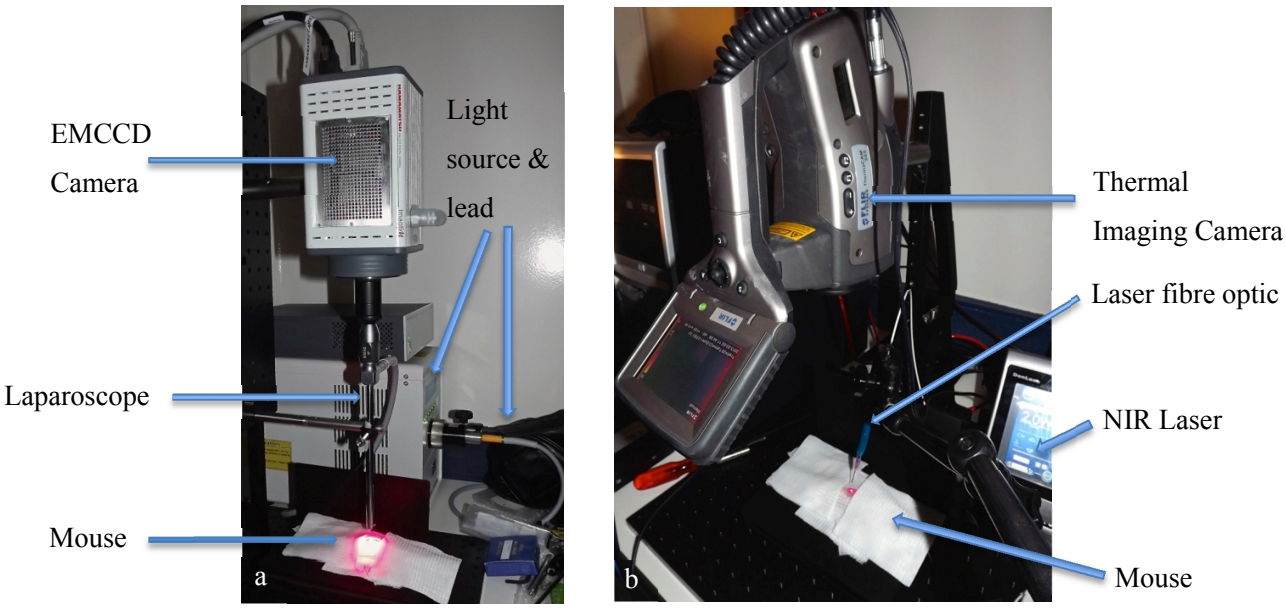
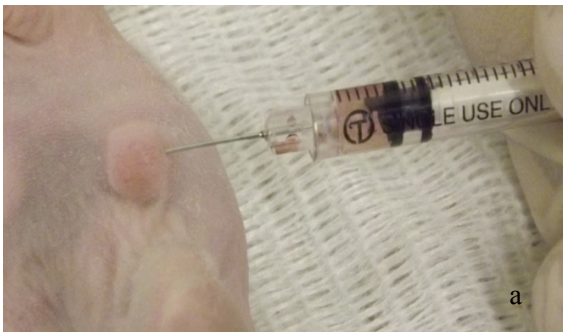
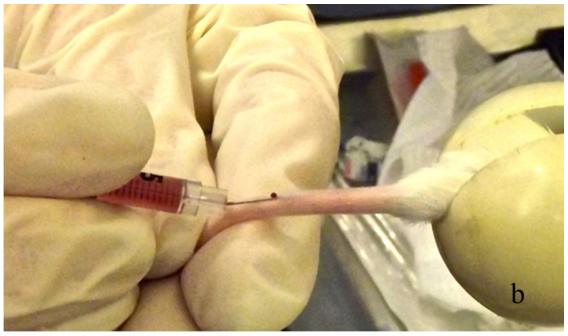


Fig. 6-2 The experimental set-up for (a) fluorescence imaging and (b) photothermal therapy.



Experiment 1.
Grow s/c tumour xenograft.





Experiment 2 (i). Inject GNRs [(a) IT or (b) IV].



Experiment 2 (ii). Assessment of GNR localisation via fluorescence imaging.



Experiment 3. Irradiate tumour site with NIR laser & record thermal response over time.

Fig. 6-3 The three fundamental experimental steps of the *in vivo* study.

6.2.4 Experimental animals

The use of animals raises considerable ethical and scientific issues. Animal studies were conducted after tests were performed on cancer cells *in vitro* and on *ex vivo* tissues with the knowledge that no further advancement can be achieved without *in vivo* experiments. Dr. William MS Russell and Mr. Rex L Burch produced the 3R's concept in animal experiments in their 1959 publication *The Principles of Humane Experimental Technique* in which they stated that all animals experiments should incorporate: Replacement (of animals with alternative methods), Reduction (the minimum number of animals used to achieve scientific objectives) and Refinement (of methods to prevent or reduce animal pain, suffering or distress) (7). These principles were adhered to throughout the duration of the animal study.

The mouse is the least sentient animal that can be used to replicate human tumour growth and is appropriate for testing the true potential of PTT. Therefore due consideration was given to guidelines published by Workman *et al.* in carrying out the research and devising the study protocol (8).

8 - 9 week old male severe combined immunodeficiency (SCID) and BALB/c nude nu/nu mice were purchased from Charles River UK Ltd. (Kent, England). SCID mice are autosomal recessive, with a single nucleotide polymorphism within the *Prkdc* gene on chromosome 16. They lack both T & B cells. Natural killer cell, macrophage and granulocyte cell numbers and function are normal. They are highly susceptible to opportunistic bacterial and viral infection, and as such strict adherence to aseptic techniques and sterility was maintained at all times. They underwent an acclimatisation period after arrival. Each animal was housed individually in a cage (polycarbonate, open on the top and covered with steel wire lid, 29.0 x 11.0 x 11.0 cm^3 deep) and fed with conventional chow [RM1 (P), Special Diets Services, England] and sterile water *ad libitum* while maintained under controlled conventional environmental conditions at 20 ± 2°C ambient temperature and 54 ± 2 % humidity, with 12/12 hour light/dark cycles. Food, sawdust and nesting material were autoclaved.

In 1913 Dr. Halsey J. Bagg, working at the Memorial Hospital, New York, obtained the white coat coloured (albino) founder animals of this strain from a mouse dealer in Ohio. Since then, Bagg albinos or BALB nude mice are among the most widely used inbred strains used in animal experimentation. BALB/c strains are hairless as a consequence of spontaneous mutation of the $Foxn1^{nu}$ gene on chromosome 11. They are athymic and thus

are T-cell deficient, whereas B cells function as normal. The term *nu* refers to the recessive nude mutation introduced into inbred BALB/c mice by crossing them with congenitally athymic nude mutants (nu/nu).

6.2.5 Sample Size

A pilot study was initially conducted with 15 mixed SCID and BALB/c mice, with a further 30 BALB/c mice used in the experimental and control arms. Of these 30, some mice with tumours were used for complementary studies such as TEM imaging of GNR localisation, measurement of [Au] in tumours and organs using ICP-MS, depth of energy penetration, histological assessment of organs and blood profile studies. After completing the pilot, control and the aforementioned studies, 20 of these 30 mice were included into the main study assessing tumour regression after PTT in mice randomly allocated to receive either IT or IV GNRs, thus there would be 10 mice receiving each method of GNR administration. Control mice (with tumours) received either IV GNRs, IT GNRs or laser alone and the experiments were repeated thrice. If there was any noticeable decrease in the size of these tumours in control mice, it would be a clinically relevant observation as it is not perceived that any of these interventions could singularly induce tumour regression, nor is the tumour self-limiting. As this is primarily a proof of concept and feasibility study, true statistical analysis has not been applied**,** but the likelihood of success of treatment will be calculated for each treatment arm to give a measure of predictability of success with each treatment modality.

6.2.6 Experimental outcomes

1. Evaluate fluorescence imaging in correctly identifying cancerous tissue by exploiting the physiological ability of functionalised GNPs to target tumours.
2. Confirm the ability of PTT in successfully reducing or destroying tumours.
3. Determine the safety of GNRs *in vivo* and establish the depth of energy penetration.
4. To determine what factors would allude to successful photodestruction of tumours.
5. To propose a suitable approach to theranostics in clinical practice.

6.2.7 Characteristics of the functionalised GNRs used in *in vivo* studies

The functionalised GNRs had an excitation peak at 675 nm and a corresponding emission peak at 692 nm. This is shown in Figure M1 in Methods and Materials. The filters that were chosen and the fluorescence imaging set-up used in our experiments were based on these spectra. The absorption spectra of the functionalised GNRs show very little in the way of spectral deviation or attenuation of the peak optical densities (OD) from the original CTAB-GNRs growth solution and the process of PEGylation. This consistency is paramount to ensure that we would be applying a pure and concentrated solution of GNRs *in vivo*. The final solution of PEG-GNR-Cy5.5-anti-EGFR-antibody had a peak $OD_{\lambda = 808}$ of 26.4 and 100 μl was used for intravenous administrations. The concentration of this solution is 5.50 nmols/l, or 5.50 nM.

For IV injections, the number of GNPs in 100 μl of GNR solution can be calculated using the formula: n (mols/l) = C x V x N_A
Where the concentration, C = 5.50 x 10^{-9} M (concentration of GNR solution)
The volume, V = 100 x 10^{-6} l (100 μl solution)
Avogadro's Number, N_A = 6.022 x 10^{23}
Thus the number of GNPs at this concentration (OD = 26.4): n = 3.3 x 10^{11} GNPs/100 μl.
Or 3.3 x 10^{12} GNPs/ml.

For IT injections, half the volume (50 μl solution) and half the concentration (2.75 nM) was used, thus the number of particles per ml was also halved, n = 1.66 x 10^{12} GNPs/ml, or 8.3 x 10^{10} GNPs/50 μl.

6.3 Results

6.3.1 Fluorescence Spectroscopy of mice injected with functionalised GNRs

Fluorescence spectroscopy was performed as a preliminary validation experiment. *In vivo* fluorescence spectroscopy (fibre-coupled HR4000 spectrometer) was performed on mice with mature oesophageal tumour xenografts which had received functionalised GNRs. Fig. 6-4 shows the absorption and emission spectra of the functionalised GNRs acquired using a UV-Vis spectrometer, and the experimental set-up is shown in Fig. 6-5. During fluorescence spectroscopy, the surface of the mouse was excited with excitation from a 300 W Xenon lamp (MAX-303 Asahi Spectra) adapted with a 655 nm band-pass filter (bandwidth 50 nm).

In order to acquire fluorescence spectra, a multimode fibre in conjunction with a long-pass (LP) filter with a cut-off at 690 nm was placed a few mm from the excited area and fed to a compact HR4000 spectrometer. The addition of a long pass filter at 690 nm removed any interfering emission signals prior to this cut-off wavelength. The fluorescence signal directly from the tumour was also compared with the signal received from other parts of the body such as the back, right shoulder and leg. Fluorescence spectroscopy from both IV and IT administered GNRs were recorded and an example of the readings observed directly over the tumour site are given in Fig. 6-6.

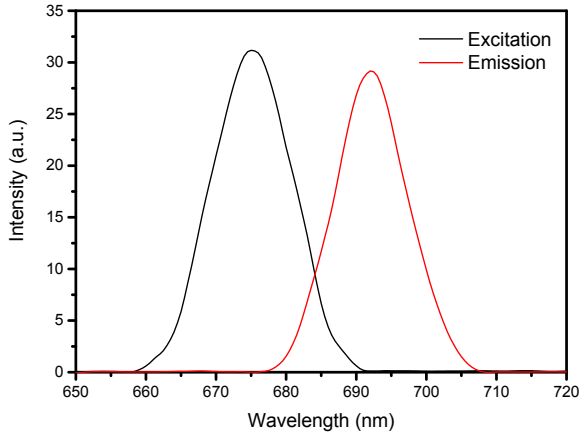


Fig. 6-4 Fluorescence absorption and emission spectra from functionalised GNRs (normalised).

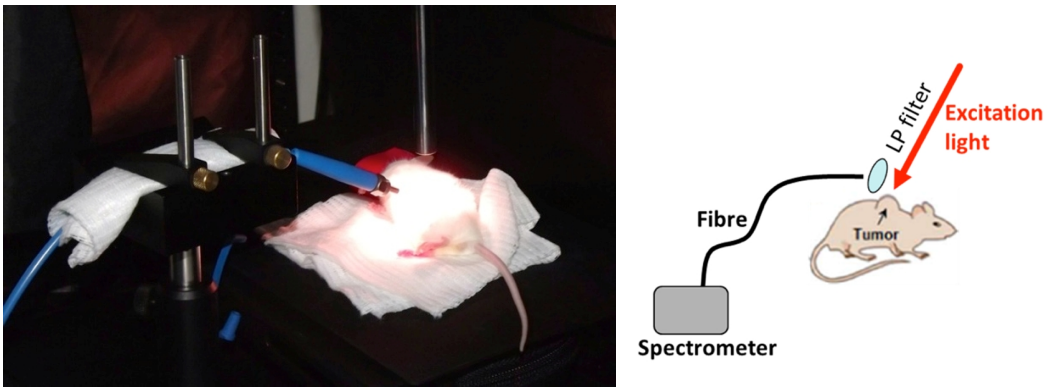


Fig. 6-5 Use of a fluorescence spectrometer with a 690 nm long pass (LP) filter over the probe. The excitation light is emitted from a laparoscope mounted above.

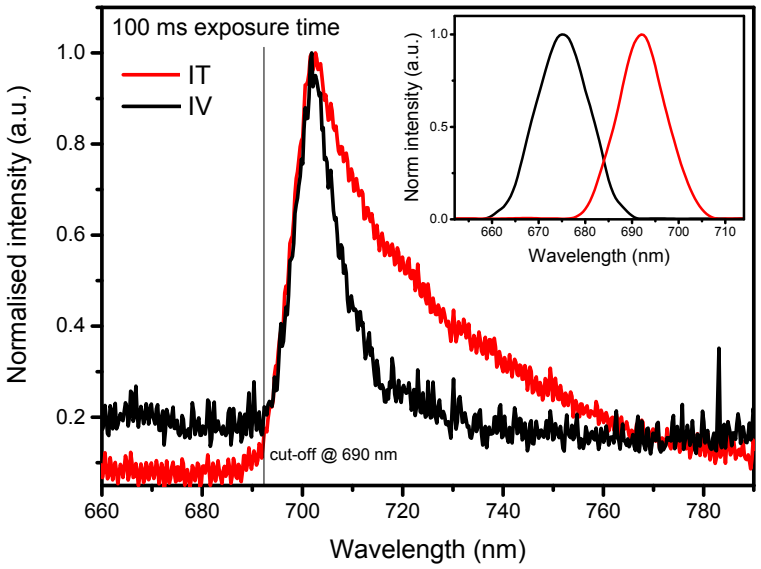


Fig. 6-6 Fluorescence spectroscopy readings with both IV and IT GNRs, which were noted to be specifically enhanced over the area of tumour. Inset: Normalised UV-Vis spectroscopy of the GNR solution.

With reference to Fig. 6-6, high amplitude signal peaks at approximately the same wavelength were obtained specifically over visually confirmed tumour sites in mice which had received GNRs via both IT (30 minutes prior) and IV routes (24 hours prior). The difference in the emission spectra shape between the two routes is likely to be related to a concentration/dose effect (photoquenching) as there is a much higher concentration of GNRs being delivered into the tumour with the intratumoural injection route. Although perhaps a less sensitive and crude method compared to fluorescence imaging via an EMCCD camera, fluorescence spectroscopy provided proof of concept that we should be able to detect and record fluorescence emission spectra following IV and IT delivery of GNRs, which was detected with spectroscopy signals specifically over the tumour site and corresponded well to the absorption spectrum of GNRs. This spectrum was not detected elsewhere on the mouse, indicating a high degree of specificity, and was thus evaluated further by fluorescence imaging.

It was hoped that should fluorescence imaging concur with these fluorescence spectroscopy results, it would provide clear indication of their potential diagnostic value in identifying the location of a neoplastic lesion. This would then also be further characterised and corroborated by TEM imaging showing the presence of GNRs within the cancerous cells of the tumour and by ICP-MS, which would measure the [Au] within tumours.

6.3.2 The application of functionalised GNRs for fluorescence imaging of tumours

The experimental set-up for fluorescence imaging is shown in Fig. 6-7. The tumour area was excited by radiation with a central wavelength of 655 nm light (50 nm bandwidth), obtained from a 300 W Xenon lamp which passed through a bandpass filter. The light was then directed into a conventional 0° laparoscope. A 690 nm LP filter was inserted between the laparoscope and the camera in order to block the reflected light from the tumour. Fluorescence emissions were recorded by a Hamamatsu EM-CCD camera through the laparoscope. The image was then constructed using 19 mm or 30 mm achromatic lens (depending on the distance of the tumour from the tip of the laparoscope) and EM-CCD camera. The excited area of the mouse was dependant upon the distance between the tip of the laparoscope and the mouse; this distance was varied to achieve different fields of view for fluorescence imaging. The field of view was further dependent on the specification of the achromatic lens (19 mm or 30 mm). The camera was operated with MatLab programming language and the images were subsequently processed and analysed using Origin software (OriginLab Corporation).

Background fluorescence of mice was measured pre-injection. After mice with tumours received systemic GNRs through the tail vein (IV), fluorescence imaging was again performed at 0, 2 and 24 hours post injection and the intensity of the signals were compared between these times. This was performed with acquisition times ranging from 40 ms to 5 s. Images were taken from various regions of the mice; on the sides with and without tumours for comparison. Images were subsequently processed and analysed using Origin software (OriginLab Corporation).

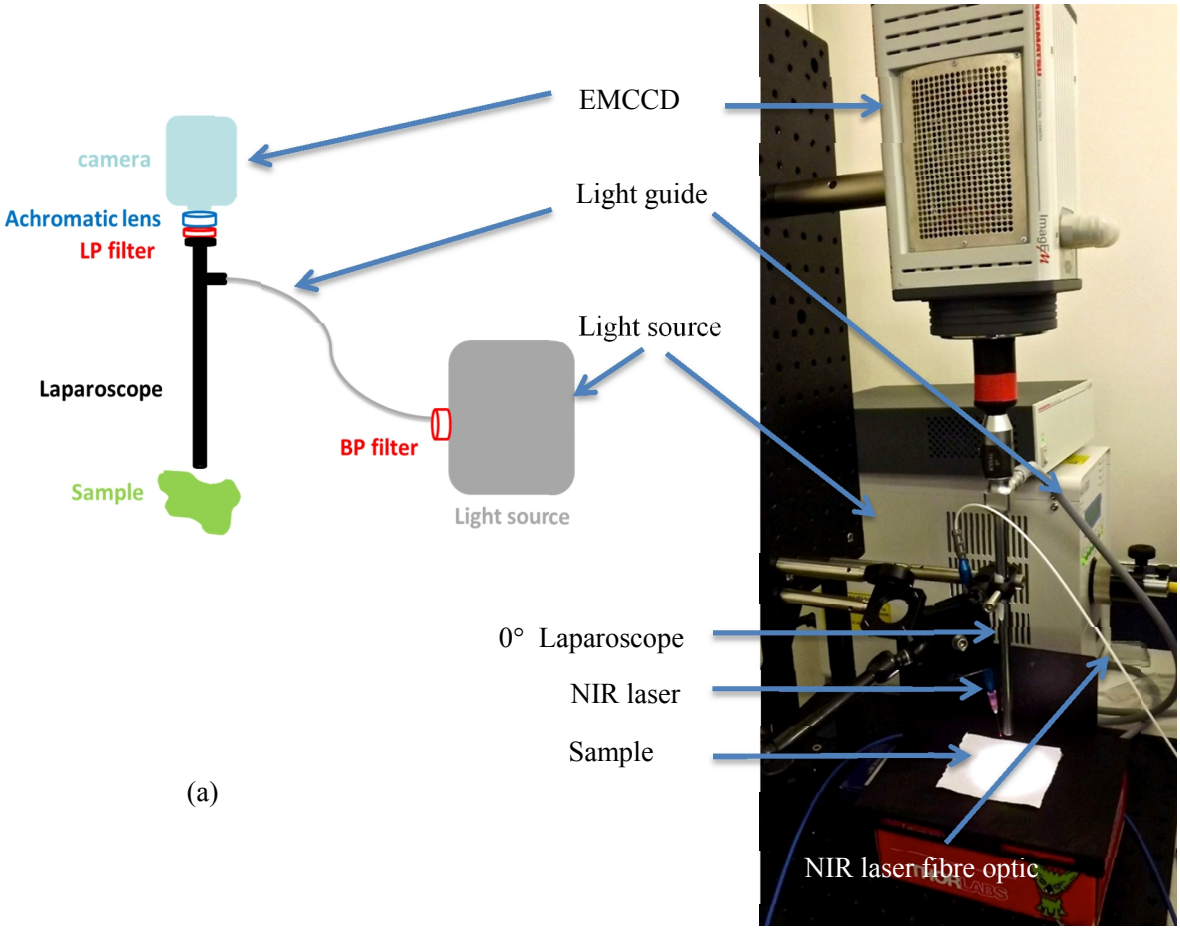


Fig. 6-7 (a) Schematic of fluorescence imaging set-up. Key LP = Long pass, BP = Band pass (b) Fluorescence imaging experimental actual set-up (with laser fibre optic in-situ).

6.3.3 Fluorescence imaging results for IV GNRs

Prior to the administration of GNRs, there was a constant area of fluorescence in all study mice on the abdominal area, regardless of the presence or absence of GNRs (Fig. 6-8). This was thought to be intrinsic to the animal because it was omnipresent and only on the left side and so this was explored further under live fluorescence-image-guided surgery performed under terminal anaesthesia to determine which internal structure could be attributed to this illumination. It was found that it was due to the colon of the mouse which predominantly occupies the left side (Fig 6-9).

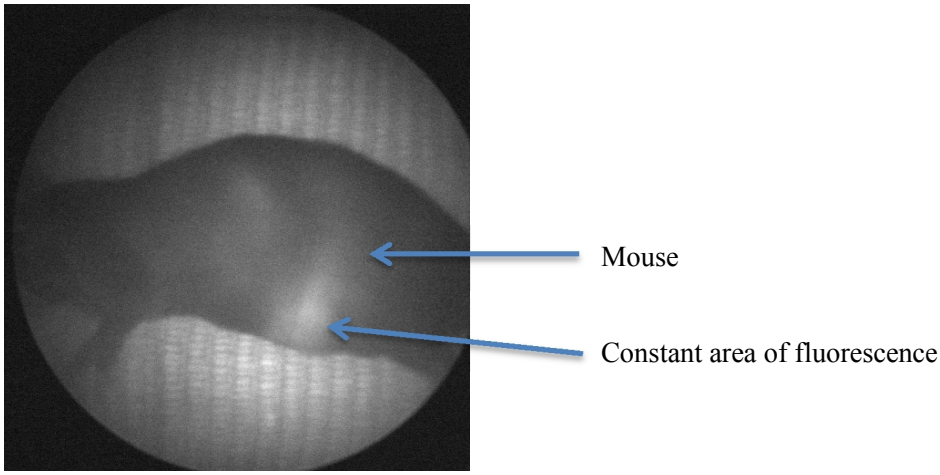


Fig. 6-8 Live fluorescence image pre-IV injection with a constant area of fluorescence.

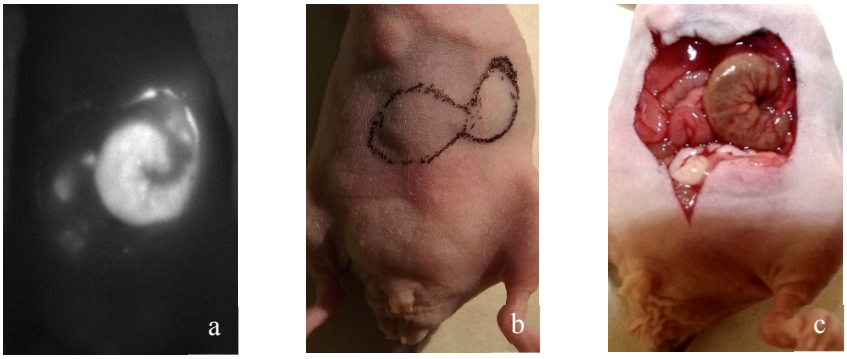


Fig. 6-9 (a) Constant fluorescence noted on left flank, (b) area demarcated under fluorescence image-guidance, (c) laparotomy to confirm bowel as the cause of the fluorescence.

Within the first hour of administration of GNRs, it would appear that there was a good fluorescence signal which corresponded well to the external appearance of the tumour, with clear delineation of tumour margins. This was noted with good regularity with freshly prepared samples of functionalised GNRs, however the signal was poor to non-existent when the GNR sample was more than three weeks old. When the tumour region was marked externally using needles, live fluorescence imaging conclusively demonstrated well-defined tumour margins, as represented in Fig. 6-10(b) and Fig. 6-11(a). Fluorescence was also detectable 24 hours post-injection, as shown in the comparison Fig. 6-11(b), even for subtle tumours. With the use of the image processing software Origin, it was possible to digitally subtract the background, and this would highlight the region of tumour clearly [as demonstrated in Fig. 6-11(c)]. This was highly reproducible using the fluorescence imaging set-up and would be a useful adjunct in routine endoscopy for highlighting subtle tumours.

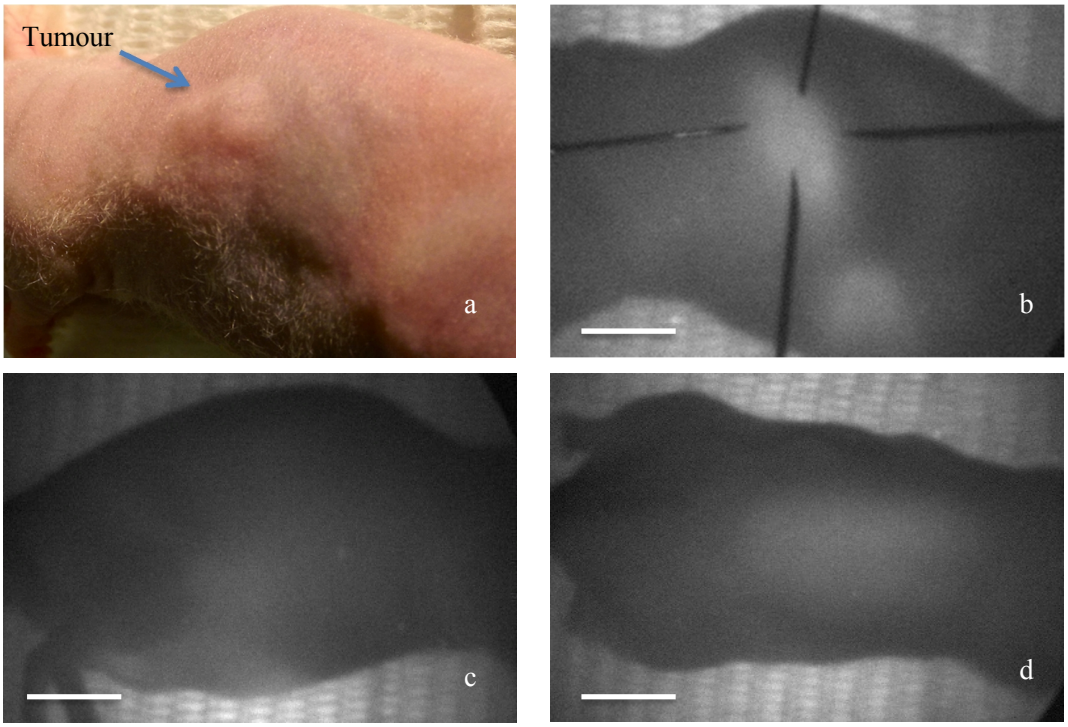
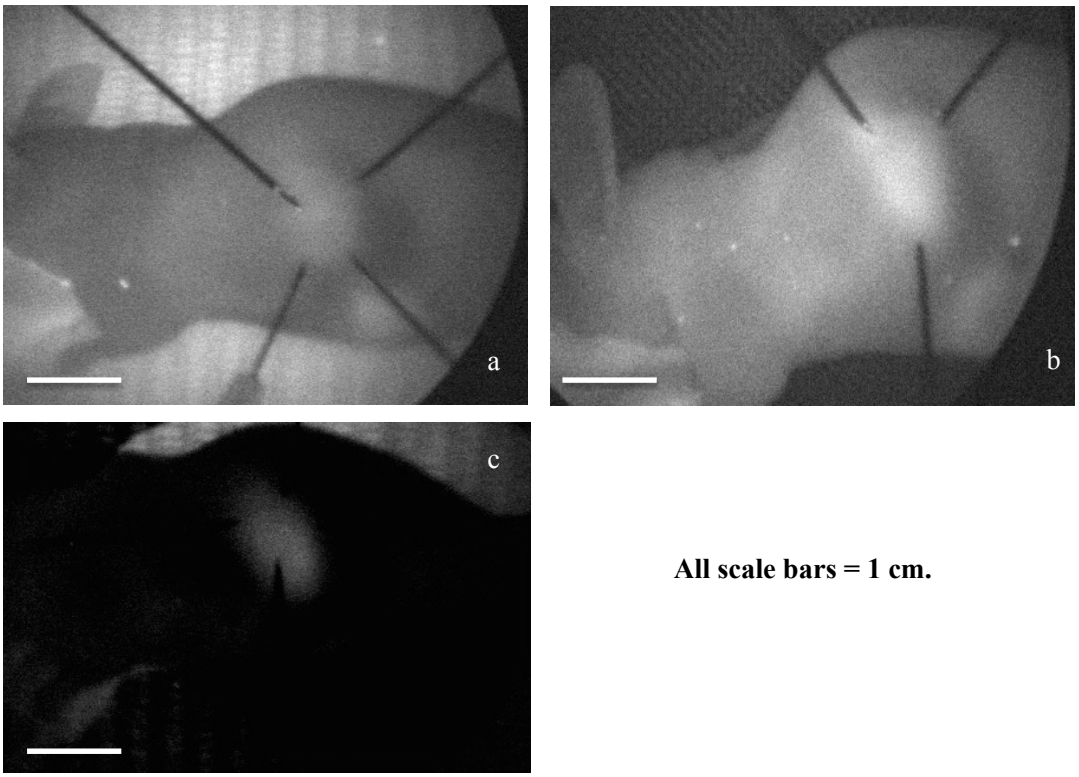


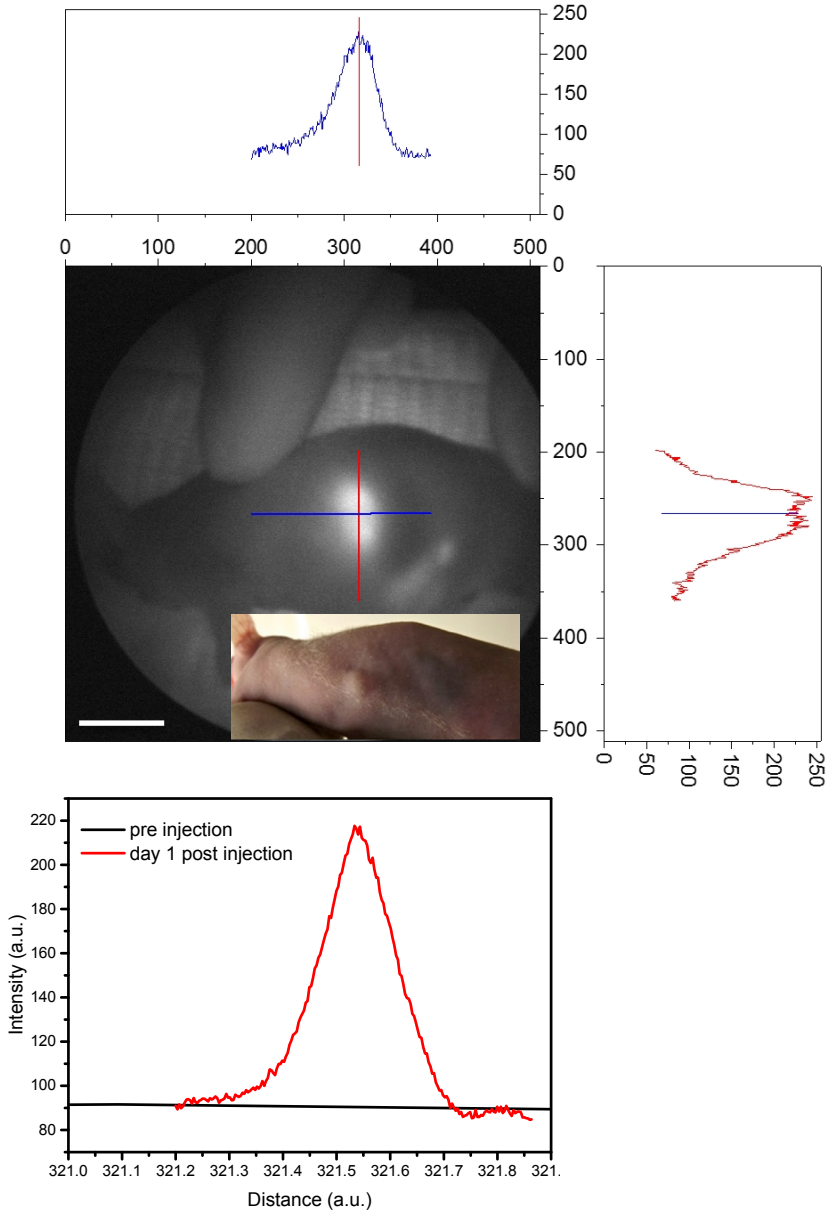
Fig. 6-10 Images seen during live fluorescence imaging (needles in situ correspond to the external visible boundaries of tumour) in a mouse with tumour (b) and the absence of any fluorescence signal on the contralateral (tumour-free) flank (c) and the back (d).



All scale bars = 1 cm.

Fig. 6-11 Live fluorescence signal (a) on the day of IV GNRs and (b) 24 hours post injection in the same mouse, (c) processed fluorescence image with background subtracted showing the fluorescence emission arising specifically from the tumour area.

It was also possible to quantify the fluorescence emission seen using a line profile over the region which would process arbitrary units of intensity. This combination of fluorescence emission, its clear delineation of boundaries and the quantification of signal amplitude would be of interest for both surgeons and endoscopists alike as it affords more information regarding suspicious or irregular lesions seen during endoscopy or laparoscopy (e.g. a sessile polyp or an isolated peritoneal nodule). The presence of fluorescence together with a high amplitude signal peak would provide an indication that the area warrants further investigation, such as a biopsy, which could therefore be image-guided. This concept of quantifying fluorescence signal feedback is illustrated in two study mice with their corresponding tumours shown as an inset picture in Fig. 6-12. The contrast of fluorescence signal intensities between pre- and post-injection is further demonstrated in a graph.



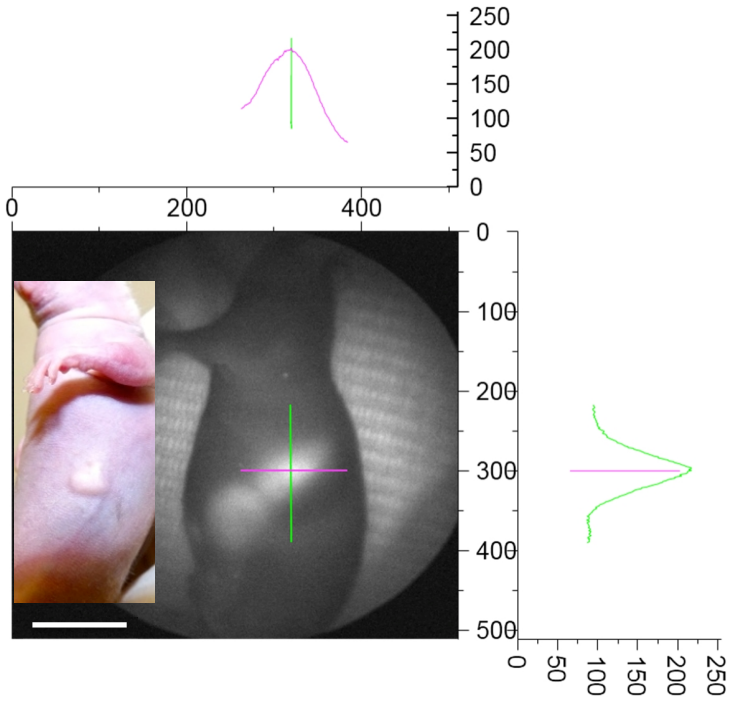


Fig. 6-12 Line profiles of fluorescence emission signals over the tumour site correspond to peak fluorescence intensities in two different mice receiving IV GNRs. Scale bars = 1 cm. Graph also demonstrating the contrast in fluorescence intensity signals between pre- and 24 hours post-IV injection of GNRs (background subtracted).

The presence of fluorescence on the same day of IV injection was however not compatible with the time quoted in the literature for GNP accumulation within tumour tissues, which is normally 24 hours post systemic delivery. The rapid fluorescence often seen in our experiments were thus thought to be due to the presence of free Cy5.5-anti-EGFR-antibody which was presumed to be unbound and present within our aqueous sample of functionalised GNRs. An experiment was done to clarify this further, whereby only Cy5.5-anti-EGFR-antibody (without GNRs) was administered IV to the animal, and immediate (within 10 minutes) and delayed fluorescence imaging was performed. The results are shown in Fig. 6-13 and it is apparent that there is good emission seen just from the fluorophore alone by account of the fact that the Cy5.5-anti-EGFR-antibody particles are smaller than the GNRs, and localisation is also fairly rapid because of its conjugation to the appropriate antibody. The principles of active (antibody driven) and passive (EPR effect) accumulation would synergistically amplify tumour targeting. This intensity gradually decayed over the next seven days (Fig. 6-14).

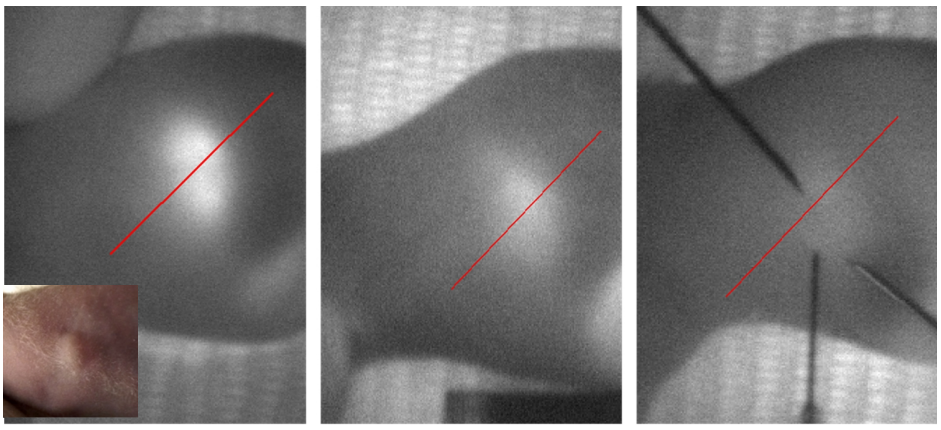


Fig. 6-13 Live fluorescence imaging performed on a pilot mouse receiving only Cy5.5-anti-EGFR-antibody (without GNRs) demonstrating a gradual drop in fluorescence intensity over time.

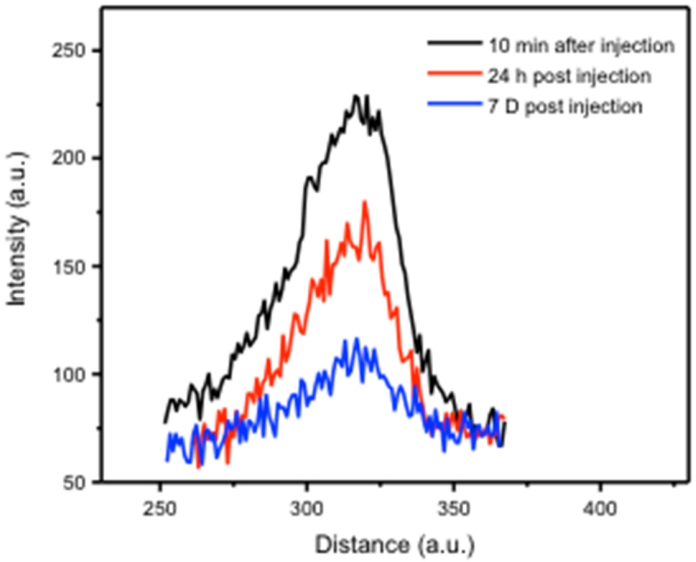


Fig. 6-14 Degradation of fluorescence intensity over time in a pilot mouse receiving only Cy5.5-anti-EGFR-antibody, indicating a high initial signal intensity.

This phenomenon was further expounded in another pilot mouse which for comparison was given fully functionalised GNRs and fluorescence imaging was performed prior to, immediately after, then at 2 and 24 hours post IV injection (as shown in Fig. 6-15). This demonstrated a gradual diminution in the intensity as illustrated in Fig. 6-16. It is perceived that the free antibody-conjugated fluorophore within the GNR solution that would arrive at the tumour site more rapidly than the functionalised GNRs. This hypothesis was challenged by applying PTT to another pilot mouse soon after an injection of Cy5.5-anti-EGFR-antibody-functionalised GNRs given IV had confirmed high intensity fluorescence from the region of the tumour. The application of NIR laser to the tumour site was performed within one hour of the confirmation of high fluorescence signal. Although there was a reasonable

temperature rise observed with this attempted PTT, it was likely to have been from only a small number of GNRs in within the tumour. Within a week, this irradiated tumour site demonstrated residual tumour which continued to grow. This is discussed further in Section 6.7.5 "Allow 24 hours after IV administration of functionalised GNRs". It is highly suggestive that the functionalised GNRs would need 24 hours to permeate and percolate before being incorporated within the tumour, while early fluorescence is likely to arise from the free antibody-conjugated fluorophore within the solution.

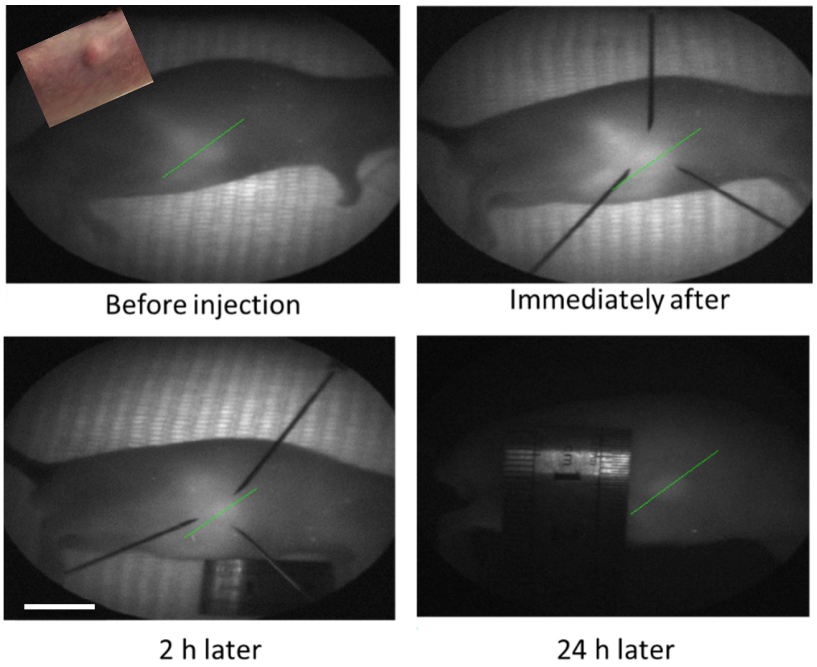


Fig. 6-15 Fluorescence imaging performed immediately before, after, and at 2 and 24 hours post IV injection of functionalised GNRs. Scale bar = 1 cm.

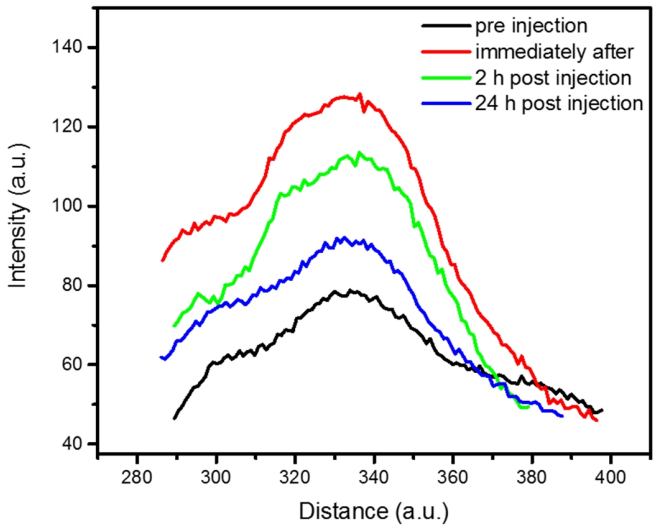


Fig. 6-16 Decay of fluorescence imaging intensity signals from tumour sites at various time points after an IV injection of functionalised GNRs.

In summary it is perceived the Cy5.5-anti-EGFR-antibody component of the functionalised Cy5.5-GNR-anti-EGFR-antibody solution could potentially provide fairly rapid (within minutes of IV injection) diagnostic information about the location and margins of tumour, but for PTT to be effective it should be performed after 24 hours of IV administration. The fluorescence signal is preserved at this time point, albeit slightly weaker than the initial intensity. In a theranostic set-up, it is plausible that an endoscopic/laparoscopic diagnosis of cancer could be enhanced during live fluorescence imaging very soon after systemic administration of an aqueous solution of functionalised GNRs. It is anticipated that this solution would contain a certain degree of unbound antibody-conjugated fluorophore that will aid in the diagnosis or biopsy. Should there be a need to return to photothermally ablate the tumour, it can be performed by pre-marking the fluorescent mucosal surface to be irradiated at the index procedure, then perform NIR irradiation by revisiting this site after a period of 24 hours, which will allow a sufficient time lapse in order to further characterise the tumour's grade and stage. This potiential for a combined theranostic application is discussed further in the Section 6.5 "The theranostic application of GNRs *in vivo*".

6.3.4 Fluorescence imaging results for IT GNRs

After delivery of IT GNRs, fluorescence imaging demonstrated a darkened area shown here in two mice in Fig. 6-17 and Fig. 6-18. The fluorescence quenching experienced here is from a decrease in the fluorescence intensity from the GNRs and likely due to aggregation from a heavily concentrated sample of GNRs.

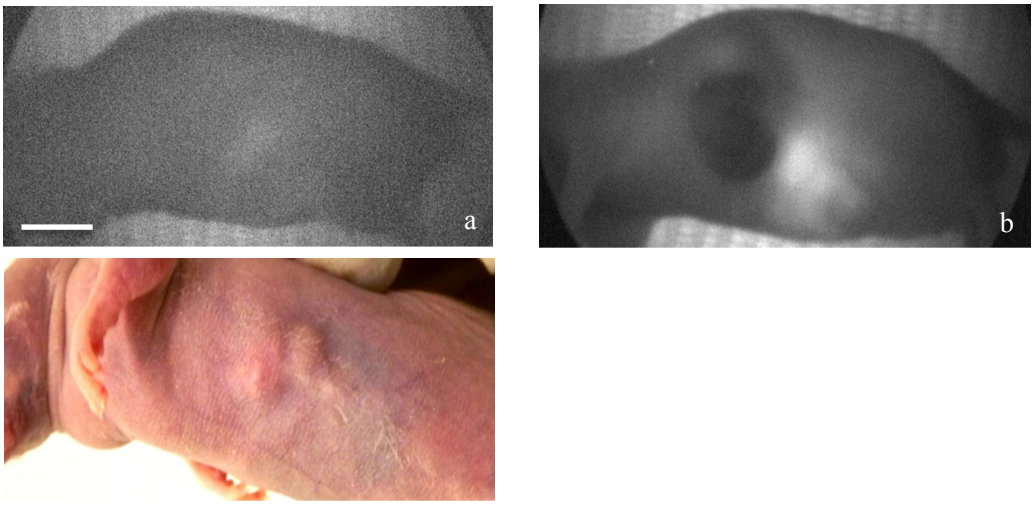


Fig. 6-17 Live fluorescence imaging of a mouse (a) pre- and (b) post- IT GNR injection. Scale bar = 1 cm.

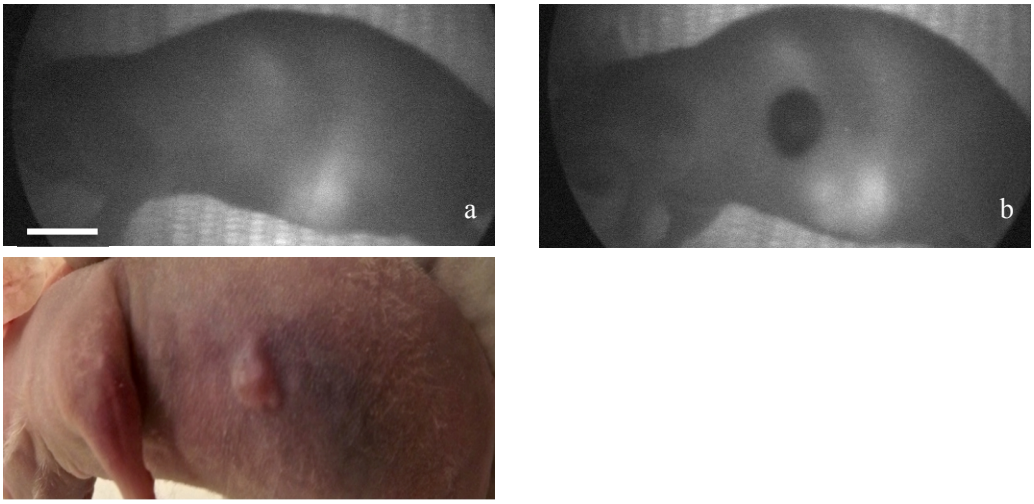


Fig. 6-18 Live fluorescence imaging of another mouse (a) pre- and (b) post- IT GNR injection. Scale bar = 1 cm.

As the delivery of GNRs to the tumour would neither be aided by the physiological EPR effect nor an immunological antigen-antibody coupling which is relied upon for the IV accumulation of GNRs in tumours, fluorescence imaging of this area provided a reliable indication that the injected tumour area had been sufficiently covered with GNRs which is essential information prior to targeted laser application. In one experiment it was noted that the tumour area did not receive a full coating of GNRs, thus it was then possible to "top up" the barren area with further GNRs to ensure that the entire tumour was well prepared prior to irradiation (Fig. 6-19). Without such image referencing, one can appreciate there might be areas of tumour irradiation that would not be photothermally ablated as the hyperthermia in this area of the tumour would be inadequate or uneven, leaving potential for continued tumour growth.

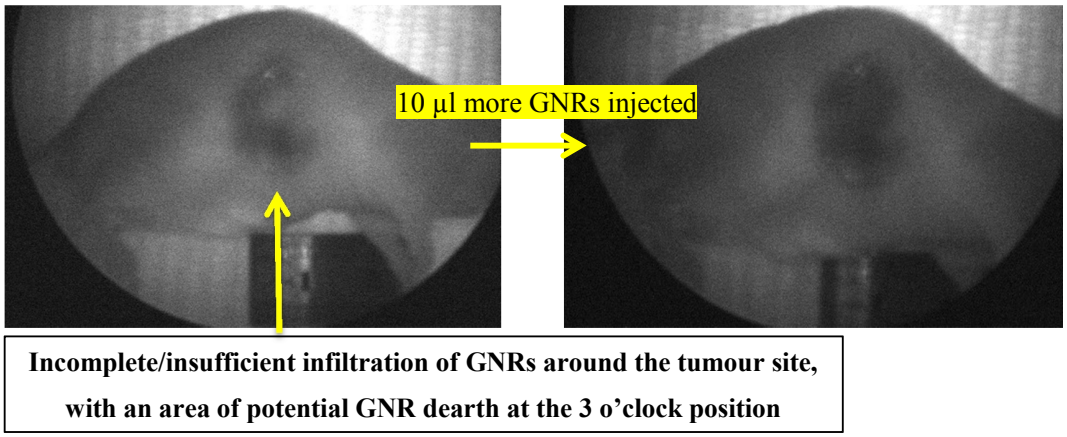


Fig. 6-19 (a) Fluorescence imaging illustrating the importance of photoquenching in highlighting GNR-deficient areas around the tumour pre-irradiation site with complete circumferential delivery of IT GNRs around the tumour site in (b) confirmed by fluorescence imaging after a 'top-up' GNR injection to the previously deficient region.

6.3.5 Hepatorenal metabolism of GNRs

Fluorescence signals from vital organs such as spleens, kidneys and livers were also examined 24 hours post IV GNRs and immediately after IT GNRs by harvesting the organs at these time points (Fig. 6-20 – Fluorescence images from mouse given IT GNRs).

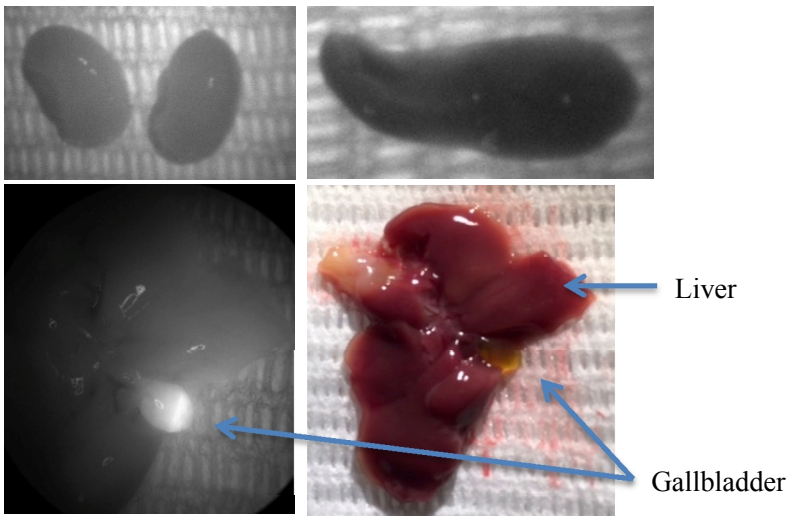
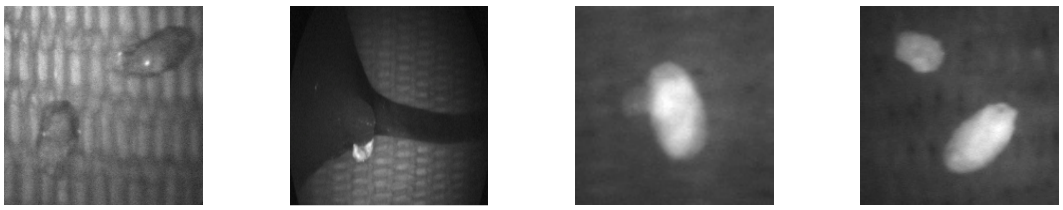


Fig. 6-20 Fluorescence images from the kidneys, spleen and liver (with picture of liver and gallbladder) of a mouse injected with IT GNRs.

The organs did not show fluorescence except for an area within the liver (the gallbladder), which contains bile. This was shown in mice receiving both IV and IT GNRs. It is known that gold nanoparticles are cleared predominantly via the renal system (9). Hainfield *et al.* demonstrated that the kidneys acquire the highest tissue concentration of gold 15 min post IV injection with 77.5% of the total injected gold cleared after five hours (9). The organ which retains the largest amount of gold after this time period was usually the liver, irrespective of the size of NPs (10). GNPs are predominantly metabolised and biodistributed in the liver and spleen (10-13). If GNPs are larger than the renal filtration cut-off, they are not excreted in urine but instead eliminated from the blood by the reticuloendothelial system thus having a tendency to accumulate in the spleen and liver (11, 14). The liver plays an active role in the metabolism and biliary excretion of blood-borne particles and eliminates foreign substances via phagocytosis (15). GNRs that become excreted via the biliary system are first metabolised through hepatocytes. GNPs that are processed by hepatocytes then potentially undergo biliary excretion. Although the hepatic uptake of GNPs from blood may occur relatively rapidly, hepatic processing and biliary excretion of these particles is

relatively slow, which results in a prolonged retention of GNPs within the liver parenchyma (16). ICP-MS analysis was performed to determine the concentration of Au in all organs of mice injected with IV and IT GNRs in our study. This suggested that although the values were infinitesimal, the three organs that accumulated the most Au were the spleen, followed by the liver and kidneys.

The hepatobiliary metabolism and excretion of GNRs was also noted to be manifest in the faeces of mice which were given IV GNRs (Fig. 6-21). This is presumed to be from bile which flows into the small intestines where it mixes with chyme (partially digested food from the stomach). Fluorescence imaging was performed on mice feed, control mice (which were not given any GNPs), and mice which were given 100 μl of IV GNRs (measured on Day 1 & Day 2 post injection). The mice feed did not show fluorescence apart from a micro-spiculation pattern of fluorescence emanating from their coarse, hard and irregular surfaces. The results in Fig. 6-21 demonstrate the bright intensity observed from the faeces of mice on Day 1 and Day 2 post IV GNRs, which was not observed in control mice. This experiment was repeated three times in six mice (three controls and three given IV GNRs) with similar and consistent results.



Control Mice | Mouse given IV GNRs 24 hours previously | Faeces on Day 2

Fig. 6-21 The lack of fluorescence in the faeces of control mice, and fluorescence from faeces after 1 and 2 days in mice that received IV GNRs.

It is likely that the main route of GNP excretion within the circulation is via the hepatorenal pathway, and this would concur with other studies (17-19). The fluorescence signals seen emerging from the gallbladder and faecal matter from mice receiving GNRs in our study would also suggest that despite being delivered outwith the GI tract, hepatic metabolism and urinary excretion is the mainstay of Au elimination from the body. Although auto-fluorescence emanating from the colon was demonstrated prior to the delivery of any GNRs in mice (Section 6.3.3), a selective fluorescence seen in the faeces of mice receiving IV GNRs demonstrates that the GI tract is also likely to be a route of GNR excretion/metabolism.

6.4 The application of functionalised GNRs for photothermal therapy

6.4.1 Control Mice

Before mice were randomised into their respective treatment arms of having IV GNR and laser irradiation or IT GNRs and laser irradiation as therapeutic combinations, it was necessary to determine the individual responses of tumours to laser irradiation alone or GNRs alone administered either IT or IV in control studies. These control studies were performed when tumour xenografts reached at least 5 mm, and terminated either at day 30 or when the sizes of tumours had become considerably large. The same volumes and concentrations of GNRs and laser fluence settings as used in the treatment arms were given appropriate to the tumour sizes and adequate time was given for a possible response.

The varying parameters for GNRs and laser in the control group are listed in Table 6-1. The laser modality of control was repeated thrice, while the GNRs only control was repeated twice for each route of administration.

Control Method	Vol. GNR (μl)	Conc. (GNR) nM	Laser Power (W)	Beam diam. (mm)	Laser time (min)	Tumour at Day 0 (mm)	Tumour size at end (mm)	No. of days
Laser only 1		-	1.00	6	3	5.5 x 5.1	14.5 x 11.4	30
Laser only 2	-	-	1.15	5	3	5.4 x 5.0	14.3 x 8.3	17
Laser only 3	-	-	2.20	8	3	5.8 x 4.9	6.0 x 5.5	30
IV GNRs - 1	100	5.50	-	-	-	5.5 x 4.3	11.3 x 9.8	17
IV GNRs - 2	200*	5.50	-	-	-	5.5 x 5.3	12.0 x 10.5	20
IT GNRs - 1	50	2.75	-	-	-	6.0 x 4.6	10.3 x 8.6	17
IT GNRs - 2	50	2.75	-	-	-	8.3 x 5.5	16 x 7.6	23

Table 6-1 The parameters of GNRs and laser used in the control groups, with the tumour sizes measured at the start and end dates of the control arm.

* This mouse received double the regular volume of IV GNRs.

Inoculations of FLO-1 cells develop fairly rapidly and aggressively into large adenocarcinomas in immunocompromised mice, and no tumours in the study were found to be self-limiting. As such, any ablative response that would potentially be seen with GNR-induced PTT would be a clinically relevant finding and not a chance occurrence.

It can be seen that the tumours continued to grow in all the control mice and hence large tumours were readily evident at the end of the study period (see Fig. 6-23). There was no tumour regression or dissolution response that could be elicited by the single modality option of either GNRs or irradiation. A temperature rise within the 7.6–9.9°C range (Fig. 6-22) was observed in the laser only control tumours and is likely to have been from superficial (skin surface/hair follicles) or pin-point heating, thus not generating a homogeneous heating profile throughout the entire tumour tissue. No eschars or scabs were noted with the laser only group. The lack of any clinical improvement or noticeable damage to the irradiated skin surface demonstrates the innocuous nature of NIR irradiation in the absence of GNRs as long as it remains within the fluence range used in the study.

Tumours in SCID mice did not behave any differently to the tumours in BALB/c nu/nu mice. As an experiment one mouse received double the normal IV volume of GNRs, and it was evident that even this higher dose:

i) was not capable of inducing any tumour regression
ii) did not cause any systemic side-effects or morbidity in the mouse

One mouse receiving IT GNRs developed an ulcer overlying the tumour after a fortnight, but this neither caused harm nor did it retard tumour growth. It remains unclear if the ulceration was due to the tumour itself or from a local irritative skin reaction to the GNRs. However it did not worsen over the subsequent 10 days.

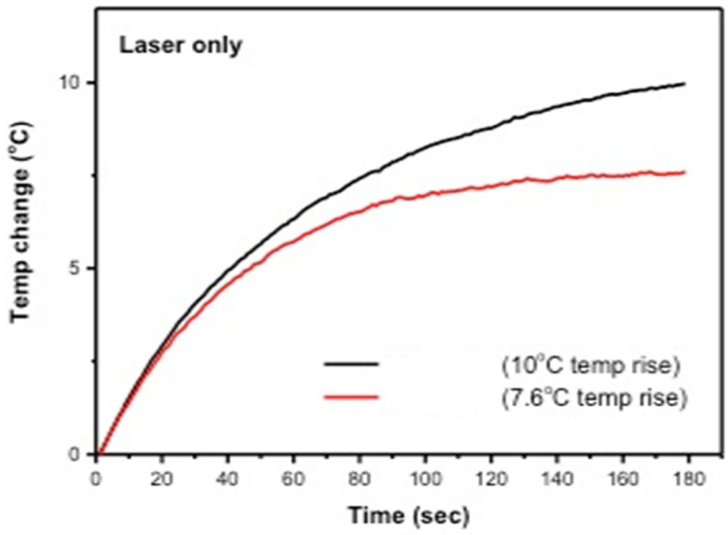


Fig. 6-22 Temperature responses to laser irradiation of tumours without GNRs.



Fig. 6-23 Tumours of the mice in the control group, showing images pre-intervention (Day 0), then at stated days post-intervention, indicating continued tumour proliferation in all control arms.

6.4.2 Results - Intratumoural (IT) GNRs and NIR irradiation

Ten mice were randomised from twenty to receive IT GNRs and 808 nm laser irradiation for three minutes. All tumours were at least 5 mm in a single axis before the treatment commenced. Mice were anaesthetised and injected with 50 µl of GNRs at a concentration of 2.75 nM (8.3 x 10^{10} GNPs). After twenty minutes, fluorescence imaging was performed to confirm that the area of tumour was sufficiently covered with GNRs (refer to section 6.3.4 "Fluorescence imaging results for IT GNRs"). Should an area be felt to be GNR-depleted after the first injection, a further 10 µl 'top-up' GNR solution was injected into the relevant region. The parameters of the ten mice that received IT GNRs are shown in Table 6-2. It was imperative to ensure that the laser beam diameter would be at least 1 mm greater than the circumference of the tumour, to ensure adequate coverage. This was factored in during fluence (power density) calculation by adding an additional 1 mm to the maximal single dimension of the tumour (and disregarding the smaller dimension).

Laser beam size = Largest single dimension of the tumour + 1 mm

Should the temperature rise observed live during irradiation noted from the thermal imaging camera be deemed excessively high (i.e. > 50°C rise), there was an option to manually cease the irradiation prior to completing the full three minutes. However, of the twenty mice studied, this was only required in one mouse, and this was in the IT-administered GNRs group.

The Gaussian distribution pattern of the heat derived from the laser's emission varied over the surface of the tumour, where it was normally hottest at its epicentre and cooler in the peripheral margins of the tumour. When analysing temperature fluctuations occurring during PTT, regions of interest (ROIs) were selected as line profiles across the centre of the tumour (as shown in Fig. 6-24) and also the distant ambient temperature to distinguish the temperature changes occurring within the tumour tissue from the background temperature. The mean and standard deviation of the pixels within the regions of interest was calculated. Then any background heating was subtracted from the heating occurring from within the tumour site to give a measurement of the true temperature rise within the tissues due to the laser. Plots of temperature rise over time were created using a Matlab program.

Mouse No.	Tumour size (mm) at Day 0	Vol. GNR (μl)	Conc. [GNR] nM	OD (GNR)	Laser Power (W)	Beam diam. (mm)	Laser time (min)
1	7.3 x 5.7	50	2.75	13.2	2.0	7	3
2	7.2 x 6.0	50	2.75	13.2	2.0	7	3
3	5.3 x 4.9	50	2.75	13.2	2.2	8	3
4	9.1 x 6.3	50	2.75	13.2	2.5	9	3
5	5.5 x 4.8	100*	2.75	13.2	1.6	6	130 s
6	5.1 x 5.1	50	2.75	13.2	1.1	5.5	3
7	8.5 x 5.5	50	2.75	13.2	2.2	8	3
8	6.4 x 6.2	50	2.75	13.2	1.8	9	3
9	7.3 x 4.8	70	2.75	13.2	2.1	8	3
10	5.0 x 4.7	40	2.75	13.2	1.0	6	3

Table 6-2 The parameters of the ten mice which received IT GNRs and PTT with NIR irradiation.

* This mouse received double the normal volume of IT GNRs.

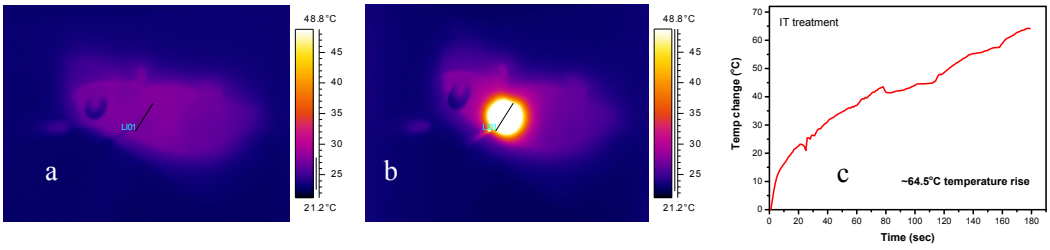


Fig. 6-24 Temperature charts recorded live during photothermal therapy from the thermal imaging camera, showing (a) the starting and (b) the final temperature rise after three minutes of NIR laser irradiation. The line across image (b) is a line profile across the measured region of the temperature change and can be processed into a temperature profile graph as shown in (c).

Once the concentration (OD) of GNRs to be given IT was known, it was crucial to determine the volume to be given, and in one mouse (Mouse 5), an attempt to deviate from the normal dose demonstrated a very high temperature (73°C) rise during the irradiation process such that it was ceased at 130 seconds. This clearly demonstrates that there is an upper limit to the amount of GNRs that can be applied safely for PTT beyond which may cause harm to the animal. Excessive injected volume may result in a predominantly high concentration of GNRs accumulating focally under the skin, resulting in a very high local temperature that would ultimately burn the skin and/or encompassing area. While it could be argued that the volume of GNRs administered should be proportional to the size of the tumour, the crux lies in ensuring an even distribution of GNRs during the injection procedure. Larger tumours may require larger volumes, and vice versa.

Thus the concept of tumour size should be brought to bear as a consideration of GNR volume to be administered during PTT experiments, as long as it can be established what the upper limits should be. This is explored further in Sections 6.7.3 and 6.7.6.

All mice demonstrated a good photothermal response with macroscopic and microscopic disappearance of tumour and absence of proliferating cells on post-termination histology at the end of study (day 30) as shown in Fig. 6-25. There was an early thermal reaction by the crinkling/puckering of skin around the tumour immediately after PTT. Early signs of tumour necrosis were commonly seen 3-4 days post therapy with eschar formation which would eventually be replaced by a dry scab. This scab usually sloughed off spontaneously by the third week revealing an underlying healed irradiation site which was evident by day 30. All mice demonstrated complete healing by day 30 with neo-epithelialisation as a result of thermal therapy. This area was subsequently resected with deep and wide margins and sent for histopathological analysis. Apart from the ablation of tumour, there was regeneration of epithelium through the process of neo-collagenesis, which was appreciated under polarised light microscopy (Fig. 6-26 and Fig. 6-27).

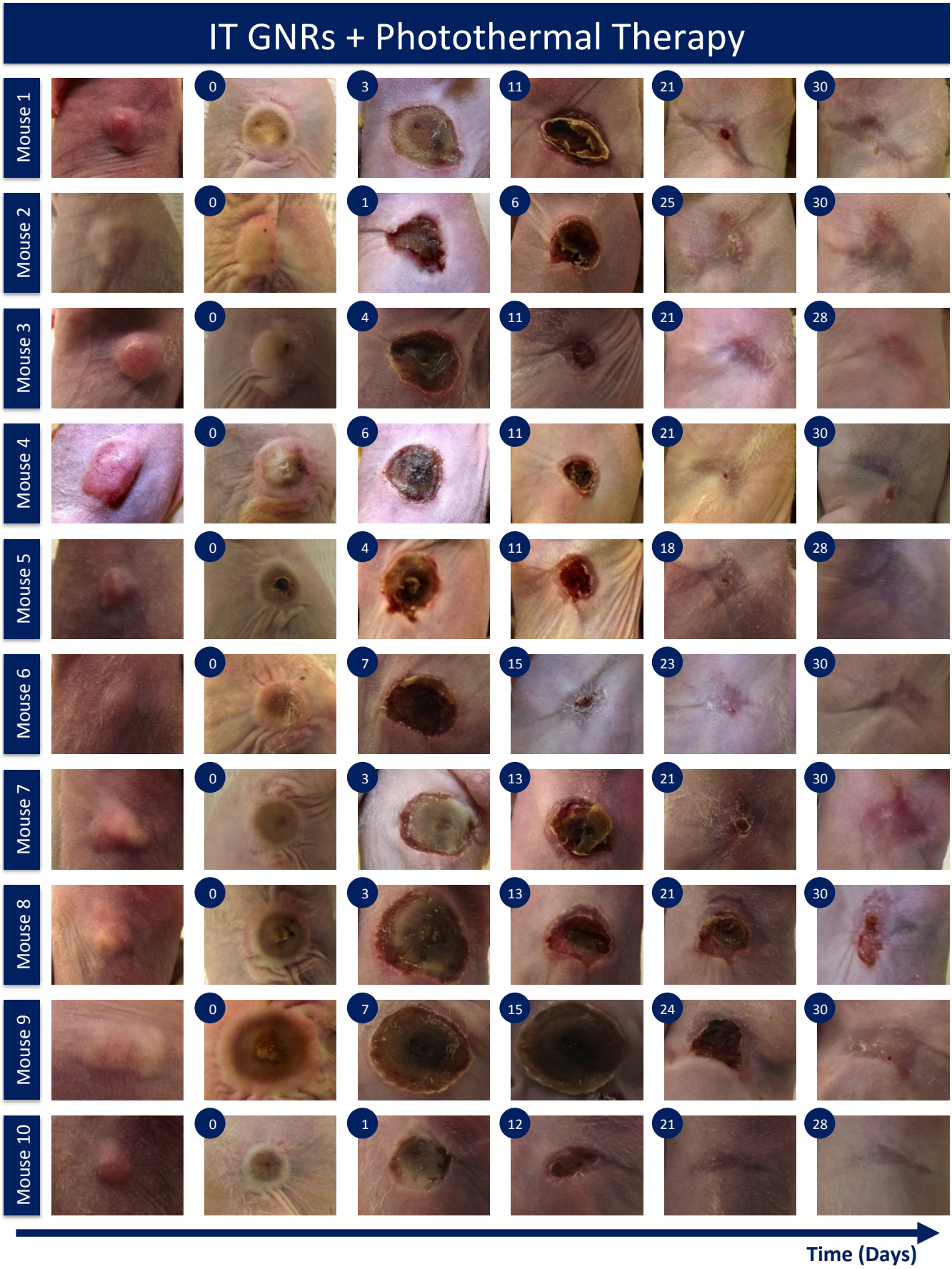


Fig. 6-25 The PTT responses in tumours of the ten mice (initial tumours on the left column) which received IT GNRs, with their progression over days.

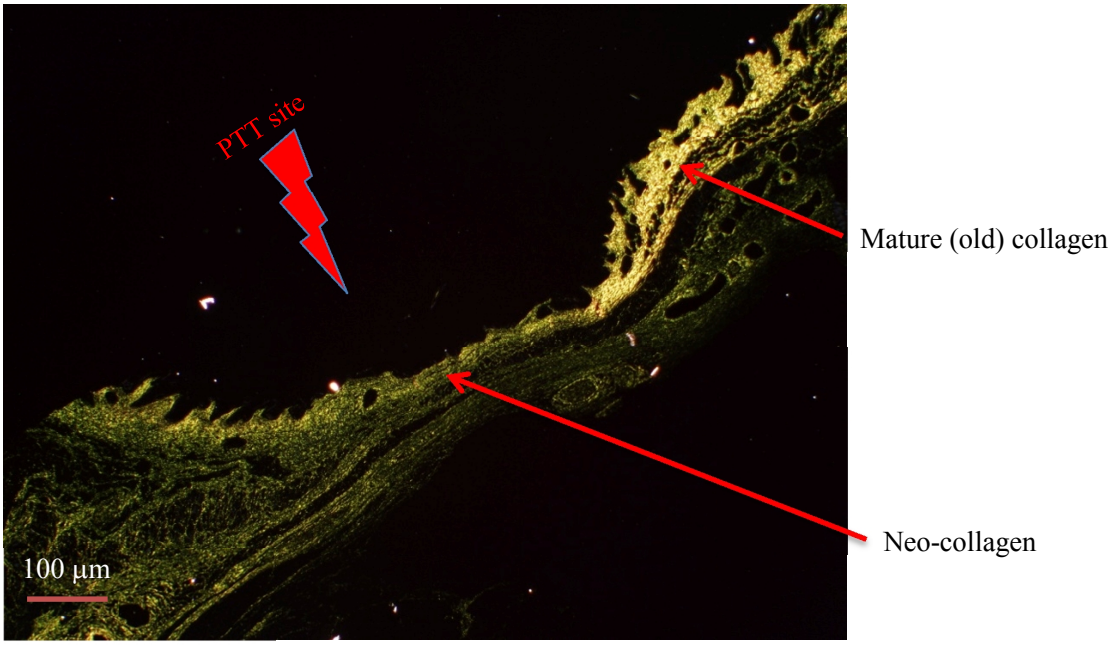


Fig. 6-26 Contrast seen from re-epithelialisation and regeneration of neo-collagen post PTT seen under polarised light microscopy (100x magnification).

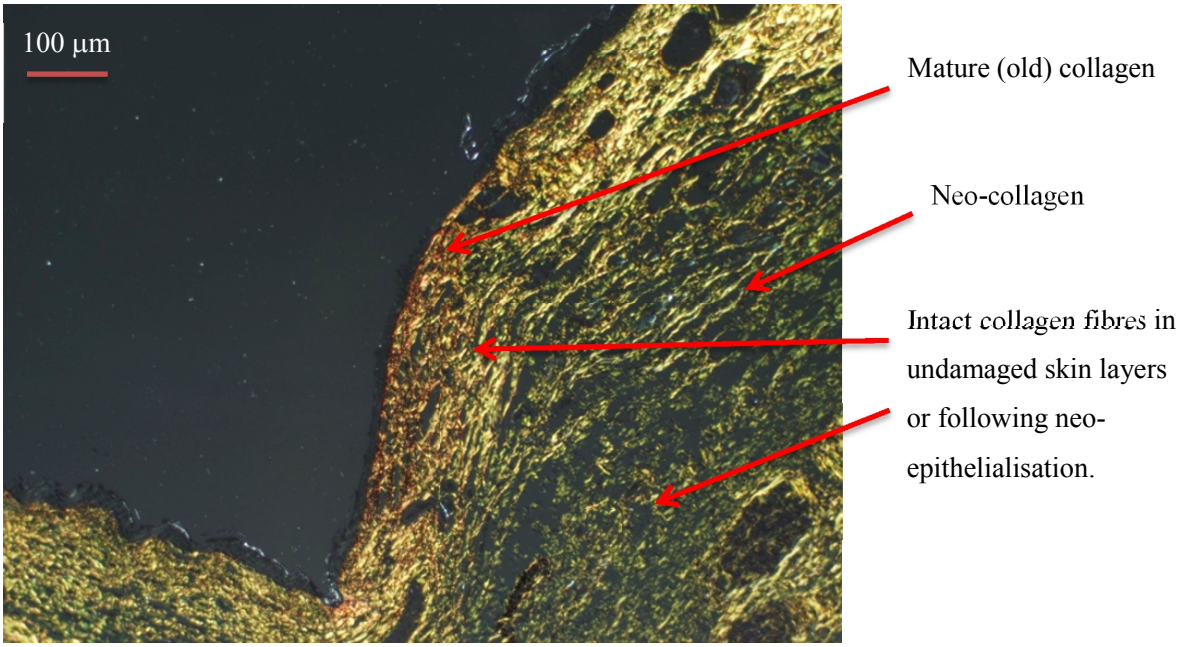


Fig. 6-27 Intact collagen fibres in skin layers demonstrated following PTT. Shown here under polarised light microscopy after staining with Picrosirius red with Miller's elastic stain added (100x magnification).

0.1% Picrosirius red with Miller's elastic stain was used to demonstrate collagen with standard light microscopy and polarised light microscopy. The staining used resulted in collagen fibres showing as red under light microscopy while other tissue elements appear

bright yellow. However under polarised light microscopy, the collagen fibres appear as orange/red bands against a black background (20).

As can be seen in the images of PTT (Fig. 6-25), tumours that were ablated quickly formed eschars which made estimation of any remaining tumour volume or size impossible to measure. Consequently there was no residual tumour 'lump' to size after intention-to-treat PTT was administered.

Temperature profiles of the successfully ablated tumours in these mice were analysed and it would seem that a mean 42.3°C ± 9.4°C rise would lead to adequate PTT and successful tumour ablation (see Fig. 6-30). However it must be cautioned that our earlier pilot studies have demonstrated that should there be incomplete distribution of GNRs within the tumour, achieving these temperatures (or higher) would still be insufficient for complete tumour ablation. In the case of uneven distribution of GNRs, tumours that initially appear ablated due to the thermal reaction and temperatures achieved would eventually re-surface and proliferate from the peripheries of the ablation site before the end of the 30-day period. Thus it is imperative that all four quadrants and the base of the tumour receive equal volumes of IT GNRs prior to any attempts at irradiation. This is discussed further in Section 6.7.1.

Published values on the level of hyperthermia required to achieve successful PTT or tumour ablation suggest that a temperature range of 42-47°C *in vivo* would be sufficient to induce tumour cell death (21-23). When considering the translational potential of this form of therapy, this is not particularly high considering that the core (internal) human body temperature is 37°C. In our mice tumour xenograft model it was apparent that the initial (skin surface) temperature was much lower, often being around 21–23°C. It is thus postulated that a 30°C rise should be more than adequate to achieve complete thermal therapy and this thermal response would be adjusted for a human study. From the experiments performed, we found that temperature rise is clearly related to the concentration of GNRs as well as the laser fluence. Hence the accumulation of GNRs in tumours is crucial to the overall thermal and ablative effect. In direct IT injections, the GNR concentration will always be higher than if relying on EPR or the antibody-antigen targeting required for IV GNRs, as such it falls to reason that the temperature rise will be higher in IT GNR route of administration. It is reassuring to have established that these temperature rises and thermal ablations can be achieved relatively constantly with a single GNR injection and a quick laser application.

The degree of heat dissipation after the laser was turned off was also determined in a pilot mouse, and a Newtonian cooling behaviour was observed. This is represented in Fig. 6-28 where the temperature returned to baseline in two minutes.

Mouse type	Tumour size (mm) at Day 0	Vol. GNR (µl)	Conc. [GNR] nM	OD (GNR)	Laser Power (W)	Beam diam. (mm)	Laser time (min)
Pilot	8.0 x 7.5	50	3.85	18.5	2.0	8	3

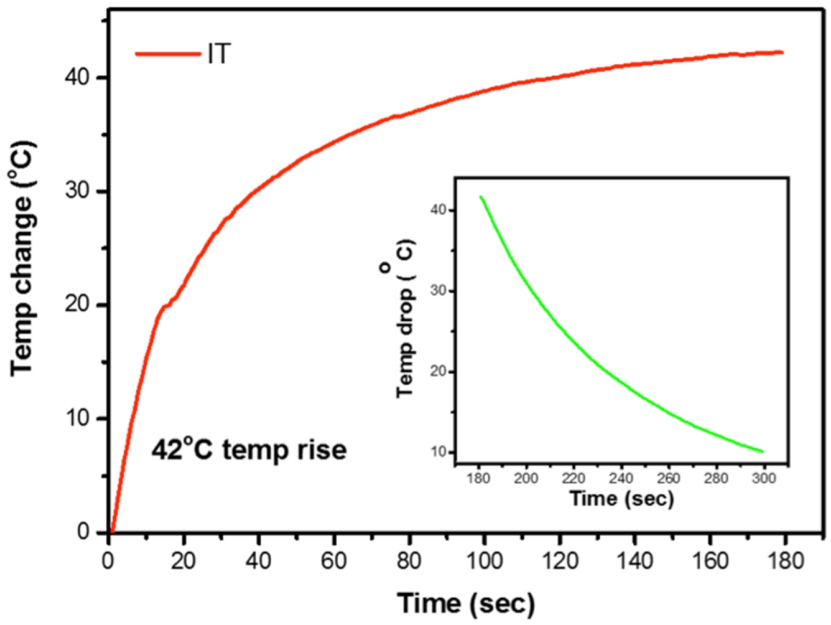


Fig. 6-28 Representative temperature changes in a pilot mouse. Inset graph demonstrating the principle of Newtonian cooling behaviour observed after the laser was turned off, with a return to baseline after approximately two minutes.

6.4.3 Results - Intravenous (IV) GNRs and NIR irradiation

A further ten randomised mice received IV GNRs and 808 nm laser irradiation for three minutes. All tumours were at least 5 mm in a single axis before the treatment commenced. Mice were anaesthetised and injected in the tail vein with 100 µl of GNRs at a concentration of 5.50 nM (3.3 x 10^{11} GNPs) and an OD of 26.4. The parameters of the ten mice which received IV GNRs are shown in Table 6-3.

At various time points, fluorescence imaging was performed to determine the presence of a fluorescence signal from functionalised GNRs at the site of tumour. However, despite the

intensity signal, (see results in section 6.3.3 “Fluorescence imaging results for IV GNRs”) it was decided that PTT would be conducted 24 hours post injection. The power of the laser was calculated to incorporate at least a 1 mm additional circumferential dimension with respect to the largest dimension of tumour, ensuring adequate beam coverage, in the same manner as described in the IT section. The laser position, triggering mechanism and image analysis were all identical to mice receiving IT GNRs and PTT.

Mouse No.	Tumour size (mm) at Day 0	Vol. GNR (μl)	Conc. [GNR] nM	OD (GNR)	Laser Power (W)	Beam diam. (mm)	Laser time (min)
1	6.6 x 4.6	100	5.50	26.4	1.7	7.0	3
2	7.5 x 6.0	100	5.50	26.4	2.0	8.0	3
3	6.2 x 7.0	100	5.50	26.4	2.5	8.5	3
4	6.6 x 5.0	100	5.50	26.4	2.1	7.0	3
5	7.5 x 7.0	100	5.50	26.4	2.5	8.0	3
6	9.6 x 7.2	100	5.50	26.4	2.6	10.0	3
7	5.0 x 6.2	100	5.50	26.4	1.7	6.5	3
8	6.5 x 4.7	100	5.50	26.4	1.7	7.0	3
9	5.8 x 6.3	100	5.50	26.4	1.7	6.5	3
10	5.7 x 4.3	100	5.50	26.4	1.7	6.5	3

Table 6-3 The parameters of the ten mice which received IV GNRs and PTT with NIR irradiation.

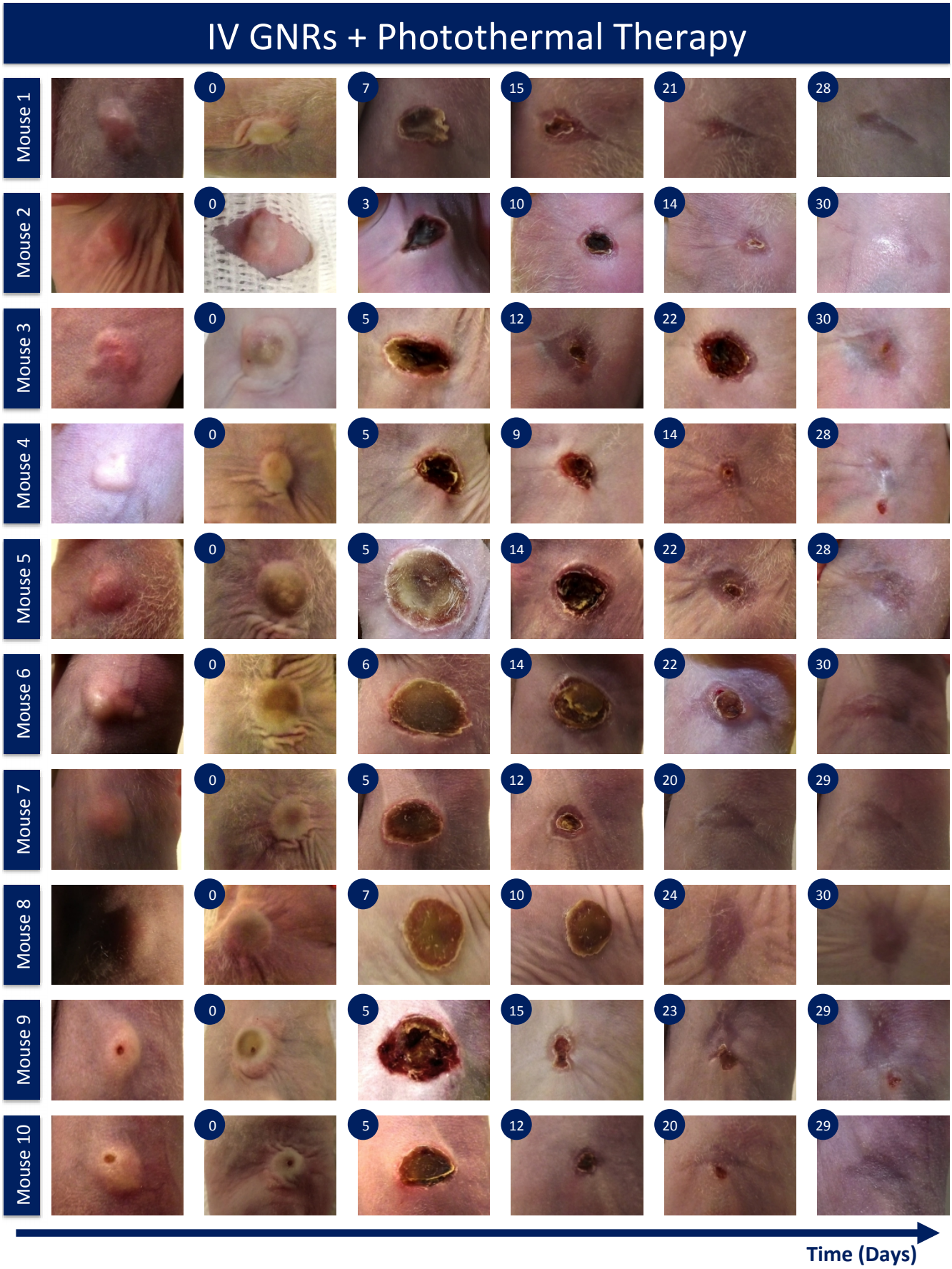


Fig. 6-29 The PTT responses in tumours of the ten mice (initial tumours on the left column) which received IV GNRs, with their progression over days.

All mice in the IV GNRs and PTT group also demonstrated a good photothermal effect with macroscopic and microscopic disappearance of tumour and absence of any proliferating cancer cells on post-termination histology at the end of study (day 30) as shown in Fig. 6-29. There was a similar indication of early thermal reaction by the crinkling/puckering of skin around the tumour immediately after PTT (day 0). Early signs of tumour necrosis were commonly seen 1-5 days post therapy with a less intense eschar formation than in the IT group, which would subsequently develop into a dry scab. This scab usually resolved spontaneously by the third week revealing an underlying healed irradiation site. All mice demonstrated complete healing by day 30 with neo-epithelialisation at the site of thermal therapy. These irradiated areas were resected with deep and wide margins and histopathological analysis confirmed the ablation of tumour and an identical picture to that seen in the IT group of epithelial regeneration through neo-collagenesis under polarised light microscopy was observed (as seen in Fig. 6-26 and Fig. 6-27).

Temperature profiles of the successfully ablated tumours in these mice were analysed and it would seem that a mean of 38 ± 9°C rise would lead to adequate PTT and successful tumour ablation (see Fig. 6-30). All mice received the same volume, concentration and OD of IV GNRs in aqueous solution. This was irrespective of the tumour size, as it was not possible to calculate the increased volume to be required for larger tumours without a substantially larger comparative *in vivo* study. Despite this limiting factor, as it can be seen in Mouse 6 which has the largest tumour dimension, all tumours responded to the same dose of GNRs when irradiated as the tumours were adequately covered by the laser beam. Despite the sequestration of GNRs by the RES organs there seemed to be a sufficient uptake of systemic GNRs into tumour tissues, as subsequently determined by ICP-MS (see Fig. 7-9 in Chapter 7). The mean concentration of Au measured in tumours by mass spectrometry in IV-delivered GNRs was approximately a quarter of that seen in IT-injected GNRs. This is likely to be due to the synergistic combination of ensuring the combined targeting approach of passive EPR localisation and the active antigen-antibody targeting would increase the efficiency of delivery of functionalised GNRs specifically to the tumour site. A large proportion of the IV administered GNRs would be sequestered by the liver and spleen, as results from ICP-MS demonstrate (refer to Table 7-3 and Figure 7-9). Thus, if the initial tumour size is very large, it is unlikely that the same volume, concentration and OD of IV GNRs and irradiation parameters used in this regime would lead to complete or lasting tumour ablation. This principle is expounded further in Section 6.7.3 “Size consideration of large tumours”.

6.4.4 Comparison between photothermal temperature responses with IV and IT GNRs

The mean temperature rises for all mice in the study during PTT is depicted in Fig. 6-30. Standard deviations within the groups were measured at 30, 60, 90, 120, 150 and 180 s. The mean temperature rise after three minutes of irradiation in the IT group was higher (42.3 ± 9.4°C) than in the IV group (38 ± 9°C). This would be explained by the intuitively higher concentration of GNRs within the tumour site in the IT group, as also evidenced by ICP-MS analysis (see Fig. 7-9 in Chapter 7). The minimum temperature rise after three minutes in the IT group was 32.6°C and 29°C for the IV group. As the minimum core skin temperature of mice was 21°C, even the minimum temperature rises in each group would be sufficient to induce the level of hyperthermia necessary for successful thermal ablation. This indicates that all mice in both groups received adequate hyperthermia and this corresponded well with the elimination of tumours. When considering a human translation of this principle the higher core body temperature (37.2°C) would require a much lower temperature rise for intratumoural hyperthermia to be effective, and consequently a tailored or personalised approach with respect to tumour size, GNR concentration and volume, and laser power and duration would need to be taken into consideration.

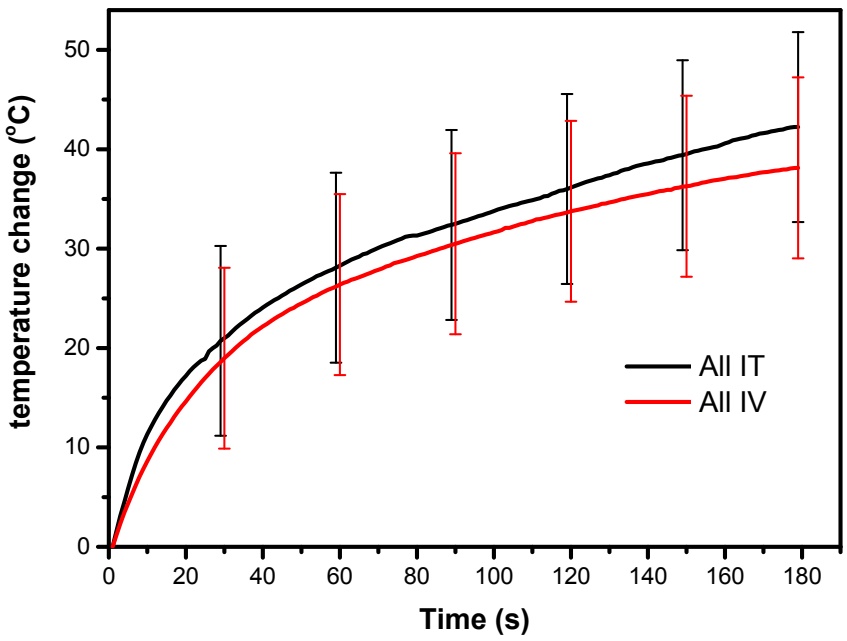


Fig. 6-30 The mean and standard deviation of temperature rise in mice observed during PTT from all ten mice in both IT and IV GNRs groups.

In Chapter 4, the maximal concentration of GNRs which was used to incubate porcine *ex vivo* tissues with was 6.6 x 10^{-12} M (with an OD of 1). In the experiments here the concentration of GNRs delivered *in vivo* to mice with tumours was 5.5 nM with IV GNRs (with an OD of 26.4) and 2.75 nM for IT GNRs (with an OD of 13.2). When reviewing the temperature profile of porcine *ex vivo* tissues, it would appear that the highest concentration of GNRs produced a temperature rise of approximately 40°C, and a similar temperature rise would be noted in mice receiving PTT following the delivery of IT GNRs (average = 42°C rise) and IV GNRs (average = 38°C rise). Although at first glance the temperature rise appear to be similar despite the 1000-fold lower GNR concentration in porcine *ex vivo* tissues, it must be borne in mind that the *ex vivo* tissues were exposed and incubated with topical GNRs within a solution, which were then absorbed on their surface or endocytosed (similar therefore to an IT delivery of GNRs). However for an IV injection of GNRs, the GNRs would have to initially evade opsonisation by the organs of the reticuloendothelial system and rely on both active and passive tumour targeting before arriving at the tumour site. Thus in this regard, the temperature rise is significant and an important factor in the consistently successful ablations of tumours seen in the IV GNRs arm of the study.

6.5 The theranostic application of GNRs *in vivo*

While it has been shown separately that functionalised GNRs are potentially able to provide live diagnostic information during endoscopy, and are capable of inducing thermally-assisted photoablation of tumours, it would be prudent to be able to combine this technology for the endoscopic setting. A proposal for *in situ* merging of fluorescence imaging and PTT is envisioned whereby tumours can be precisely identified, their dimensions measured and boundaries marked, followed by NIR irradiation. This theory was put to practice during the latter stages of the *in vivo* study where tumour identification was followed by NIR therapy (immediately for IT GNRs, and the next day for IV GNRs). The combined theranostic set-up is an amalgamation of the set-ups of the individual components of imaging and therapy, and illustrated in Fig. 6-31**.** The set-up comprises aligning the NIR laser alongside the laparoscope, and a thermal imaging camera mounted above the specimen (tumour). This enabled fluorescence imaging to localise and mark out the tumour (this was conducted in the study using hypodermic needles). Once localisation was achieved, the fluorescence light would be turned off and the laser aim-beam turned on. The aim beam would coincide with the pre-marked area and the tumour was thus ready to be irradiated. This set-up, along with corresponding images is depicted in Fig. 6-32 (a)–(d).

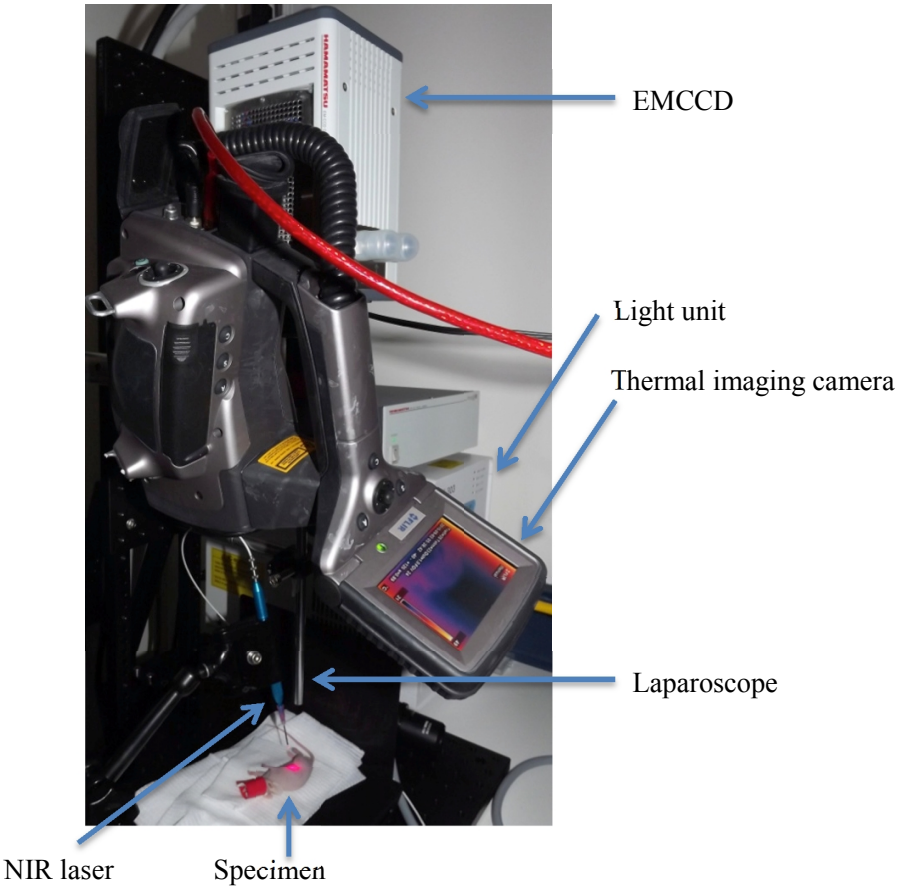


Fig. 6-31 The set-up for coupling fluorescence imaging with photothermal therapy. Fluorescence excitation light was delivered through the laparoscope and NIR light through the laser delivery fibre.

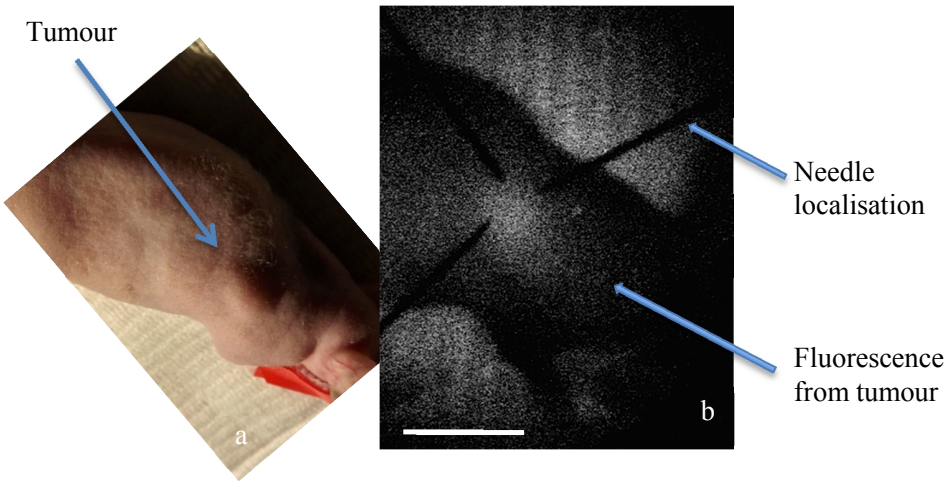
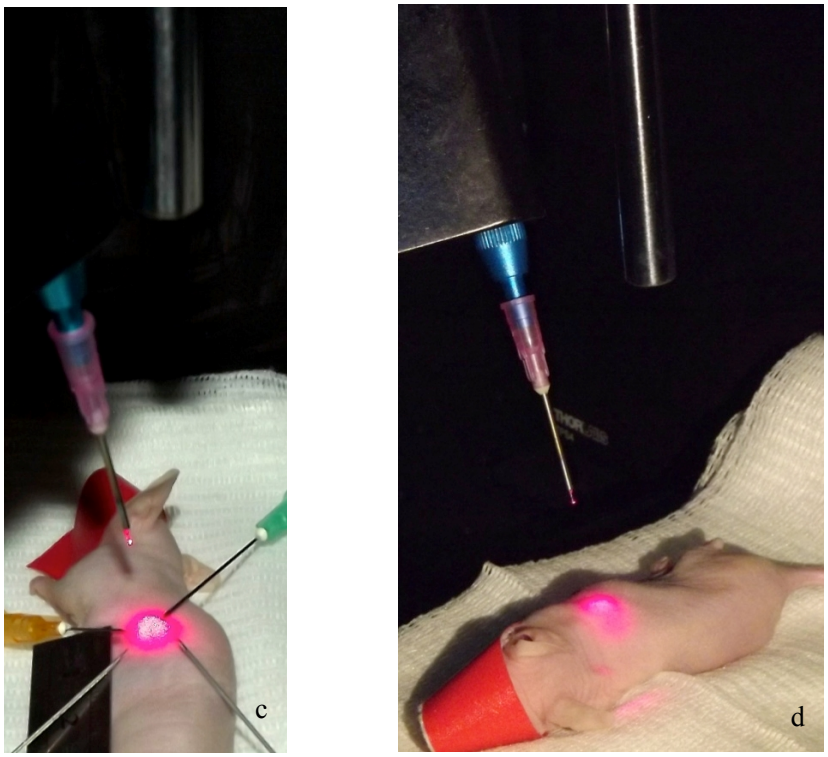


Fig. 6-32 The tumour xenograft (a) is initially identified and mapped [with hypodermic needles, (b)] while under fluorescence guidance following an administration of IV GNRs. Scale bar = 1 cm.



Following fluorescence-guided needle localisation, the laser's aim-beam was directed to the area (c). The marking needles were removed, and NIR laser applied *in situ* (d).

Several experiments in the study were conducted using this combined theranostic approach. A representation of the results seen in mice receiving IV GNRs is described here, using Mouse 8 (from the IV GNRs and PTT group) as the example **(**Table 6-4**).**

Mouse No.	Tumour size (mm) at Day 0	Vol. GNR (μl)	Conc. [GNR] nM	OD (GNR)	Laser Power (W)	Beam diam. (mm)	Laser time (min)
8	6.5 x 4.7	100	5.50	26.4	1.65	7	3

Table 6-4 Parameters used in Mouse 8.

The tumour was identified under fluorescence imaging and localised with needles placed at the margins of the fluorescent region. The area was also measured with a ruler and without moving these markers, the fluorescence emission light was switched to the laser's aim-beam by focusing it on the pre-marked position (Fig. 6-33).

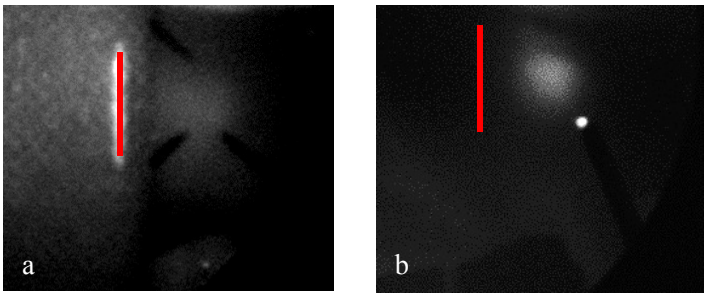


Fig. 6-33 The fluorescent area was measured and marked (a), and without moving the markers, the laser aim-beam was brought into position (b). Scale bar = 1 cm.

Photothermal therapy was then performed and a 29.5°C temperature rise can be observed in Fig. 6-34(a)-(c). The thermal effect on the tumour can be seen in Fig. 6-29 (Mouse 8), with histologically confirmed ablation of all tumour cells.

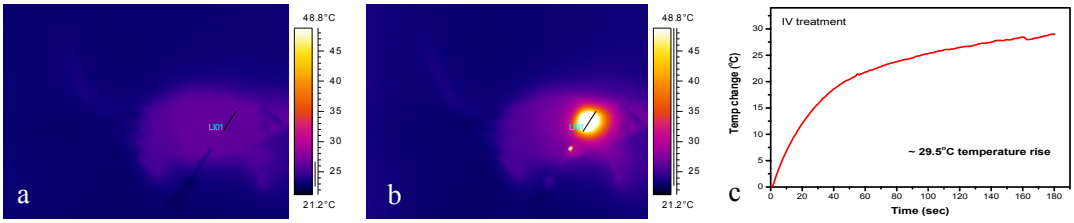


Fig. 6-34 Temperature measurements obtained using the theranostic approach, at (a) 0 s and (b) 180 s, with a graphical representation of the measured temperature rise in (c).

It is plausible to transfer this set-up to a clinical endoscopic setting, with the excitation light replacing standard Xenon white light, and after endoscopically marking the fluorescent margins of the tumour, delivering NIR light through a fibre optic inserted into the working channel of the endoscope for tumour ablation. The procedure could also be performed endoscopically with an IT injection of GNRs, using the same principles and findings discussed in the IT GNRs treatment arm of the study.

6.6 Histological confirmation of tumour ablation

Following the end of the 30-day study, all mice in the IV and IT treatment arms of the study had an excision biopsy performed of their irradiated tumour sites and H & E staining for histological examination. Representative histology images from the ten mice in each group are shown in Fig. 6-35 and Fig. 6-36. All mice showed tumour regression clinically. Histologically both treatment arms demonstrated healthy cells with fully regenerated and well-defined layers of epidermis and dermis which had experienced neo-collagenesis. There was no evidence of tumour proliferation or cancer cells.

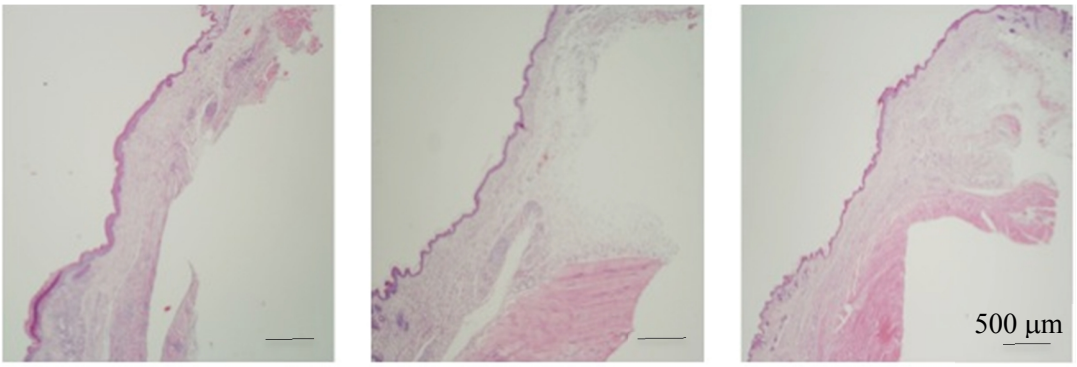


Fig. 6-35 Representative histological appearances of three mice in the IT GNRs and PTT group showing fully regenerated epidermal & dermal layers with no evidence of tumour or proliferating cells (x20 magnifications, scale bars = 500 μm).

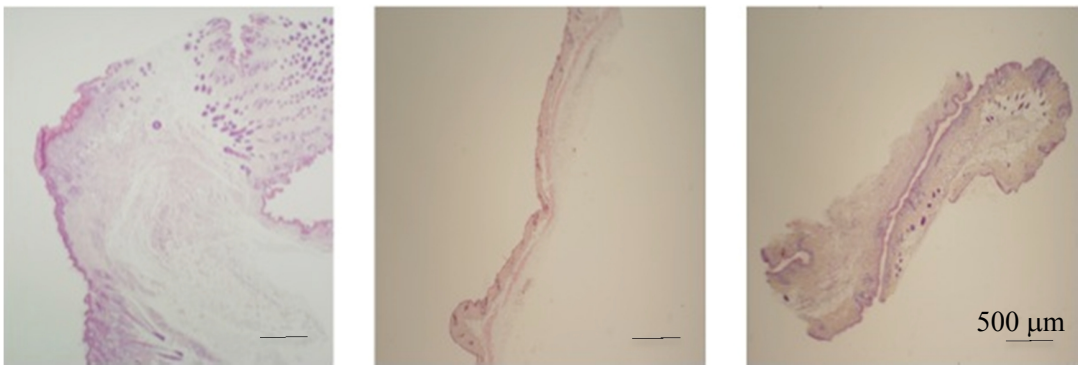


Fig. 6-36 Representative histological appearances of three mice in the IV GNRs and PTT group showing fully regenerated epidermal & dermal layers with no evidence of tumour or proliferating cells (x20 magnifications, scale bars = 500 μm).

Not infrequently, clusters of 'black dots' were seen under light microscopy in the post-irradiated IT group and this is represented in Fig. 6-37. In the absence of other entities which

were artificially 'added' into the tumour tissues apart from an intratumoural injection of GNRs, this was presumed to be very large aggregations of GNRs, as they were being detected under relatively low magnification light microscopy. These black dots were not visible in tumours from laser-only control mice, nor were they visible in the IV GNRs group. Upon 200x magnification, there was evidence that most of these particles were in the submuscularis layer [Fig. 6-37(b)].

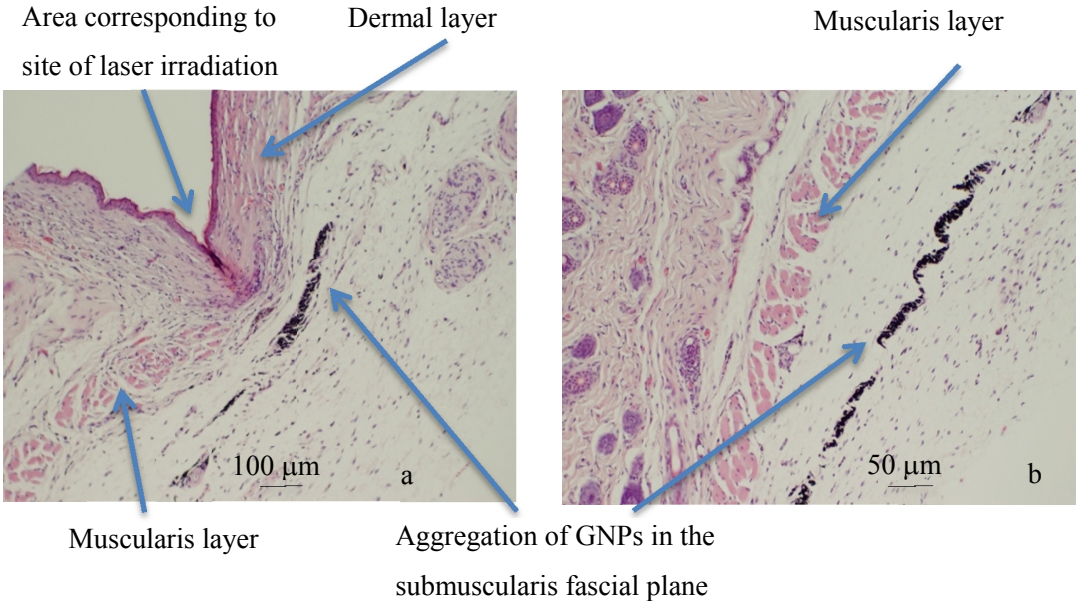


Fig. 6-37 Histology from a study mouse showing potential aggregation of irradiated GNPs along a submuscularis fascial plane [(a)100x and (b) 200x mag.].

While not under the ideal imaging modality of electron microscopy (EM), however with only 1000x magnification under light microscopy and H & E staining there occasionally appeared to be both an aggregation of GNPs and a reshaping of nanorods into more spherical constructs post irradiation, which were noted in the submuscularis fascial plane. It also shows some evidence that the nanoparticles are within the cytoplasm of cells (perinuclear) and not inside the nuclei [stained purple in Fig. 6-38(a)]. These cells could well be macrophages as they seem to be normal cells 'mopping up' the GNPs [Fig. 6-38(b)]. These appearances were further characterised by TEM (see the next section 6.6.1).

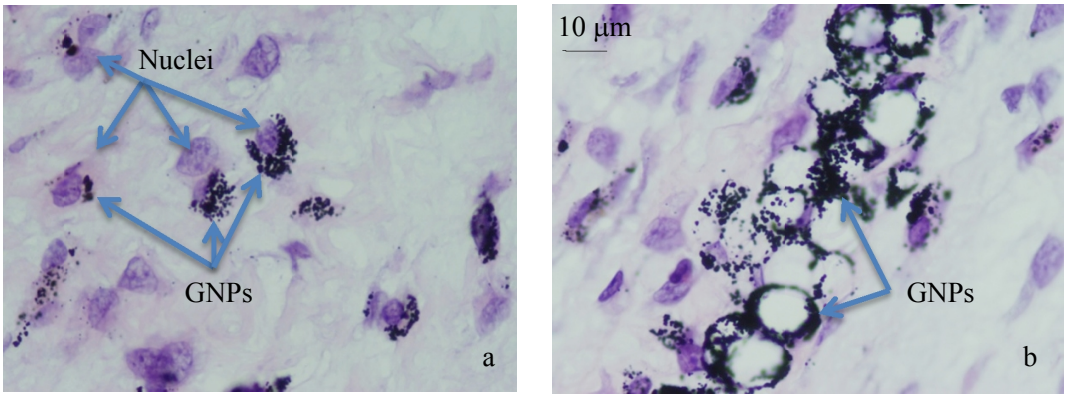


Fig. 6-38 (a) Perinuclear 'black dots' seen that may be GNPs under 800x & 1000x mag. in an area that received IT GNRs and PTT 30 days prior. (b) Large cells presumed to be macrophages phagocytosing GNPs.

6.6.1 TEM – Evidence of intracellular endocytosis of GNRs in tumour cells

Although there was sufficient evidence to conclude that GNRs given IV and IT did accumulate at the tumour site with ICP-MS, fluorescence imaging and the temperatures seen during irradiation, it was important to determine whether GNRs administered *in vivo* had actually been endocytosed by cancer cells and were hence poised for subsequent targeted therapy and to quantify the numbers, location and shape of GNRs. TEM is able to provide appropriate magnification to resolve these issues and ascertain that they were not merely 'floating' freely within the extracellular matrix or interstitial space, which could arguably also account for the results seen from fluorescence imaging, thermal measurements and ICP-MS.

We obtained tissue from tumour sites that received GNRs (without laser) on Day 0 post IT injection, and on Day 1 post IV injection, as well as microscopically ablated tumour sites which had been treated with PTT 30 days prior. For confirmation of the presence or absence of cancer cells in the samples, tumour tissue from mice which received IT GNRs only on the day of sampling was divided into two sections - one half of which was observed under light microscopy to confirm that it was from an area of proliferating cells within a GI adenocarcinoma. The other half of the tumour tissue was processed and sectioned for TEM imaging analysis using the methods previously described.

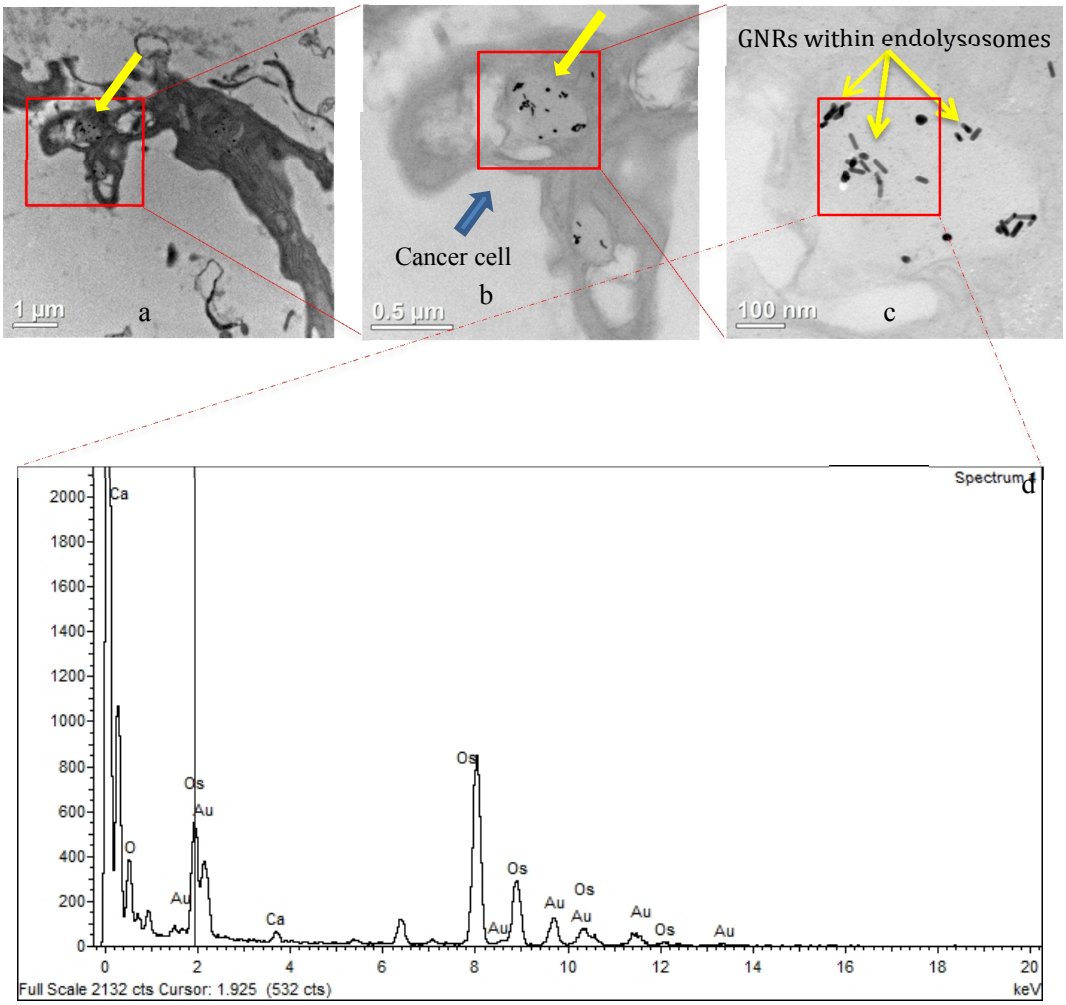


Fig. 6-39 (a) TEM of a group of cells within the tumour tissue with gradual increase in magnifications in the ROI (b-c). Yellow arrows correspond to vesicles within cancer cells which gradually become more defined through higher magnification. (c) higher magnification of (b), now focused on a single cancer cell demonstrating intravesicular GNRs, (d) energy-dispersive X-ray spectroscopy graph showing the chemical analysis of the magnified ROI with the presence of gold indicated by peaks of 'Au' within the EDX.

Fig. 6-39 from the tumour site of a mouse which received IT GNRs on the day of sampling demonstrates that there were vesicles with black spots within – these are marked with arrows in the diagram. Upon increased magnification (up to 120k times), it could be resolved in Fig. 6-39(c) that these appeared to be intracellular GNRs within endolysosomes which lay within the cytoplasm and not in the nucleus of cancer cells. A reasonable number of these intracellular vesicles could be visualised in the specimen with lower magnification in Fig. 6-39(a-b) and although it could be fairly certain that these were in fact all vesicles containing intracellular GNRs, energy-dispersive X-ray spectroscopy (EDS/EDX) was used for further characterisation. This technique is widely used in conjunction with TEM or SEM in the chemical characterisation or elemental analysis of samples. Corresponding peaks within the

processed EDX graphical analysis showed that these intracellular 'black dots' corresponded to peaks of gold (Au), which conclusively proved that the particles seen were indeed the administered GNRs. The other peaks corresponded to carbon, calcium (Ca) and osmium (OsO_4), which are elements which were either found naturally intracellularly or used as our sample fixative. Thus this provided conclusive evidence that anti-EGFR-antibody-GNRs injected directly into the tumour site retain their rod-like structure once they fairly rapidly become endocytosed within cancer cells, where they are optimally positioned for their function in photothermal therapy.

When examining tumour specimens that received IV GNRs with TEM, it was difficult to locate the GNRs. It is known with ICP-MS that there were less GNRs within the tumour matrix than in IT-administrated GNRs and it is therefore more difficult to obtain the precise location of these particles within sections performed with an ultramicrotome. However work is currently on-going with this regard, and some progress has been made in identifying gold nanorods within control mice which received IV GNRs alone.

6.6.2 Evaluation of metastasis

All mice were autopsied at the end of the study and a visual examination of their internal organs was performed. A thorough inspection of the peritoneum, liver, spleen, omentum and lungs indicated that there were no detectable metastases from the primary tumour. In addition to primary tumour regression, it was important to be cognisant of this finding which reinforces the strength in eliminating the primary tumour. Although not scrutinised in great detail due to the subcutaneous nature of the tumour xenograft, is likely that the sentinel lymph node was also destroyed by the radiation of energy. Thus in humans it may be worth imaging or sampling the sentinel lymph node prior to application of photothermal therapy in certain tumours such as breast cancer. It can be seen from a tumour in a mouse in the pilot study which persisted after PTT (Section 6.7.3), that GNPs do disperse into the lymphatics and the sentinel lymph node, thus it may be possible in future studies to examine the use of fluorescence or other pre-existing modalities to identify positive lymph nodes pre-treatment.

6.7 The 7 principles of highly effective photoablation

"I have not failed; I've just found 10,000 ways that won't work" – Thomas Edison.

Upon completing the pilot study, a number of key lessons were learnt which became essential when planning and executing the actual study. These principles helped to ensure reproducibility of good results with PTT and also to elucidate the potential pitfalls in the application of this technology for complete tumour ablation. The lessons learnt from the pilot studies thus directed modifications which were made in the actual study experiments. These are listed below and discussed in turn:

1. Multidirectional injection of GNRs for IT administration
2. Ensuring the beam size is larger than the largest dimension of tumour
3. Size consideration of large tumours
4. Administer a fresh and pure sample of fully functionalised GNRs
5. Allow 24 hours after IV administration of functionalised GNRs
6. Determine the appropriate OD (and volume) of GNRs to administer
7. Observe for 30 days and evaluate pathology

6.7.1 Multidirectional injection of GNRs for IT administration

Having observed some tumour recurrences in the pilot studies, it was decided that it was imperative that approximately the same volume of GNRs was injected homogeneously into the entire tumour volume. Thus with a single entry point, the needle of the syringe containing an aqueous solution of GNRs was directed into all four quadrants and finally into the base of the tumour. Each region thus received approximately 10 μl of the GNR solution. As recurrences usually emerged from the peripheral zone of irradiation, it was learnt that a single bolus of GNRs into the epicentre (core) of the tumour would not dissipate evenly by itself into the edges of the tumour. A good example of this is in a pilot mouse where only a core injection GNRs was performed into the tumour, and initial results looked promising (in Fig. 6-40) with a temperature increase of 39°C after three minutes of NIR irradiation.

Mouse type	Tumour size (mm) at Day 0	Vol. GNR (μl)	Conc. [GNR] nM	OD (GNR)	Laser Power (W)	Beam diam. (mm)	Laser time (min)
Pilot	8.2 x 7.4	50	2.75	13.2	2.2	8	3

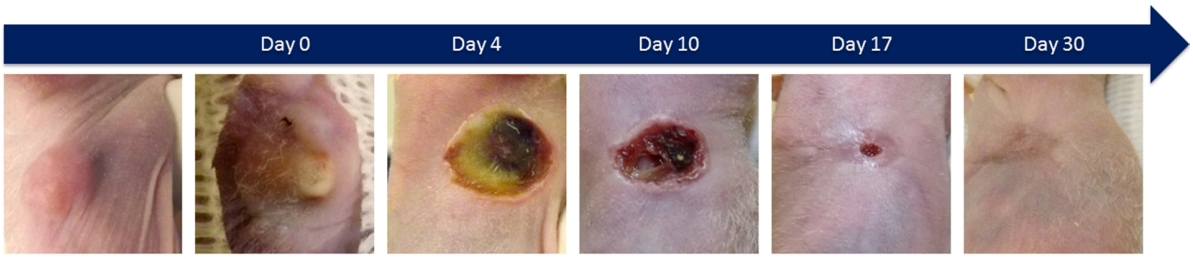


Fig. 6-40 Pilot mouse that received a core delivery of GNRs into its tumour, with promising results and a clinical resolution of tumour by day 30.

A histological examination performed of the tumour site at day 30 however revealed that there was proliferating tumour within the muscularis layer, which could not be appreciated clinically (Fig. 6-41). The epidermis, dermis and superficial muscularis layers appeared free of tumour and proliferating cells. It was thence decided that it was imperative to obtain histological confirmation of all irradiated sites, despite the outward clinical appearance of tumour resolution. This may have not been appreciated in some published PTT studies which report solely on clinical or macroscopic disappearance of tumour at the irradiation sites. It indicated that subsequent injections of GNPs into tumour should incorporate an injection into the base of the tumour, as well as all four quadrants. This refinement to the procedure of administering the GNRs, would attempt to ensure homogeneity in GNR distribution within tumours prior to irradiation.

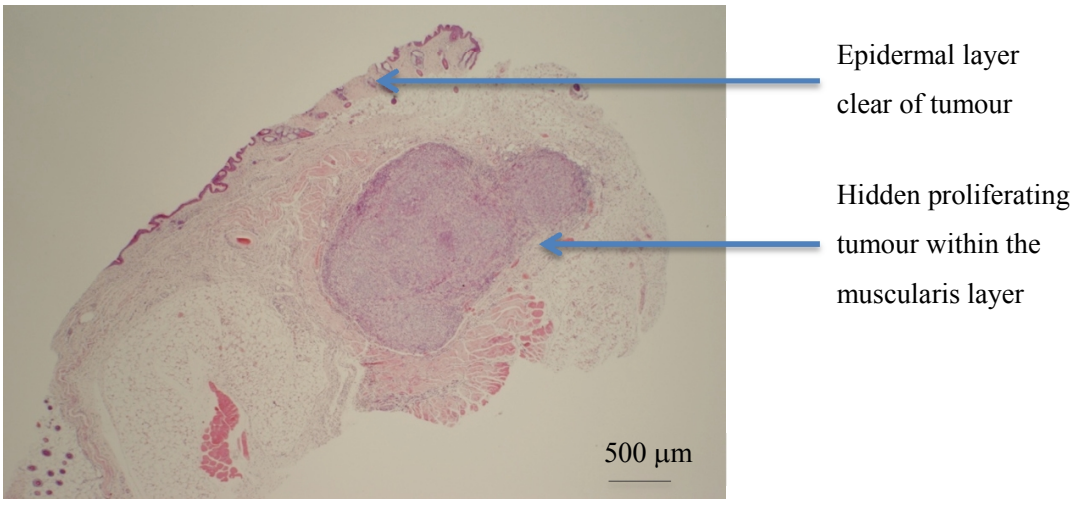


Fig. 6-41 Hidden microscopic tumour within the muscularis layer despite a clinical (macroscopic) disappearance on its surface (20x mag.).

6.7.2 Ensuring the beam size is larger than the largest dimension of tumour

Selecting the appropriate laser power was dependant on the tumour size, and it was crucial to maintain a laser beam diameter of at least 1 mm larger than the longest single dimension of the tumour, to ensure adequate tumour coverage. In some pilot mice it was noticed that a recurrence of tumour would be found emerging from the edges of the irradiated zone, likely due to the presence of proliferating cells outwith the zone of irradiation. The application of fluorescence imaging in guiding PTT was found to be useful in marking out the area of intended irradiation, but would not be sensitive in delineating the margins of cancer cells. Consequently when an additional 1 mm diameter laser spot size was used over and above the maximal axial dimension of the tumour, it would appear, at least for these tumour xenografts, to incorporate a safe margin of error. The beam diameter was defined as 1/e as it had a Gaussian shape with no sharp edges. This would augur well with the basic tenets of surgical cancer resection in humans, incorporating a (relatively wide) margin of macroscopically normal tissue in the resection specimen in the endeavour to be clear of microscopic disease within the resection margins.

6.7.3 Size consideration of large tumours

One of our pilot mice demonstrated this principle in that the standard volume and concentration of IV GNRs and irradiation regime (shown in Table 6-5**)** as in the experimental study was administered to a mouse with a rather large tumour measuring 11.5 x 8.4 mm. The tumour in this mouse however also did not receive adequate laser coverage (the laser beam size was initially kept at a constant 8 mm for comparative reasons), which is a confounding factor. According to our formula for power density, the actual laser power that would be required for an adequate spot size coverage (i.e. 12.5 mm) would need to have been 6.1 W. This would be an exceptionally high laser power to be delivered to a mouse, and thus a safe and logical balance between tumour size and laser fluence needs to be considered for PTT. From our literature review, the maximal power applied in rodent studies for PTT with GNPs was 3 W, but the maximum power used in all the mice in our experimental studies was 2.6 W, irrespective of the size of the tumour. Although in this pilot mouse a high temperature rise was seen (44°C rise at the end of three minutes of irradiation) along with an appropriate initial macroscopic thermal response, by the end of the third week a proliferating tumour had evidently arisen from the peripheries of the irradiation site, and this continued to enlarge (see Fig. 6-42**).**

Mouse type	Tumour size (mm) at Day 0	Vol. GNR (µl)	Conc. [GNR] nM	OD (GNR)	Laser Power (W)	Beam diam. (mm)	Laser time (min)
Pilot	11.5 x 8.4	100	5.50	26.4	2.2	8	3

Table 6-5 The parameters for a pilot mouse in which the tumour regrew from the peripheries due to its large initial size.

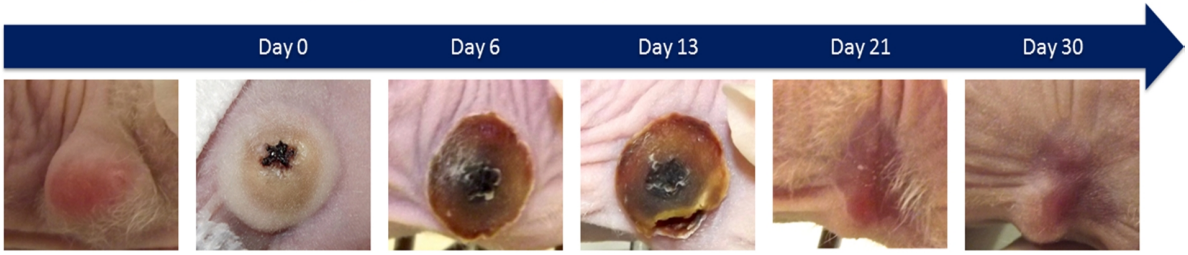


Fig. 6-42 Pilot mouse demonstrating a large tumour with a reasonable initial photothermal effect but developed a noticeable recurrence of tumour from day 21.

The high temperature achieved was likely to have been concentrated at the epicentre and not homogenously distributed throughout the tumour. The Gaussian distribution of thermal energy induced by the CW laser, being hottest at its centre of focus and cooler at the peripheries, can explain this. Thus it is possible that there was a diminution in energy delivered to the peripheral (extremity) zone. The beam size also fell short of covering the dimensions of the tumour, and thus it is retrospectively apparent that this would have resulted in incomplete tumour ablation. It was therefore considered that a less intense temperature change with complete laser coverage of a smaller tumour would ensure a better photothermal result. Hence the additional 1 mm additional circumferential margin in the beam size in relation to the tumour's single largest dimension was utilised in the actual study for both IT and IV groups, with better outcomes.

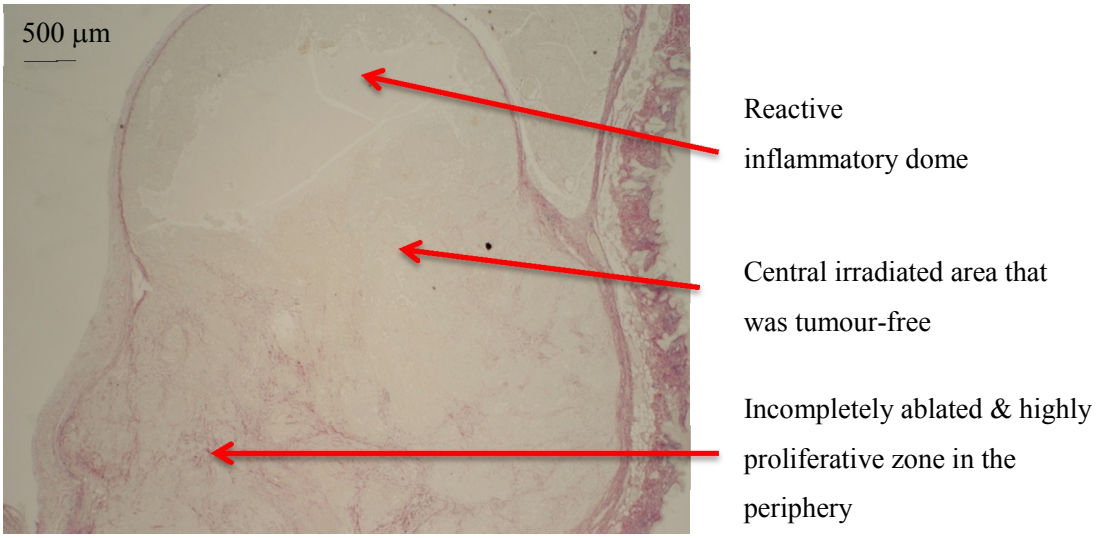


Fig. 6-43 Histology of the pilot mouse (on termination at day 30 post PTT, x20 mag.).

Histological examination of this site as seen in Fig. 6-43 showed that there was a central area of tumour ablation where the collagen was destroyed (paler in comparison to areas of original collagen shown as pink). However, there was certainly an area of residual tumour (or tumour recurrence) that encroached upon the irradiated and tumour-free area, with signs of cancer cells invading this central area from the periphery. There was also a noticeable reactive inflammatory dome at the tumour ablation site (Fig. 6-43).

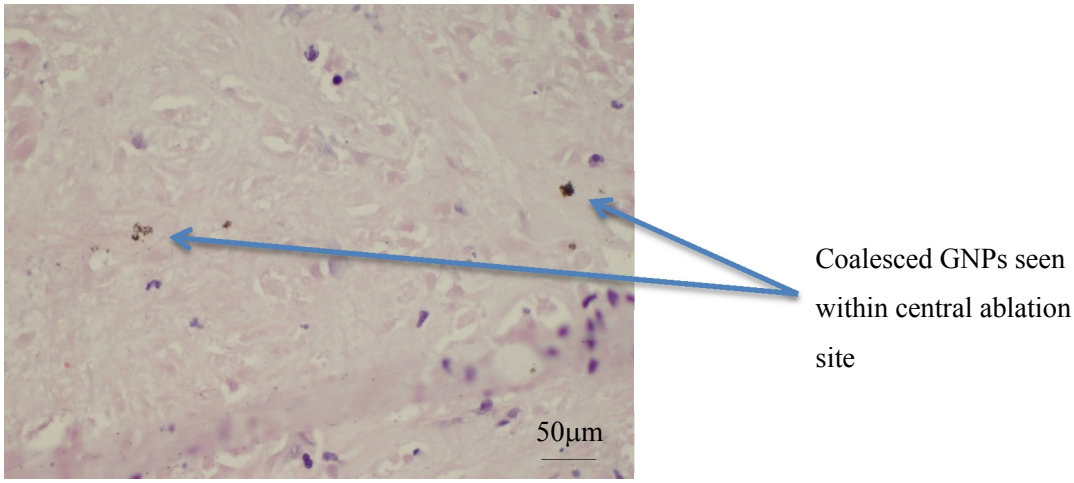


Fig. 6-44 Within the central area of the tumour ablation site, there was some evidence of probable coalescing of GNPs (200x mag.).

While there appeared to be at least some potential GNPs seen within the centrally ablated site (Fig. 6-44), no GNPs were seen within the proliferative zone. This may have led to incomplete ablation. This would be due to a non-homogeneous distribution of GNRs and heating that should ideally occur evenly throughout the tumour matrix.

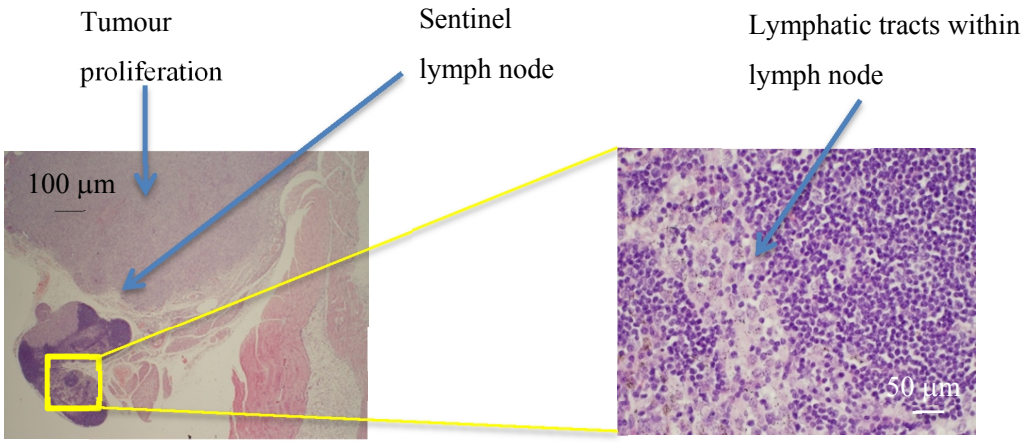


Fig. 6-45 A sentinel lymph node seen adjacent to the tumour site with lymphatic tracts within the lymph node (100x mag. and 200x mag.).

A sentinel lymph node was seen adjacent to the tumour site and upon higher magnification, GNPs were seen within lymphatic tracts (Fig. 6-45) as black dots (Fig. 6-46).

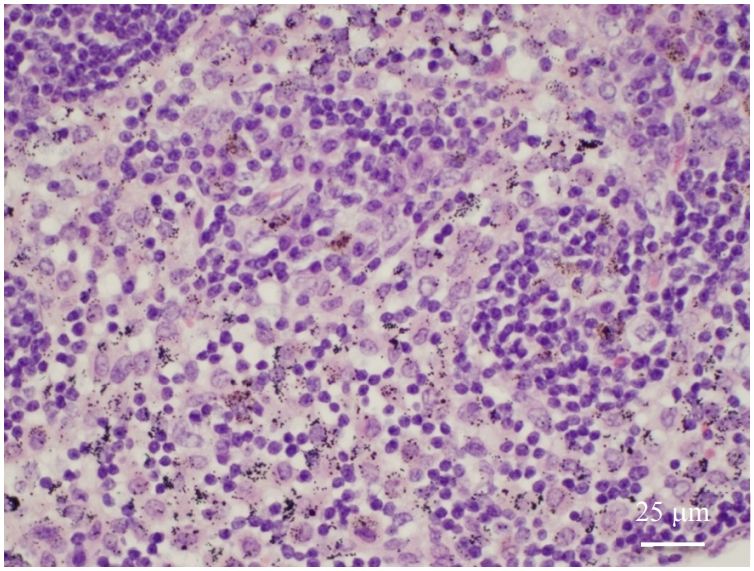


Fig. 6-46 GNPs seen inside lymphatic tracts of the lymph node as black dots (400x mag.).

This demonstrates that given the large size of the initial tumour, GNPs can and do drain into a sentinel (pathological) lymph node as there was substantial accumulation of GNPs within this node as seen in Fig. 6-46. This would be compatible with the usual route of cancer spread, invading local lymph nodes prior to haematogenous routes, and given that this was a large tumour, this may be the way in which GNPs are cleared from the site. Although there has only been one such case examined in detail by histology, as it was an unexpected deviation from our main study, it does bring to bear a theoretical possibility of photothermally ablating the sentinel lymph node, along with the tumour. However this clearly deserves further confirmation studies *in vivo*, which is beyond the scope of our study.

In due consideration of the pre-PTT size of this tumour, it is very likely that the area of tumour recurrence:

1) Did not receive enough GNRs
2) Did not receive adequate laser fluence

As the amount of GNRs administered was limited to the same amount that would be given to a tumour measuring 5 x 5 mm, to ensure consistency in the case of multiple variables, it is plausible that there were insufficient GNRs and consequently poor heating at the edges of the initial tumour leading to recurrence/proliferation. It may be possible that for very large tumours in palliative cancer, that a dual route of GNR administration or treatment course may be considered for enhanced or cumulative photothermal effect, as the laser beam area would be limited by a laser power that would need to be both safe and effective.

6.7.4 Administer a fresh and pure sample of fully functionalised GNRs

Early evidence of incomplete tumour ablations and/or recurrences seen in a few consecutive mice was ultimately traced back to the application an older stock of functionalised GNRs. Although there were reasonable initial temperature rises of 27-42°C, it soon became apparent that for both IV/IT injections, all the tumours had been incompletely ablated. The aggressiveness of the inoculated adenocarcinoma would soon become apparent in that the size of the treated tumours eventually became larger than (and in some cases doubled) their initial pre-PTT size. The recurrences were usually macroscopically evident from day 7 to 14, and would be seen to proliferate from the periphery into the central irradiation area. This was seen in four sequential mice that had received GNRs from the same batch of older GNRs. It transpired that the sample was more than two months old since its functionalisation process. It was further observed that it was difficult to obtain fluorescence signals *in vivo*, which could be an initial indication of a weakening of fluorophore-GNR binding. However once this was replaced by a fresh and pure sample of functionalised GNRs, both the fluorescence and PTT aspect of the study demonstrated significantly better and consistent results.

Thus while there is no published information about the life-span or shelf-life of multi-functionalised GNRs, our results indicated that they were approximately useful for *in vivo* purposes if utilised within three weeks following their functionalisation. The fresher the sample of functionalised GNRs were, the more reliable and consistent the results were from their application for *in vivo* theranostics. Functionalised GNRs should be kept in a sterile test tube/eppendorf covered with aluminium foil in a sterile refrigerated environment until such time it is intended for *in vivo* administration. Where possible tests of sample purity and tests of bioconjugation should be performed *in vitro* prior to *in vivo* administration.

6.7.5 Allow 24 hours after IV administration of functionalised GNRs

When functionalised GNRs are given IV, studies have shown that it does take approximately 24 hours for peak accumulation of GNRs within the tumour. This accumulation is enhanced by the use of a tumour targeting ligand attached to the surface of the GNRs. We tested this theory *in vivo* by attempting PTT early after the administration of GNRs in a pilot mouse which resulted in incomplete ablation. This mouse was given IV GNRs followed by fluorescence imaging within an hour of systemic administration, and PTT was performed immediately after this. Initial fluorescence imaging images demonstrated a high fluorescence intensity signal which corresponded well to the precise location of the tumour.

Mouse type	Tumour size (mm) at Day 0	Vol. GNR (μl)	Conc. [GNR] nM	OD (GNR)	Laser Power (W)	Beam diam. (mm)	Laser time (min)
Pilot	5.6 x 4.6	100	5.50	26.4	1.8	6	3

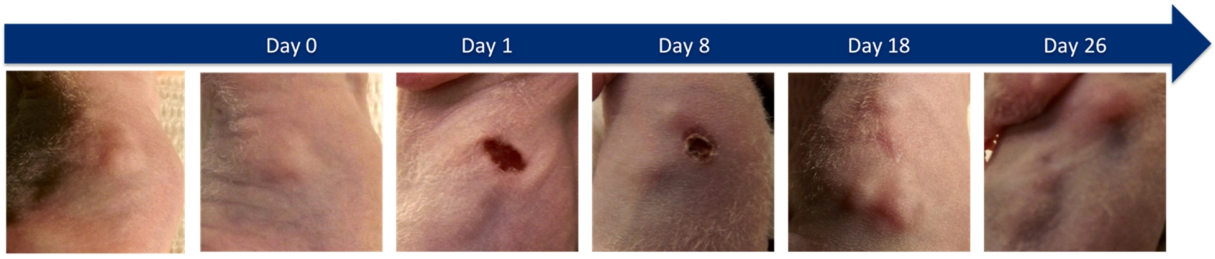


Fig. 6-47 Pilot mouse received immediate PTT after IV administration of GNRs, demonstrating a reasonable initial photothermal effect but a recurrence of tumour noticeable from day 8.

The temperature rise observed here was 29°C, which would indicate adequate heating transpired, but the region of tumour was incompletely ablated and this was noticeable after a week, with gradual proliferation of tumour in the incompletely ablated zone (Fig. 6-47). It is likely that the temperature rise was focal to the laser point and ultimately there were insufficient GNRs to generate an even temperature gradient across the entire area of proliferation. There was thus a discrepancy between the immediate fluorescence signal seen and the interpretation that this was from the rapid accumulation of functionalised GNRs at the tumour area. In retrospect the fluorescence was more likely to arise from unbound Cy5.5-anti-EGFR-antibody particles within the GNR solution. In the main study, mice were given 24 hours after IV delivery of GNRs and all achieved a complete tumour response with PTT.

Following this, all mice that received IV GNRs were subjected to a 24 hour "GNR targeting" time period prior to the application of NIR irradiation. This would allow a sufficient time lapse for functionalised GNRs to embed within the tumour matrix and to also become endocytosed within proliferating cells through a combination of both the passive EPR and active ligand-targeting routes of GNR accumulation. Although 24 hours was taken as an arbitrary time point, it was with correlation of ICP-MS values of Au concentration at the tumour site after IV and IT administration (refer to Section 7.5 in Chapter 7). It was not feasible to perform a more accurate measurement of Au concentration at various time points from 0 – 48 hours to determine an optimal time for PTT, as this would require a substantial number of mice that would need to be culled immediately after IV administration without undergoing PTT. From the pilot study and published data, it was discerned that 24 hours post IV injection of GNRs was the optimal time for PTT.

6.7.6 Determine the appropriate OD (and volume) of GNRs to administer

One of the other determining factors of successful PTT is the OD of the intravenously injected GNRs, which in the experimental study was consistently 26.4. This was decided upon after an initial attempt at delivering half this OD (13.2) for PTT was met with a critical failure of any form of tumour regression in a pilot mouse (shown in Fig. 6-48). The reason for this is depicted in Fig. 6-49. As a comparison, the results seen in this pilot mouse is compared to Mouse 2 in the study group which received IV GNRs and PTT and exposed to the same irradiation parameters (refer to Mouse 2 in Fig. 6-29).

Mouse No.	Tumour size (mm) at Day 0	Vol. GNR (μl)	Conc. [GNR] nM	OD (GNR)	Laser Power (W)	Beam diam. (mm)	Laser time (min)
Pilot	8.0 x 7.5	100	2.75	13.2	2.0	8	3
Mouse 2	7.5 x 6.0	100	5.50	26.4	2.0	8	3



Fig. 6-48 Pilot mouse receiving half the normal OD/concentration of IV GNRs, with failure of tumour control.

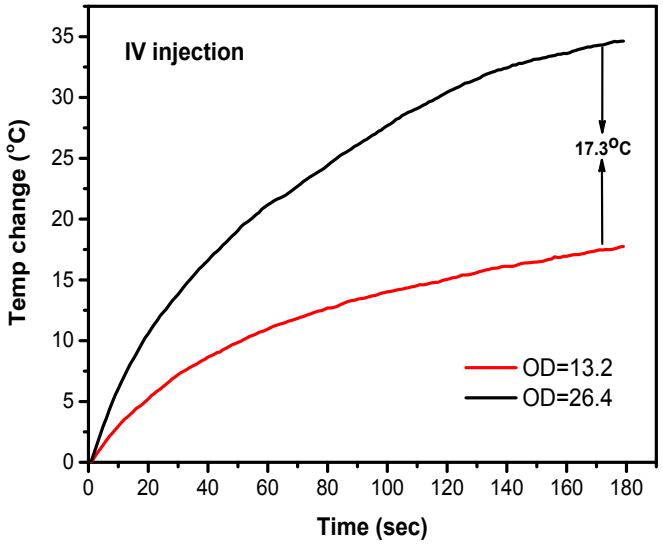


Fig. 6-49 Temperature increases seen from the irradiation of two mice receiving IV GNRs at different ODs but the same irradiation parameters.

From Fig. 6-49 it can be appreciated that in the pilot mouse which received IV GNRs at an OD of 13.2, inadequate heating was generated, which in turn allowed the tumour cells to continue to proliferate at more or less the same high mitotic rate as if there was no intervention. There was no visible thermal effect on day 1 after PTT. When the OD of GNRs was 26.4 as administered in Mouse 2 in the IV study (with identical irradiation parameters), it provided a higher temperature rise (17.3°C increase) than that of the tumour in the pilot mouse. It provided some evidence of essentially using the appropriate (in this case higher) OD for targeted therapy when administering GNRs intravenously for PTT. Chosing the appropriate volume of GNRs is also an important factor, as previously explained in Section 6.4.2, using Mouse 5 of the IT arm of the study as an example where the usual volume of GNRs adminstered was doubled even though it was of the same OD (13.2), resulting in a need to pre-emptively cease the irradiation early due to the temperature rise shown in Fig. 6-50.

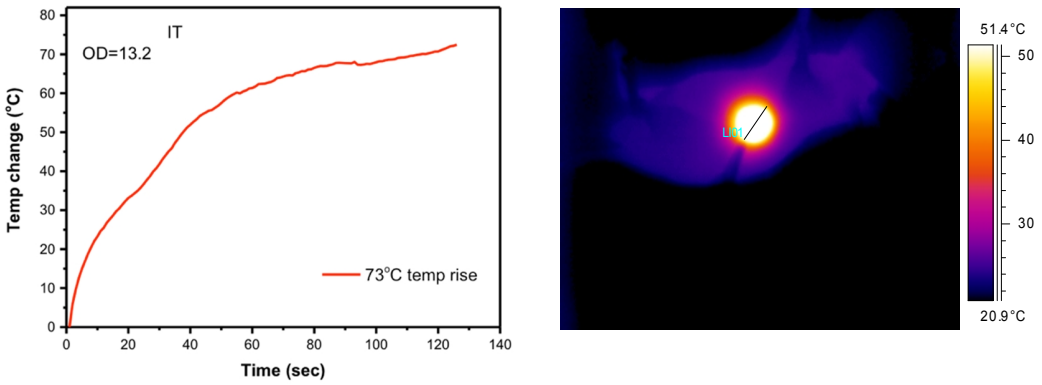


Fig. 6-50 Alarming temperature rise seen at the tumour site in a study mouse (Mouse 5) which received double (100 µl) the regular volume of IT GNRs at the same OD. The irradiation was ceased rapidly, and the mouse recovered satisfactorily.

6.7.7 Observe for 30 days and evaluate pathology

The mice in our study were observed for 30 days, even if initial macroscopic/clinical regression of tumour was evident, and the tumour ablation sites in the study were examined histologically with a wide excision biopsy of the treated area. This is to allow adequate time to ensure that tumours do not re-surface once the distracting thermal reaction on the skin had completely healed, and there were no hidden subdermal tumours (as described in the pilot mouse in Section 6.7.1). Some studies fell short of this observation period and microscopic examination [such as a 13 day observation period (24)], and it is possible that tumours can

deceptively appear to have been cured after a fortnight. However in our pilot studies, we learnt that the visual thermal effect on the skin and temperature rises seen can occasionally be a red herring. This is exemplified in one of the pilot SCID mice which received IT GNRs as a bolus solely into the core of the tumour (without confirming all quadrants and the tumour base was covered). The tumour appeared initially to respond well to PTT with a temperature rise of 37.6°C, however it became evident only in the last four days of the 30 day-study period that there was a still a tumour present (see Fig. 6-51).

Mouse type	Vol. GNR (μl)	Conc. [GNR] nM	OD (GNR)	Laser Power (W)	Beam diam. (mm)	Laser time (min)	Tumour size (mm) at Day 0	Tumour size at Day 30
Pilot	50	2.75	13.2	2.2	8	3	5.2 x 4.5	7.3 x 5.6

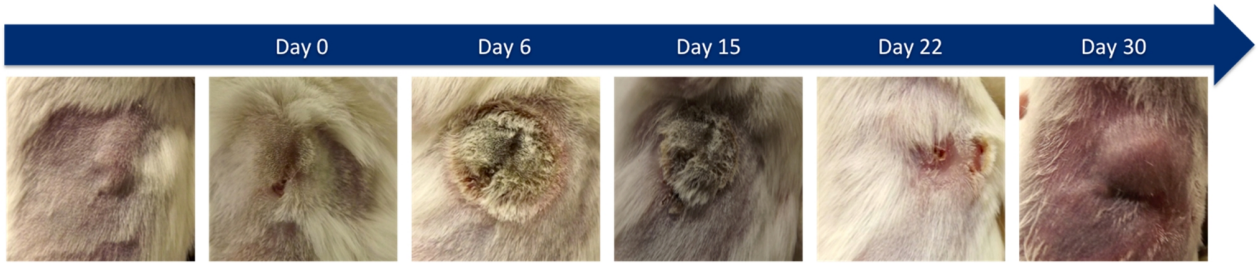


Fig. 6-51 Pilot SCID mouse receiving IT GNRs and PTT with a good initial response, until a tumour was detected at the end of the study period.

This tumour may have surreptitiously grown aggressively towards the end of the study period, as it was larger on Day 30 than the initial pre-PTT size. Histology of the irradiated tumour site with H & E staining demonstrated that even though there was regeneration of epidermis & dermis, there was still a significant tumour present with original tumour cells and some new recurrent cells (Fig. 6-52).

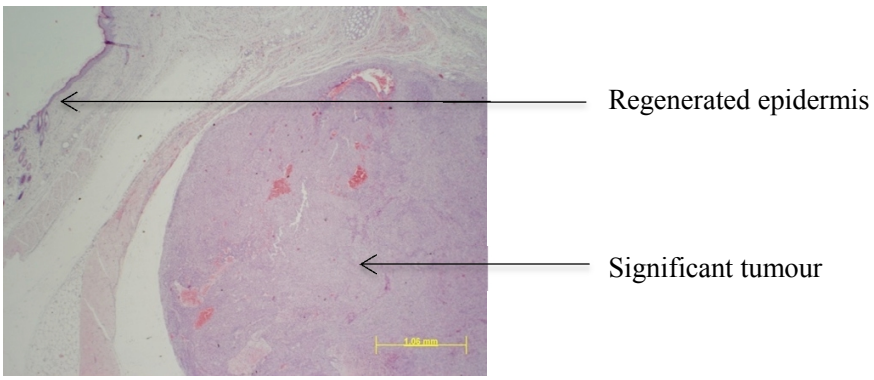


Fig. 6-52 Histology from pilot SCID mouse: Regenerated epidermis and dermis with an underlying tumour present in the submuscularis plane (20x mag., scale bar = 1 mm).

Upon closer examination of the tumour site, scarcely distributed clusters of probable GNPs were seen within the tumour matrix under light microscopy (Fig. 6-53).

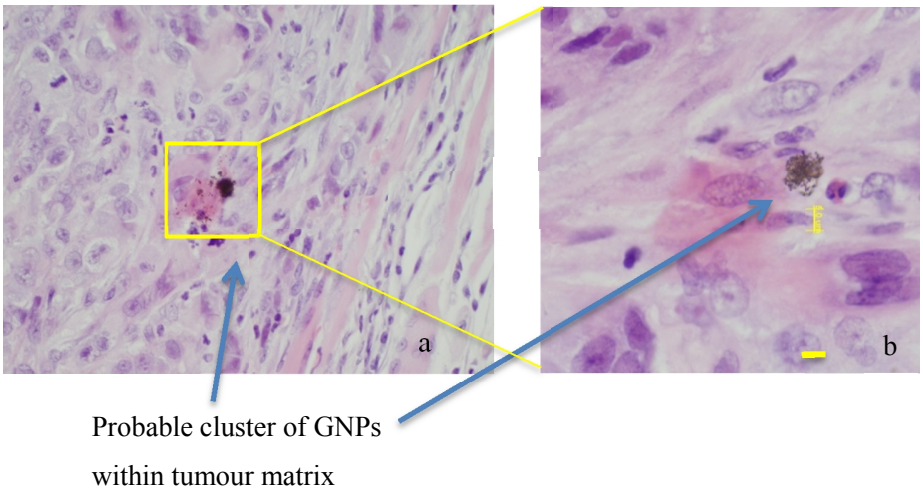


Fig. 6-53 A cluster of GNPs seen within the tumour matrix of pilot mouse [(a)400x and (b) 1000x mag.]. Scale bar = 5 μm.

There may have been inadequate administration and distribution of GNRs during the IT injection. While it is clear that some of the GNRs were injected into the tumour as the histological slides testify, having an inadequate number or uneven GNR distribution pre-irradiation may have ultimately accounted for continued tumour proliferation. It is thus worth waiting for 30 days for any latently growing tumours to become apparent and to confirm irradiation sites with histology in the circumstances where tumour ablation is seen or anticipated.

6.8 Summary of findings

- PEGylated GNRs were functionalised with a fluorophore (Cy5.5) modified with anti-EGFR antibody. The peak $OD_{\lambda = 808}$ of 26.4 was used in IV administrations *in vivo* while GNRs with an $OD_{\lambda = 808}$ of 13.2 were administered IT
- With fluorescence spectroscopy high amplitude signal peaks at approximately the same wavelength were obtained specifically over visually confirmed tumour sites in mice which had received GNRs via both IT and IV routes. These matched the fluorescence emission of the functionalised GNRs, indicating specific accumulation of GNRs in the region of cancer

- Fluorescence imaging was able to provide good contrast between healthy and cancerous regions, by detecting IV administered fluorescent GNRs accumulating at the site of tumours. This fluorescence corresponded well to the external margins of even subtle tumours, which will be useful clinically in cases of diagnostic uncertainty and to assist in optically guiding endoscopic biopsies
- The level of intensity feedback from fluorescent areas was quantifiable with line profiling across the fluorescent area
- Fluorescence imaging was able to delineate the margins of tumours, and possibly even of its less visible peripheral borders
- It is likely that the free Cy5.5-anti-EGFR-antibody component in an aqueous solution of functionalised Cy5.5-GNRs-anti-EGFR-antibody is responsible for the early fluorescence seen because of its small size and through its rapid binding to tumours which over-express the EGFR antigen
- Fluorescence feedback signals decay over time, but the tumour site was usually still well illuminated 24 hours post IV injection
- It was important to allow 24 hours for the intratumoural endocytosis of IV administered GNRs before applying PTT
- IT GNRs demonstrated a darkened area due to a quenching effect under fluorescence imaging, which was useful in ensuring the tumour area was adequately infiltrated with GNRs prior to PTT
- It was suggested that GNRs were metabolised and excreted primarily through the hepato-renal pathway
- In the experimental study, control mice subjected to GNRs or laser alone showed that these modalities were by themselves incapable of inhibiting tumour proliferation
- In the IT GNRs and PTT group, all ten mice in the study demonstrated complete tumour ablations at the end of the study, which were confirmed histologically
- In the IV GNRs and PTT group, all ten mice in the study demonstrated complete tumour ablations at the end of the study, which were confirmed histologically
- No metastatic lesions were identified at the end of study, which reinforces the strength in eliminating the primary tumour
- Mean temperature increases of 42.3 ± 9.4°C was seen from PTT in the IT GNRs group and 38 ± 9°C in the IV GNRs group. A return to baseline temperature was seen within two minutes of laser energy cessation
- All mice in the study demonstrated histological disappearance of proliferating cells, and irradiated sites showed regeneration of new epidermis through the process of neo-collagenesis

- Endocytosis of functionalised GNRs into tumour cells was confirmed by TEM analysis and EDX characterisation of Au
- A combined theranostic application of GNRs is demonstrated and shown to be feasible and effective for clinical translation using endoscopy
- Seven key principles are suggested to increase the success rates of photothermal tumour ablation.

6.9 DISCUSSION

Clinical Applications

It would be prudent to consider the clinical translation of this form of nanotechnology, given the findings presented. The theranostic set-up that we have used in the latter stages of the *in vivo* study has worked well in identifying tumours and performing image-guided PTT at the same sitting. The theranostic potential offered by functionalised GNRs can be seen to have an application in both the early and late stages of cancer. It is envisaged as a valuable adjunct to both surgery and endoscopy. One of the primary advantages of this form of therapy lies in its capacity of providing both rapid diagnosis and targeted treatment during the same endoscopic procedure, therefore application of this technology *in vivo* and in humans would best be performed either during endoscopy or minimally invasive surgery. The endoscopic and laparoscopic approaches would be similar and seamless in its application.

Early or occult cancers – Fluorescence imaging and photothermal therapy

For the diagnosis of occult or subtle (unknown) tumours, an aqueous solution of IV GNRs could be given immediately prior to commencement of endoscopy, and during the procedure, regions of interest could be explored further by switching the standard Xenon white light illumination setting to fluorescence excitation light. It is envisaged that if the fluorescent imaging aspect of this *in vivo* work is successfully translatable, the results could potentially be beneficial in avoiding early or small mucosal or submucosal cancers from being missed during endoscopy.

For the therapeutic aspect, it is possible to deliver a small fibre optic from the NIR laser through one of the endoscopic working channels or laparoscopic ports and have it positioned directly above a ROI, where can be primed for PTT. For IV delivered functionalised GNRs,

the early diagnostic potential would allow the endoscopist to mark out the margins of a potential tumour (e.g. with short-burst diathermy) while obtaining an optically-guided biopsy from its centre for histological confirmation. The specificity of targeting after 24 hours into tumour sites would enable photothermal treatment to be commenced at this time. In the event of wanting to treat solitary lesions at the same sitting, it is possible to give an IT injection of functionalised GNRs directly into the tumour site and ensure adequate coverage of GNRs at the tumour site by live fluorescence imaging before proceeding with irradiation. Should it be necessary to monitor temperature elevation, a standard thermocouple device can be guided into position.

As clinical examples, during upper GI endoscopy, the whole of the insufflated mucosal surface of the stomach could be illuminated and visualised under fluorescence light. Should there be a fluorescent area this could then be re-inspected under Xenon white light or sampled by image-guided biopsy during the fluorescence mode. During staging laparoscopy for upper GI cancers, one could potentially apply the same principles when examining the peritoneal cavity, serosal surfaces, liver and omentum for occult metastatic lesions. It should also be possible to photothermally ablate single metastatic peritoneal lesions by IT injections of functionalised GNRs.

There could also be implications for tumour treatment in clinical applications such as early GI cancers (T1-T2) that are either not amenable to or have failed attempts at endoscopic mucosal resection (EMR) or endoscopic submucosal dissection (ESD). These would be a subgroup of patients who are perhaps unfit for surgical resection who may benefit from an alternative modality of localised ablative treatment.

Advanced cancers and surgical applications – Photothermal therapy

There is a further subgroup of patients that may benefit from PTT under light sedation or a quick general anaesthetic, which are those who have advanced cancers that are deemed palliative but require localised tumour debulking. These patients could be experiencing symptoms of dysphagia from inoperable oesophageal tumour, liver capsular pain from hepatic metastasis, or bowel obstruction from colonic tumours. Some patients may present with tumour ingrowth into self-expanding bare metal stents, which can further occlude the lumen of the hollow viscus, and as such a further intervention would be required.

A further potential application is complementary to surgery, being applicable post-operatively to tumour cavities or in R1/R2 resections and even to targeted regional lymphatic

tissues in order to reduce the risk of recurrence. In R1 resections, although the tumour is cleared macroscopically, the resection margins are microscopically positive (infiltrated or inadequate margin clearance) according to the pathologist. As resection status is strongly associated with prognosis and survival, an R1 outcome could implicate additional surgery in some cancers (such as breast, GI and some skin cancers). There may be a role here in the application of combined fluorescent imaging for tumour cell labelling and/or localised PTT with GNRs at the area of concern, which could provide a less invasive, timely and effective adjuvant means achieving margin clearance. Frequently surgery is performed with curative intent, but occasionally it can become apparent intra-operatively that only a R2 (partial) resection can be performed, leaving grossly visible tumour behind. It should also be possible to attempt tumour mass debulking while the patient is being operated, during open surgery or through intracorporeal (laparoscopic) delivery of GNRs and fibre-optic laser. Providing an alternative means of treatment that is effective, cheap and rapid will ultimately represent a significant improvement in patient care, treatment and quality of life, with considerable financial implications to the NHS and health services worldwide.

References

1. Cancer Research UK. Oesophageal Cancer Incidence and Mortality. http://wwwcancerresearchukorg/health-professional/cancer-statistics/statistics-by-cancer-type/oesophageal-cancer - heading-Zero.
2. National Oesophago-Gastric Cancer Audit. http://wwwhscicgovuk/catalogue/PUB11093/clin-audi-supp-prog-oeso-gast-2013-reppdf. 2013.
3. Kilkenny C, Browne WJ, Cuthill IC, Emerson M, Altman DG. Improving Bioscience Research Reporting: The ARRIVE Guidelines for Reporting Animal Research. Plos Biol. 2010;8(6).
4. Dickerson EB, Dreaden EC, Huang X, El-Sayed IH, Chu H, Pushpanketh S, McDonald JF, El-Sayed MA. Gold nanorod assisted near-infrared plasmonic photothermal therapy (PPTT) of squamous cell carcinoma in mice. Cancer Lett. 2008;269(1):57-66.
5. Junqueira LC, Bignolas G, Brentani RR. Picrosirius staining plus polarization microscopy, a specific method for collagen detection in tissue sections. Histochem J. 1979;11(4):447-55.
6. Puchtler H, Waldrop FS, Valentine LS. Polarization microscopic studies of connective tissue stained with picro-sirius red FBA. Beitr Pathol. 1973;150(2):174-87.
7. Russell W, Burch R. The Principles of Humane Experimental Technique 1959. London UK: Methuen An on-line publication of this book is available through http://altwebjhsphedu/pubs/books/humane_exp/het-toc.
8. Workman P, Aboagye EO, Balkwill F, Balmain A, Bruder G, Chaplin DJ, Double JA, Everitt J, Farningham DAH, Glennie MJ, Kelland LR, Robinson V, Stratford IJ, Tozer GM, Watson S, Wedge SR, Eccles SA, Navaratnam V, Ryder S, Inst NCR. Guidelines for the welfare and use of animals in cancer research. Brit J Cancer. 2010;102(11):1555-77.

9. Hainfeld JF, Slatkin DN, Focella TM, Smilowitz HM. Gold nanoparticles: a new X-ray contrast agent. Brit J Radiol. 2006;79(939):248-53.
10. De Jong WH, Hagens WI, Krystek P, Burger MC, Sips AJAM, Geertsma RE. Particle size-dependent organ distribution of gold nanoparticles after intravenous administration. Biomaterials. 2008;29(12):1912-9.
11. Semmler-Behnke M, Kreyling WG, Lipka J, Fertsch S, Wenk A, Takenaka S, Schmid G, Brandau W. Biodistribution of 1.4-and 18-nm Gold Particles in Rats. Small. 2008;4(12):2108-11.
12. Chen YS, Hung YC, Liau I, Huang GS. Assessment of the In Vivo Toxicity of Gold Nanoparticles. Nanoscale Research Letters. 2009;4(8):858-64.
13. Balasubramanian SK, Jittiwat J, Manikandan J, Ong CN, Yu LE, Ong WY. Biodistribution of gold nanoparticles and gene expression changes in the liver and spleen after intravenous administration in rats. Biomaterials. 2010;31(8):2034-42.
14. von Maltzahn G, Park J-H, Agrawal A, Bandaru NK, Das SK, Sailor MJ, Bhatia SN. Computationally guided photothermal tumor therapy using long-circulating gold nanorod antennas. Cancer Res. 2009;69(9):3892-900.
15. Kuntz E, Kuntz H-D. Hepatology: principles and practice: history, morphology, biochemistry, diagnostics, clinic, therapy. 2nd ed Vol 3 Springer; Heidelberg. 2006:19-24.
16. Choi HS, Liu W, Misra P, Tanaka E, Zimmer JP, Ipe BI, Bawendi MG, Frangioni JV. Renal clearance of quantum dots. Nature Biotechnology. 2007;25(10):1165-70.
17. Guerrero S, Herance JR, Rojas S, Mena JF, Gispert JD, Acosta GA, Albericio F, Kogan MJ. Synthesis and in vivo evaluation of the biodistribution of a 18F-labeled conjugate gold-nanoparticle-peptide with potential biomedical application. Bioconjug Chem. 2012;23(3):399-408.
18. Kwon KC, Ryu JH, Lee JH, Lee EJ, Kwon IC, Kim K, Lee J. Proteinticle/Gold Core/Shell Nanoparticles for Targeted Cancer Therapy without Nanotoxicity. Advanced Materials. 2014;26(37):6436-41.
19. Kao HW, Lin YY, Chen CC, Chi KH, Tien DC, Hsia CC, Lin WJ, Chen FD, Lin MH, Wang HE. Biological characterization of cetuximab-conjugated gold nanoparticles in a tumor animal model. Nanotechnology. 2014;25(29):295102.
20. Greenberg SR. Histology - a New Method for the Histological Study of Collagen. Lab Med. 1986;17(8):474-5.
21. Huang XH, Jain PK, El-Sayed IH, El-Sayed MA. Plasmonic photothermal therapy (PPTT) using gold nanoparticles. Laser Med Sci. 2008;23(3):217-28.
22. Chatterjee DK, Diagaradjane P, Krishnan S. Nanoparticle-mediated hyperthermia in cancer therapy. Ther Deliv. 2011;2(8):1001-14.
23. Svaasand LO, Gomer CJ, Morinelli E. On the Physical Rationale of Laser Induced Hyperthermia. Lasers Med Sci. 1990;5:121-8.
24. Dickerson EB, Dreaden EC, Huang XH, El-Sayed IH, Chu HH, Pushpanketh S, McDonald JF, El-Sayed MA. Gold nanorod assisted near-infrared plasmonic photothermal therapy (PPTT) of squamous cell carcinoma in mice. Cancer Letters. 2008;269(1):57-66.

Chapter 7 Safety considerations in the application of functionalised GNRs for *in vivo* theranostics

7.1 Introduction

While is has been demonstrated that functionalised GNRs used for *in vivo* theranostics are effective, it raises the natural question of their safety. Initial publications that concentrated on the cytotoxicity of CTAB-GNRs generated a cauldron of controversy and propelled antagonists to admonish against its human application. In the last decade however the number of publications that attest to the inherent safety of *coated* GNRs in (rodent) *in vivo* studies have increased exponentially. The setting of an *in vivo* study in mice allowed us to scrutinise this aspect closely, which may, as a sole entity, be hindering the 'leap of faith' required to elevate this technology from bench to bedside.

Some of the issues that remain to be quantified from the *in vivo* studies are the safe levels of both the GNRs themselves and the power of the laser that can be applied. In the context of application of GNRs for *in vivo* therapy, it was important to determine the minimum concentration of IV GNRs required to successfully ablate tumours, and the maximum concentration that could be applied IT to tumours before thermal damage to (healthy) tissue would offset any potential benefit to be gained by tumour ablation. To this regard critical information was gained from our literature review and the pilot study, and the subsequent experimental study utilised this by refining the protocol for GNR dose and laser fluence.

Cytotoxicity of GNPs *in vitro* has been studied, and it has been demonstrated that they are safe up to 250 mM (1). However this does little to provide reassurances of the toxicity of GNPs *in vivo*, as there is a dearth of toxicity evaluation studies in animal models, which is an ideal means of evaluating toxicity on because of the complex physiological interplay between reticuloendothelial and immune systems. It would be important to know whether these gold nanoparticles can cause parenchymal structural or cellular damage to the main organs in which they tend to accumulate, especially in the RES. A quantification of the levels of Au within organs and the tumour itself would be useful to obtain, and towards this aim, a live animal model given both IV and IT GNRs would be optimal.

The principle underlying PTT is the ablation of tumours by GNRs through the conversion of SPR to thermal energy. The thermal reaction and temperatures seen are evident from the *in vivo* study described in the previous chapter. However it has not been previously quantified to what extent the potential transmission of energy through underlying tissues is, i.e. the depth of energy transfer. Although there was a constant area of thermal reaction evident on the skin of the subcutaneous tumour noted on the early stages post NIR irradiation, nothing is yet known about the state of the structures that lie beneath this area. This is important because although it appeared that the mice were unharmed by PTT, the extent of energy radiation could have subclinical effects on organs and tissues which lie adjacent to, or directly below the irradiated surface. A BALB/c mouse with a very thin skin layer would be an ideal model to study this element, as immediately underlying the subcutaneous tumour in the flank would be organs such as lung, spleen and liver. Histological analysis of these organs soon after PTT would reveal information about the effects seen from PTT. The issue of energy transfer depth needs to be determined before this technology can be tested in humans, as it is relevant to know if PTT could possibly induce a perforation of the hollow viscus in which it was applied, or, as in the case of the oesophagus, rupture the aorta which lies immediately posterior.

Parameters such as weights, behaviour and routine blood tests were also evaluated in the mice study and they add to the overall picture in assessing the suitability and safety of GNRs as a viable treatment adjunct to the surgical armamentarium.

This chapter is an extension of the *in vivo* study and is devoted to the assessment of the safety considerations in the application of GNRs and PTT *in* vivo. The main aims are to:

1. Determine what power of laser irradiation would cause harm to healthy tissues or to the animal itself
2. Determine the maximal safe dose for IT injection of GNRs for PTT, which provides the greatest temperature rises of the two routes of GNR administration
3. Determine the depth of energy transfer in ambient organs and tissues from thermal reaction caused by PTT
4. Evaluate the toxicity and biodistribution of circulating Au by inductively coupled mass spectrometry (ICP-MS) and histological assessment of the organs
5. Perform haematological and biochemical blood analysis of mice receiving GNRs and PTT after 30 days
6. Objectively provide evidence of weight changes throughout the study, and to evaluate psychosocial attributes and morbidities of mice receiving GNRs and PTT.

7.2 Determination of the maximal safe laser fluence

In performing *in vivo* experiments, boundaries of dosage were unintentionally determined from mice that were inadvertently harmed. This only happened on two occasions during the experiments, with each providing crucial information about the maximal safe radiation dose and intratumoural concentration of GNRs. The parameters of laser fluence which was applied for PTT was guided by a result from inadvertent harm caused by NIR treatment in one pilot mouse which received IT GNRs. The parameters of this mouse are listed in Table 7-1.

Mouse type	Vol. GNR (μl)	Conc. [GNR] nM	OD (GNR)	Laser Power (W)	Beam diam. (mm)	Laser time (min)	Temp. rise (°C)
Pilot	50	3.00	13.2	5.0	11	5	54

Table 7-1 Parameters of pilot mouse which received IT GNRs and PTT at a high setting.

Although this mouse did not exhibit any immediate post interventional signs of concern, it was apparent that it failed to thrive the next morning and had developed a thermal radiation burn (as shown in Fig. 7-1) measuring 1.6 x 1.8 cm. It was thus euthanised and histological examination confirmed a full thickness burn of all skin layers, including healthy tissue.

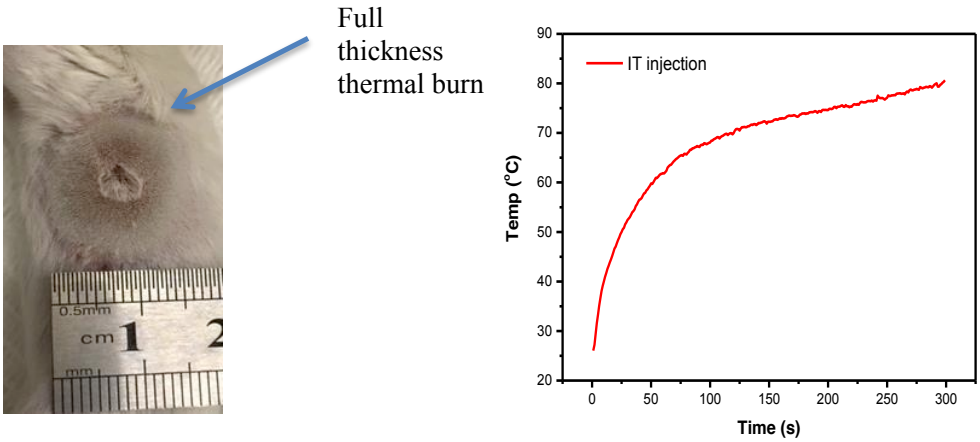


Fig. 7-1 Full thickness thermal burn in this pilot mouse with graph demonstrating the temperature rise during PTT.

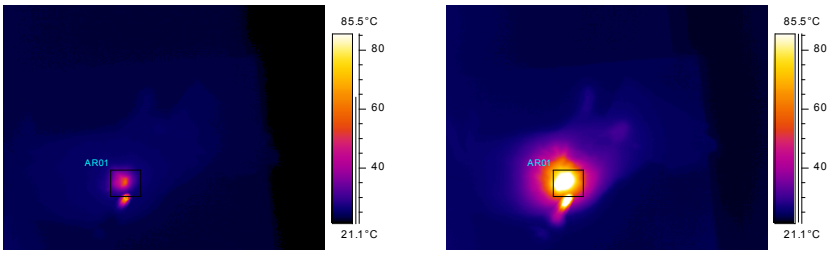


Fig. 7-2 Thermal camera images showing the heating (immediately upon the commencement of irradiation) with corresponding temperature rise showing extension into the surrounding healthy tissues (at the concluding time point).

The temperature rise of 54°C was deemed critically high and it was evident from the thermal images (Fig. 7-2) that it had radiated laterally across leading to the inevitable destruction of healthy tissues. It was subsequently decided not only to reduce the laser power but also the duration of irradiation. For the experimental study, the **maximal laser fluence** used for PTT was therefore limited to **2.6 W/ cm^2**. The **duration of irradiation** was reduced to **3 minutes**. Within these lower irradiation parameters, no mouse in the study experienced a thermal injury. The skin layer in BALB/c nude mice is extremely thin and practically transparent, and thus is comparable to the mucosal layer of the GI tract. A quantification of the vertical transmission of thermal energy through the skin is expounded in Section 7.4.

7.3 Determination of the maximal safe concentration of IT GNRs

The experimental study showed that the mean PTT temperature rise from IT-administered GNRs was higher than IV-administered GNRs. Thus a further consideration is the maximal safe dose for IT GNR administration which would not only prevent a detrimental temperature increase with PTT, but would need to be balanced against a dose that provided an appropriate photothermal effect on the tumour and be compatible with the preservation of adjacent healthy tissues. The answer to this was obtained from another pilot mouse which was given IT GNRs, and followed soon after with NIR therapy (refer to Table 7-2).

Mouse type	Vol. GNR (µl)	Conc. [GNR] nM	OD (GNR)	Laser Power (W)	Beam diam. (mm)	Laser time (s)	Temp. rise (°C)
Pilot	100	5.50	26.4	2.20	8	156	37

Table 7-2 Parameters of pilot mouse which received a high dose of IT GNRs before PTT.

During PTT in this mouse, it became apparent that a thermal burn (Fig. 7-3) was occurring and the NIR irradiation was ceased prematurely (at 156 s) and the animal was euthanised whilst under general anaesthesia. Subsequent analysis of the temperatures achieved demonstrated a 37°C rise, which was initially perplexing (Fig. 7-3). This temperature rise was compared to another animal which achieved a similar and slightly higher temperature profile but with half the OD of GNRs. It was hypothesised that this pilot mouse was given too high a volume and concentration of GNRs (**OD 26.4**, **volume 100 µl**) and this induced a concentrated burn at the core of its highest concentration (corresponding to its injection site).

From this it was learnt that mice in the experimental study would receive half the concentration of GNRs (OD of 13.2) in half the volume (50 µl), which would be distributed more evenly throughout the tumour. This would be done while maintaining the laser irradiation parameters. It can be seen from the temperature graph below that reducing the concentration and volume of GNRs administered IT did not reduce the overall temperature rise when compared to the higher dose received in the tumour of the pilot mice (OD 26.4, volume 100 µl). Instead this reduction in GNR dose made thermal absorption safer, more homogeneous in its distribution and more tolerable to the animal. This is in contrast to an IV injection, whereby administering a lower OD of GNRs resulted in a proportionately much lower temperature rise, and failure in tumour ablation, as the lower concentration of IV GNRs would lead to a significantly lower percentage of GNRs accumulating at the tumour site due to a relatively constant uptake by the RES organs. This was previously illustrated in Fig. 6-50 (see Section 6.7.6 in Chapter 6).

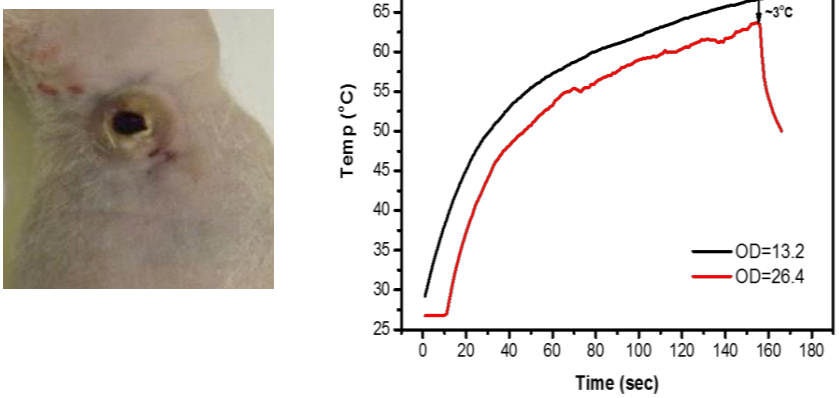


Fig. 7-3 Pilot mouse demonstrating thermal spot burn and its associated temperature rise (in red) compared to another mouse receiving half the OD and volume of GNRs.

7.4 Depth of Energy Transfer

As the outward skin changes and temperature rises were noted most significantly in irradiated tumours which received IT GNRs, it was prudent to determine the depth of transmission of energy being delivered both to healthy and underlying tissues and examine the degree of damage that may inadvertently be occurring.

Fig. 7-4 demonstrates the early post-irradiation clinical appearance of the tumour site, and it would thus be useful to assess the contemporaneous depth of energy transfer within the tissues. Day 3 post delivery of GNRs and irradiation was determined to be the optimal time to be able to quantify this histologically. Thus in one mouse which was given a routine dose of IT GNRs followed by PTT, a dissection was performed of the irradiated tumour site in the left flank, along with its underlying intercostal muscles and ribs taken *en bloc* for histological examination. Under terminal anaesthesia, a thoraco-laparotomy was performed in order to harvest the tumour site, a left hemi-hepatectomy and left pneumonectomy, as these were the organs that lay immediately underneath the irradiated site (Fig. 7-5). The dissection was done along with Professor Paul Sibbons, Northwick Park Institute for Medical Research, London, who subsequently also examined the H & E stained sections under light microscopy. The microscopic examination from these sites would provide evidence and information of the depth of energy transfer from PTT and the collateral dispersion of this energy. It would be clinically useful to ensure that the depth of energy is not unduly large or collaterally destructive, as it could cause unintentional or critical damage to the underlying structures.

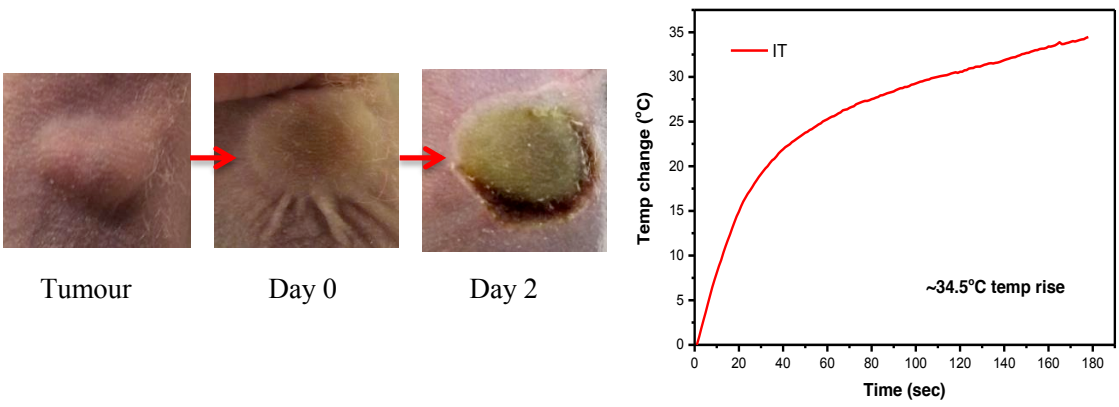


Fig. 7-4 Typical clinical appearance of the early thermal reaction seen with PTT, with the corresponding temperature rise at the site of irradiation.

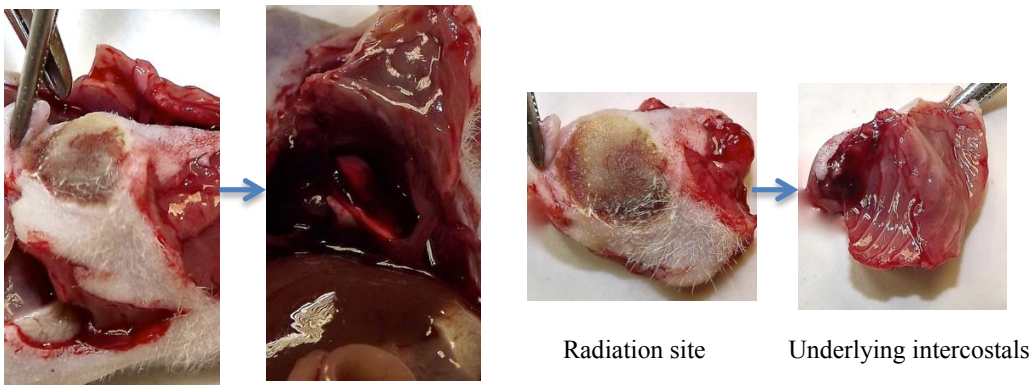


Fig. 7-5 Dissection of the irradiated site on day 2 post-PTT, exposing the underlying intercostals, left lung and left lobe of liver.

From the histological assessment in Fig. 7-8, it would appear that the bone marrow immediately underneath the line of irradiation has been depleted, but the bones (ribs) immediately adjacent to this appeared normal. This illustrates the very limited lateral thermal spread and consequently the precision of thermal effect, whereby ribs immediately adjacent to the straight line of the laser's beam were completely spared from any cortical or bone marrow destruction. The line of energy transmission extended further inside the thoraco-abdominal cavity whereby the left lobe of the liver and left lung were marginally affected (Fig. 7-6 and Fig. 7-7). Thus when measured from the surface of the skin to the average depth of thermal spread seen from histologically measured depths within the liver and lung, the total depth of energy transfer was calculated at 5.73 mm (4.13 + 1.6 mm).

Although there was histological evidence that thermal energy reached below the surface of the thin layer of the mouse's skin to the left lung and left liver lobe parenchymal surface, this would not exert a clinically significant effect on the liver due to the extremely superficial nature of thermal effect. The liver parenchyma also has the ability to regenerate and hence compensate whilst the superficial thermal effect on the lung would in the worst perceivable scenario possibly lead to a small degree of fibrosis without any appreciable effect on breathing or oxygenation. In summary, the energy transmission was noted to be collimated along a linear line of transmission from its source and did not dissipate widely laterally from this line, such that only organs/structures immediately underlying its path received some superficial and gradually diminishing thermal effect, up to a total depth of approximately 5.7 mm from the skin surface. This is likely to be a consequence of a peak concentration of GNRs within the tumour and our endeavours at keeping the laser beam focused precisely above the tumour site, which in turn minimised the potential for collateral thermal damage.

The tip of the laser's fibre was also kept close to the surface of the tumour, maintaining an average of approximately 1.5 cm above the tumour. Images from the thermal imaging camera showed that although the entire tumour was heated due to the homogeneous distribution of GNRs, the maximal temperature activity was always seen at a single spot at the epicentre of the tumour where the laser was precisely focused. This was confirmed by reducing the ROI to examine the specific heat from the centre of the tumour (high) when compared to the global heat gradient across the entire tumour volume (lower).

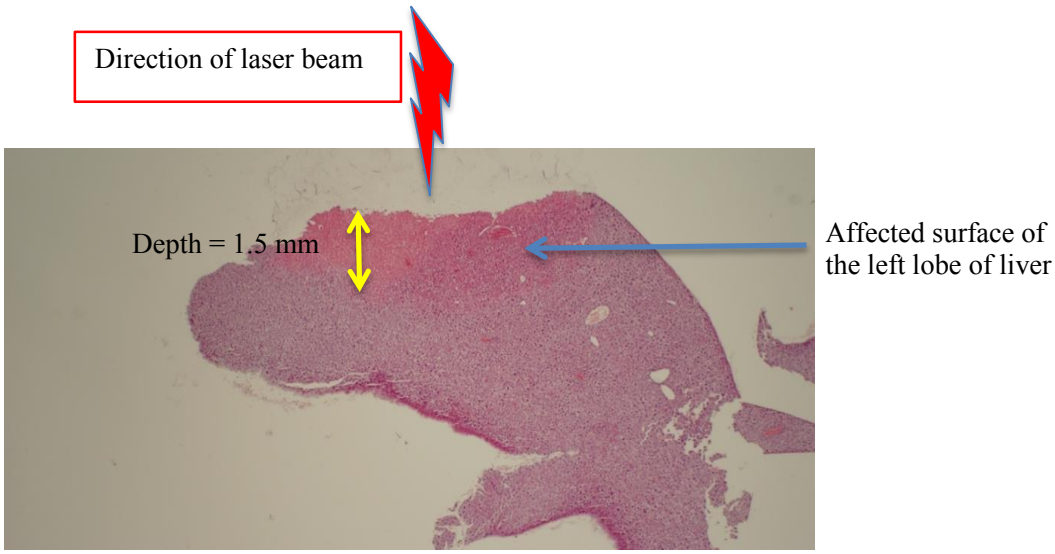


Fig. 7-6 Distance from surface of left lobe of liver affected by energy dissipation.

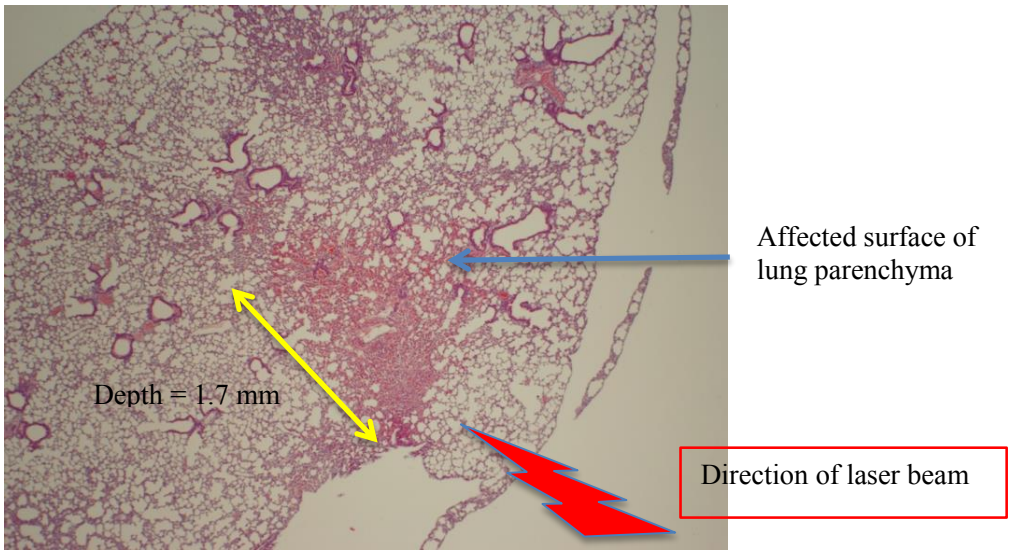


Fig. 7-7 Distance affected from the surface of the left lung by energy transmission.

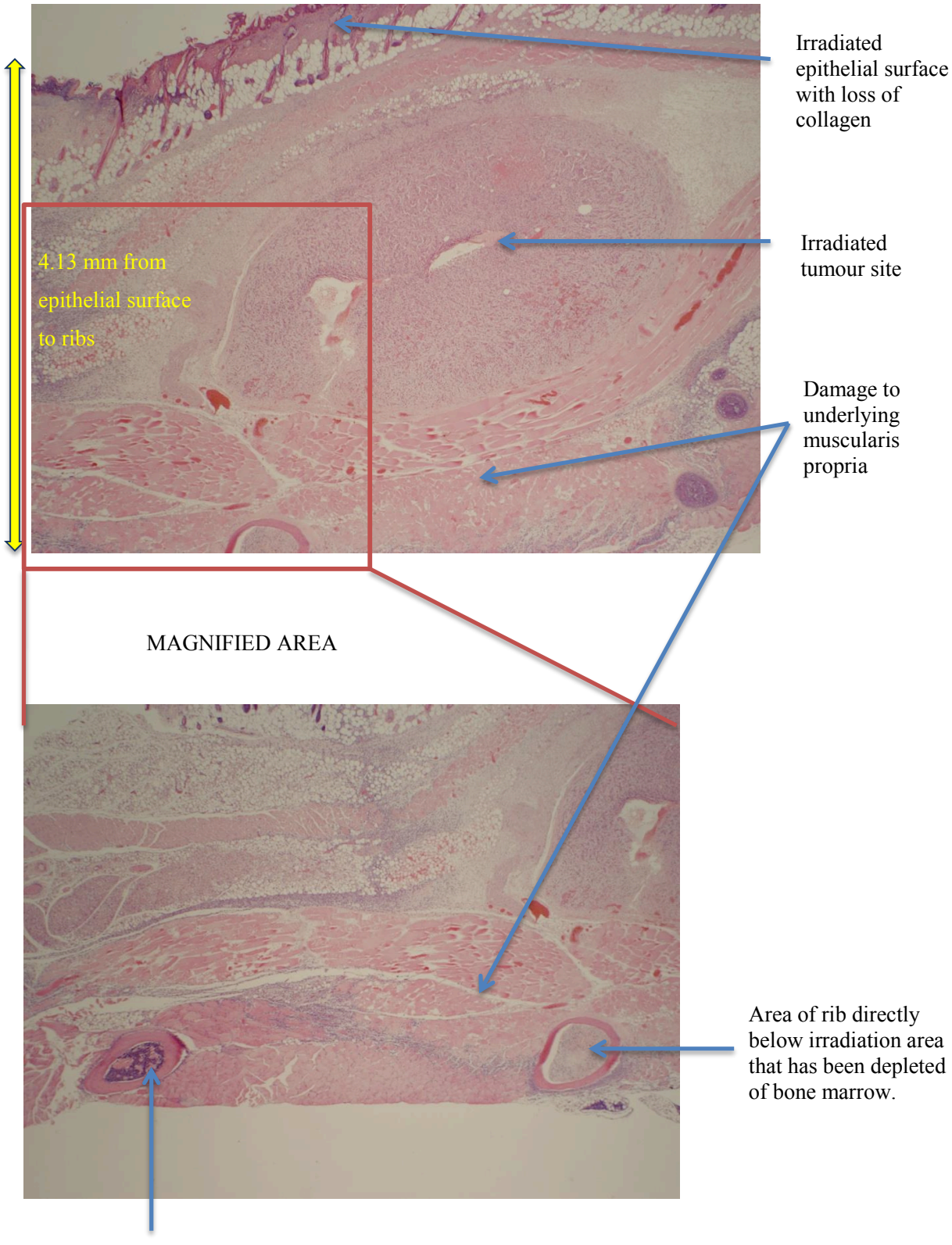


Fig. 7-8 Depth of energy transfer from PTT and its histological extension from the epidermal layer to the underlying intercostal rib directly below the tumour.

7.5 Toxicity and biodistribution of gold

7.5.1 Methods

This study was performed using inductively coupled plasma mass spectrometry (ICP-MS). The concentration of gold ([Au]) within organs was tested 30 days after injection of GNRs. The blood sample obtained was nearly the entire circulating blood volume, obtained through intracardiac venesection while under terminal anaesthesia. This blood sample was retained in a potassium-ethylenediaminetetraacetic acid (EDTA) blood bottle. Tumour sites were also resected, and organs such as liver, spleen, kidneys, lungs, heart and brain were harvested for analysis. All organs were weighed dry after washing with sterile water and drying and kept in cryovials in -80°C until ready to be processed.

The [Au] at 30 days (end of study) was contrasted with [Au] at the tumour sites and in vital organs on Day 1 (for IV injections of GNR) and Day 0 (for IT injections) to see the initial [Au] concentration values at the time of PTT and its variation at the end of 30 days. As an observation, one mouse without any tumour and which was not subjected to laser, was instead given 1.5x the standard IV volume of GNR (150 μl, OD 13.2) purely to study toxicity, biodistribution and behavioural changes/morbidity.

All sample preparation work was performed by and in the MAGIC isotope research group clean lab facilities at the Department of Materials, Imperial College London. The samples were processed and analysed by Miss Rebekah Moore, a doctoral student, in conjunction with Dr. Adam Laycock PhD from the Department of Materials. Tissue samples were placed in individual microwave digestion vessels with 7 ml of concentrated (15.4 M) HNO_3 and 3 ml of 30% H_2O_2 (Suprapur 30% H_2O_2 from Merck) and left overnight at room temperature. Blood samples were weighed into the microwave digestion vessels. Sample solutions were produced using an Ethos EZ microwave digestion system, whereby the samples were increased up to a temperature of 210°C over one hour. Once clear sample solutions were obtained, they were evaporated to dryness before dissolving in 5% aqua regia. Samples were analysed for the gold concentration using an Agilent 7700x ICP-MS at The Natural History Museum, London. The 15.4 M HNO_3 and 12 M HCl used in the aqua regia were purified in-house using sub-boiling distillation with quartz stills.

7.5.2 ICP-MS Results

The average concentration of Au [Au] obtained from various mice organs and blood at the end of study (day 30) was measured and contrasted with values obtained from mice receiving only GNRs at Day 0 (akin to control mice). Day 0 values correspond to post-GNR-administration values and were included to give a representation of what the [Au] was at the point at which PTT would be instituted, however irradiation was withheld but instead the organs, blood and tumour sites were harvested. The tumour sites harvested had similarly not been exposed to radiation, and the [Au] was measured at days 0 and 17, which was the end point due to gradual increase in the size of tumour without PTT. The exact values are represented in Table 7-3 and the results are illustrated in Fig. 7-9. As the values were extremely small, the [Au] in the samples were shown in logarithmic scale on the graph for clarity.

Tissues	Average [Au] IV (μg/g)	Average [Au] IT (μg/g)
Liver	28.11 (0.791)	0.786 (0.078)
Spleen	59.423 (6.841)	1.073 (0.845)
Kidneys	0.801 (1.132)	0.025 (0.105)
Lungs	0.477	0.011
Heart	0.491	0.007
Brain	0.015	0.001
Tumour	2.609 (3.205)	10.083 (103.863)
Blood	0.015 (20.573)	0.004 (0.297)

Table 7-3 The average values of the concentration of Au ([Au]) found in tissues/blood at the end of study (given in μg of Au detected per gram of organ). Values in brackets correspond to the [Au] at Day 0.

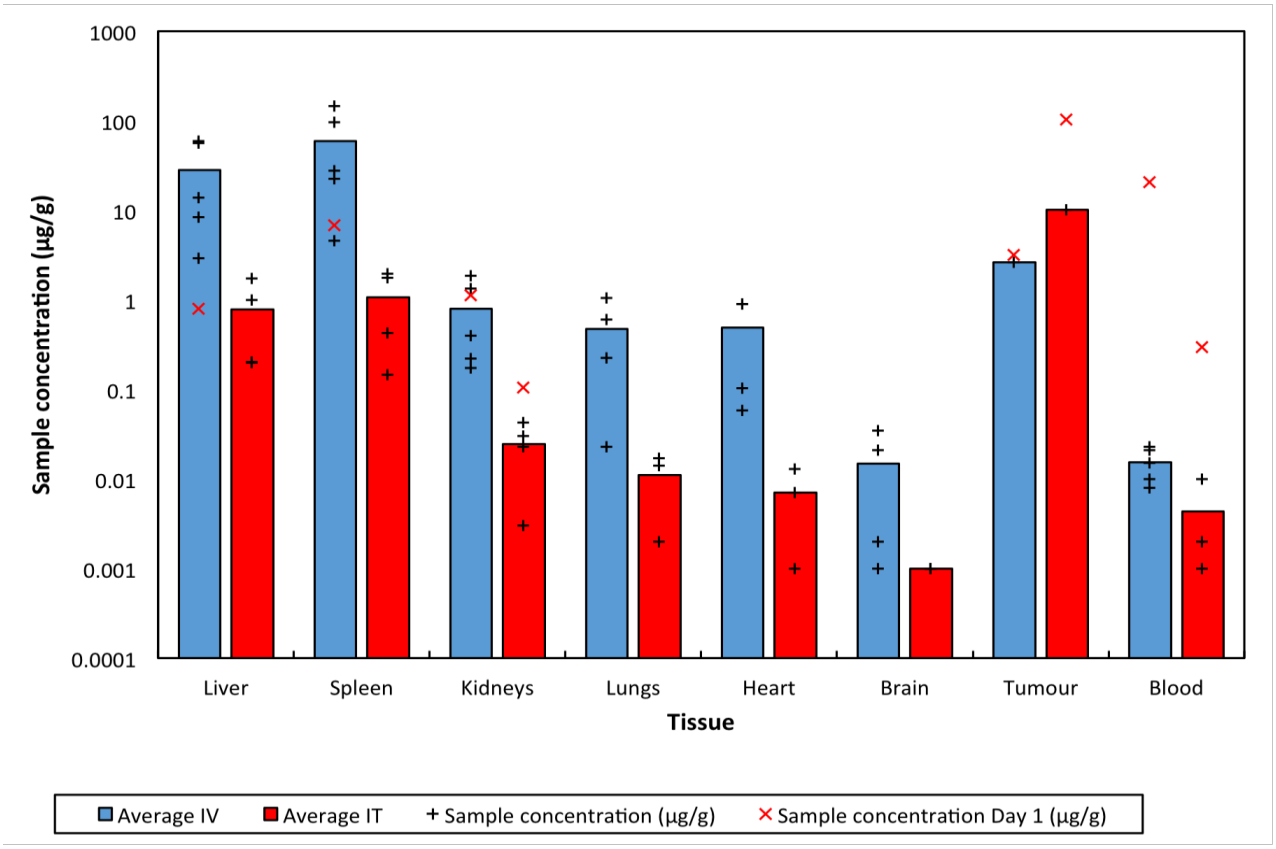


Fig. 7-9 The average [Au] in tissues/blood at the end of study. X's correspond to [Au] at Day 0/1.

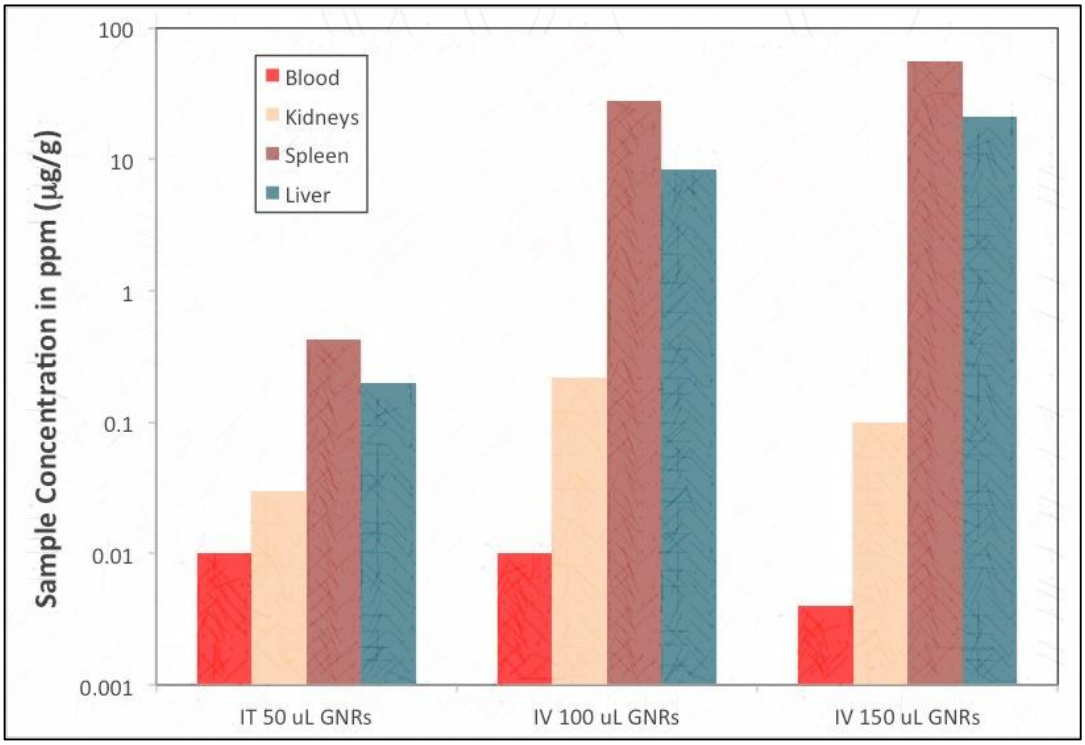


Fig. 7-10 Proportionate increase in [Au] seen in the RES organs of three mice receiving varying volumes of GNRs.

7.5.3 Discussion

Apart from tumour sites, it can readily be observed from Table 7-3 and Fig. 7-9 that intravenously administered GNRs result in a higher accumulation of Au in all studied organs when compared to IT delivery. This is likely to reflect the proportionately more volume and OD given via IV route, providing 100 µl of GNRs at an OD of 26.4 systemically while IT administrations contained 50 µl at an OD of 13.2 locally. This proportional increase in [Au] and distribution to the liver and spleen was similarly seen when exceptionally, 150 µl GNRs was given IV (Fig. 7-10). It would seem that considerably more GNRs are absorbed by the liver and spleen when administered systemically than when delivered locally to the tumour site. Organs such as the brain, lungs, heart and kidneys showed an extremely low and virtually negligible Au accumulation in comparison to a proportionally higher accumulation in the RES organs.

In line with other published studies, the results from ICP-MS from this study further confirm that administered GNRs do not induce undue accumulation of Au within the blood stream or kidneys as the values of Au remain consistently low as shown in Fig. 7-9 and Fig. 7-10. This is demonstrated to be true even when increasing the volumes and concentration of administered GNRs. Even in the mouse that received the highest IV dose of GNRs (150 µl, which is 1.5x more than the IV dose and 3x the IT dose), there was virtually no detectable Au present in blood or kidneys after 15 days (Fig. 7-10). It is clear that RES organs show Au dose-dependant results on ICP-MS where livers and spleens absorb proportionately larger quantities of Au when higher volumes of GNRs were administered. In mice that received IV GNRs, it would appear that the majority of the remaining circulating Au would be metabolised by the organs of the reticuloendothelial system, chiefly the spleen and liver. It is known that the spleen and liver are primary organs of GNP biodistribution and metabolism (2-12), and the main hub of phagocytotic activity. Fig. 7-9 suggests there is a gradual accumulation of Au particles within the liver and spleen from the day of administration to the end of study, which is counterpoised by the gradual ebb from blood and tumour sites. The higher [Au] seen in the spleen may also be partly due to the relatively smaller size of the spleen in comparison to the liver, thus accounting for more Au per gram of organ.

The data of [Au] within tumours provided conclusive evidence that the functionalised GNRs were in fact arriving at tumour sites from systemic administration, as evidenced by ICP-MS.

This proved the value in fabricating multi-functionalised GNRs as they were reaching their target destination through a combination of active and passive processes. A comparable percentage of the injected Au was seen within tumours as quoted in previous publications [<5% (13) and 0.16-1.22% of injected doses (14)]. Concordance with Maeda & Matsumura's EPR theory (15, 16) was demonstrated here in that systemically-administered GNRs do accumulate at the site of tumour from leaky tumour vasculature resulting from fenestrations within vascular endothelial walls large enough to permit GNRs to passively accumulate at the tumour site. The [Au] at the tumour sites also prove that GNRs are retained within the tumour matrix due to the poor lymphatic drainage around the site of tumour, resulting in a similar [Au] found at both the start and end of the study in the IV group. However there was considerable clearance of GNRs from the IT-injected tumour site, with a 10-fold decrease in [Au] at the end of study compared to the day of delivery. This is compatible to macrophagic activity seen under 1000x magnification under light microscopy [see Fig 6-39(b), in Section 6.6 of Chapter 6]. This would result from the fact that despite the intention, most of the injected GNRs would not be directly absorbed by tumour cells; a vast majority would be lying freely within the interstitium and extracellular matrix, and as such a phagocytic reaction to 'foreign material' by macrophages would ensue, clearing up GNP 'debris' lying dormant within the epithelial layers. Without the application of PTT, at the end of the study there were approximately 4 times more GNRs persisting in IT-administered tumour sites compared to IV delivery.

There was a proportionately larger [Au] in tumours found on Day 0 in mice receiving IT GNRs (30-fold higher) than mice receiving IV GNRs (103.8 vs. 3.2 μg/g). However, as it can be seen in Fig. 6-30, the temperature rise during PTT (Day 0) following IT GNRs was on average only 4.3 ± 9°C higher than IV GNRs. This temperature rise in IT GNRs could perhaps be limited because the absorption from GNRs within the tumour is sufficiently high to convert all NIR light into heat within the tumour, therefore there is no incremental benefit to be gained by increasing the concentration of GNRs. It is known that much higher temperatures can be achieved with more concentrated GNRs especially when administered IT and with higher laser fluences (refer to Sections 7.2 and 7.3), but this would be detrimental to the mouse, as such it was endeavoured to maintain temperature rises within a certain photothermal therapy range. In our experiments this was performed by halving the concentration, OD and volume of GNRs delivered IT in comparison to the IV dose.

Clearance of Au from the bloodstream after 30 days is important in ensuring there are no long-term effects from systemic reservoirs of GNPs which may aggregate/coalesce or

precipitate to propagate as emboli. The values show a barely detectable quantity of Au within the circulation from both methods of administration at the end of the study (30 days), and it is worth being cognisant that virtually the entire blood volume was sampled and analysed through mass spectrometry by means of (terminal) intracardiac venesection.

7.6 Histological evaluation of RES organs exposed to GNRs and PTT

In view of the higher [Au] in the liver and spleen compared to other organs, RES organs were examined at Day 30 post GNR and PTT to establish the actual degree of hepatocyte, splenocyte and renal cell damage that may be appreciated microscopically from the accumulation of Au. The histology of the organs shown in Fig. 7-11 and Fig. 7-12 is representative of the changes visualised from both IT and IV GNRs 30 days after PTT.

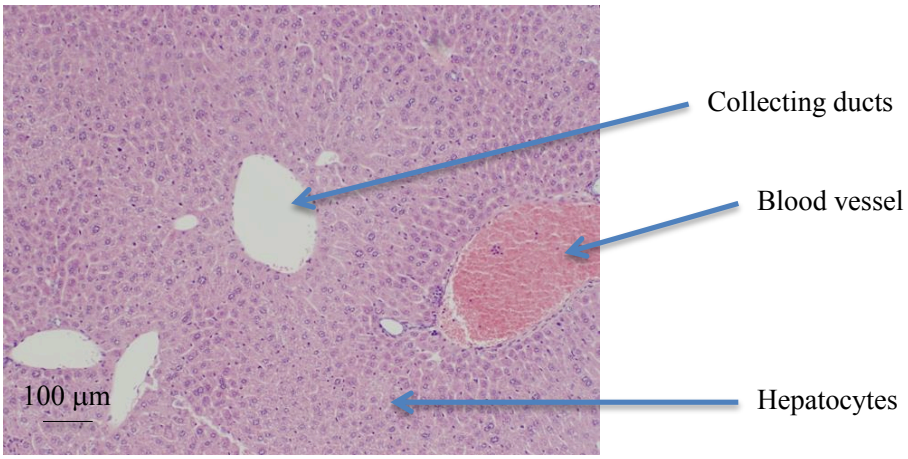


Fig. 7-11 Histology from the liver 30 days post GNRs and PTT demonstrating no hepatocellular damage (100x mag.).

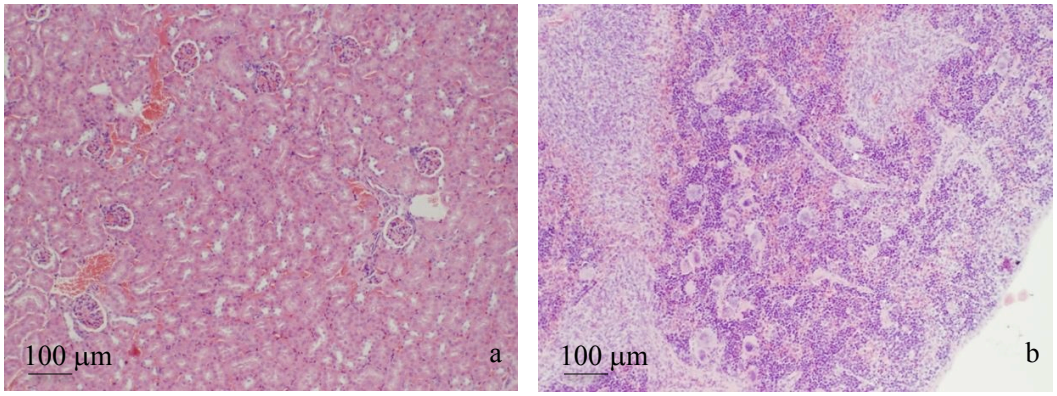


Fig. 7-12 Histology from the (a) kidneys and (b) spleen 30 days post GNRs and PTT showing no damage to renal cells (100x mag.), a morphologically active spleen but no splenocyte damage (100x mag.).

The histology from the liver, spleen and kidneys of mice examined at the end of the 30 day study period demonstrated that there was no structural damage to these organs, despite there being clear accumulation of Au within the parenchyma of the organs identified on ICP-MS which persisted through to the end of the study. The spleen has been identified through ICP-MS as the organ that retains the most Au. Although morphologically active sites were demonstrated histologically within the splenic parenchyma, there was no indication that there was any long-lasting splenocyte damage. Combined with the fact that there was no physiological or psychological insult to the mice during the study period, this provides further evidence that GNPs should be considered safe and biocompatible *in vivo* and the measurable Au which persists in organs after 30 days really is minute and clinically inconsequential. This would concur with other *in vivo* studies of PEGylated GNPs (17).

An *in vivo* study by Zhang *et al*. (18) examined toxicity of 13.5 nm GNPs in mice whereby animal survival, weights of organs and animals, haematological and morphology of GNPs in blood and bone marrow cells were determined at varying concentrations of GNPs administered via different routes (oral, intraperitoneal and intravenous) over 14-28 days. The authors concluded that injecting gold nanoparticles via the tail vein (IV) demonstrated the least toxicity over more adverse outcomes observed with oral and intraperitoneal routes of GNP administration. This would augur well with our two chosen methods of safe *in vivo* GNP delivery – intravenous (IV) and intratumoural (IT).

7.7 Haematological & biochemical analysis

Blood tests were carried out on mice receiving PTT with both IV and IT routes of administration to evaluate any haematological or biochemical changes occurring as a result of GNRs or PTT. We were only able to perform these tests at the end of study (after 30 days post-treatment) as the analysis required a volume of blood which was only attainable through cardiac venesection. This was thus performed three minutes after terminal general anaesthesia (comprising intraperitoneal ketamine and xylazine). The main aims were to evaluate if there was any functional and intrinsic damage occurring primarily to the kidneys or liver. Blood from three mice in each group were evaluated, and the averaged results are tabulated (Table 7-4 and Table 7-5).

Haematology test	Results	Comment
Haemoglobin	14.8 g/dL	Normal
White Blood Cells (WBC)	6.73 x 10^3 µl	Normal
Red Blood Cells	9.94 x 10^6 µl	Normal
Haematocrit	0.469 l	Normal
Platelets	1009 x 10^3 µl	Normal
WBC Differential	Normal	Normal

Biochemistry test	Results	Comment
Urea	6.8 mg/dl	Normal
Creatinine	38 mg/dl	Normal
AST	215 IU/l	Normal
ALT	68 IU/l	Normal
ALP	60 IU/l	Normal

Table 7-4 The average blood results in the IV GNRs + PTT group (after 30 days).

Haematology test	Results	Comment
Haemoglobin	14.6 g/dL	Normal
White Blood Cells (WBC)	7.11 x 10^3 µl	Normal
Red Blood Cells	10.12 x 10^6 µl	Normal
Haematocrit	0.462 l	Normal
Platelets	1043 x 10^3 µl	Normal
WBC Differential	Normal	Normal

Biochemistry test	Results	Comment
Urea	5.8 mg/dl	Normal
Creatinine	37 mg/dl	Normal
AST	110 IU/l	Normal
ALT	46 IU/l	Normal
ALP	69 IU/l	Normal

Table 7-5 The average blood results in the IT GNRs + PTT group (after 30 days).

PTT with GNRs did not incur any deviation of blood biochemistry values. It can therefore be inferred that the intrinsic function of the liver and kidney is preserved. There was also no haematological abnormality noted as a consequence of the nanorods themselves or the therapeutic intervention. These results, when seen together with the histological samples from organs, provide further objective evidence of the innocuous nature of GNRs and PTT.

7.8 Physical and psychosocial attributes of treated animals

The mice were weighed at the start of tumour induction and weekly thereafter until the end of study. These weight changes can be seen from the values in Table 7-6 and are represented in Fig. 7-13. The median weight gain in the IT group was 3 g while it was 4.5 g in the IV group. More importantly, no mouse in either treatment arm lost weight from the period of inoculation to the end of study. No mouse demonstrated muscle atrophy or emaciation, and no animal experienced anorexia (loss of appetite) or appeared dehydrated at any point during the study.

	IT GNRs + PTT	IV GNRs + PTT
Min (g)	1	1
Q1 (g)	1.25	3
Median (g)	3	4.5
Q3 (g)	4	5
Max (g)	6	6

Table 7-6 The minimum, median, maximal and 1st and 3rd quartiles of weight gained by mice in each treatment arm of the study. All measurements are in gram.

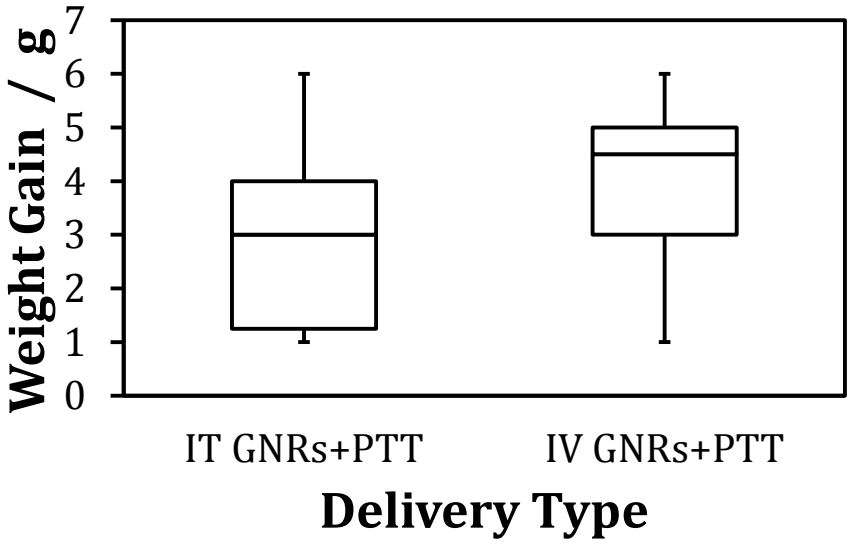


Fig. 7-13 Box and whisker diagram of weight distribution of the mice, demonstrating an increase in both groups with the medians, quartiles and minimum and maximum weight gains.

Survivability of the animals was key to ensuring GNR and irradiation therapy would not be grossly harmful, nor would the effects from having a large tumour burden or metastasis. In our study no systemic side effects or morbidity were observed during the study period and there was no unexpected mortality. Control mice with GNRs and laser alone did not suffer from any ill effects, even when 1.5x the usual IV dose of GNRs was administered to a control mouse without any tumour. As control mice were terminated within 30 days (or when the tumour size was > 12 mm) and there was no mortality, it is not possible to comment on long-term survivability of the treated mice in comparison to controls, as this was not designed to be a longitudinal study.

Mice were routinely observed at least once daily, but on the day of PTT and on day 1 post PTT, each animal was monitored closely and observed at least four times. Once awake from general anaesthesia, it was apparent that the animals did not experience undue pain as a consequence of PTT, such that no animal appeared to require analgesia before, during or after PTT. The sites of tumour inoculation and of PTT were consistently dry and no radiation site infections were noted and no prophylactic or treatment antibiotics were required.

All animals were monitored assiduously for changes in physical appearance, behaviour and social interaction. There was no observable change in the physical or psychosocial attributes of mice receiving GNRs alone or PTT, even when administered at the higher (1.5x or 2x the normal) IV dose. These findings are consistent with other reported *in vivo* studies, which agree that there is no pain, suffering, distress or lasting harm to be derived from clinically relevant doses of *in vivo* GNP administration or irradiation (17, 19-21).

7.9 Summary of findings

- The parameters for safe and effective laser fluence and maximal GNR concentrations used for *in vivo* PTT were learnt and adapted from initial pilot studies
- It became apparent from pilot studies that half the concentration and volume of GNRs was better tolerated by mice and could produce similarly effective heat profiles for IT administrations
- Energy transmission appeared to propagate in a relatively collimated manner to the tumour surface. This was likely to be due to the maximal GNR concentration within the tumour itself and the laser beam focused proximately and directly over the tumour, which minimised lateral energy dissipation. The depth of energy transfer was

approximately 5.7 mm from the surface, with a gradual attenuation in the thermal effect

- Underlying structures did not appear to be unduly traumatised by this propagation
- Biodistribution studies revealed that the volume of GNRs administered is proportionate to [Au] found within the RES organs
- Blood clearance of GNRs was notably prominent, and systemic GNRs were predominantly metabolised by the liver and spleen, and excreted by the kidneys. Other organs showed negligible quantities of Au
- Evidence of the permeation and retention of GNRs at tumour sites was demonstrated
- Histological evaluation of the liver, spleen and kidneys showed no evidence of structural, parenchymal or cellular damage, despite showing the highest [Au] on mass spectrometry
- Haematological and biochemical parameters within the blood did not demonstrate any deviation from normal values, and demonstrated preservation of intrinsic kidney and liver function
- No weight loss, anorexia, pain, morbidity or change in physical or psychosocial attributes were seen in mice throughout the duration of the study.

7.10 Discussion

The findings from our *in vivo* study are highly suggestive that the initial concern of cytotoxicity and biocompatibility of GNPs has been addressed by the addition of PEG coating, at least in this short-term *in vivo* study. Recent studies which have incorporated some form of 'stealth' coating onto CTAB-GNPs have also not shown any *in vitro* or *in vivo* cytotoxicity, immunogenic response or mortality, even when administered to immunodeficient or transgenic mice. Although there was a small quantity of Au that persists within the liver and spleen after both IV and IT administration, it is perhaps the safest refuge for them as they do not linger within the blood stream to propagate as emboli from their aggregation. It has been shown that the liver, spleen and kidneys are not structurally or functionally affected by the presence of Au within their parenchyma. The hepatorenal metabolic pathway is the most likely route of GNR elimination. Although it is beyond the capacity of this study to conclude, it is likely that the infinitesimal quantities of GNPs remaining within these organs would continue to be innocuous with the passage of time.

Multi-functionalised GNRs do seem to be more affective at tumour targeting than relying solely on the physiological principles underlying the EPR effect of GNR accumulation. The quantity of Au identified within tumour tissue from systemic administration of GNRs is a strong testament to this, as it has been effective for photothermal therapy. There was a comparable percentage of GNRs arriving at the tumour site from the IV-injected dose as with other published studies.

Having previously demonstrated the photothermal effect on porcine and human *ex vivo* tissues, it was important to establish the effects of applying PTT onto live tissue, and the adaptations that could be made to enhance its safety and efficiency. Towards this aim, an extensive literature review and the *in vivo* pilot studies were crucial in understanding the right combinations of GNR concentrations and laser power that are applicable *in vivo*. This led to refinements in the doses used in the study for both control and PTT groups, in particular to avoid collateral damage to healthy tissues during PTT. Furthermore it was imperative to resolve the spread of energy from this technology, in due consideration of its adoption as a viable application in humans. The relatively vertical spread of energy from the surface, with most of the heating effect observed within the tumour, resulted in only a slight collateral extension of the energy. This is not expected to have any clinical bearing on humans.

The translational potential of GNRs would inevitably also be dependant on the results from blood tests, along with the fundamental physical and psychosocial aspects that were studied. With this regard, having provided a blemish-free safety profile of all the individual components, it strongly suggests that when viewed as a whole, the application of GNRs as a theranostic tool is both safe and effective for cancer detection and therapy.

References

1. Connor EE, Mwamuka J, Gole A, Murphy CJ, Wyatt MD. Gold nanoparticles are taken up by human cells but do not cause acute cytotoxicity. Small. 2005;1(3):325-7.
2. De Jong WH, Hagens WI, Krystek P, Burger MC, Sips AJ, Geertsma RE. Particle size-dependent organ distribution of gold nanoparticles after intravenous administration. Biomaterials. 2008;29(12):1912-9.
3. Sonavane G, Tomoda K, Makino K. Biodistribution of colloidal gold nanoparticles after intravenous administration: effect of particle size. Colloids Surf B Biointerfaces. 2008;66(2):274-80.
4. Kim JH, Kim JH, Kim KW, Kim MH, Yu YS. Intravenously administered gold nanoparticles pass through the blood-retinal barrier depending on the particle size, and induce no retinal toxicity. Nanotechnology. 2009;20(50):505101.

5. Chen YS, Hung YC, Liau I, Huang GS. Assessment of the In Vivo Toxicity of Gold Nanoparticles. Nanoscale Res Lett. 2009;4(8):858-64.
6. Cho WS, Kim S, Han BS, Son WC, Jeong J. Comparison of gene expression profiles in mice liver following intravenous injection of 4 and 100 nm-sized PEG-coated gold nanoparticles. Toxicol Lett. 2009;191(1):96-102.
7. Semmler-Behnke M, Kreyling WG, Lipka J, Fertsch S, Wenk A, Takenaka S, Schmid G, Brandau W. Biodistribution of 1.4- and 18-nm gold particles in rats. Small. 2008;4(12):2108-11.
8. Cho WS, Cho M, Jeong J, Choi M, Cho HY, Han BS, Kim SH, Kim HO, Lim YT, Chung BH, Jeong J. Acute toxicity and pharmacokinetics of 13 nm-sized PEG-coated gold nanoparticles. Toxicol Appl Pharmacol. 2009;236(1):16-24.
9. Balasubramanian SK, Jittiwat J, Manikandan J, Ong CN, Yu LE, Ong WY. Biodistribution of gold nanoparticles and gene expression changes in the liver and spleen after intravenous administration in rats. Biomaterials. 2010;31(8):2034-42.
10. Balogh L, Nigavekar SS, Nair BM, Lesniak W, Zhang C, Sung LY, Kariapper MS, El-Jawahri A, Llanes M, Bolton B, Mamou F, Tan W, Hutson A, Minc L, Khan MK. Significant effect of size on the in vivo biodistribution of gold composite nanodevices in mouse tumor models. Nanomedicine. 2007;3(4):281-96.
11. Zhang G, Yang Z, Lu W, Zhang R, Huang Q, Tian M, Li L, Liang D, Li C. Influence of anchoring ligands and particle size on the colloidal stability and in vivo biodistribution of polyethylene glycol-coated gold nanoparticles in tumor-xenografted mice. Biomaterials. 2009;30(10):1928-36.
12. Lipka J, Semmler-Behnke M, Sperling RA, Wenk A, Takenaka S, Schleh C, Kissel T, Parak WJ, Kreyling WG. Biodistribution of PEG-modified gold nanoparticles following intratracheal instillation and intravenous injection. Biomaterials. 2010;31(25):6574-81.
13. Schwartz JA, Price RE, Gill-Sharp KL, Sang KL, Khorchani J, Goodwin BS, Payne JD. Selective nanoparticle-directed ablation of the canine prostate. Lasers Surg Med. 2011;43(3):213-20.
14. Gormley AJ, Malugin A, Ray A, Robinson R, Ghandehari H. Biological evaluation of RGDfK-gold nanorod conjugates for prostate cancer treatment. J Drug Target. 2011;19(10):915-24.
15. Maeda H. Tumor-selective delivery of macromolecular drugs via the EPR effect: background and future prospects. Bioconjug Chem. 2010;21(5):797-802.
16. Matsumura Y, Maeda H. A new concept for macromolecular therapeutics in cancer chemotherapy: mechanism of tumoritropic accumulation of proteins and the antitumor agent smancs. Cancer Res. 1986;46(12 Pt 1):6387-92.
17. Liu XS, Huang N, Li H, Wang HB, Jin Q, Ji J. Multidentate Polyethylene Glycol Modified Gold Nanorods for in Vivo Near-Infrared Photothermal Cancer Therapy. Acs Appl Mater Inter. 2014;6(8):5657-68.
18. Zhang XD, Wu HY, Wu D, Wang YY, Chang JH, Zhai ZB, Meng AM, Liu PX, Zhang LA, Fan FY. Toxicologic effects of gold nanoparticles in vivo by different administration routes. Int J Nanomed. 2010;5:771-81.
19. Cheng L, He WW, Gong H, Wang C, Chen Q, Cheng ZP, Liu Z. PEGylated Micelle Nanoparticles Encapsulating a Non-Fluorescent Near-Infrared Organic Dye as a Safe and Highly-Effective Photothermal Agent for In Vivo Cancer Therapy. Adv Funct Mater. 2013;23(47):5893-902.
20. Cheng L, Yang K, Chen Q, Liu Z. Organic Stealth Nanoparticles for Highly Effective in Vivo Near-Infrared Photothermal Therapy of Cancer. Acs Nano. 2012;6(6):5605-13.
21. Thakor AS, Luong R, Paulmurugan R, Lin FI, Kempen P, Zavaleta C, Chu P, Massoud TF, Sinclair R, Gambhir SS. The Fate and Toxicity of Raman-Active Silica-Gold Nanoparticles in Mice. Sci Transl Med. 2011;3(79).

Chapter 8 Summary, future work and conclusion

From the outset, this work crossed the threshold of becoming a truly multidisciplinary team project with the chemistry involved in the fabrication of functionalised GNRs, the physics involved with the application of fluorescence imaging and NIR laser energy to coincide with the surface plasmon resonance of GNRs, the molecular biology involved with immunohistochemistry and electron microscopy, the animal science and tumour biology aspects, geochemical analysis using mass spectrometry, combined with a foray into the clinical aspects of medicine which constantly strived to ensure that the theranostic aspect of the project's aims, methods and findings would be able to develop a technology that would ultimately be beneficial and translatable to humans. It also involved collecting and analysing a variety of samples ranging from aqueous samples of GNRs to *ex vivo* human tissues, *in vitro* cancer cells, and finally *in vivo* mice tissues.

GNRs have attracted much interest in biomedical application due to their ability to be synthesised in bulk, high optical absorption in the NIR and their ability to be functionalised to target peptides and receptors which are over-expressed on the surface of malignant cells. Their size and functionality permits the application of nanoparticles for surgical imaging and targeted therapy.

Current hyperthermic techniques such as radiofrequency ablation, microwave therapy and hyperthermic intraperitoneal perfusion for inducing heat within tumours are rather limited in their applicability to selectively deliver heat towards cancer tissues (1), in many cases causing damage to healthy surrounding tissues, as well as significant discomfort. Furthermore, commercially available instruments for these conventional hyperthermic treatment options are often limited to shallow depth penetration (less than 3 cm) (1). Precise treatment can be achieved through focused (fibre-optic) delivery of incident radiation (2, 3). The clinical practicality of NIR light resides in its minimal attenuation by water, haemoglobin and endogenous chromophores, such that it can penetrate soft tissues at depths up to 10 cm (4). It has also been shown that blood flow to tumour is essentially obliterated three hours after NIR therapy (5). Our NIR light delivery system involves a small, cheap and portable dental CW diode laser.

The functionalised PEG-GNR-Cy5.5-anti-EGFR-antibody complex appears to offer great potential in conjunction with NIR irradiation at ablating human oesophageal adenocarcinoma tumours *in vivo*. Within the tumour sizes in this study, therapy seemed to be effective with

just a single application of GNRs and a short irradiation period with relatively low energy. Although anti-EGFR antibody was used as a targeting agent on the surface of GNRs in our *in vivo* model, it is perfectly feasible to substitute this with another peptide/ligand for application in other cancers. The heterogeneity of expression of molecular markers make the specificity of targeting challenging, which is one reason for opting for the more generically abundant over-expression of EGF receptors, which can be then applied in a variety of other similar antigen expressing tumours.

The GNRs and carefully researched irradiation regime was well tolerated by mice and there was no unexpected mortality due to either component. This is possibly due to the process of PEGylation which has made GNPs biocompatible. The quantity of Au identified within tumour tissue from systemic administration of GNRs is a strong testament to the use of multifunctionalised GNRs, which have been effective in targeted photothermal therapy. Toxicity studies have shown exceedingly low concentrations of Au, particularly in organs associated with their metabolism and excretion. The rapid excretion of Au resulted in a virtually negligible circulating concentration of Au at the end of the study, and when examined histologically, did not result in any lasting effect on major organs.

The aims of this work as listed at the beginning were:

1. The assessment of the viability of applying photothermal therapy in human (*ex vivo*) adenocarcinoma tissues
2. Determine its efficiency in rodent (*in vivo*) cancer
3. Develop the application of fluorescence imaging for cancer detection *in vivo*

In Chapter 3, *in vitro* assessments of GNR showed them to change shape due to heat generated by CW irradiation. They also experienced a blue shift and a diminution in their absorption spectral peaks thus rendering any subsequent CW irradiation at the identical previous wavelength largely ineffective. Aggregation was also shown as an additional phenomenon post-irradiation *ex vivo*. GNRs did not demonstrate the extent of heating and spectral blue shift with PA laser as when compared to the changes observed with CW laser. Aggregation and reshaping of GNRs was also demonstrated to occur *in vivo* by examining irradiated tumour sites with TEM. This has an implication for CW lasers which are the most commonly used light sources for tumour PTT as sequential therapy performed by irradiating the same batch of previously irradiated GNRs is unlikely to provide any additional photothermal effect.

Chapter 4 involved experiments with aqueous solutions of GNRs, porcine and *ex vivo* human tissues. A linear relationship was found between the concentration of aqueous GNRs and the

temperatures generated by their irradiation. Healthy porcine tissues incubated with the most concentrated solution of GNRs experienced instantaneous charring/carbonisation under 2 W of NIR irradiation with a similar and prominent dose-effect seen on tissues irradiated with varying concentrations of GNRs. *Ex vivo* human oesophago-gastric cancer tissues incubated with CTAB-GNRs elicited a maximal temperature rise of at least 20°C after just 3.5 minutes of NIR light exposure, while tissues not exposed to any GNRs only achieved a modest 2°C rise. This is the first time that the plasmonic photothermal effect from GNRs has been evaluated on human *ex vivo* oesophagogastric tissues.

Chapter 5 dealt with the formation of stable and functionalised PEGylated GNRs that were conjugated with both a fluorophore and anti-EGFR-antibody. FLO-1 human oesophageal adenocarcinoma cells demonstrated an overexpression of the EGF receptor by a good uptake of free anti-EGFR antibody. Incubation of FLO-1 cancer cells with the functionalised GNRs showed a high degree of binding when compared to healthy Het-1A oesophageal cells. The concept of photothermal therapy using cancer cells was introduced along with the formation of tumour xenografts by a subcutaneous inoculation of FLO-1 cells in immunocompromised mice.

Chapter 6 fulfilled *in vivo* objectives by performing an in-depth analysis into the tumour theranostic potential of GNRs. The main findings of the *in vivo* study are summarised below:

1. Fluorescence spectroscopy obtained high amplitude signal peaks specifically over visually confirmed tumour sites in mice which had received GNRs via both IT and IV routes. These matched the fluorescence emission of the functionalised GNRs, indicating the specific accumulation of GNRs in the region of cancer
2. Fluorescence imaging was able to provide good contrast between healthy and cancerous regions, by detecting IV administered fluorescent GNRs accumulating at the site of tumour. These fluorescence areas corresponded well to the external margins of even subtle tumours, which will be clinically useful in cases of diagnostic uncertainty and image-guided biopsies
3. The degree of intensity feedback from fluorescent areas was quantifiable with line profiling across the fluorescent area
4. Fluorescence imaging was able to delineate the tumour margins, and possibly even of its less visible peripheral borders
5. It is likely that the free Cy5.5-anti-EGFR-antibody component in an aqueous solution of functionalised Cy5.5-GNRs-anti-EGFR-antibody is responsible for the early fluorescence seen because of its small size and through its rapid binding to tumours which over-express the EGFR antigen

6. Fluorescence signals decay over time, but the tumour site was usually still well illuminated 24 hours post IV injection
7. IT GNRs demonstrated a darkened area under fluorescence imaging due to a quenching effect, which was useful in ensuring the tumour area was adequately infiltrated with GNRs prior to PTT
8. It was suggested that GNRs were metabolised and excreted primarily through the hepato-renal pathway
9. In the experimental study, control mice subjected to GNRs or laser alone showed these modalities were by themselves incapable of inhibiting tumour proliferation
10. In the IT GNRs and PTT group, all ten mice in the study demonstrated complete tumour ablations at the end of the study, which were confirmed histologically
11. In the IV GNRs and PTT group, all ten mice in the study demonstrated complete tumour ablations at the end of the study, which were confirmed histologically
12. No metastatic lesions were identified at the end of study, which reinforces the strength in eliminating the primary tumour timely and completely
13. Mean temperature increases of 42.3 ± 9.4°C was seen from PTT in the IT GNRs group and 38 ± 9°C in the IV GNRs group. A return to baseline temperature was seen within two minutes of laser energy cessation. However thermal imaging only detects surface heating, is unable to provide live thermal information and was found to have a poor correlation with the elimination of tumour
14. All irradiated sites demonstrated neo-epithelialisation which occurred through the process of neo-collagenesis with histological disappearance of proliferating cells
15. Endocytosis of functionalised GNRs into tumour cells was confirmed by TEM analysis and EDX characterization of Au

Pilot mice studies were instrumental in formulating seven key principles which are likely to enhance photothermal tumour ablation success rates.

1. Multidirectional injection of GNRs for IT administration

It was imperative that equal volumes of GNRs was injected homogeneously into the entire tumour volume, by directing the needle of the syringe into all four quadrants and finally into the base of the tumour. This principle effectively and significantly reduced post-ablation cancer recurrence from the peripheral zone of irradiation. This was discovered after noticing that injections of GNRs solely into the epicentre (core) of the tumour did not dissipate GNRs evenly to all the edges of the tumour thereby inducing tumour persistence/recurrence.

2. Ensuring the beam size is larger than the largest dimension of tumour

It was crucial to maintain a laser beam diameter of at least 1 mm larger than the longest single dimension of the tumour, to ensure adequate tumour coverage and incorporate a margin of safety. The beam diameter was defined as 1/e as it had a Gaussian shape with no sharp edges. This was important in ensuring that any marginal cancer cells that were present in the periphery of the central (visible) tumour were also thermally ablated, so as to effectively minimise the likelihood of tumour recurrence.

3. Size consideration of large tumours

Larger tumours require proportionally more GNRs for successful photothermal therapy with adequate laser fluence as there was a gradual diminution in energy delivered to the peripheral (extremity) zone. However, safety consideration of the maximal laser power was essential in order to prevent collateral tissue damage, irrespective of the size of the tumour. As such, a gradated PTT approach should be considered for large tumours.

4. Administer a fresh and pure sample of fully functionalised GNRs

A fresh and pure sample of functionalised GNRs affords better fluorescence and thermal effects, leading to more reliable and consistent results. This was discovered after noticing diminished fluorescence signals and photothermal efficiency from using functionalised GNRs *in vivo* that were older than three weeks. Fresh samples of functionalised GNRs were found to yield consistently good theranostic results.

5. Allow 24 hours after IV administration of functionalised GNRs

Although the optimal time for detecting fluorescence signals and commencing PTT for tumours remains to be determined after IV administration of GNRs, immediate PTT after IV delivery of GNRs was associated with a poorer outcome. A 24-hour lapse after delivery of GNRs for PTT saw complete tumour ablations in all mice within the IV group of the study. This allowed sufficient time for passive GNR accumulation at the tumour site via the complex physiological interplay between EPR and the active biochemical antigen-antibody interaction between GNRs and cell membrane receptors.

6. Determine the appropriate OD (and volume) of GNRs to administer

An appropriate volume and OD of GNRs was crucial for targeted therapy when administering GNRs for PTT. This principle was discovered from pilot studies where insufficient OD of GNRs would lead to tumour reccurence and too large a volume of GNRs would lead to inappropriate hyperthermia levels. Achieving a fair balance between concentration and volume of GNRs with irradiation parameters was paramount to successful photothermal therapy. A systematic review of literature and the *in vivo* pilot studies were crucial in determining the optimal parameters for both GNRs and laser.

7. Observe for 30 days and evaluate pathology

This allowed adequate time to ensure that tumours do not re-surface once the skin had completely healed, both macroscopically and microscopically. This was significant as the initial visual thermal effect on the tumour site and the temperature rise following photothermal therapy was often similar in almost all irradiated mice but not always consistent with the final result. Performing histological assessments of tumour ablation sites and a thorough post-mortem evaluation at day 30 was the gold standard approach adopted in the *in vivo* studies to confirm successful tumour eradication.

Chapter 7 endeavoured to address the safety issues that persist about the application of GNRs and PTT *in vivo*. The main findings were:

1. The parameters for safe and effective laser fluence and maximal GNR concentrations applicable for PTT *in vivo* were established from initial pilot studies
2. Half the concentration and volume of GNRs was better tolerated by mice and could produce similarly effective heat profiles with IT administrations of GNRs
3. Energy transfer from the laser's irradiation appears to propagate in a relatively straight line from the tumour surface with minimal lateral extension. The depth of energy transfer was approximately 5.7 mm from the surface, with a gradually diminishing thermal effect. Underlying structures appear not to be unduly traumatised by the propagation of this energy
4. Biodistribution studies revealed that the volume of GNRs administered is proportional to [Au] found within RES organs (spleen, liver)

5. Blood clearance of GNRs was notably prominent, and systemic GNRs were predominantly metabolised by the liver and spleen, and excreted by the kidneys. Other organs showed negligible quantities of Au
6. Evidence of the enhanced permeability and retention of GNRs at tumour sites was observed
7. Histological evaluation of the liver, spleen and kidneys showed no evidence of structural, parenchymal or cellular damage, despite showing the highest levels of [Au] on mass spectrometry
8. Haematological and biochemical parameters within blood did not demonstrate any deviation from normal values, and showed preservation of intrinsic kidney and liver function.
9. No weight loss, anorexia, pain, morbidity or change in physical or psychosocial attributes were seen in mice throughout the duration of the study.

8.1 Clinical applications

8.1.1 Early Cancers

From this study, a combined theranostic application of GNRs was demonstrated and shown to be feasible and effective for clinical translation via endoscopic delivery. The theranostic potential offered by functionalised GNRs can be seen to have an application in both the early and late stages of cancer. It is envisaged as an adjunct to both surgery and endoscopy/laparoscopy. For the diagnosis of occult or subtle tumours, fluorescent imaging could potentially avoid early mucosal or submucosal cancers being missed during endoscopy. The feedback signals from fluorescence imaging could alert the endoscopist of an abnormal region which requires closer examination and allow the endoscopist to perform image-guided biopsies for histological confirmation. Large areas such as the entire mucosal surface of the stomach or peritoneal cavity could be visualised while under fluorescence imaging during endoscopy, which could potentially lead to more optically guided and targeted biopsies. There could also be implications for tumour treatment in clinical applications such as early GI cancers (T1-T2) that are either not amenable for surgical intervention or have failed attempts at endoscopic mucosal resection (EMR) or endoscopic submucosal dissection (ESD). When coupled endoscopically for intracorporeal use, NIR fibre optics can easily be introduced into the working channel of any commercially available flexible endoscope or through a 5 mm laparoscopic port during minimally invasive surgery.

8.1.2 Advanced cancers

Curative strategies for primary tumours located in poorly accessible regions and with poorly defined boundaries remain both a diagnostic and therapeutic challenge. Palliative treatment for cancers which are symptomatic from their size or advanced stage could be a further potential application for GNRs. IT injection followed by PTT could be done for tumour debulking, and this could be used in oesophageal, colonic or hepatic tumours. Other potential applications would be in isolated lung or peritoneal metastatic lesions, tumour ingrowth into intraluminal stents, intraluminal polypoid lesions and malignant melanoma.

8.1.3 Adjunct to surgery

It is envisioned that PTT could be directed to tumour cavities post-operatively, or be applied in margin positive or partial resections. It is further possible that PTT could be useful when applied at regional lymphatic tissues in order to reduce the risk of recurrence.

8.2 Key challenges remaining and future work

1. Ability to detect and treat the sentinel lymph node

Apart from fluorophore labelling, it is also possible that GNRs can be conjugated to radionuclide polymers (a low-activity radioactive substance) and thus become useful in the identification of the sentinel lymph node (SLN) which drains the primary tumour. Should detection of the SLN be positive, it is plausible then to treat that regional echelon of lymph nodes photothermally. In Section 6.7.3 “Size consideration of large tumours”, sentinel lymph node involvement was shown in a large tumour that remained incompletely ablated in a pilot mouse. Upon higher magnification, it was possible to see that the functionalised GNRs had infiltrated into the lymphatic tracts. As this was only demonstrated once, more studies would need to be conducted to determine if this was a chance occurrence, but it is possible that GNRs could be retained within the lymphatics surrounding tumours, and in particular, the SLN. Should this be a persistent feature, detecting the SLN with fluorescence imaging or gamma probes (for GNRs conjugated with radionuclide), determining its nodal status and then delivering concomitant PTT to regional lymph nodes remains a potential future challenge.

2. Drug Delivery

One of the features of nanoparticles is their ability to be used for drug delivery at targeted sites, and 'activated therapy' involves administering enzyme-cleavable prodrugs whereby the active moiety of the prodrug is released or becomes activated within the target cancer cell. The commonly used examples already in existence are Paclitaxel (Abraxane®, Abraxis BioScience Inc.) in metastatic breast cancer, and Doxorubicin (Doxil), which has been validated in a phase III multiple-myeloma trial and further indicated in metastatic ovarian cancer and AIDS-related Kaposi's sarcoma (6). While the functionalised GNRs used in this work were not conjugated to any drug, it may be possible to do so. The drug of choice could be a chemotherapy prodrug which would enhance the tumour effect while reducing systemic side-effects through its target-specific delivery. Collaboration with the pharmaceutical industry will be required to functionalise this prodrug to GNRs along with the appropriate receptor antibodies. The combined effect of drug delivery to tumour cells could be synergistic with PTT. It would merit some research into ensuring that long length linkers are attached to the prodrug such that it stands proud of the bare GNR surface (and does not shield the GNR, which may then preclude the desired effect from PTT).

3. Ensuring translatable results for *in situ* tumours

While the *in vivo* study used a subcutaneous tumour xenograft model, it would be useful to know if the results seen with fluorescence imaging and PTT are also effective for *in situ* tumours. For example, the depth of energy radiation has been determined for subcutaneous tumours but it would be important to also establish this depth for *in situ* oesophago-gastric tumours, such as to ensure that there would be contrast enhancement from luminal tumours and assess any complications arising from PTT. Care must be taken to avoid full thickness damage to the GI tract wall. An orthotopic tumour model would be ideal for this assessment, using for example immunosuppressed rabbits induced with gastric cancer, as the tumour model may allow an assessment of gastric wall integrity and offer a more robust intermediary assessment when intending to elevate the results from this study to the arena of a clinical trial.

4. Longitudinal studies

While it is known that there were no 30 day effects seen histologically within hepatocytes and splenocytes, and mice did not experience any apparent physical, physiological or psychosocial deterioration, it would be noteworthy to ensure this could be sustained over a longer period, and to repeat the biodistribution profiling at this juncture. This could also be

performed in control rodents which are given slightly more GNRs than what is clinically required for fluorescence or PTT.

5. Determination of optimal time for fluorescence imaging and PTT

In this study it was found that fluorescence imaging provided contrast enhancement to distinguish healthy from cancerous regions. The intensity of feedback signals from tumours was quantifiable with line profiling across the fluorescent areas. It was presumed that the early fluorescence seen from tumour sites was due to free Cy5.5-anti-EGFR-antibody component in an aqueous solution of functionalised Cy5.5-GNRs-anti-EGFR-antibody. It was further noted that fluorescence feedback signals decayed over time, but the tumour site remained well-illuminated 24 hours post IV injection, which was arbitrarily set as the time point when PTT was commenced. However the study fell short of determining the optimal time for imaging and therapy, which would involve a more extensive scrutiny into this specific component. This would involve regularly screening and measuring the fluorescence intensity signals, as well as performing PTT at similar time points. A large dataset would be required to definitively establish these parameters. An alternative would be to perform biopsies of tumours at various time points and establish the [Au] within the tissues.

6. Development of a flexible endoscope for fluorescence imaging

Although there are commercially available endoscopes which can detect indocyanine green (ICG) as a fluorescent dye, it would be useful to have a flexible endoscope which can detect more fluorophores than just ICG. This would enable imaging of a wider variety of dyes which can be conjugated to GNRs, such as Cy5.5 used in this study. For this to occur, the flexible endoscope has to ideally be able to be connected to suitable light sources which permit filters to be incorporated between the light source and the scope. The endoscope would also ideally have two working ports for image-guided biopsies and for PTT.

In conclusion the cancer theranostic potential of GNRs delivered by endoscopy has been described in detail for the first time by the results from this work. The use of this technology for surgical imaging and targeted treatment with its highly effective and reproducible results could significantly reduce the incidences of missed lesions, and also maximise tumour cell death while minimising damage to healthy tissues. Being shown to be a safe adjunct to surgery, when coupled with pre-existing minimally invasive procedures, the clinical application of photothermal therapy would enable rapid recovery and a shorter hospital stay. As such the theranostic potential of GNRs holds the capacity of not only saving but improving the quality of lives in a highly cost effective manner.

References

1. Wust P, Hildebrandt B, Sreenivasa G, Rau B, Gellermann J, Riess H, Felix R, Schlag PM. Hyperthermia in combined treatment of cancer. Lancet Oncol. 2002;3(8):487-97.
2. Amin Z, Donald JJ, Masters A, Kant R, Steger AC, Bown SG, Lees WR. Hepatic Metastases - Interstitial Laser Photocoagulation with Real-Time Us Monitoring and Dynamic Ct Evaluation of Treatment. Radiology. 1993;187(2):339-47.
3. Eichler K, Mack MG, Straub R, Engelmann K, Zangos S, Woitaschek D, Vogl TJ. Oligonodular hepatocellular carcinoma (HCC): MR-guided laser-induced thermotherapy (LITT). Radiologe. 2001;41(10):915-22.
4. Weissleder R. A clearer vision for in vivo imaging. Nature Biotechnology. 2001;19(4):316-7.
5. Li ZM, Huang P, Zhang XJ, Lin J, Yang S, Liu B, Gao F, Xi P, Ren QS, Cui DX. RGD-Conjugated Dendrimer-Modified Gold Nanorods for in Vivo Tumor Targeting and Photothermal Therapy. Mol Pharmaceut. 2010;7(1):94-104.
6. Hussein MA, Wood L, Hsi E, Srkalovic G, Karam M, Elson P, Bukowski RM. A Phase II trial of pegylated liposomal doxorubicin, vincristine, and reduced-dose dexamethasone combination therapy in newly diagnosed multiple myeloma patients. Cancer. 2002;95(10):2160-8.